Terms and Conditions of Use of Digitised Theses from Trinity College Library Dublin

Copyright statement

All material supplied by Trinity College Library is protected by copyright (under the Copyright and Related Rights Act, 2000 as amended) and other relevant Intellectual Property Rights. By accessing and using a Digitised Thesis from Trinity College Library you acknowledge that all Intellectual Property Rights in any Works supplied are the sole and exclusive property of the copyright and/or other IPR holder. Specific copyright holders may not be explicitly identified. Use of materials from other sources within a thesis should not be construed as a claim over them.

A non-exclusive, non-transferable licence is hereby granted to those using or reproducing, in whole or in part, the material for valid purposes, providing the copyright owners are acknowledged using the normal conventions. Where specific permission to use material is required, this is identified and such permission must be sought from the copyright holder or agency cited.

Liability statement

By using a Digitised Thesis, I accept that Trinity College Dublin bears no legal responsibility for the accuracy, legality or comprehensiveness of materials contained within the thesis, and that Trinity College Dublin accepts no liability for indirect, consequential, or incidental, damages or losses arising from use of the thesis for whatever reason. Information located in a thesis may be subject to specific use constraints, details of which may not be explicitly described. It is the responsibility of potential and actual users to be aware of such constraints and to abide by them. By making use of material from a digitised thesis, you accept these copyright and disclaimer provisions. Where it is brought to the attention of Trinity College Library that there may be a breach of copyright or other restraint, it is the policy to withdraw or take down access to a thesis while the issue is being resolved.

Access Agreement

By using a Digitised Thesis from Trinity College Library you are bound by the following Terms & Conditions. Please read them carefully.

I have read and I understand the following statement: All material supplied via a Digitised Thesis from Trinity College Library is protected by copyright and other intellectual property rights, and duplication or sale of all or part of any of a thesis is not permitted, except that material may be duplicated by you for your research use or for educational purposes in electronic or print form providing the copyright owners are acknowledged using the normal conventions. You must obtain permission for any other use. Electronic or print copies may not be offered, whether for sale or otherwise to anyone. This copy has been supplied on the understanding that it is copyright material and that no quotation from the thesis may be published without proper acknowledgement.

VIBRATION CONTROL OF STRUCTURES USING ACTIVE AND SEMI-ACTIVE TUNED MASS DAMPERS

by

Ruth Collins

Thesis submitted to the University of Dublin, Trinity College, for the Degree of Doctor of Philosophy

November 2005

DECLARATION

The author hereby declares that this thesis, in whole or in part, has not been submitted to any other University as an exercise for a degree. Except where reference has been given in the text, it is entirely the author's own work.

The author confirms that the Library may lend or copy this thesis upon request, for academic purposes.

Ruth Collins

Ruth Collins

November 2005

SUMMARY

This study addresses the vibration control of tall and flexible structures, such as wind turbine towers (WTTs). Investigations into the use of single and multiple tuned mass dampers (TMDs) with passive, active and semi-active control strategies in single- and multi-degree of freedom structures are carried out.

Two control strategies using bang-bang control with minimax shaping of the frequency response function (FRF) have been proposed. The first of these combines the principle of minimizing the maximum value of the FRF for a coupled structure-active TMD (ATMD) system with the application of a bang-bang control force to the TMD. This approach is shown to be effective at reducing the response of the structure with relatively small control forces. The second control strategy employs semi-active TMDs with bang-bang control and online shaping of the FRF. By retuning the TMD in real time, it is ensured that the peaks of the FRF of the coupled structure-TMD system never match the frequency of an external excitation, allowing the response to be decreased to a desired level with smaller control forces. Both proposed control strategies are applied to SDOF and MDOF structures subjected to harmonic and random excitations. It is seen that the control strategies reduce the response of the structure considerably, even when stiffness variations in the structure are considered or the passive TMD is mistuned.

A semi-active TMD in the form of a prototype variable stiffness TMD (VSTMD) is developed, characterised and tested experimentally. The VSTMD is capable of retuning in real time according to the minimax principle, based on the measured response of the structure. The TMD stiffness can be varied due to the presence of a solenoid through which the mass of the TMD passes. When current is supplied to the solenoid, a magnetic field is created. Depending on the level of current supplied, the magnetic field resists the motion of the mass, effectively providing additional stiffness to the TMD. The stiffness and damping of the VSTMD are characterised for different levels of current. When no current is supplied to the solenoid, the VSTMD acts as a passive device. Online tuning of the VSTMD is achieved by using wavelet analysis to identify the frequency of the response of the structure and tune the TMD

accordingly. The novel advantage offered by the developed VSTMD is that an electromechanical actuator is not required to change the properties of the TMD, hence control requirements are low. The VSTMD is tested experimentally using a model SDOF structure and shown to achieve considerable response reductions.

The above control strategies are incorporated into a multiple TMD (MTMD) configuration for a WTT. The response reductions achieved by each are evaluated numerically, and compared with the performance of passive MTMDs in the WTT. To assess the robustness of the different schemes, the stiffness of the WTT is varied by ±15%. The proposed control strategies are shown to reduce the response considerably and are to be particularly effective at controlling vibrations when the stiffness of the WTT is uncertain.

ACKNOWLEDGEMENTS

My work was carried out in the Department of Civil, Structural and Environmental Engineering. I am very grateful to the Department, RPS-MCOS and Enterprise Ireland who funded my studies over the past three years. My research was supervised by Dr Biawajit Basu and Dr Brian Broderick, and I thank them for all the knowledge and encouragement they have given me, their advice and support has been invaluable.

This work could not have been completed without the help of the technical staff in the structural laboratory. In particular, thanks must go to Gerard McGranaghan for the amount of time he spent with the experimental set-up in order to get it perfect (I know, I'm very fussy!). Also, thanks to George Jones, Dave McAuley and Chris O'Donovan, for always being there to help when needed.

I would like to acknowledge Prof. Satish Nagarajaiah of Rice University Texas, for the use of MATLAB programmes used in the numerical analysis in Chapters 3 and 4 of this thesis.

My heartfelt thanks must go to my parents, Fergus and Sandra, for the support they have given me, both financial and emotional over the past three years. To my fiancé Alan, for putting up with all my moaning when things were bad, you kept me sane and always made me laugh when I needed it the most. Thanks to my sisters Susan and Orla and to my brother Mark and his wife Teri and their children for all their support and encouragement

I would like to acknowledge the encouragement Dr Roger West gave me, not just to pursue a PhD but to get involved in other areas of College life as well. I would also like to thank my Rugby coach, Alwyn Thomas, for being so understanding of my absence from training sessions over the last few months!

TABLE OF CONTENTS

LIST OF ACRONYMS

AMD – Active Mass Damper

ATMD – Active Tuned Mass Damper

CI – Controllability Index

CMS – Critical Mode System

DOF – Degree of Freedom

EDR – Energy Diddipating Restraint

EMD/HT – Empirical Mode Decomposition/Hilbert Transform

ER – Electrorheological

FLC – Fuzzy Logic Controller

FMS – First Mode System

FRF – Frequency Response Function

LQC – Linear Quadratic Controller

LQG – Linear Quadratic Guassian

LSB – Limited Slip Bolt

LVDT – Linear Variable Differential Transducer

MDOF – Multi Degree of Freedom

MR – Magnetoheological

MTMD – Multiple Tuned Mass Damper

PSDF – Power Spectral Density Function

ROS – Reduced Order System

SAIVS-TMD – Semi-active Variable Stiffness Tuned Mass Damper

SDOF – Single Degree of Freedom

SMC – Sliding Mode Control

SROS – State reduced order system

SSA – Sequential Search Algorithm

SSSA – Simplified Sequential Search Algorithm

TLCD – Tuned Liquid Column Damper

TLD – Tuned Liquid Damper

TMD – Tuned Mass Damper

VDW – Viscous Damping Wall

VE – Viscoelastic

VF – Viscous Fluid

VSTMD – Variable Stiffness Tuned Mass Damper

WTT – Wind Turbine Tower

LIST OF FIGURES

LIST OF TABLES

CHAPTER 1

INTRODUCTION AND LITERATURE REVIEW

1.1 INTRODUCTION AND MOTIVATION

In today's growing economy and population, the need for tall structures in urban areas is becoming more and more of a reality in all areas of the world and not just the major capital cities. These tall structures are required to withstand high wind loads and in earthquake regions, large base excitations. Dampers are used for the vibration control of these structures. With the introduction of a damper in a structure, bracing members and large columns are less necessary, reducing the amount of material in the structure and making it more economically feasible.

The growing population and increasing number of structures around the world result in a strain on energy resources. Renewable energy is the way of the future and one such renewable is wind energy. Wind turbine towers (WTTs) offer the means by which wind energy is used to generate mechanical power and electricity. One of the issues with WTTs, which are tall and flexible structures, is that they must be shut down when wind speeds are too high and cause excess vibrations in the tower. Dampers may once again be employed to reduce such vibrations, making the WTT more efficient and improving its economic potential.

The aim of this thesis is to investigate passive, active and semi-active tuned mass dampers (TMDs) for the mitigation of vibration in both tall structures and WTTs. A procedure to identify the optimal number, location and tuning parameters of multiple TMDs (MTMDs) is developed. A new control strategy for active and semi-active dampers is examined and a prototype semi-active damper is designed and built in the lab. Both experimental and theoretical studies have been carried out on this damper.

1.2 BACKGROUND INFORMATION AND LITERATURE REVIEW

1.2.1 Classification of dampers

Vibration dampers can be classified on the basis of their functional performance and power supply requirements as passive, semi-active or active. In all cases, the role of the damper is to absorb and dissipate energy from the structure that originates from a source of loading, (e.g. wind or earthquakes), and to reduce the vibrations experienced by the structure.

Passive dampers do not require an external power supply; their properties are chosen based on apriori design criteria and do not change during the response of the structure. The effect of employing a passive device is primarily to reduce the vibrations of a structure when a resonant condition occurs. The advantage of a passive damper is that it is reliable and rarely fails to operate during critical periods, being independent of external power. However, the main disadvantage of the passive damper is its inability to recognise structural changes due to the applied excitation or changes in the level or nature of the excitation. Active and semi-active dampers are employed to alleviate this problem. An active damper requires a large power source for operation. The control forces supplied by the power source are based on the actual response of the structure and change as the response of the structure changes. A control strategy must be developed to command the actuator to apply the correct control force. For some applications, the power requirements of active dampers may be so large that they are not economically feasible; in these cases semi-active dampers can be introduced. A semi-active damper does not require an external control force to be applied; rather the mechanical properties of the damper can be varied, normally using considerably less power than an active damper. Further, semi-active strategies do not cause instability to the structure as no force is applied. In addition to the three classifications of dampers, combined or hybrid control systems also exist. These are combinations of passive and active or passive and semi-active control systems.

While passive dampers have been employed in tall structures in various areas of the world over the past 50 years, e.g. a tuned mass damper was placed at the top of the

Sears Tower in Chicago in 1974, full scale active dampers were not employed until 1989 when two active mass dampers were placed in the Kyobashi Centre in Toyko (Kobori et al., 1991). Since then, a number of active control strategies have been employed in buildings and bridges throughout the world. Semi-active systems have not as yet been applied to real structures, even though the benefits of the semi-active systems are considerable compared to the active and passive devices. Little experimental research into such control strategies has been carried out, and few prototype semi-active devices have been developed.

1.2.2 Types of Dampers

1.2.2.1 Passive dampers

'A passive control system may be defined as a system which does not require an external power source for operation and utilises the motion of the structure to develop the control forces' (Symans and Constantinou, 1999). It is shown in the block diagram of Figure 1.1 that the control is designed when the structure is passive and unmoving. When the structural properties change due to the applied excitation, the control will not change. The control system and the structure do not behave independently of each other, but rather interact with each other; as indicated in the block diagram by the dashed arrow between the control system and the structure.

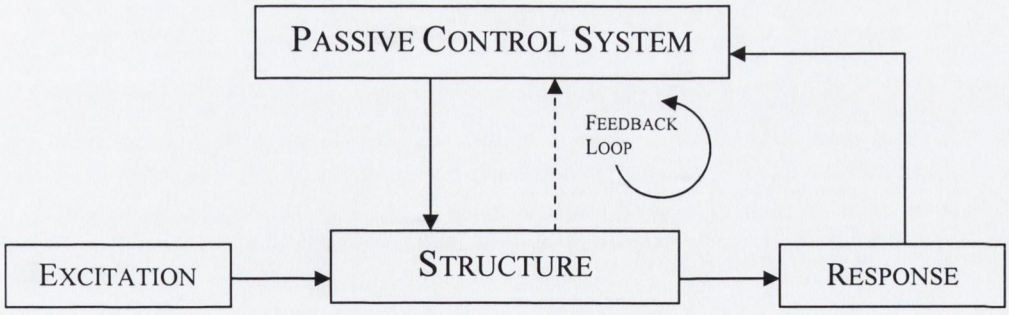

Figure 1.1 – Block diagram of passive control system (Symans and Constantinou, 1999)

Examples of passive dampers are bracing systems, tuned liquid dampers (TLDs), friction dampers, viscoelastic (VE) dampers, viscous fluid (VF) dampers and TMDs.

One of the most common practices of passive damping is the bracing system. Simply put, this is two pieces of reinforcement placed diagonally across each other at a section of the structure, to strengthen the structure and carry the excitation forces to the base of the structure. Much research into the bracing system has been carried including Balendra et al. (1991), Perotti et al. (1996), Kalyanaraman et al. (1998), Kameshki and Saka (2001), Bartera and Giacchetti (2004), Raftoyiannis (2005), and Spyrakos and Ermopoulos (2005).

Friction dampers are used to slow down the motion of structures 'by braking rather than breaking' (Pall and Marsh, 1982, Soong and Dargush, 1997). By achieving this, the kinetic energy of the motion is dissipated. There are a number of different types of friction dampers. The limited slip bolted (LSB) joint is used in conjunction with cross bracing in framed structures. Brake lining pads are used between the sliding surfaces in order to provide a consistent force-displacement response. The slippage of the brake lining pads is calculated so that maximum response reduction will be achieved for the passive structure. The Sumitomo friction damper has been applied to structures in Japan (Aiken and Kelly, 1990), where friction pads are employed to dissipate the energy in the structure. The energy dissipating restraint (EDR) is a more sophisticated friction damper and is described by Nims et al. (1993a, 1993b). Other studies on friction dampers have been carried by, Feigin (1961), Alspaugh (1978), Dowell (1983), Dowell and Schwartz (1983a; 1983b), Ostachowicz (1989), Colajanni and Papia (1995), Whiteman and Ferri (1997), Csaba (1998), Levy et al. (2001), Qu et al. (2001), Mualla and Belev (2002), Nacivet et a. (2003), López et al. (2004) and Lee et al. (2005).

A typical VE damper is shown in Figure 1.2. The VE material, typically copopolymers or glassy substances, is bonded to a steel plate. The energy is dissipated when the structural vibration causes shear motion between the outer steel plate and the centreplate. VE dampers were first used in aircraft in the 1950s to control the vibration-induced fatigue in airframes. Ten thousand VE dampers were installed in the twin towers of the World Trade Centre in New York in order to reduce the vibrations caused by wind excitations (Mahomoodi, 1969; Mahmoodi et al., 1987; Caldwell, 1986). Samali and Kwok (1995) investigated the effectiveness of VE

dampers in tall structures. VE dampers were shown to be very effective at dissipating the kinetic energy in a structure, achieving considerable reduction in vibrations. Cho et al. (1998) tested a scale model of a five-storey building in a wind tunnel. VE dampers were used to control the vibrations in the structure and considerable reductions were achieved. Other studies on VE dampers have been carried out by Tzou and Schiff (1987), Mahmoodi and Keel (1990), Tsai (1993), Tsai and Lee (1993), Lee and Tsai (1994), Li and Tsai (1994), Shen et al. (1995), Horr and Schmidt (1996), Munshi (1997), Park (2001), Lee et al. (2002), Tezcan and Uluca (2003), Xu et al. (2004) and Hryniewicz (2004).

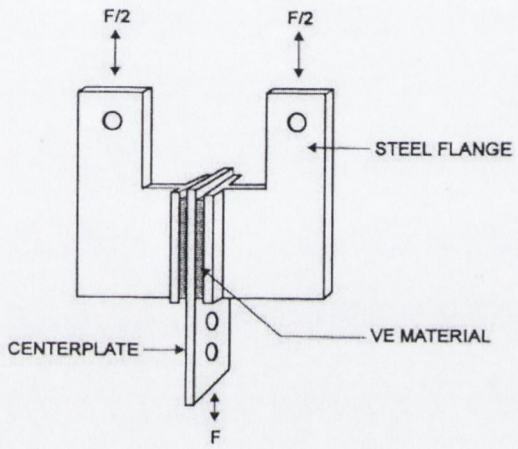

Figure 1.2 – VE damper (Soong and Dargush, 1997)

Fluids can also be applied to reduce the vibrations in structures. A VF damper is one such device. There are several different ways of employing a VF damper. The VF damper can be modelled as a dashpot to provide damping to the structure, reducing the structural vibrations. This is achieved by converting mechanical energy into heat by moving a piston in and out of a highly viscous fluid. Another approach is the viscous damping wall (VDW) (Arima et al., 1988). The VDW consists of a steel plate immersed in a viscous fluid in a narrow steel container. The container of the VDW is attached to the lower floor and the steel plate is attached to the upper floor. The motion of the plate through the viscous fluid as the structure vibrates dissipates the energy. An example of a VDW is shown in Figure 1.3. Other studies on VF dampers have been carried out by Slocum (1994) and Martinez-Rodrigo and Romero (2003).

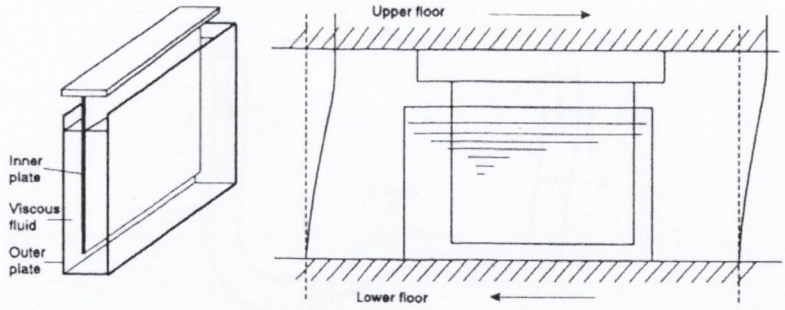

Figure 1.3 – VF damper (Soong and Dargush, 1997)

A TMD is a type of dynamic vibration absorber, consisting of a mass, M, a spring, K and a dashpot, C, as shown in Figure 1.4. When the natural frequency of a TMD is tuned to the natural frequency of a structure, the TMD absorbs some of the vibrations in the structure hence reducing the response of the structure. Further discussion on TMDs, the damper of interest in this thesis, is included separately in Section 1.2.3.

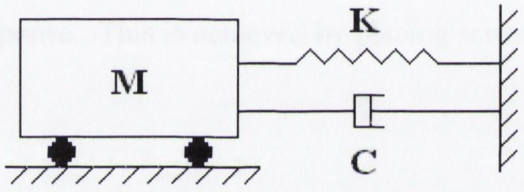

Figure 1.4 – TMD

The TLD is another type of dynamic vibration absorber, which is basically a tank of water placed at the top of a building. The liquid tank provides the mass of the damper and the sloshing of the water provides damping through viscous action. The frequency at which the water moves in the tank can be tuned to the natural frequency of the structure by changing the dimensions of the tank and the quantity of water placed in the tank. The tuned liquid column damper (TLCD), shown in Figure 1.5, is similar to the TLD, except that the fluid moves between two columns connected by an orifice. The dimensions of the orifice are modified so that the natural frequency of the damper matches that of the structure. Studies on the TLCD have been carried out by Xu et al. (1992), Balandra et al. (1995), Gao et al. (1997), Won et al. (1997), Gao et al. (1999), Xue et al. (2000a), Xue et al. (2000b), Ghosh and Basu (2004), Shum and Xu (2004), Ghosh and Basu (2005), Min et al. (2005) and Wu et al. (2005)

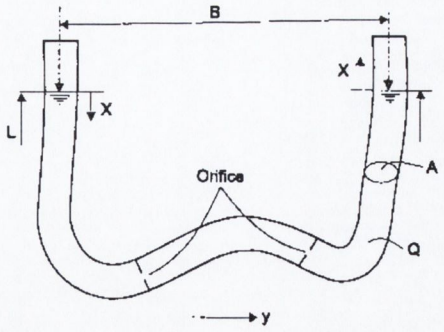

Figure 1.5 – TLCD (Soong and Dargush, 1997)

1.2.2.2 Active dampers and control strategies

'An active control system may be defined as a system which typically requires a large power source for operation of electrohydraulic or electromechanical actuators, which supply control forces to the structure' (Symans and Constantinou, 1999). The block diagram in Figure 1.6 shows how the control forces are generated based on feedback from the structural response. This is achieved by placing sensors at strategic locations in the structure.

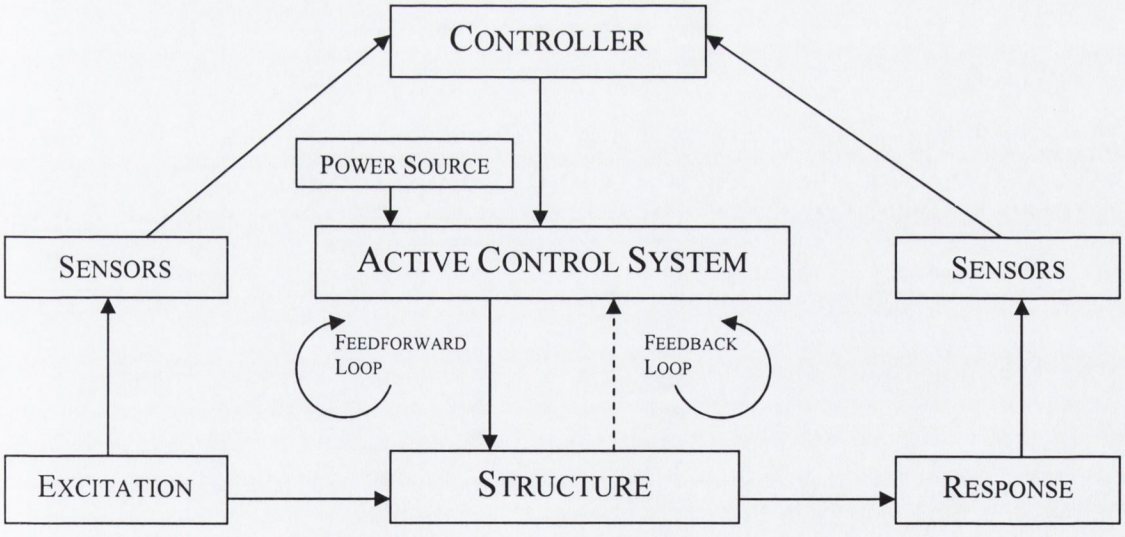

Figure 1.6 – Block diagram of active control system ((Symans and Constantinou, 1999)

A passive device can be turned into an active device by applying a control force to it. The advantage of the active device is that the properties of the damper can change based on the response of the structure and the variation in the stiffness of the

structure. An active damper requires a control strategy in order to apply the control force. Examples of control strategies are the linear quadratic controller (LQC), sliding mode control (SMC), pole location technique, H_2 and H_∞ and bang-bang control.

The LQC is an example of a classical control strategy. This method is defined by designing a control input that drives the system from some initial state to a constant final state (Meirovitch, 1995). The method is based on feedback control and applies a gain matrix to the state space equations, which is obtained by solving the Ricatti equation. Zhang and Xu (2001) derived a closed-form solution to the wind-induced response of actively controlled tall buildings. The active control scheme was obtained using linear quadratic guassian (LQG) controllers (similar to the LQC). A number of different examples were studied to achieve maximum reduction in the response with different control parameters. Other studies on the LQG controller have been carried out by Grimble (1984), Bansal and Basar (1987), Hsiao and Chen (1988), Sternad and Söderström (1988), Grimble (1990), Hsiao and Hsieh (1991), Von Bokern et al. (1992), Haddad (1993), Halevi et al. (1993), Hakvoort et al. (1994), Moore et al. (1999), Petersen and Pota (2003), Chen and Chou (2004) and Munteanu et al. (2005).

The purpose of SMC is to design a controller to drive the response trajectory into the sliding surface. The motion on the sliding surface is stable and the external excitation is ignored in its design. Yang at al (1995a) studied SMC for nonlinear and hysteretic structures subjected to strong earthquakes. The controllers presented are robust and result in considerable reductions in the response of the structure; they also have no undesirable chattering effects. The controller takes into account the earthquake excitation although the excitation needs to be known for the design. Yang et al. (1995b) examined the use of SMC for seismically excited linear structures. The method presented is similar to the previous paper and similar conclusions are drawn. It is also concluded that sliding mode controller methods are applicable to active variable dampers, active variable stiffness systems and friction controllable sliding bearings. Yang et al, (1995c) examined the use of SMC in buildings subjected to seismic excitation. A numerical study was carried out and to verify the results a scaled model, with four frictional sliding bearings, was tested on a shaky platform. A

reduced order model was taken for the numerical analysis and it was found that this model is comparable to that of the full order model, the control methods also proved satisfactory. The correlation between the peak response of the numerical and experimental analysis was reasonable however, the time history response was not as good. In order to get a more realistic time history response, the actuator dynamics and the interaction of the actuator with the system should be taken into account. Other studies on SMC have been carried out by Su et al. (2001), Chang and Zhu (2001), Shkolnikov and Shtessel (2002), Herrmann et al. (2003), Liang and Su (2003) and Yu et al. (2004).

Many control techniques are effective because they force the closed-loop poles of a system to be located on the complex plane. Pole location technique is one such method of achieving this. Chang and Yu (1998) examined a simple optimal pole location technique in order to control a structure subjected to seismic excitation. Three optimal pole locations are prescribed that incorporate the technique of rotating the poles to a particular constraint and/or shifting the natural frequency to a particular constraint. These techniques are then applied to two different structural models; a single-degree of freedom (SDOF) model and an eight-degree of freedom (DOF) model. It is found that this technique is effective for the design of control of tall buildings subjected to seismic excitation. Other studies on pole location techniques have been carried out by Ramar and Appukuttan (1991), Yang and Munro (1991), Valásek and Olgaç (1999).

The H_2 and H_∞ control techniques minimize the maximum amplification of the transfer function between the input excitation and the response of the structure. Suhardjo et al. (1992), examined the frequency domain based, H_2 optimal control method and applied the algorithm to a 60 storey building subjected to along-wind excitation. The balanced model reduction method was used to represent the building as a 20-degree of freedom model for ease of calculation. The controller was designed using the reduced order model but is applied to the full order model. The weighting parameters are chosen based on the frequency to be controlled and therefore a number of modes of the structure can be controlled depending on the number of dampers chosen. Considerable reduction in the acceleration response of the structure is

observed. Spencer et al. (1994) examined the H_2 and H_∞ frequency domain control techniques. The methods were represented using block diagrams and numerical examples of both were considered. It is seen that frequency domain techniques are successful in achieving a desired output response. Control strategies for the H_∞ and SMC techniques are verified experimentally, by Yang et al. (1996), using the shaking table. Considerable reductions were achieved in both cases and these compared well with the experimental results, the actuator dynamics and actuator structure were not taken into account, resulting in the error. Chase et al. (1999) developed an algorithm for the design of the H_∞ output feedback controller and examined its stability in the presence of non-linear actuator saturation effects. Numerical studies concluded that satisfactory reductions in the response of the structure were achieved with minimal control effort. Other studies on the H_2 and H_∞ control techniques have been carried out by Madiwale et al, (1989), Mohamed and Magdi (1999), Assawinchaichote et al. (2004), Hwang et al. (2005) and Berman and Shaked (2005).

Comparisons on SMC, linear quadratic regulator (LQR) (similar to the LQC) and H_∞ control techniques have also been examined. Wu et al. (1998) examined the H_∞ and LQR controller for three reduced order systems (ROS); the state-reduced order system (SROS), the critical mode-system (CMS) and the first-mode system (FMS). A reduced order system is used as it is impractical to place sensors on every floor, however, the reduced order model must incorporate all the important modes of vibration. The structure is subjected to a wind excitation modeled by the Davenport wind load spectrum. It is concluded that as long as the important modes are accounted for in the ROS, the SROS and SMS systems are satisfactory; however, the FMS system is not because of spillover effects. Wu and Yang (1998) present three methods of control for an active mass driver (AMD); LQG, H_∞ and SMC, which are employed in the Nanjing Tower in order to reduce the accelerations in the upper observation deck. The LQG controller minimizes some performance criteria assuming that the excitation input is based on Gaussian white noise. The H_∞ controller minimizes the maximum amplification of the transfer function between the input excitation and the response of the structure. The objective of the SMC controller is to drive the response trajectory onto the sliding surface, which is

designed to be stable. It is seen that all three methods result in considerable reductions in the acceleration response.

The principle of bang-bang control assumes that the components of the optimal control are piecewise constant functions of time. Studies on the bang-bang principle have been carried out by Cerf (1994), Bressan and Piccoli (1995) and Zhang et al. (2004) for general applications. The bang-bang control law based on the bang-bang principle has been examined in detail for vibration control applications by some researchers. Choi and Kim (1996) proposed a non-linear control scheme including a H_∞ controller that prevents the persistent switching of the bang-bang. An experimental validation was also carried out. Nandy and Sengupta (1996) proposed a simple mid-point bang-bang switching strategy in order to eliminate the multi-point switching strategy, which can be complex and expensive. Wu and Soong (1996) suggested a modified bang-bang control law based on a series expansion of singular functions. The modified control law is examined numerically and verified experimentally. The control law provides improved peak-response control performance.

1.2.2.3 Semi-active dampers

'A semi-active control system may be defined as a system which typically requires a small external power source for operation and utilises the motion of the structure to develop the control forces, the magnitude of which can be adjusted by the external power source' (Symans and Constantinou, 1999). As with active control, the control forces are generated from the feedback of the structure, the difference is that the magnitudes of the control forces are designed to take into account the response of the structure. The block diagram in Figure 1.7 for the semi-active control system is the same as that given in Figure 1.6 except that the power source is now a low-level power source.

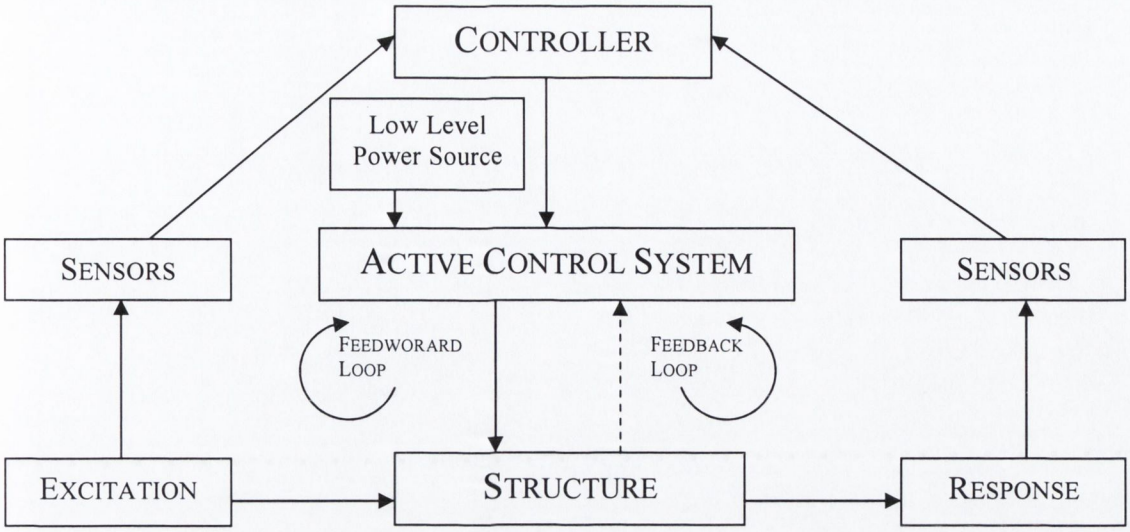

Figure 1.7 – Block diagram of semi-active control system (Symans and Constantinou, 1999)

A semi-active damper is developed from a passive damper in that it is modified so that the mechanical properties of the damper can change. This is achieved with little or no control force, hence providing a more economically feasible system than the active damper. Examples of semi-active dampers are: variable stiffness dampers, variable friction dampers, controllable fluid dampers, electrorheological (ER) dampers and magnetorheological (MR) dampers.

Variable stiffness control devices are employed in order to modify the stiffness and therefore change the natural vibration characteristics of a structure (Symans and Constantinou 1999). The advantage of the variable stiffness device is that the structure can be modified so that a resonant condition will not occur when subjected to wind or seismic forces. Kobori et al. (1994) proposed a full-scale variable orifice damper. The system is engaged or released so as to include or not include the stiffness of the damper. However, there are some disadvantages to the system regarding discontinuous modifications of the stiffness leading to increased accelerations and excitation of the higher modes. Also, the system provides mainly variable damping and limited varying stiffness capability. Nasu et al. (2001) carried out further research on the active variable stiffness damper proposed by Kobori et al (1994). The variable stiffness damper was placed in a building on a trial basis and observed for ten years. The system was found to be highly reliable and easy to maintain.

Variable friction devices are similar to the passive friction damper described in Section 1.2.2.1. Based on the response, the frictional interface of the lining pads is adjusted to allow for different amounts of slippage. Studies on variable frction dampers have been carried out by Akbay and Aktan (1991; 1992), Pandya et al. (1996), Feng and Shinozuka (1990), Feng et al. (1992; 1993), Feng (1993), Dowdell and Cherry (1994a; 1994b) and Fujita et al. (1994).

By changing the size of the orifice of the TLCD described in Section 1.2.2.1, the natural frequency of the device can be varied based on the response of the structure. Tamura et al. (1995) examined the effectiveness of TLDs showing that TLDs can significantly reduce the vibration response of tall structures. Balendra et al. (2001) subjected a SDOF tower to wind excitation and used a TLCD for active control. The TLCD was compared to an active passive TMD and the results showed that the proposed system offers a good alternative, which may be more effective for vibration control in wind-induced towers. Other studies on semi-active TLCD have been carried out by Lou et al. (1994), Haroun et al. (1994), Kareem et al. (1994) and Abe et al. (1996).

Two other kinds of semi-active devices are the ER and MR dampers. The potential of the ER fluid as a control device was first recognised by Winslow (1949). The ER damper consists of a container containing micron-sized dielectric particles suspended within a fluid, usually oil (Symans and Constantinou, 1999). When a current is applied to the fluid, an electric field is created and the dielectric particles are polarised and thus aligned. The ER fluid is simple and provides a rapid response, hence reducing instability due to time delay. This offers a resistance to the flow and therefore by changing the current, the resistance is changed depending on the response of the structure. Studies on the ER damper have been carried out by Ehrgott and Masri (1992a; 1992b; 1993), Gavin et al. (1993; 1994; 1996a; 1996b; 1996c), Gavin and Hanson (1994), Gavin (1996; 1997), Makris et al. (1995; 1996a; 1996b), Makris and McMahon (1996a; 1996b), Makris (1997), Burton et al. (1996; 1997), Burton and Makris (1996), McMahon and Makris (1997) and Gordoninejad et al. (1994).

The MR damper is very similar to the ER damper. Here the fluid contains micron sized magnetically polarised particles which are polarised and aligned due to the presence of a magnetic field. The advantage of the MR damper over the ER damper is their ability to provide high yield strength, low viscosity and stable hysteretic behaviour over a broader temperature range (Carlson et al, 1995). Zhang and Roschke (1999) tested a flexible multi-DOF (MDOF) structure, which employed active control and an MR damper to control the along-wind structural response. Other studies on MR dampers have been carried out by Spencer et al. (1996; 1997a; 1997b), Dyke et al. (1996a; 1996b; 1997a; 1997b), Dyke and Spencer (1996;1997), Carlson and Spencer (1996a; 1996b) and Hansen et al. (1997).

1.2.2.4 Hybrid Dampers

The control force in an ATMD can often be quite large and therefore impractical; other types of control systems have been proposed. A hybrid control system is one, which incorporates a combination of passive and active devices. The hybrid strategy can alleviate some of the control problems that occur when each device is acting on its own. Several studies on hybrid control strategies have been carried out in the past. Spencer and Nagarajaiah (2003) examined the advantages and disadvantages of passive, active, hybrid and semi-active damping devices to protect structures against natural hazards. Cheng and Jiang (1998) present a hybrid control system comprising of a hydraulic actuator and a VF damper. A stochastic theory on the seismic response of controlled structures is established and based on this the optimal location of the device is determined. Considerable response reduction of the structure is seen with the inclusion of the device and it is shown that the effectiveness of the device is greatly influenced by its location. Yang and Agrawal (2002) examined the combination of a passive base isolation system with various passive or semi-active control devices for non-linear buildings against near-field earthquakes. The base isolation system alone is not sufficient to protect the structures and therefore the addition of the passive and semi-active devices improves the performance of the design. Ricciardelli et al. (2003) examined the use of TMDs, AMDs and active TMDs (ATMDs) for the control of the response of tall buildings to wind gustiness. The active control law was based on the Linear Quadratic Regulator strategy. It was

shown that the hybrid device required much lower control forces than that of the other two methods studied. Earlier studies on hybrid control have been carried out by Glauser et al. (1997), Yang et. al. (1992) and Nagarajaiah et al. (1993).

1.2.3 Tuned mass dampers

The TMD given in Figure 1.4 is basically a dynamic vibration absorber, consisting of a mass, a spring and a dashpot, attached to a structure. Den Hartog (1956) was the first to examine the optimum parameters of the vibration absorber in the absence of damping in the main structure. It was found that the frequency at which the maximum vibration occurs in a structure is independent of damping. From this the optimum tuning ratio for a TMD was determined as that which minimised the maxima of the peaks of the transfer function, i.e. making the peaks equal in magnitude. Based on this principle, the optimum damping in the TMD could also be determined.

The TMD and multiple TMDs (MTMDs) are increasingly popular dampers used in structural vibration control. Rana et al (1998) examined a simplified procedure for TMD design and performed a parametric study to enhance the understanding of the behaviour of a TMD. As one TMD can only control one mode of vibration, the use of MTMDs has also been examined to allow control of multiple modes. MTMDs were proposed by Xu and Igusa (1992) and further investigations in this area of research was carried out by Yamaguchi and Harnpornchai (1993), Tsai and Lin (1993), Abe and Fujino (1995), Abe and Igusa (1995), Kareem and Kline (1995), Jangid and Datta (1997), Li (2000) and Li (2002), Ghosh and Basu (2004). Igusa et al. (1993) studied the effectiveness of MTMDs compared to a single TMD for the case where the natural frequencies of each TMD were spaced closely together. It was observed that the optimum frequency characteristics of each TMD did not exactly match those of the primary structure, and that the maximum vibration reduction in the structure was achieved with 'mis-tuned' conditions. For practical purposes, the stiffness and damping parameters of TMDs are constant while the mass is varied to control the natural frequency. As a single TMD is tuned to a unique frequency, Igusa et al. (1993) concluded that MTMD systems are more effective. Joshi et al (1996) investigated the stochastic response of a structure with MTMDs subjected to a base

excitation and also found that a MTMD system was more effective than a TMD system. It was also concluded that the damping in the primary system does not influence the optimum-damping ratio in either MTMD or TMD systems. Research has also been carried out into the optimum parameters of a MTMD system. Jangid (1999) investigated the optimum parameters of an MTMD system for an undamped primary system subjected to a harmonic base excitation using a numerical searching technique. Li and Liu (2003) investigated the control performance of eight different MTMD models. The optimum parameters were identified using extensive numerical analysis and the most effective model selected. Ricciardelli et al. (2000) optimised the properties of the TMD based on the measured response of a wind-excited structure. It was found that by optimising the TMD, the structural response did not vary significantly, however, the displacement of the added mass was reduced.

TMDs are most effective when the excitation force matches the natural frequency of the structure, i.e. under a resonant vibration condition of the structure. If a non-resonant vibration condition occurs, the TMD is generally ineffective as the response of the structure is marginal. However, the frequency of a non-resonant excitation may match the frequency at which a peak occurs in the frequency response function (FRF) of the response of the coupled structure-TMD system. If this happens, the structural response may increase and may even exceed the response of the system without any TMD. In order to overcome this problem, which could be caused due to uncertainty in the excitation frequency or structural properties, ATMDs are employed. An ATMD requires a force to control the response of the TMD and a control strategy to achieve this. Xu (1996) examined the parameters of ATMDs to obtain the maximum possible vibration reduction in a wind-excited tall building. It was observed that the vibrations could be greatly reduced if appropriate ATMD parameters were employed along with acceleration sensors. Aldawod et al. (2001) examined the vibration control of tall buildings under along-wind excitation. An ATMD, driven by a Fuzzy Logic Controller (FLC) was used to control the system, and it was shown that the FLC was more effective than the more commonly used LQG controller.

The disadvantage of ATMDs is that they require large power sources. A semi-active variable stiffness TMD (VSTMD) is introduced in order to reduce the power source.

The VSTMD has the capability of retuning its natural frequency, in real time, to match the natural frequency of the structure. Nagarajaiah developed a semi-active variable-stiffness device that modifies the stiffness and damping continuously and smoothly [U.S. Patent No. 6,098,969 (2000)]. Nagarajaiah and Mate (1998) have shown the effectiveness of this device in a scaled structural model. Varadarajan and Nagarajaiah (2004) proposed a semi-active VSTMD (SAIVS-TMD). This device is capable of continuously modifying its stiffness, alleviating the problems associated with on-off devices. It can retune in real time, thereby avoiding response amplification due to mis-tuning. Other studies on variable stiffness dampers have been carried out by Kobori et al.(1993), Nemir et al. (1994), Loh and Ma (1994), Yamada and Kobori (1995), Yang et al. (1996) and Nagarajaiah (1997).

1.2.4 Wind turbine towers

From previous research it can be concluded that TMDs are effective at suppressing vibrations in flexible structures. A wind turbine tower is a typical tall structure, which is flexible with considerable mass of the nacelle and rotating blades at the top. Wind is caused by the uneven heating of the earth's surface due to irregularities on the surface and the rotation of the earth as it moves around the sun. Wind energy turbines offer the means by which wind energy is used to generate mechanical power and electricity. Wind energy is a free renewable source, and wind farms emit no atmospheric or other pollutants. Once a wind turbine is in operation it is relatively cheap to run as Capital costs represent approximately 80% of the total expenditure.

Many studies have been carried out on the design of WTTs. Varol et al. (2001) performed an experimental study of the efficiency of a WTT. Bazeos et al. (2002) calculated the load bearing capacity and the seismic behaviour of a steel wind turbine tower. Lavassas et al. (2003) presented the analysis and design of a 1MW steel WTT. Studies on different components of a WTT by Fuglsang and Madsen (1999), Ronold and Larsen (2000), Ekelund (2000), Ronold and Christensen (2001) and Maalawi and Negm (2002) have also been conducted. Recently, studies on the interaction between the blades and the tower have been carried out by Murtagh et al. (2004).

1.2.5 Sequential search algorithm

In order to achieve the maximum reduction in the vibrations of tall flexible structures including wind turbine towers, it is important to identify the optimums locations for the dampers. Zhang and Soong (1992) suggested the use of a Sequential Search Algorithm (SSA) to determine the optimal location of VE dampers in a structure. A controllability index (CI), based on the response of the structure is defined. The response of the primary structure is calculated and the first damper placed where the CI is highest. The properties of the structure are altered by the presence of this additional damper; hence the response of the structure is recalculated. The next damper is now placed where the new CI is highest. The procedure is repeated until additional dampers cause insignificant changes to response of the structure. Garcia and Soong (2002) developed a simplified version of the SSA, the Simplified Sequential Search Algorithm (SSSA). A number of models with different parameters were examined and the study provided further insight into the effectiveness of the SSA. Shukla and Datta (1999) also examined the optimal locations of VE dampers in a structure. A CI was determined based on the root mean square (RMS) of the displacement response and a similar sequential procedure was applied.

1.3 SCOPE OF RESEARCH STUDY

This research study examines passive MTMDs, ATMDs and VSTMDs applied to tall structures and WTTs. Passive TMDs are investigated by employing MTMDs in a WTT to control the first and second modes of vibration, as these are the dominant modes affecting the displacement and acceleration responses, respectively. The WTT is subjected to four power spectral density functions (PSDFs), two based on base excitation and two based on wind excitation. The SSA is employed to find the optimal number and location of MTMDs in the WTT. The values for the tuning parameter that achieves the maximum reduction in the response of the WTT are also obtained. Based on the results, a general configuration for the optimal number, location and tuning parameter of the MTMDs is obtained. To determine the robustness of the design, the stiffness of the WTT is varied by ±15%.

ATMDs are examined with a view to reducing the number of TMDs in the structure while achieving the same response reduction. A control strategy for the vibration control of structures using ATMDs is proposed. The control strategy incorporates bang-bang control and the minimax principle. A SDOF coupled structure-ATMD system is subjected to harmonic excitations at resonant and non-resonant frequencies and the effectiveness of the control scheme is examined. The magnitude of the control force applied to the TMD is then compared to the control force required to achieve similar response reductions in the SDOF structure without any TMD. To determine the effectiveness of the proposed strategy, it is compared to another conventional controller, the LQC with FRF shaping, while to determine the robustness of the control scheme, the SDOF system is examined under random excitations. The proposed control scheme for a MDOF structure is then applied to the 76-story benchmark problem proposed by Yang et al (2004). The set of structural performance criteria, based on the peak and RMS responses of the structure, developed by Yang et al. (2004) is evaluated for the structure. Constraints are also placed on the actuator stroke and the actuator control force. The results are then compared to the ATMD with LQR proposed by Yang et al. (2004).

Semi-active TMDs are also investigated. This type of TMD has the ability of retuning in real time and is therefore more efficient than the ATMD. The bang-bang control strategy developed for the ATMD is modified to incorporate the change in stiffness of the semi-active TMD based on the value of the control force. A coupled SDOF structure semi-active TMD system is subjected to harmonic excitations at resonant and non-resonant frequencies and the effectiveness of the control scheme is compared to the ATMD control strategy. The semi-active TMD is then employed in the 76-storey model developed by Yang et al. (2004) and the results are compared to those obtained by Yang et al. (2004), a semi-active control strategy proposed by Varadarajan and Nagarajaiah (2004) and the ATMD with bang-bang control.

A prototype VSTMD is developed in the laboratory. The TMD stiffness is varied due to the presence of a solenoid through which the mass of the TMD passes. When current is supplied to the solenoid, a magnetic field is created. Depending on the level of current supplied, the magnetic field resists the motion of the mass, effectively

providing additional stiffness to the TMD. The stiffness and damping of the VSTMD are characterised for different levels of current. When no current is supplied to the solenoid, the VSTMD acts as a passive device.

Online tuning of the VSTMD is investigated using wavelet analysis to identify the frequency of the response of the structure and tune the TMD accordingly. The response of the structure and the base excitation can be determined using sensors at strategic locations. If the structure is stiff, it will vibrate close to the frequency of the base excitation. Therefore, if the frequency of the base excitation matches the natural frequency of the structure, a resonant condition will occur. By applying wavelet analysis to identify the frequency at which the structure is vibrating, the VSTMD can be retuned to this frequency according to the minimax principle.

Finally, the use of passive MTMDs and MTMDs with the ATMD and VSTMD control strategies are compared in a numerical study. A WTT model is subjected to a random excitation and the response of the structure is examined. The stiffness of the structure is varied by ±15% to assess the robustness of each control strategy. Optimal damping is also considered for the passive MTMD design, in order to determine its effectiveness for future design.

1.4 ORGANISATION OF THESIS

Chapter 2 examines passive MTMDs. The optimal number, location and tuning parameters of the MTMDs in a WTT are determined, using the SSA.

Chapter 3 introduces an ATMD. A control strategy incorporating the minimax principle and bang-bang control is obtained. The proposed control strategy is investigated for a number of numerical examples.

Chapter 4 introduces a VSTMD. The VSTMD is capable of retuning the TMD in real time according to the minimax principle and bang-bang control. A proposed control strategy is investigated for a number of numerical examples.

The design of a prototype solenoid-based VSTMD is presented in Chapter 5. Detailed description of the structural laboratory set-up and experimental programme is given. The stiffness and damping of the VSTMD are characterised for static and dynamic response conditions. A deliberately mistuned TMD is placed on a model SDOF structure and the current applied to the VSTMD solenoid varied to retune the TMD according to the minimax principle.

The capability of retuning the VSTMD in real time is examined in Chapter 6. This is achieved using wavelet analysis. The response of the structure at a given time step is obtained. Using wavelet analysis, the local dominant frequency of the response is calculated and the VSTMD is retuned in real time according to the minimax principle. Finally, the SDOF structure is subjected to a base excited white noise excitation and the effectiveness of the VSTMD examined.

In Chapter 7, passive MTMDs and MTMDs with the ATMD and VSTMD control strategies are applied to the WTT subjected to a random excitation. Variation in the stiffness of ±15% is considered and optimal damping in the TMDs is examined.

CHAPTER 2

PASSIVE MTMDS FOR MDOF STRUCTURES USING SSA

2.1 INTRODUCTION

TMDs are placed in a structure in order to reduce the vibrations of the structure caused by external excitations acting on the structure. Multiple TMDs are employed to further reduce the vibrations. In order to achieve the maximum reduction in vibrations, it is important to identify the optimum location of the MTMD system. There are a number of ways MTMDs can be employed in a structure. MTMDs may be placed at the top of the structure and their natural frequencies distributed around the fundamental natural frequency. This alleviates the problem of mistuning the TMDs. It has also been observed that MTMDs strategically placed in a structure reduce the structural vibrations.

2.2 OPTIMAL DESIGN OF MTMDS

To determine the optimal location of the MTMDs, the SSA, developed by Zhang and Soong (1992) can be employed. In this approach, a CI, based on the RMS response of the structure is defined. The RMS response of the primary structure is calculated and the first TMD placed where the CI is highest. The properties of the structure are altered by the presence of this additional TMD; hence the response of the structure is recalculated. The next TMD is now placed where the new CI is highest. The procedure is repeated until additional TMDs cause insignificant changes to the response of the structure. The FRF of the structure is also obtained to determine the tuning frequency of each TMD. The MTMD configuration is optimised to reduce the RMS displacement and acceleration response.

The structure examined in this chapter is a WTT, subjected to a number of base motions and wind loading PSDFs, modelled as the Kanai-Tajimi spectrum, base excited white noise, the Harris spectrum and wind excited white noise. The WTT is assumed to act as a vertical cantilever and the stiffness matrix is obtained from the flexibility of the structure. Classical structural damping of the Rayleigh type is

assumed. The transfer matrix is obtained using the state space equations and the RMS response of the structure is calculated using the H_{rms} norm control technique. The CI is based on the RMS acceleration and displacement response of the structure. The optimum MTMD configuration is determined for each loading type, and a generalised configuration based on all four PSDFs is determined. To determine the robustness of the MTMD design, the generalised configuration is assumed for a WTT with a variation of ±15% in its stiffness. The observed reduction in response is expressed as a set of performance criteria, based on the RMS displacements and accelerations in a structure. The performance criterion is a modified version of that given by Yang et al (2004).

2.3 TRANSFER MATRIX AND STOCHASTIC RESPONSE

The transfer matrix is defined as the matrix that algebraically relates a system's output to its input. Here, the system input is the PSDF and the output includes the displacement, velocity or acceleration response for which the transfer matrix is formulated. By employing a Laplace Transform, these inputs and outputs can be obtained in the frequency domain. For a MDOF structure, the theory of state space, modelled in the frequency domain, is employed. The equation of motion for a MDOF system is given as

$$[m]\{\ddot{x}\} + [c]\{\dot{x}\} + [k]\{x\} = [F]\{z\} = \{W\} \tag{2.1}$$

where [m], [c] and [k] are the mass, damping and stiffness matrices of the structure respectively, [F] is the force influence matrix, x is the displacement of the structure, $\{z\}$ is the excitation force vector and the overdot implies differentiation with respect to time. The system can be represented in state space using the following equations (Nise, 1994).

$$[\dot{X}] = [A][X] + [B]\{z\} \tag{2.2}$$

$$[Y] = [C][X] + [D]\{z\} \tag{2.3}$$

where [X] is the state vector given in Eq (2.4) and [Y] is the output vector given in Eq (2.5)

$$[X]=[\{\dot{x}\}\ \{x\}]^T \tag{2.4}$$

$$[Y]=[\{\ddot{x}\}\{\dot{x}\}\ \{x\}]^T \tag{2.5}$$

For single point base excitations, the force influence matrix [F] is equivalent to the mass matrix [m] of the structure; therefore the input matrix [B] is given by

$$[B]=\begin{bmatrix}[0]_{nxn}\\ -[I]_{nxn}\end{bmatrix} \tag{2.6}$$

For wind excitations the force influence matrix [F] is an identity matrix and therefore the input matrix [B] is given by

$$[B]=\begin{bmatrix}[0]_{nxn}\\ -[m]^{-1}_{nxn}\end{bmatrix} \tag{2.7}$$

The system matrix, [A], the output matrix, [C], and the feed-forward matrix [D] are given by

$$[A]=\begin{bmatrix}[0]_{nxn} & [I]_{nxn}\\ -[m]^{-1}_{nxn}[k]_{nxn} & -[m]^{-1}_{nxn}[c]_{nxn}\end{bmatrix} \tag{2.8}$$

$$[C]=\begin{bmatrix}[I]_{2nx\,2n}\\ -[m]^{-1}_{nxn}[k]_{nxn} & -[m]^{-1}_{nxn}[c]_{nxn}\end{bmatrix} \tag{2.9}$$

$$[D]=\begin{bmatrix}[0]_{nxn}\\ [B]_{2nxn}\end{bmatrix} \tag{2.10}$$

where n is the number of DOFs in the structure. From the state space equations (as in Equations (2.2) and (2.3)), the transfer matrix, $[H(i\omega)]$, is obtained using the Laplace Transform. The resulting matrix is given as follows

$$[H(i\omega)] = [C][(i\omega[I]-[A])]^{-1}[B] + [D] \tag{2.11}$$

where ω is the frequency over the applied loading and i is the complex function such that $i^2 = -1$. The transfer matrix can also be expressed, as a function of the frequency ratio β,

$$\beta = \frac{\omega}{\omega_n} \tag{2.12}$$

where ω_n is the fundamental natural frequency of the structure. The relationship between the PSDF of any input, S_W and any output, S_X at each point in the system can now be obtained using the following equation.

$$S_x(\beta) = H(\beta)S_W(\beta)H^*(\beta) \tag{2.13}$$

where, $H^*(\beta)$ is the complex conjugate of $H(\beta)$. The RMS value of the response of the structure is determined by

$$H_{RMS} = \left(\frac{1}{2\pi}\int_{-\infty}^{\infty} H(\beta)S_W(\beta)H^*(\beta)d\beta\right)^{1/2} \tag{2.14}$$

This value is employed as the basis on which the vibration response of the tower is minimised.

2.3.1 Base excitations

A ground acceleration process applied to the structure is represented by its PSDF, $S_{\ddot{z}}(\beta)$, for this $\{z\}$ is given by $[I]_{nx1}\,\ddot{g}$, where $\ddot{g}$ is the base acceleration. To investigate the applicability of the proposed procedure to different seismological

settings, two distinct representations are employed: base excited white noise and the Kanai-Tajimi spectrum. Base excited white noise is represented by a constant value of $\phi_0 = 1\text{cm}^2/\text{s}^3$ over the entire frequency domain; the Kanai-Tajimi spectrum is given as follows

$$S_{\ddot{z}}(\omega) = \phi_0 \frac{1 + 4\zeta_g^2(\omega/\omega_g)^2}{[1-(\omega/\omega_g)^2]^2 + 4\zeta_g^2(\omega/\omega_g)^2} \tag{2.15}$$

The parameters ζ_g and ω_g are the damping ratio and natural frequency of the ground respectively, which may be chosen to represent specific local soil conditions. Here, general firm ground conditions are assumed, for which an analysis of recorded ground motions suggests values of 0.6 and 5π for ζ_g and ω_g, respectively (Clough and Penzien, 1993). For the numerical study considered in the following section, $\phi_0 = 1\text{cm}^2/\text{s}^3$ is assumed in Eq (2.15) without any loss of generality.

2.3.2 Wind excitations

For wind excitations, the PSDF, $S_W(\beta)$ is obtained from the along-wind excitation applied to the structure and the turbulence between two points, for this $\{z\}$ is given by $\{\overline{W}\}_{nx1}$, where the wind acceleration applied to each DOF of the structure is given by $[m]^{-1}\{\{\overline{W}\}\}$. The along-wind excitation $S_{WW}(\beta)$ is modelled by the Harris spectrum and wind excited white noise. The Harris Spectrum is given by

$$[S_{WW}(\beta)]_{nxn} = S_0 \frac{4k_0[\overline{F}]^2_{nxn}[\gamma]_{nxn}}{\beta} \tag{2.16}$$

where

$$[\gamma]_{nxn} = \frac{[U_r]^2_{nxn}\pi^4\psi\beta}{[2+(\pi^3\psi\beta)^2]^{5/6}} \tag{2.17}$$

The parameters in Eqs (2.16) and (2.17) are given by

$$\psi = \frac{\omega_1 l_x}{2\pi^4 U_{10}} \tag{2.18}$$

$$[\overline{F}]_{nxn} = \frac{[F_0]_{nxn}\pi^4}{\omega_1^2 M_{11}} \tag{2.19}$$

$$[F_0]_{nxn} = \rho_0 A_0 C_0 [U_z]^2_{nxn} \tag{2.20}$$

$$[U_r]_{nxn} = \frac{U_{10}}{[U_z]_{nxn}} \tag{2.21}$$

$$[U_z]_{nxn} = U_{10}\left(\frac{[h]_{nxn}}{10}\right)^{\alpha_p} \tag{2.22}$$

and

$$[h] = \begin{bmatrix} h_1 & 0 & . & . & 0 \\ 0 & h_2 & . & . & 0 \\ . & . & . & . & . \\ . & . & . & . & . \\ 0 & 0 & . & . & h_n \end{bmatrix}_{nxn} \tag{2.23}$$

where h_n is the height of the structure at the n^{th} DOF, S_0 is $1(mm/s^2)^2$, k_0 is the ground surface drag co-efficient, l_x is the wave length, ω_1 is the fundamental frequency, U_{10} is the mean wind speed at a reference height of 10m, α^p is the power law exponent, ρ_0 is the density of air, A_0 is the frontal area of structure and C_0 is the drag coefficient. The value of α^p varies depending on the design codes for the terrain specified. The parameter M_{11} is the modal mass and is defined by equation (2.24)

$$M_{11} = \int_0^H \phi_1^T(h) m \phi_1(h) dz \tag{2.24}$$

In Eq (2.24), H is the height of the tower, $\{\phi_1(h)\}_{1xn}$ is the mode shape of the first mode and $\{\phi_1^T(h)\}_{nx1}$ is its conjugate. The mode shape is calculated from Eqs (2.25), (2.26), (2.27) and (2.28)

$$D(\omega_n) = [k] - \omega_n^2 [m] \tag{2.25}$$

$$\begin{bmatrix} D_{aa}(\omega_n) D_{ab}(\omega_n) \\ D_{ba}(\omega_n) D_{bb}(\omega_n) \end{bmatrix} \begin{Bmatrix} 1 \\ \phi_1 \end{Bmatrix} = \begin{Bmatrix} 0 \\ 0 \end{Bmatrix} \tag{2.26}$$

$$\{\phi_1\}_i = \begin{Bmatrix} \phi_{12} \\ \phi_{13} \\ . \\ . \\ . \\ \phi_{1i} \end{Bmatrix} \tag{2.27}$$

$$\{\phi_1\} = -[D_{bb}(\omega_n)]^{-1} D_{ba}(\omega_n) \tag{2.28}$$

where $D(\omega_n)$ is the determinant representing the characteristic equation to find the first mode of the structure, and $D_{aa}(\omega_n)$, $D_{ba}(\omega_n)$, $D_{ab}(\omega_n)$ and $D_{bb}(\omega_n)$ represent the sub-matrices of the matrix $D(\omega_n)$. The white noise spectrum for along wind excitation is represented by Equation (2.29)

$$[S_{WW}(\beta)]_{nxn} = S_0 4k_0 [\overline{F}]^2_{nxn} \tag{2.29}$$

The turbulence between two points, p and q, is obtained from the Davenport spectrum and is represented by Eq (2.30)

$$S_{UUpq}(P_p, P_q, \beta) = [\exp(-C_m / U_{mean})][S_{WWpp}(P_p, \beta) S_{WWqq}(P_q, \beta)]^{1/2} \tag{2.30}$$

where $S_{UUpq}(P_p, P_q, \beta)$ is the cross spectrum of the two longitudinal turbulence components at points P_p and P_q, C_m is a non-dimensional decay constant that

determines the spatial extent of the correlation in the turbulence (C_{rn} = 10 is assumed here) and U_{mean} is the mean wind velocity. Therefore, the complete PSDF matrix, S_W, can now be expressed in Equation (2.31)

$$[S_W] = \begin{bmatrix} S_{WW11} & S_{UU12} & S_{UU13} & \cdot & \cdot & S_{UU1n} \\ S_{UU21} & S_{WW22} & S_{UU23} & \cdot & \cdot & S_{UU2n} \\ S_{UU31} & S_{UU31} & S_{WW33} & \cdot & \cdot & S_{UU3n} \\ \cdot & \cdot & \cdot & \cdot & \cdot & \cdot \\ \cdot & \cdot & \cdot & \cdot & \cdot & \cdot \\ S_{UUn1} & S_{UUn2} & S_{UUn3} & \cdot & \cdot & S_{WWnn} \end{bmatrix} \tag{2.31}$$

Eq (2.14) can now be employed to calculate the RMS response of the WTT subjected to base or wind PSDFs.

2.4 SSA, PERFORMANCE CRITERIA AND WTT MODEL

2.4.1 Sequential search algorithm

A CI based on the RMS acceleration and displacement response of the structure is employed to quantify the extent to which the response of the structure is reduced using different numbers of MTMDs. The FRF of the WTT is obtained in order to determine the mode to which the TMD is tuned. The CI is first based on the RMS displacement response. The response of the structure is calculated and the first TMD is placed where the CI is the highest. The addition of this TMD will change the response of the structure, which is calculated again. The second TMD is now placed where the new CI is the highest. This procedure is repeated until additional TMDs have marginal effect on the RMS displacement response of the structure. The CI is then based on the RMS acceleration response, the procedure is repeated and TMDs are added until they have marginal effect on the RMS acceleration response of the structure.

2.4.2 Performance criteria

Based on the performance criteria proposed by Yang et al (2004) for a benchmark problem on the response control of tall buildings, a non-dimensional set of criteria is defined from the RMS responses of the structure. The first evaluation criterion is the ability of the TMD to reduce the maximum floor accelerations

$$\bar{J}_1 = \frac{max(\sigma_{\ddot{x}1}, \sigma_{\ddot{x}2} \ldots \sigma_{\ddot{x}n})}{max(\sigma_{\ddot{x}1o}, \sigma_{\ddot{x}2o} \ldots \sigma_{\ddot{x}no})} \tag{2.32}$$

where $\sigma_{\ddot{x}n}$ and $\sigma_{\ddot{x}no}$ are the RMS acceleration of the n^{th} DOF of the controlled structure and the uncontrolled structures, respectively. The second evaluation criterion is the average reduction in the RMS acceleration response of the structure

$$\bar{J}_2 = \sum_i (\sigma_{\ddot{x}i} / \sigma_{\ddot{x}io}), for \quad i = 1,2 \ldots, n \tag{2.33}$$

The third evaluation criterion is the ability of the TMD to reduce the maximum RMS displacement response

$$\bar{J}_3 = \frac{max(\sigma_{x1}, \sigma_{x2} \ldots \sigma_{xn})}{max(\sigma_{x1o}, \sigma_{x2o} \ldots \sigma_{xno})} \tag{2.34}$$

where σ_{xn} and σ_{xno} are the RMS displacement response of the n^{th} DOF of the controlled and the uncontrolled structures respectively. The fourth evaluation criterion is the ability of the TMD to reduce the average RMS floor displacement

$$\bar{J}_4 = \sum_i (\sigma_{xi} / \sigma_{xio}), for \quad i = 1,2 \ldots, n \tag{2.35}$$

and the final evaluation criterion is on the response of the TMD expressed in terms of the TMD stroke

$$\bar{J}_5 = \frac{max(\sigma_{xm1}, \sigma_{xm2} \ldots \sigma_{xmi})}{max(\sigma_{x1o}, \sigma_{x2o} \ldots \sigma_{xno})} \tag{2.36}$$

where σ_{xmi} is the RMS displacement of the i^{th} TMD.

2.4.3 MDOF WTT model

A MDOF WTT, assumed to be fixed into the ground and acting as a vertical cantilever is considered, as shown in Figure 2.1. The model is based on a wind turbine tower designed by Lavassas et al. (2003), except that the rotors are lumped as a mass at the top of the tower, which is normal practice in conventional design. So long as the fundamental frequencies of the tower and the blades are far apart, a stochastic analysis may be carried out. The mass of the tower is lumped at n nodes of interest, which leads to a discrete N-DOF system where the n^{th} mass, stiffness and damping values are designated by m_n, k_n and c_n respectively. The stiffness of a structure is related to the flexibility of the cantilever system, which can be expressed by the flexibility matrix. Elements of the flexibility matrix are known as flexibility coefficients. The coefficient f_{ij} is defined as the displacement at the i^{th} DOF due to a unit force applied at the j^{th} DOF (Ghali and Neville, 1997). The stiffness matrix [k] is found from the inverse of the flexibility matrix [f].

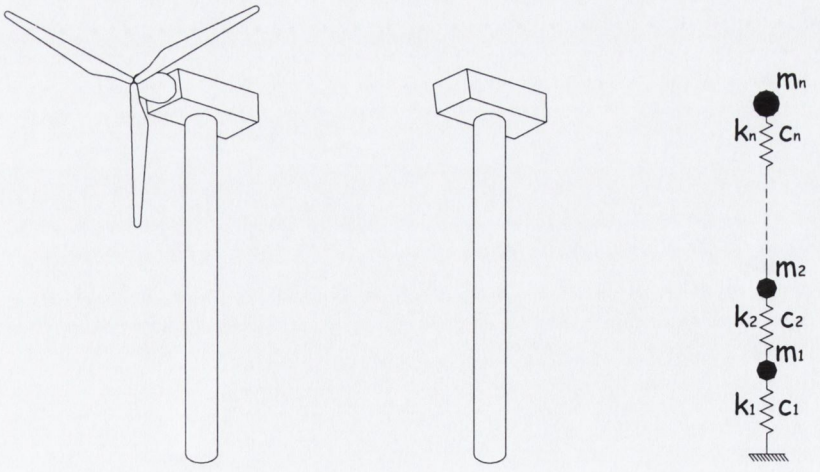

Figure 2.1 - Wind turbine tower, simplified model and discretised model

It can be assumed that the damping matrix, which is of Rayleigh type, is proportional to the mass and stiffness matrices, as in Eq (2.37)

$$[c] = a_0[m] + a_1[k] \tag{2.37}$$

The values of a_0 and a_1 are found for assumed modal damping ratios, ζ in the n^{th} and m^{th} modes of the structure, as per Eq (2.38) (Clough and Penzien, 1993).

$$\begin{Bmatrix} a_0 \\ a_1 \end{Bmatrix} = \frac{2\zeta}{\omega_m + \omega_n} \begin{Bmatrix} \omega_m \omega_n \\ 1 \end{Bmatrix} \tag{2.38}$$

The natural frequencies of the n^{th} and m^{th} modes, ω_n and ω_n respectively, are calculated from Eq (2.39)

$$\mathrm{DET}\left([k] - \omega_n^2[m]\right) = 0 \tag{2.39}$$

When TMDs are added to any DOF of the structure, the augmented model (including the additional TMD) represents an $N+p$ DOF system (where p represents the number of additional TMDs), whose response is strongly dependent on the properties of the TMD. Each TMD is placed at a DOF, chosen based on the CI and denoted by the position 'q'. For each addition of TMD, the mass, stiffness and damping matrices are amended with, m_{di} placed at positions $(N+p,q)$ and $(N+p,N+p)$ in the mass matrix; $-k_{di}$ and k_{di} placed at positions $(q,N+p)$ and $(N+p,N+p)$, respectively, in the stiffness matrix; and $-c_{di}$ and c_{di} placed at the positions $(q,N+p)$ and $(N+p,N+p)$, respectively in the damping matrix, where m_{di}, k_{di} and c_{di} are the mass, stiffness and damping of the i^{th} TMD respectively. The TMD is tuned to the structure such that

$$k_d = \gamma \omega_n^2 m_d \tag{2.40}$$

$$c_d = 2\zeta \omega_n m_d \tag{2.41}$$

where γ is the tuning parameter of the TMD.

2.5 MTMD OPTIMISATION BY SSA

The RMS response of the WTT without TMD is obtained using the H_{RMS}-norm control technique described in Section 2.1. In Figures 2.2 and 2.3, the RMS displacement and acceleration responses are plotted over the number of DOFs in the WTT model. It is observed that the maximum displacement occurs at the 20^{th} DOF and the maximum acceleration occurs at the 12^{th} DOF. The FRFs for the RMS displacement and acceleration responses of the WTT are shown in Figures 2.4 and 2.5, respectively. It is shown in Figure 2.4, that for the RMS displacement response, the dominant mode of vibrations found at the first natural frequency. However, for the RMS acceleration response shown in Figure 2.5, the second natural mode of vibration is dominant. Therefore TMDs added where the CI is based on the RMS displacement response should be tuned to the first natural frequency, whereas TMDs added where the CI is based on the acceleration response should be tuned to the second natural frequency. The tuning parameter, γ is obtained by plotting a range of γ values against the response of the structure. The chosen value of γ is identified at the lowest part of the graph.

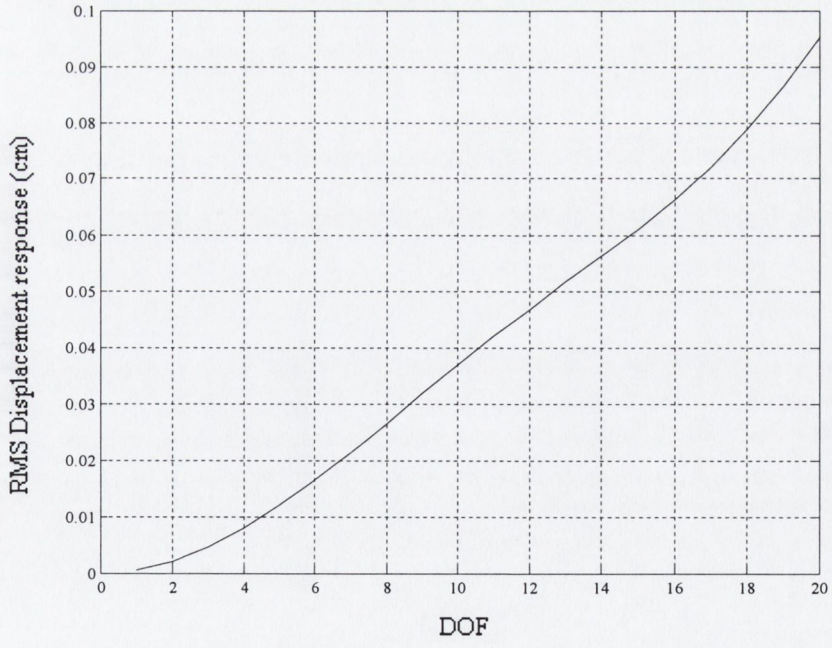

Figure 2.2 – RMS Displacement response of WTT without TMD

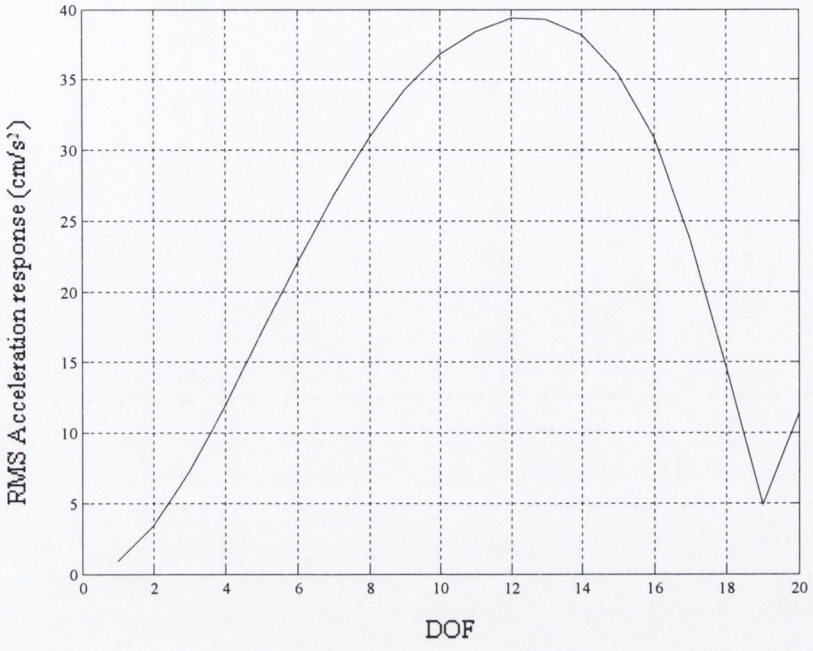

Figure 2.3 – RMS Acceleration response of WTT without TMD

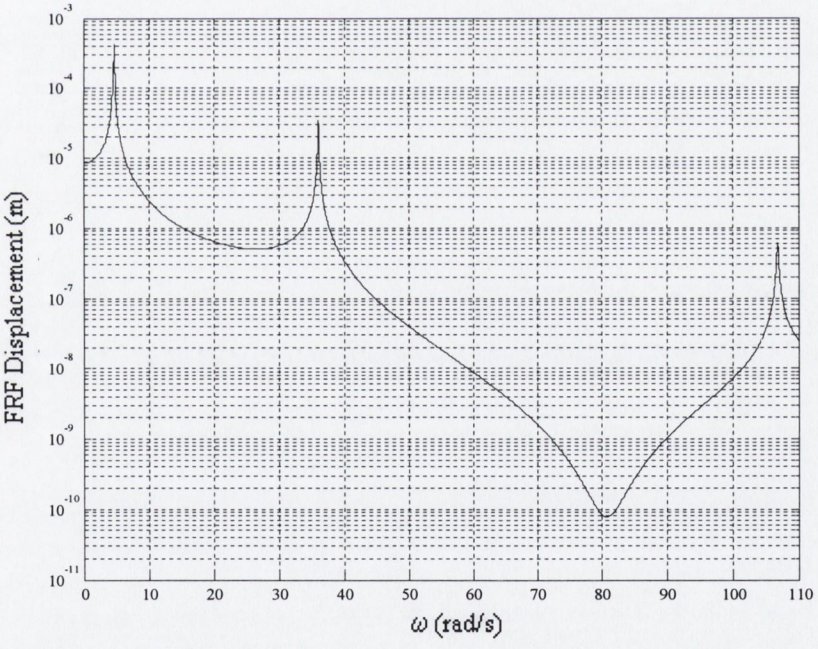

Figure 2.4 – FRF for RMS Displacement response of WTT without TMD

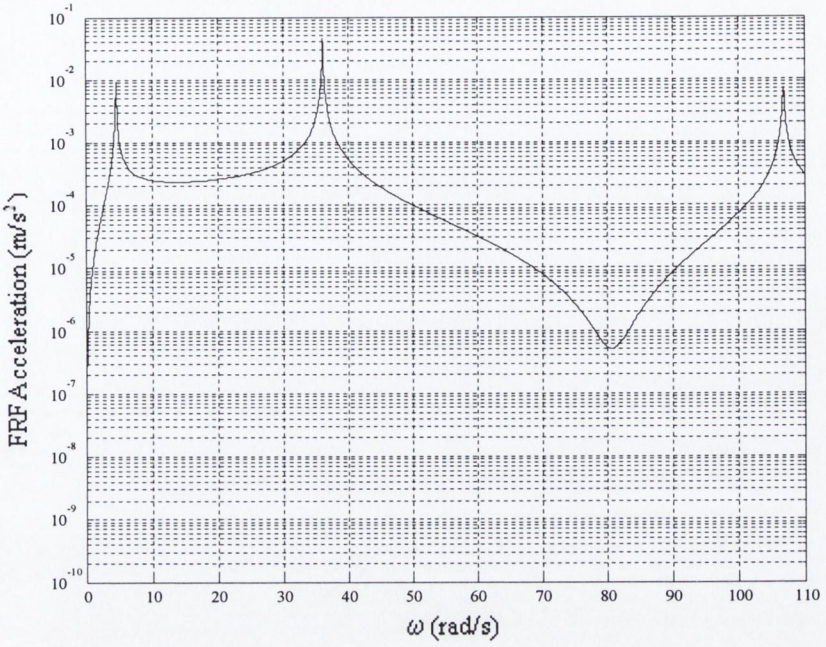

Figure 2.5 – FRF for RMS Acceleration response of WTT without TMD

2.5.1 White noise base excitation

The CI is first based on the RMS displacement response and a TMD is placed at the 20th DOF, tuned to the first natural frequency. The influence of the parameter, γ_1 on the RMS displacement response at the top of the structure is shown in Figure 2.6. It is observed that greatest reduction in the response occurs with γ_1 =1, i.e. the TMD is tuned exactly to the fundamental natural frequency of the structure. The response of the augmented structure (i.e. with a TMD placed at the top of the WTT, tuned to Eq (2.40) such that ω_n=4.69rad/s and γ_1=1) is then obtained. The maximum RMS displacement response of the structure still occurs at the 20th DOF, therefore the 19th DOF, which has the next highest CI is considered. Following this approach, three more TMDs are added to the structure at the 19th, 18th and 17th DOF with values of γ_2, γ_3 and γ_4 equal to 0.88, 1.1 and 0.8 identified from Figures 2.7, 2.8 and 2.9, respectively. As the response of the structure is consistently highest at the 20th DOF, it would also be possible to design the passive MTMD configuration by placing the additional TMDs together at the 20th DOF. However, in many cases this may not be practical due to space constraints. Also, adding a number of TMDs at one DOF could considerably add to the mass at that point, which may cause problems in the structural design of the WTT.

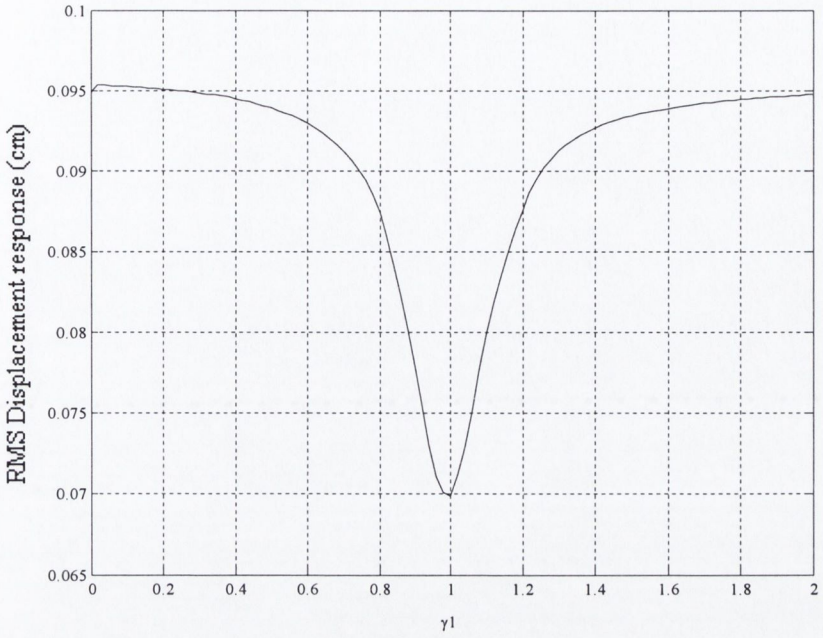

Figure 2.6 – RMS displacement response of WTT vs γ_1 @ 20th DOF

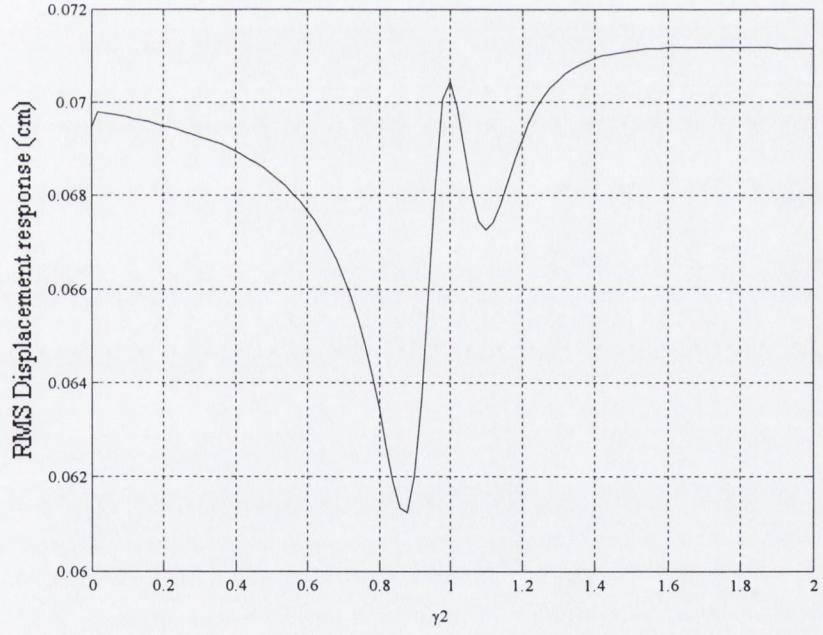

Figure 2.7 – RMS displacement response of WTT vs γ_2 @ 20th DOF

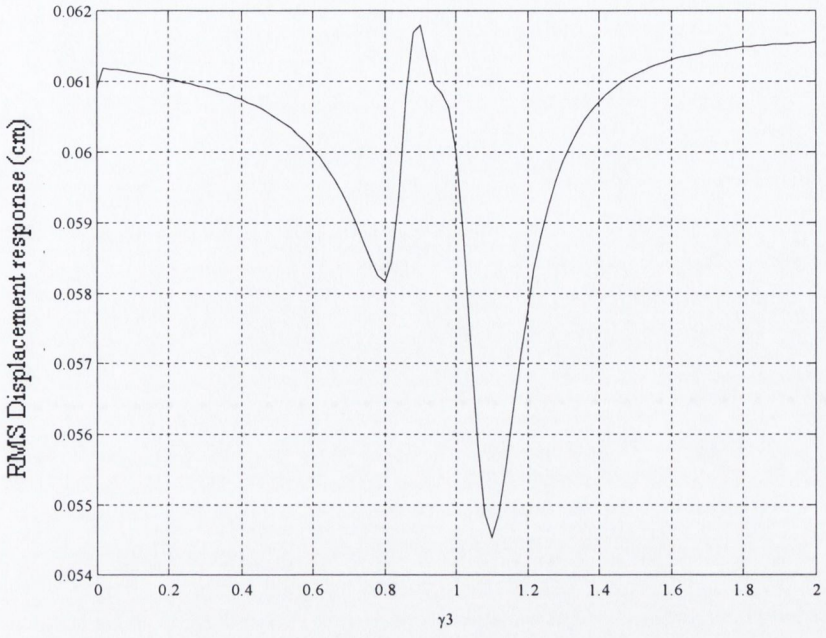

Figure 2.8 – RMS displacement response of WTT vs γ_3 @ 20th DOF

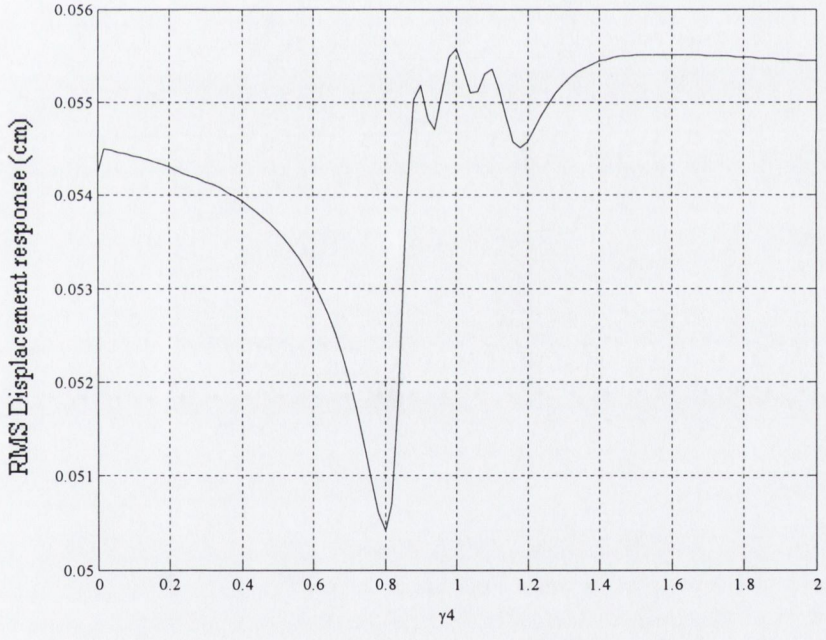

Figure 2.9 – RMS displacement response of WTT vs γ_4 @ 20th DOF

When a fifth TMD is added on the basis of a CI based on the RMS displacement response of the structure, the decrease in the response is marginal. Instead, a CI based on the RMS acceleration response is considered and the procedure repeated. Accordingly, the next TMD is placed at the 12th DOF and is tuned to the second mode of the structure as suggested by Figure 2.3 and Figure 2.5. The effect of the tuning

parameter γ_5 on the RMS acceleration response is shown in Figure 2.10. It is observed that the greatest reduction in response occurs with $\gamma_5 = 0.98$. Therefore a TMD with parameters ω_n=36.04rad/s and α_5=0.98 is added to the 12th DOF of the WTT. Following this approach, two more TMDs, are added to the structure at the 15th and 16th DOF, with tuning parameter's γ_6 and γ_7 equal to 1.14 and 0.86, respectively, identified from Figures 2.11 and 2.12.

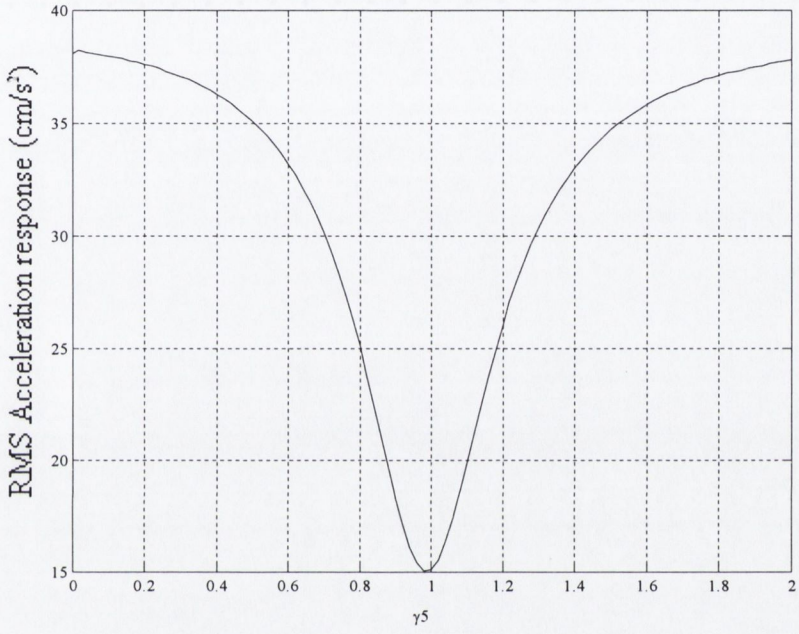

Figure 2.10 – RMS acceleration response of WTT vs γ_5 @ 12th DOF

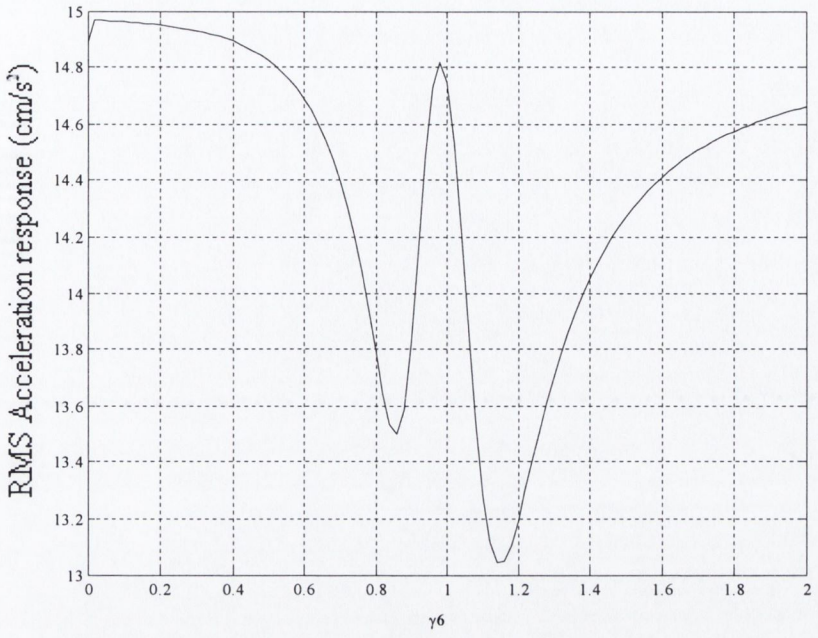

Figure 2.11 – RMS acceleration response of WTT vs γ_6 @ 12th DOF

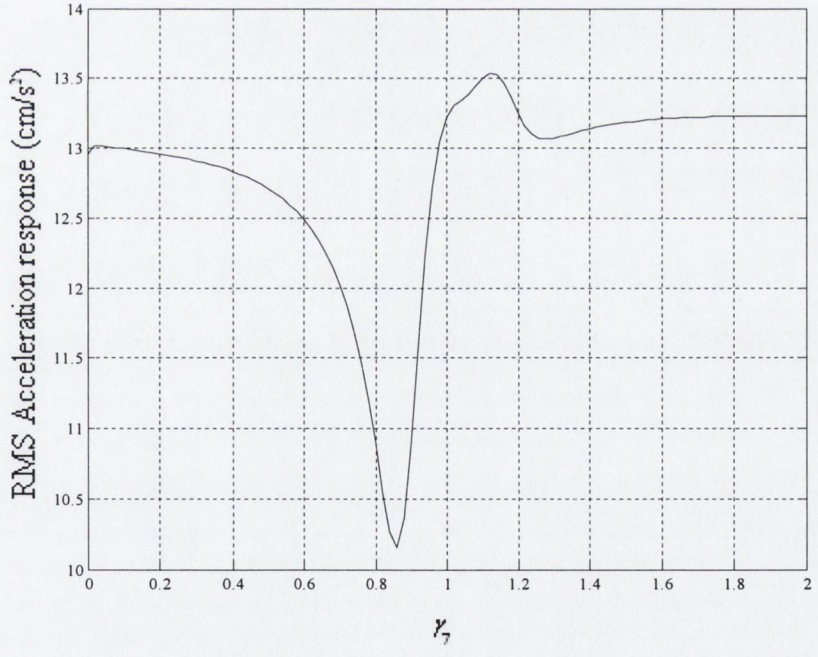

Figure 2.12 – RMS acceleration response of WTT vs γ_7 @ 12th DOF

When an eighth TMD is considered, the decrease in the response is marginal, therefore no additional TMDs are applied to the structure. The performance criteria for each additional TMD and the tuning parameter and DOF of each TMD are detailed in Table 2.1.

	1 TMD	2 TMDs	3 TMDs	4 TMDs	5 TMDs	6 TMDs	7 TMDs
DOF	20	19	18	17	12	15	16
γ	1.00	0.88	1.10	0.80	0.98	1.14	0.86
J_1	1.000	1.000	0.999	0.998	0.461	0.428	0.399
J_2	0.999	0.999	0.998	0.997	0.526	0.489	0.441
J_3	0.731	0.641	0.57	0.527	0.523	0.527	0.530
J_4	0.799	0.734	0.685	0.655	0.490	0.487	0.475
J_5	9.545	8.161	8.51	7.063	7.096	7.152	7.218

Table 2.1 – Performance criterion and optimal configuration for MTMDs with base excited white noise PSDF

It is shown in Table 2.1, that the addition of the first four TMDs where the CI is based on the RMS displacement response reduces the RMS displacement response of the structure only, however, when the fifth TMD where the CI is based on the RMS acceleration response is added, the acceleration response of the structure is reduced dramatically and the RMS displacement response reduces by 25%. It is also important to note, that the position of additional TMDs reduces performance criterion J_6, the TMD stroke. The optimal configuration of TMDs for base excited white noise is found to be 7 TMDs placed at the 20^{th}, 19^{th}, 18^{th}, 17^{th}, 12^{th}, 15^{th} and 16^{th} DOF, with γ values of 1, 0.88, 1.1, 0.8, 0.98, 1.14 and 0.86, respectively.

The MTMD arrangement is optimised to reduce the RMS displacement and acceleration response. Other MTMD configurations may be optimised for different performance objectives. For example, if it is only necessary to reduce the displacement response in the WTT, then only 4 TMDs would be required at the 20^{th}, 19^{th}, 18^{th} and 17^{th} DOF with γ values of 1, 0.88, 1.1 and 0.8, respectively. Alternatively, if the objective is to reduce the acceleration response below a defined limit, e.g. 15 cm/s^2, only 1 TMD would be placed in the structure at the 12^{th} DOF with γ=0.98. The method described can be applied to other structural forms, as long as the mass, stiffness and damping matrices of the structure are known, and the performance objective is defined.

2.5.2 Kanai-Tajimi spectrum

When the approach described in Section 2.4.1 is applied to the WTT subjected to the Kanai-Tajimi spectrum, the number, placement and tuning parameters in the optimum MTMD configuration are determined to be the same as those identified when the structure was subjected to white noise. The performance criteria for each additional TMD and the tuning parameter and DOF corresponding to each TMD are shown in Table 2.2

	1 TMD	2 TMDs	3 TMDs	4 TMDs	5 TMDs	6 TMDs	7 TMDs
J_1	1	1	0.999	0.998	0.434	0.402	0.364
J_2	0.999	0.999	0.998	0.997	0.504	0.467	0.415
J_3	0.731	0.642	0.570	0.528	0.523	0.527	0.530
J_4	0.804	0.742	0.693	0.665	0.487	0.483	0.469
J_5	9.537	8.095	8.463	7.004	7.037	7.092	7.158
γ	1	0.88	1.1	0.8	0.98	1.14	0.86
DOF	20	19	18	17	12	15	16

Table 2.2 – Performance criterion and optimal configuration for MTMDs with Kanai-Tajimi PSDF

The reductions in the response are very similar to that given in Table 2.1 for the WTT subjected to base excited white noise. Therefore it can be concluded that the MTMD configuration given in Tables 2.1 and 2.2 can be considered optimal for a wide range of base excitations.

2.5.3 White noise wind excitation

The white noise wind excitation PSDF is now applied to the structure and the process is repeated. Table 2.3 shows the performance criteria for each additional TMD and the tuning parameter and DOF corresponding to each TMD. It is observed that the number and placement of the TMDs are the same as that for the base motion PSDFs however, the values of γ differ slightly. The performance criteria confirm that the achieved reductions in the RMS response are also similar to the base motion cases.

	1 TMD	2 TMDs	3 TMDs	4 TMDs	5 TMDs	6 TMDs	7 TMDs
J_1	0.999	0.999	0.999	0.998	0.462	0.432	0.400
J_2	0.999	0.998	0.998	0.997	0.527	0.493	0.442
J_3	0.730	0.651	0.560	0.528	0.522	0.521	0.520
J_4	0.790	0.732	0.665	0.642	0.493	0.487	0.472
J_5	9.545	7.981	7.082	6.57	6.57	6.571	6.571
γ	1	0.9	1.12	0.82	1	1.18	0.88
DOF	20	19	18	17	12	15	16

Table 2.3 – Performance criterion and optimal configuration for MTMDs with wind excited white noise PSDF

2.5.4 Harris spectrum

The Harris spectrum PSDF is now applied to the structure and the process repeated. Table 2.4 shows the performance criteria for each additional TMD and the tuning parameter and DOF corresponding to each TMD.

	1 TMD	2 TMDs	3 TMDs	4 TMDs	5 TMDs	6 TMDs	7 TMDs
J_1	0.997	0.996	0.995	0.994	0.381	0.341	0.287
J_2	0.981	0.976	0.970	0.968	0.444	0.408	0.346
J_3	0.734	0.648	0.564	0.536	0.536	0.535	0.545
J_4	0.738	0.655	0.573	0.545	0.535	0.535	0.534
J_5	9.523	8.179	7.115	6.846	6.848	6.85	6.852
γ	1	0.88	1.12	0.81	0.99	1.18	0.86
DOF	20	19	18	17	12	14	15

Table 2.4 – Performance criterion and optimal configuration for MTMDs with Harris spectrum PSDF

It is observed that the number and placement of the TMDs are almost the same as those for the base motion PSDFs and the white noise wind excitation PSDF. The only exception is that TMD6 and TMD7 are placed at the 14^{th} and 15^{th} DOF, respectively, as opposed to the 15^{th} and 16^{th} DOFs previously. The values of γ are slightly different to the other 3 PSDFs. It is also observed that greater reductions in the acceleration response of the structure are achieved.

2.5.5 Optimal configuration for ±15% variation in the stiffness

Using the MTMD configurations determined for the four PSDFs considered in the previous sections, the generalised configuration shown in Table 2.5 can be determined. As the Harris spectrum PSDF was the only excitation that led to a different optimal placement of TMDs, the configuration identified for the other 3 PSDFs is adopted for the generalised configuration. The values of γ are determined from the average values of the four PSDFs.

	γ	DOF
TMD1	1	20
TMD2	0.885	19
TMD3	1.11	18
TMD3	0.81	17
TMD4	0.99	12
TMD5	1.16	15
TMD6	0.865	16

Table 2.5 – Generalised configuration for MTMDs in a WTT

When this generalised configuration is applied, and the structure is subjected to each of the four PSDFs, the performance criteria shown in Table 2.6 are obtained. It is observed that the reductions in response are almost the same as those obtained in Tables 2.1-2.4 for 7 TMDs, i.e. the MTMD configuration for the WTT subjected to each PSDF. Therefore it can be concluded that this optimum configuration for MTMDs can be considered for a wide range of base motion and wind loading PSDFs.

	Base Excited White Noise	**Kanai-Tajimi**	**Wind Excited White Noise**	**Harris Spectrum**
J_1	0.399	0.364	0.400	0.288
J_2	0.440	0.415	0.442	0.347
J_3	0.531	0.531	0.524	0.533
J_4	0.476	0.470	0.476	0.532
J_5	7.258	7.167	6.698	6.670

Table 2.6 – Performance criteria for WTT with MTMD optimum configuration for different PSDFs

To assess the robustness of the MTMD control system, the generalised configuration is now applied to the WTT with a ±15% variation in stiffness uncertainty. The resulting performance criteria comparing the WTT response to that of the uncontrolled structure (with 0% variation in the stiffness) are shown in Table 2.7.

+15% variation in the stiffness				
	Base Excited White Noise	**Kanai-Tajimi**	**Wind Excited White Noise**	**Harris Spectrum**
J_1	0.452	0.416	0.465	0.353
J_2	0.513	0.483	0.530	0.426
J_3	0.594	0.601	0.639	0.598
J_4	0.532	0.531	0.580	0.596
J_5	6.926	6.977	6.328	5.925
-15% variation in the stiffness				
	Base Excited White Noise	**Kanai-Tajimi**	**Wind Excited White Noise**	**Harris Spectrum**
J_1	0.449	0.436	0.430	0.405
J_2	0.511	0.504	0.489	0.463
J_3	0.791	0.781	0.673	0.748
J_4	0.731	0.720	0.633	0.747
J_5	8.986	8.856	7.691	8.460

Table 2.7 – Performance criterion for WTT with MTMD optimum configuration, with ±15% variation in the stiffness

It is observed in Table 2.7 that the reduction in the response of the WTT with ±15% variation in the stiffness is not as great as that achieved when there is no variation in the stiffness, with an increase in the performance measures of 10-34%. When the stiffness of the structure changes, the TMD is no longer optimally tuned, and the response reduction is not as great. Active and semi-active TMDs are known to alleviate this problem as for these types of TMD, the properties of the TMD change when the properties of the structure change.

2.6 CONCLUSION

A procedure for identifying the optimal number, location and tuning parameters for MTMDs placed in a WTT has been described. The procedure was investigated for both base and wind excitations. A CI based on the RMS displacement and acceleration response was defined and the optimum configuration of MTMDs in the

WTT for each excitation was determined. A generalised configuration for the number, placement and tuning parameters of the MTMDs was subsequently obtained. In order to determine the robustness of the design, the MTMD configuration was applied to a WTT with ±15% variation in the stiffness. It was observed that the response reduction was still high, but not as great as that when there was no variation in the stiffness. Active and semi-active TMDs may be used to alleviate this problem, as the mechanical properties of these type of TMDs can be varied as the properties of the structure change. The investigation of this topic is investigated in the following chapters.

CHAPTER 3

CONTROL STRATEGY USING BANG-BANG AND MINIMAX PRINCIPLE FOR FRF WITH ATMDS

3.1 INTRODUCTION

It was seen in Chapter 2 how MTMDs are effective in reducing the vibration response in a structure. Another approach is to provide an active external power source to the TMD to produce additional response reduction. By introducing an ATMD in a structure, the number of TMDs can be reduced, achieving similar results. A control strategy for vibration control of structures using ATMDs is proposed. The control scheme involves a combination of the use of the principle of minimizing the maximum value of the FRF for a coupled structure-ATMD system and controlling the response of the structure using bang-bang control with a control force applied to the TMD.

3.2 MINIMAX PRINCIPLE

The minimax principle of shaping the FRF has been used conventionally for optimal design of passive vibration absorbers, initially proposed by Den Hartog (1956), and is effective in vibration suppression for broad banded excitations or non-resonant excitations. For the control scheme, a control law using bang-bang control is obtained by minimising the time derivative of a Lyapunov function of the open-loop structural system (Wu and Soong, 1998). This law is used to control the ATMD, which bypasses the normal requirement of applying a force to the structure directly, e.g. by reaction against a bracing system, which may not be feasible in some cases due to physical constraints. When no control force is applied, tuning the TMD reshapes the corresponding FRF for the coupled structure-TMD system, such that the magnitudes of the peaks in the FRF of the structure are equal. When the active control is ineffective or is turned off, the damper system acts as a passive TMD, tuned using the minimax principle. If the structure is modeled as a SDOF system, the coupled structure-ATMD (a 2 degree of freedom (DOF) system) will have two peaks in the FRF. For a MDOF structure, the fundamental mode is considered and the equations

of motion relating to the fundamental mode and the equations of motion for the coupled TMD are determined.

3.3 BANG-BANG CONTROL STRATEGY

3.3.1 SDOF structure-ATMD system

A structure modelled by a SDOF system is considered. An ATMD is connected to the SDOF system as shown in Fig (3.1).

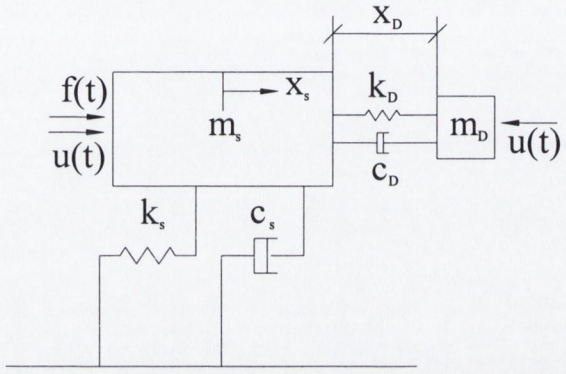

Figure 3.1 – SDOF system with ATMD

A control force is applied to the ATMD. Since the controller is placed on the structure, there will be a reaction force on the structure. The equations of motion of the coupled system are

$$m_s\ddot{x}_s(t)+c_s\dot{x}_s(t)+k_s x_s(t)-c_d\dot{x}_d(t)-k_d x_d(t)=f(t)-u(t) \tag{3.1}$$

$$m_d(\ddot{x}_s(t)+\ddot{x}_d(t))+c_d\dot{x}_d(t)+k_d x_d(t)=u(t) \tag{3.2}$$

where m_s, c_s and k_s are the mass, damping and stiffness of the structure, respectively and m_d, c_d and k_d are the mass, damping and stiffness of the ATMD, respectively. The excitation force applied to the structure and the control force applied to the ATMD (with a reaction on the structure) are represented by *f(t)* and *u(t)* respectively. The displacement of the structure and that of the ATMD with respect to the structure are

denoted by x_s and x_d respectively. On normalizing Eq (3.1) with m_s and Eq (3.2) with m_d, respectively, the following equations are obtained

$$\ddot{x}_s(t) + 2\zeta_n\omega_n\dot{x}_s(t) + \omega_n^2 x_s(t) - 2\zeta_d\omega_d\alpha\dot{x}_d(t) - \omega_d^2\alpha x_d(t) = \frac{f(t)}{m_s} - \alpha\Delta_d(t) \tag{3.3}$$

$$\ddot{x}_s(t) + \ddot{x}_d(t) + 2\zeta_d\omega_d\dot{x}_d(t) + \omega_d^2 x_d(t) = \Delta_d(t) \tag{3.4}$$

In Eqs (3.3) and (3.4), ω_n, ζ_n are the natural frequency and the damping ratio of the structure respectively; ω_d, ζ_d are the natural frequency and the damping ratio of the TMD respectively; the mass ratio is given by

$$\alpha = \frac{m_d}{m_s} \tag{3.5}$$

and the control acceleration is expressed as

$$\Delta_d(t) = \frac{u(t)}{m_d} \tag{3.6}$$

The equations of motion for the coupled structure-ATMD system can be written in the state space as follows

$$\{\dot{\hat{x}}(t)\} = [A]\{\hat{x}(t)\} + [B]\Delta_d(t) + [E]f(t) \tag{3.7}$$

where $\hat{x}(t)$ is the state vector defined by

$$\{\hat{x}(t)\} = \{x_s(t) \quad x_d(t) \quad \dot{x}_s(t) \quad \dot{x}_d(t)\}^T \tag{3.8}$$

and [A], [B] and [E] are given by

$$[A]=\begin{bmatrix} 0 & 0 & 1 & 0 \\ 0 & 0 & 0 & 1 \\ -\omega_n^2 & \omega_d^2\alpha & -2\zeta_n\omega_n & 2\zeta_d\omega_d\alpha \\ \omega_n^2 & -\omega_d^2(\alpha+1) & 2\zeta_n\omega_n & -2\zeta_d\omega_d(\alpha+1) \end{bmatrix} \tag{3.9}$$

$$[B]=\begin{bmatrix} 0 & 0 & \alpha & -(\alpha+1) \end{bmatrix}^T \tag{3.10}$$

$$[E]=\begin{bmatrix} 0 & 0 & 1/m_s & -1/m_s \end{bmatrix} \tag{3.11}$$

The control force *u(t)* is constrained in magnitude by the following condition

$$|u(t)| \leq u_{max} \tag{3.12}$$

The performance measure for the time-optimal (sub-optimal (Wu and Soong, 1996)) control for the bang-bang control law is simplified as

$$J(u)=\frac{1}{2}\int_o^{t_f}[\hat{x}^T(t)Q\hat{x}(t)]dt \tag{3.13}$$

where Q is the weighting matrix of the system. Hence, the problem can be defined as one that determines the control *u(t)*, satisfying the constraint given in Eq (3.12) that drives the initial state $x(t=0)=x_0$ to the target set *S(t)* and minimises the performance measure *J(u)*. According to the Pontryagin maximum principle (Meirovitch, 1995; Wu and Soong, 1996), the optimal control effort can be derived as

$$u(t) = -u_{\max}\,\mathrm{sgn}[B^T\lambda(t)] \tag{3.14}$$

where $\lambda(t)$ is the costate vector. The costate vector can be obtained by solving the first order differentiation equation

$$\dot{\lambda}(t)=-A^T\lambda(t)-Q\hat{x}(t) \tag{3.15}$$

However, this leads to the problem of on-line evaluation of the differential equation, which may increase the time-delay and lead to instability in the structural system. In order to overcome this problem, a sub-optimal bang-bang control law is introduced. This is derived by minimising the time derivative of a Lyapunov function of the open-loop structural system (Wu and Soong, 1996). A quadratic function of the state variable is defined as

$$V(\hat{x}) = \hat{x}^T S\hat{x} \tag{3.16}$$

where the matrix S is a positive semidefinite matrix and is a solution of the Lyapunov matrix equation

$$A^T S + SA = -Q \tag{3.17}$$

The time derivative of Eq (3.16) is

$$\dot{V}(\hat{x}) = -\hat{x}^T Q\hat{x} + 2uB^T S\hat{x} \tag{3.18}$$

Therefore, if the control force takes the form

$$u(t) = -u_{max}\, sgn[B^T S\hat{x}(t)] \tag{3.19}$$

$\dot{V}(\hat{x})$ will be a minimum. If a matrix S, which is a symmetric, square matrix, is assumed (leading to a positive semi-definite matrix) such that

$$S = \begin{bmatrix} \hat{S} & 0 & \dots & 0 \\ 0 & \hat{S} & \dots & 0 \\ . & . & \dots & . \\ 0 & 0 & 0 & \hat{S} \end{bmatrix} \tag{3.20}$$

then, for the coupled structure-TMD system considered, the value of $\hat{S}$ is given by

$$\hat{S}(t) = \frac{\ddot{x}_s(t)}{\alpha(\dot{x}_s(t) - \dot{x}_d(t)) - \dot{x}_d(t)} \tag{3.21}$$

Substituting Eqs (3.9), (3.20) and (3.21) into Eq (3.17), the matrix Q is found to be

$$Q = \hat{S}\begin{bmatrix} 0 & 0 & \omega_n^2 - 1 & -\omega_n^2 \\ 0 & 0 & -\omega_d^2\alpha & \omega_d^2(1+\alpha) - 1 \\ \omega_n^2 - 1 & -\omega_d^2\alpha & 4\zeta_n\omega_n & -2\zeta_d\omega_d\alpha - 2\zeta_n\omega_n \\ -\omega_n^2 & \omega_d^2(1+\alpha) - 1 & -2\zeta_d\omega_d\alpha - 2\zeta_n\omega_n & 4\zeta_d\omega_d(\alpha+1) \end{bmatrix} \tag{3.22}$$

The determinant of Q is calculated as

$$det(Q) = \frac{\ddot{x}_s^4(\omega_n^2(1-\omega_d^2) + \omega_d^2(1+\alpha) - 1)^2}{(\alpha(\dot{x}_d - \dot{x}_1) + \dot{x}_d)^4} > 0 \tag{3.23}$$

which implies Q is a positive semi-definite matrix. Hence there exists a matrix Q such that, the control acceleration $\Delta_d(t)$ is now determined based on the following condition

$$\begin{aligned} \Delta_d(t) &= -\eta\ddot{x}_{max}\, sgn(\ddot{x}_s), |\ddot{x}_s| \geq \ddot{x}_{max} \\ &= 0, otherwise \end{aligned} \tag{3.24}$$

where $\ddot{x}_{max}$ is the maximum control acceleration and $\eta > 0$ is a non-negative scalar, leading to a maximum control force, $u_{max} = m_d\eta\ddot{x}_{max}$. The values of $\ddot{x}_{max}$ and the scalar η can be chosen depending on the constraint on the control effort to be provided. Figure 3.2 shows an example of the applied bang-bang control law for harmonic response. It is observed that the control effort is of a typical bang-bang type with the control acceleration, $\Delta_d(t)$ switching from one extreme value to the other when $\ddot{x}_s$ (represented by the harmonic acceleration in Figure 3.2), changes sign.

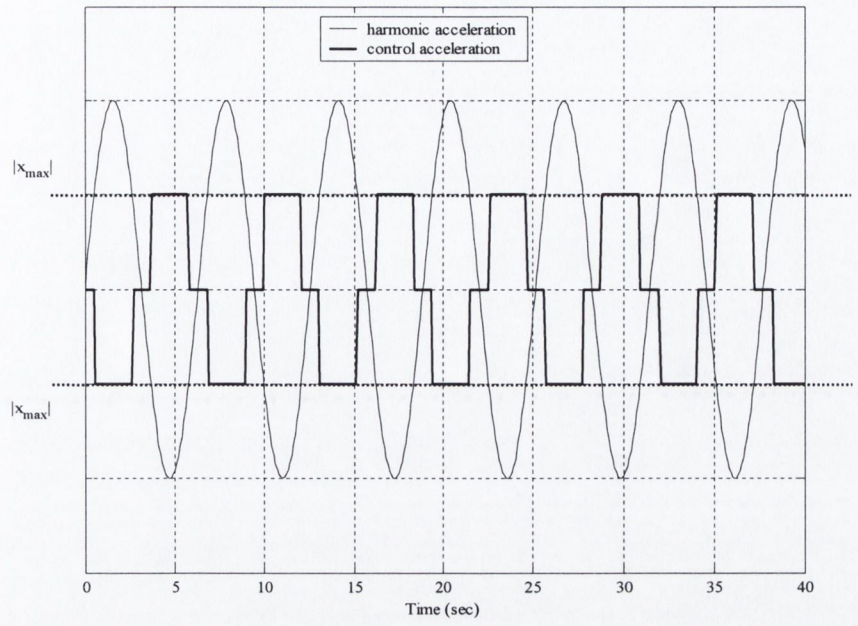

Figure 3.2 – Example of bang-bang control law for harmonic excitation

3.3.2 MDOF structure-ATMD system

A MDOF structure, having n degrees of freedom is now considered, with a TMD connected to the structure and a control force applied to the TMD. The sub optimal bang-bang control law, obtained in section 3.3.1 is applied to this MDOF-TMD structure. As the fundamental mode of vibration is likely to contribute most to the vibration response, this mode is considered in the control scheme. The first modal equation of motion of the system (with the TMD tuned to the fundamental mode) and the modal equation of motion of the TMD are given by

$$\ddot{v}_1 + 2\zeta_n \omega_{n1} \dot{v}_1 + \omega_{n1}^2 v_1 - 2\zeta_d \omega_{n1} \alpha \gamma^{1/2} \dot{v}_d - \omega_{n1}^2 \alpha \gamma v_d = -\bar{u}(t) + \bar{f}(t) \qquad (3.25)$$

$$\ddot{v}_1 + \ddot{v}_d + 2\zeta_d \omega_{n1} \gamma^{1/2} \dot{v}_d + \omega_{n1}^2 \gamma v_d = \bar{u}(t) \qquad (3.26)$$

where $\bar{f}(t)$ and $\bar{u}(t)$ are now the modal excitation force and the modal control force, respectively. The modal displacement v_j is a function of the actual displacement such that

$$\begin{aligned} x_1 &= \phi_{11}v_1 + \phi_{12}v_2 + \ldots + \phi_{1j}v_j \\ x_2 &= \phi_{21}v_1 + \phi_{22}v_2 + \ldots + \phi_{2j}v_j \\ &\cdot \\ x_i &= \phi_{i1}v_1 + \phi_{i2}v_2 + \ldots + \phi_{ij}v_j \end{aligned} \tag{3.27}$$

where, ϕ_{ij} is the i^{th} component of the j^{th} mode shape, γ is the tuning parameter of the TMD and α (mass ratio) is the ratio of the total mass of the damper, m_d to the mass of the structure, m_t, i.e.

$$\alpha = \frac{m_d}{m_t} \tag{3.28}$$

As only the fundamental mode is considered

$$x_1 = \phi_{11}v_1 \tag{3.29}$$

Assuming that the first mode shape is maximum at the top of the structure and normalised such that $\phi_{11} = 1$, then the vibration response in the first mode can be expressed in terms of the response at the top of the structure. The control law given in Eq (3.24) can then be applied to a MDOF system, where the fundamental mode is considered for the control scheme.

3.4 SHAPING OF FRF

The bang-bang control law is employed to determine the control force to be applied to the coupled structure-ATMD system. However, depending on the excitation applied to the structure, this active force may not always be necessary. In these cases, the TMD can be tuned so that the system response is reduced using passive control. This is achieved by shaping the FRF of the system. To shape the FRF, the TMD is tuned such that

$$k_d = \gamma\omega_n^2 m_d \tag{3.30}$$

where γ is the tuning parameter of the TMD. The natural frequency of the damper, ω_d is related to ω_n by

$$\omega_d^2 = \gamma\omega_n^2 \tag{3.31}$$

and the equations of motion for a SDOF system without control are given by

$$\ddot{x}_s(t) + 2\zeta_n\omega_n\dot{x}_s(t) + \omega_n^2 x_s(t) - 2\zeta_n\omega_n\alpha\gamma^{1/2}\dot{x}_d(t) - \omega_n^2\alpha\gamma x_d(t) = \frac{f(t)}{m_s} \tag{3.32}$$

$$\ddot{x}_s(t) + \ddot{x}_d(t) + 2\zeta_n\omega_n\gamma^{1/2}\dot{x}_d(t) + \omega_n^2\gamma x_d(t) = 0 \tag{3.33}$$

The FRF of the coupled equations will have two peaks. Figure 3.3 shows a plot of the amplitude, R, of the response of a coupled structure TMD system, against the frequency ratio, β. The system with a mass ratio, α equal to 0.5, tuning parameter, γ equal to 1 and various values of damping, ζ_a, in the TMD are illustrated (Den Hartog, 1956). It is observed in Figure 3.3 that without damping, two infinite peaks of the FRF are obtained. With infinite damping, these two peaks are fused to each other, resulting in a SDOF system and the amplitude is again infinite. Therefore, there must be some level of damping in between these two extreme points, where the peak becomes a minimum. It is interesting to note that all four curves in Figure 3.3 intersect at two points, P and Q independent of damping. Therefore, if the locations of these two peaks P and Q are known, by varying the tuning parameter in the TMD, the magnitude of the peaks could be adjusted so that they are equal, as illustrated in Figure 3.4. This leads to an optimum value of the tuning parameter. Also, if the value of damping in the TMD is varied so that curve is adjusted to pass with a horizontal tangent through one of the peaks (it does not matter which), optimal damping in the structure is obtained. For this study, only optimal tuning is considered for a given value of damping.

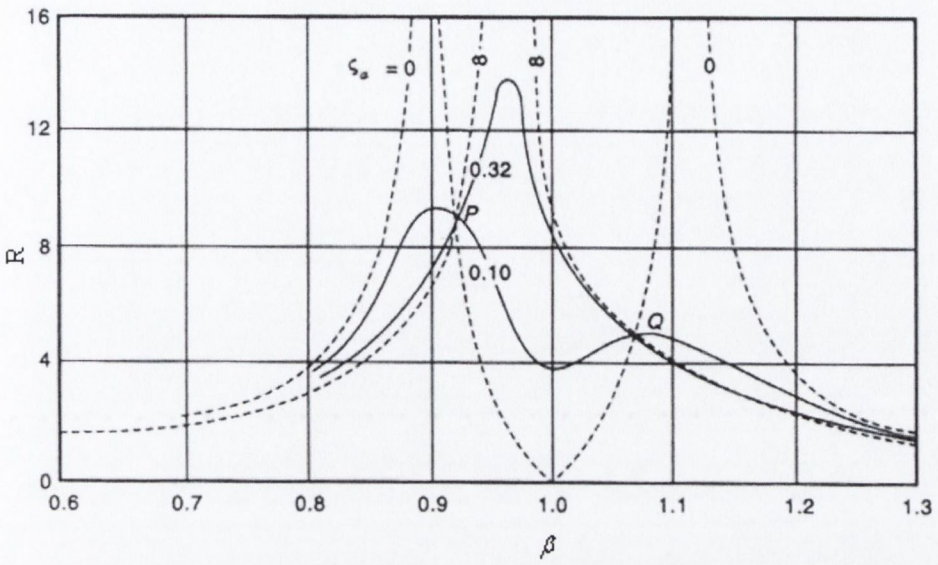

Figure 3.3 – FRF dependent on damping

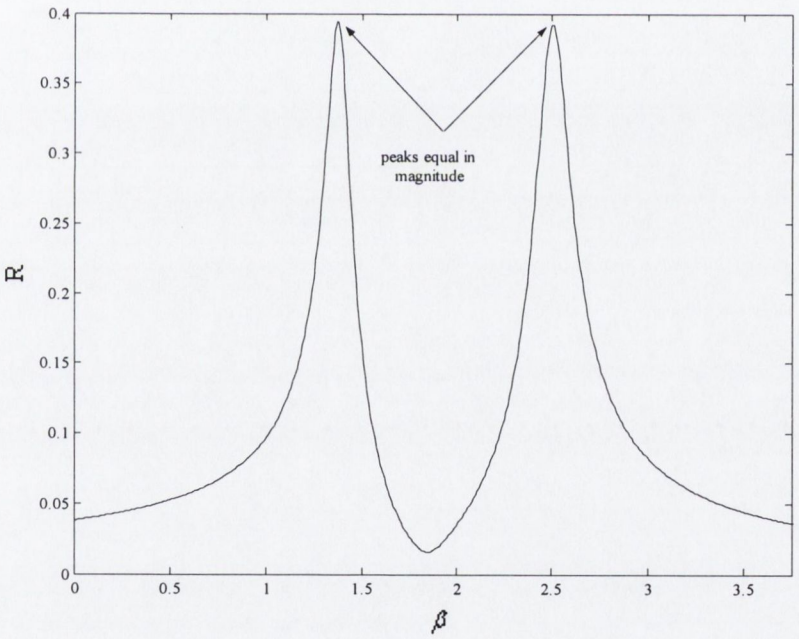

Figure 3.4 – FRF with peaks of equal magnitude

Based on Den Hartog (1956), the tuning parameter γ is characterised such that the maxima of the FRF of the displacement are minimum, leading to a minimax principle of optimisation where

$$\gamma = \left(\frac{1}{1+\alpha} \right)^2 \tag{3.34}$$

As the tuning parameter changes, the two peaks of the FRF are shaped, such that one peak moves up and the other moves down. When γ is obtained using Eq (3.34), the two peaks will be equal. For a MDOF system, the TMD is tuned to the fundamental mode of the structure. Using the modal equations given in Eqs (3.25) and (3.26), and following the method given by Den Hartog (1956) to obtain the tuning parameter for a two DOF system, using the minimax principle, the expression derived in Eq (3.34) is again obtained.

3.5 NUMERICAL EXAMPLE

3.5.1 SDOF-ATMD model subjected to harmonic excitations

A SDOF system with an ATMD is examined. The natural frequency of the SDOF system is assumed to be 5.7Hz (35.85 rad/sec). A TMD with mass, m_d, equal to 2% of the mass of the structural system is added to the structure. As mentioned in Section 3.4, optimal damping of the TMD is not considered, however, in order to avoid an infinite response, a nominal value for the damping ratio of the TMD is taken as 1%. By applying the Fourier transform to Eqs (3.32) and (3.33), the displacement FRF shown in Figure 3.5 is obtained. The minimax principle is applied to the passive structure-TMD system and the displacement FRF of the structure is shaped numerically so that the two peaks are equal in magnitude, as shown in Figure 3.6. This occurs at $\gamma = 0.96$, the value suggested by Eq (3.34).

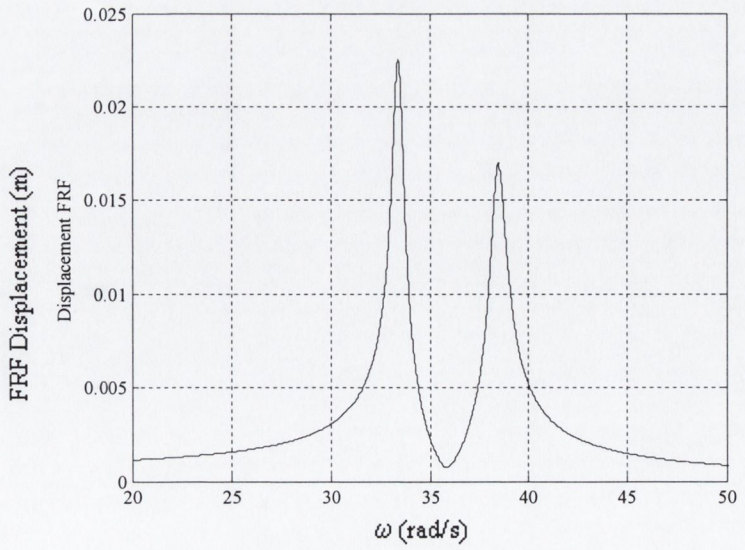

Figure 3.5 – FRF of SDOF system with TMD, $\gamma = 1$, $\eta = 0$

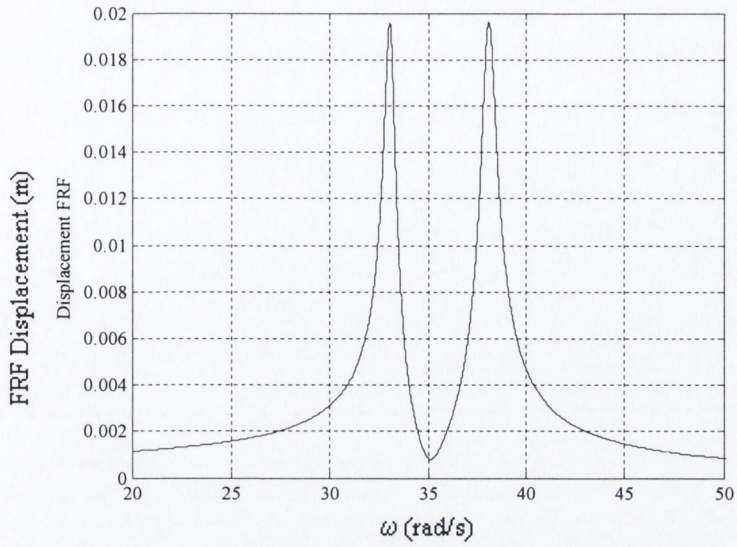

Figure 3.6 – FRF of SDOF system with TMD, $\gamma = 0.96$, $\eta = 0$

If a harmonic excitation with a frequency equal to the natural frequency of the structure is applied, the presence of the TMD will limit the response, and no control force need be applied to the TMD. However, the frequency of a non-resonant excitation may match that of a peak in the transfer function of the response of the coupled structure-ATMD system. In Figure 3.6, this occurs at $\omega = 33.04$rad/s. The control law is now applied to the TMD when the response of the coupled SDOF-TMD structure exceeds 0.3m/s^2. For increasing values of η, Table 3.1 presents the coupled structure-ATMD system steady state response, the control accelerations and the control force for an excitation with amplitude 1 m/s^2 at a frequency of 33.04rad/s and assuming the mass of the structure, $m_s = 1$kg.

It is clear from the first two rows of Table 3.1 that the addition of the TMD without control causes the response of the structure to increase considerably. However, when the control force is applied to the TMD, in accordance with the control law obtained from Eq (3.24), the response reduces, and greater reductions are observed with stronger control forces (i.e. higher values of η). It is also observed that the response reduces slowly with initial increases in values of η. As η increases there is a dramatic reduction between the values, 10 and 15. If values of η beyond 17 are applied to the system, the response begins to increase. Therefore, there is a definite range of control values with which the control force takes effect, and exceeding this range has an adverse effect on the structure. The addition of the TMD causes the response of the

structure to increase by 384%. With the addition of control, for a value of Δ_d = 5.1m/s^2, the response of the coupled structure-TMD system is now reduced by 53% compared to the structure without any TMD.

η	γ	x(mm)	$\ddot{x}$ (m/s^2)	Δ_d(m/s^2)	$u(t)$ (kN)
0	0	5.08	5.6	0	0
0	**0.96**	**19.5**	**21.2**	**0**	**0**
1	0.96	19.4	21	0.3	0.006
2	0.96	19.15	20.7	0.6	0.012
3	0.96	18.8	21.4	0.9	0.9
4	0.96	18.5	19.75	1.2	0.018
5	0.96	18	19.5	1.5	0.03
7.5	0.96	16.6	18	2.25	0.045
10	0.96	14.6	15.8	3	0.06
15	0.96	7.8	8.4	4.5	0.09
16.5	0.96	4.7	4.3	4.95	0.099
17	0.96	2.4	2.6	5.1	0.102

Table 3.1 – Response of coupled structure-ATMD system at non-resonant frequency, ω = 33.04 rad/s, with bang-bang control and FRF shaping

To compare the value of the control force required for the proposed system with that required to be directly applied to a SDOF structure without any TMD, the bang-bang control law, given in Eq (3.24) is applied to a SDOF system without a TMD. For the coupled structure-ATMD system the peak response of the system is observed when the frequency of a non-resonant excitation matches the frequency at which a peak occurs for the transfer function of the response of the coupled structure-TMD system. For the SDOF structure without TMD, the peak response of the system is observed when the excitation frequency matches the natural frequency of the structure. To ensure consistency, two equivalent cases are compared by evaluating the responses of both systems to harmonic loading at their respective resonant frequencies.

Table 3.2 shows the value of the steady state responses of the system, the control acceleration and the control force for increasing values of η, due to a harmonic excitation of amplitude 1m/s^2 and frequency of 35.85rad/s, assuming the mass of the structure, m_s = 1kg. The values of Δ_d given in Table 3.1 for the coupled structure-ATMD system are approximately 5 times the value of Δ_s given in Table 3.2 for the

SDOF system without a TMD. However, as Δ_d is the ratio of the control force to the mass of the TMD, which is only 2% of the mass of the structural system, the control force required for the coupled structure-ATMD system given in Table 3.1 is 90% less than that required for the SDOF system without a TMD given in Table 3.2. This would clearly have substantial benefits when considering the practical feasibility of control strategy implementation.

η	x(mm)	$\ddot{x}$ (m/s^2)	Δ_s (m/s^2)	$u(t)$ (kN)
0	38.9	49.4	0	0
0.5	36.6	46.6	0.16	0.16
1	32.8	41.8	0.33	0.33
1.5	26.8	34.7	0.49	0.49
2	17.6	22.3	0.65	0.65
2.5	3	4.3	0.82	0.82
3	2.1	2.9	0.98	0.98

Table 3.2 – Response of SDOF system at resonant frequency, ω = 35.85rad/s, with bang-bang control and FRF shaping

Also, from an implementation perspective, the application of active control forces to structural systems normally requires provision for the associated reaction force, such as through bracing or other stiff elements. However, it may be difficult to provide such bracing systems in some structures (for example a wind turbine tower or a chimney). In this case, the application of the control force to the TMD, with reaction against the structure itself offers a clear advantage.

3.5.2 Comparison with LQC-FRF shaping

The performance of bang-bang control with minimax shaping of the FRF is evaluated through comparison with that of another conventional method, the LQC with minimax shaping of the FRF. This method is defined by designing a control input that drives the system from some initial state to a constant final state (Meirovitch, 1995). The method is based on feedback control

$$\Delta_d = -G\hat{x}(t) \tag{3.35}$$

where G is the gain matrix which is obtained by solving the Riccati equation (Meirovitch, 1995). Substituting Eq (3.35) into Eq (3.7) yields the following

$$\{\dot{\hat{x}}(t)\} = [A - BG]\{\hat{x}(t)\} + [E]f(t) \tag{3.36}$$

For comparison with the bang-bang method performance indicated in Table 3.1, with [A], [B] and [E] as defined in Eqs (3.9) to (3.11), a harmonic excitation of ω = 33.04rad/s is applied to the structure and the control force imposed. The value of the gain matrix [G] is calculated for increasing values of Δ_d, until additional increases have only a marginal effect on the response of the structure. This is similar to applying increasing values of η in the bang-bang control system with FRF shaping.

γ	x(mm)	$\ddot{x}$ (m/s^2)	Δ_d (m/s^2)	$u(t)$ (kN)
0	5.1	5.6	0	0
0.96	**19.4**	**21.1**	**0**	**0**
0.96	11.2	11.9	2	0.04
0.96	8.8	9.6	3	0.06
0.96	7.6	8.2	4	0.08
0.96	6.9	7.6	5	0.1
0.96	6.5	7.2	6	0.12
0.96	6.3	6.9	7	0.14
0.96	6.1	6.8	8	0.16
0.96	6	6.7	9	0.18
0.96	6	6.7	10	0.2

Table 3.3 – Response of coupled structure-ATMD system at non-resonant frequency, ω = 33.04 rad/s, with LQC and FRF shaping

Table 3.3 shows the response of the structure with increasing values of $\Delta_d/u(t)$ for an excitation of amplitude 1m/s^2 at a frequency of 33.04rad/s and assuming the mass of the structure, m_s = 1kg. As seen from the first two rows of Table 3.3 and also in Table 3.2, the addition of the ATMD increases the response of the structure by 384%. With the addition of the LQC and minimax shaping of the FRF, the response of the structure is reduced by 120%, compared to the structure without any TMD, but additional increases in Δ_d beyond 9m/s^2 does not reduce the response any further. The observed response reduction is much less than that achieved using bang-bang control and minimax shaping of the FRF. Also, the value of $u(t)$ required using the LQC with

minimax shaping of the FRF is twice that required for bang-bang control with FRF shaping.

3.5.3 Random excitation

A coupled structure SDOF-TMD structure, with a low natural frequency, is now considered. A random excitation generated from the Davenport wind spectrum with a predominant energy at the resonant frequency of the structure is applied to the system. The Fourier spectrum and the acceleration time history of the excitation are shown in Figures 3.7 and 3.8 respectively. Figure 3.9 compares the response of the structure with and without a TMD. The provision of a TMD reduces the peak displacement response from 0.916m to 0.457m. This represents a considerable response reduction and the application of a control force is not required.

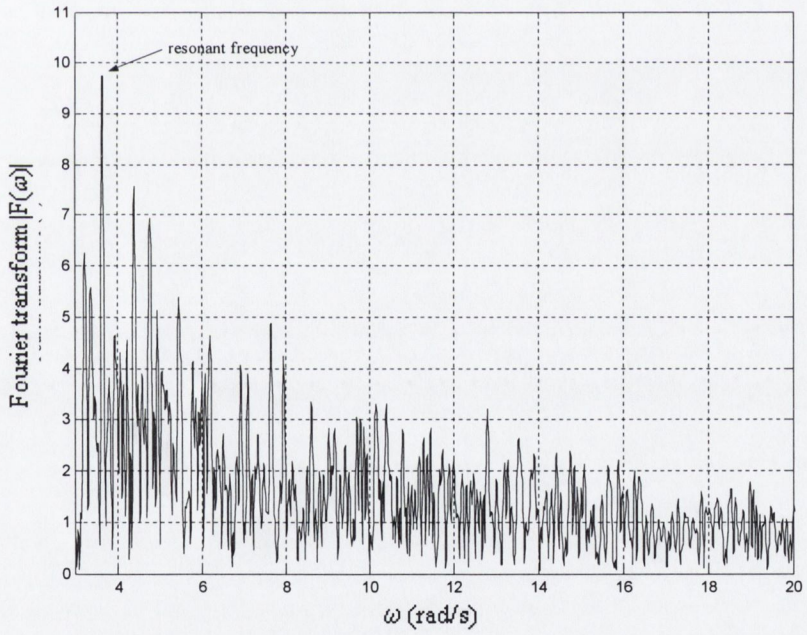

Figure 3.7 – Fourier transform of wind excitation close to the resonant frequency of a SDOF structural system with a low natural frequency

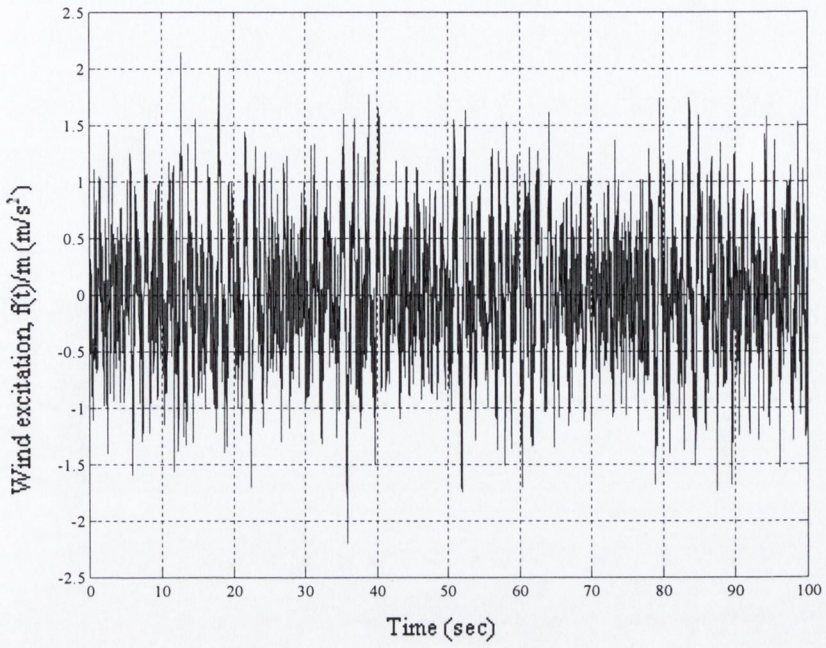

Figure 3.8 – Wind excitation close to the natural frequency of a SDOF structural system with a low natural frequency

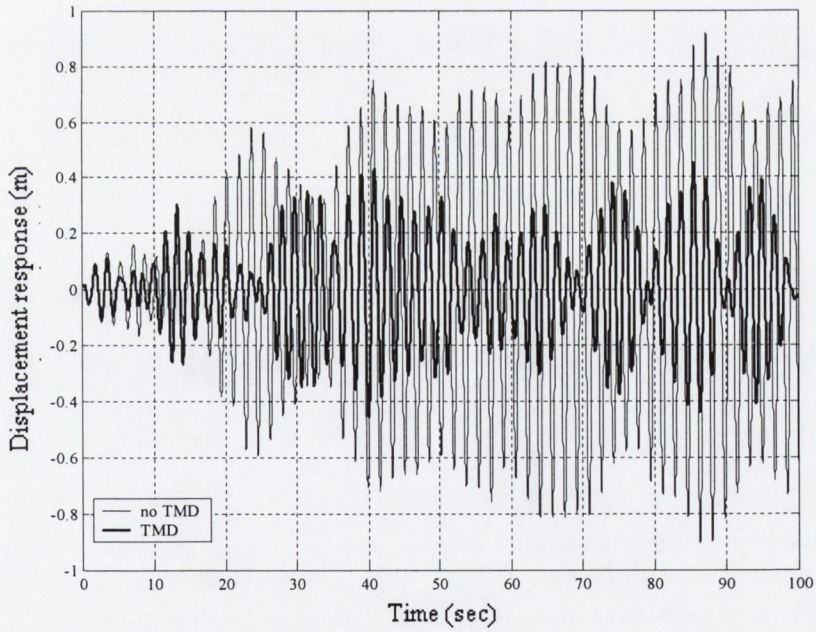

Figure 3.9 – Response of low frequency SDOF structure with and without TMD, under random wind excitation (loading spectrum peak close to resonant frequency of structure)

Different behavior is observed with an excitation with dominant frequency equal to that at which a peak occurs in the transfer function of the response of the coupled structure-TMD system. The Fourier spectrum and the acceleration time history of the

excitation are shown in Figures 3.10 and 3.11 respectively. It is shown in Figure 3.12 that the addition of the TMD increases the peak displacement response of the structure from 0.508m (without any TMD) to 0.740m. However, Figure 3.13 shows that when bang-bang control with minimax shaping of the FRF is applied to the TMD, the peak displacement response of the structure is reduced to 0.47m. The history of the control force is given in Fig 3.14, where Δ_d = 1.675m/s^2. These results show that the proposed control strategy can be used to achieve consistent response limits for all loading frequencies.

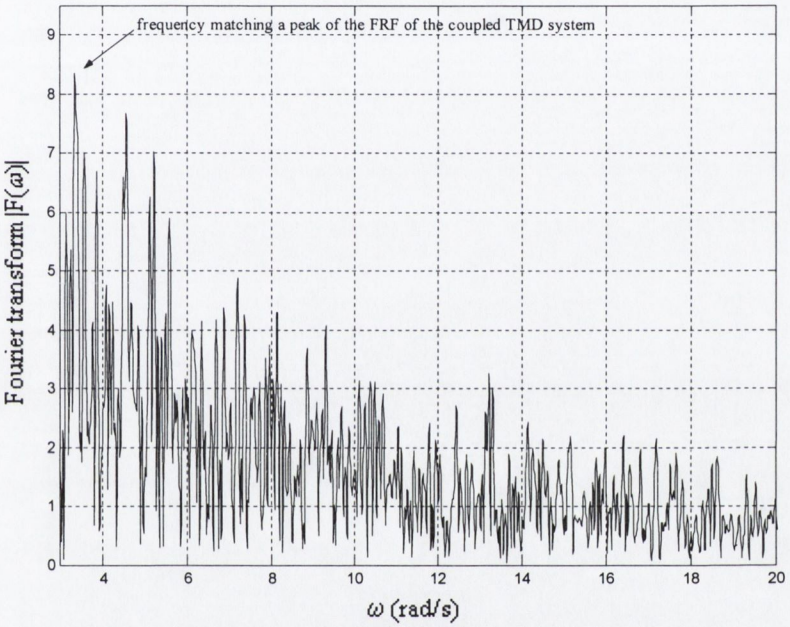

Figure 3.10 – Fourier transform of wind excitation with frequency close to the frequency matching a peak of the FRF of SDOF structure-TMD system with a low natural frequency

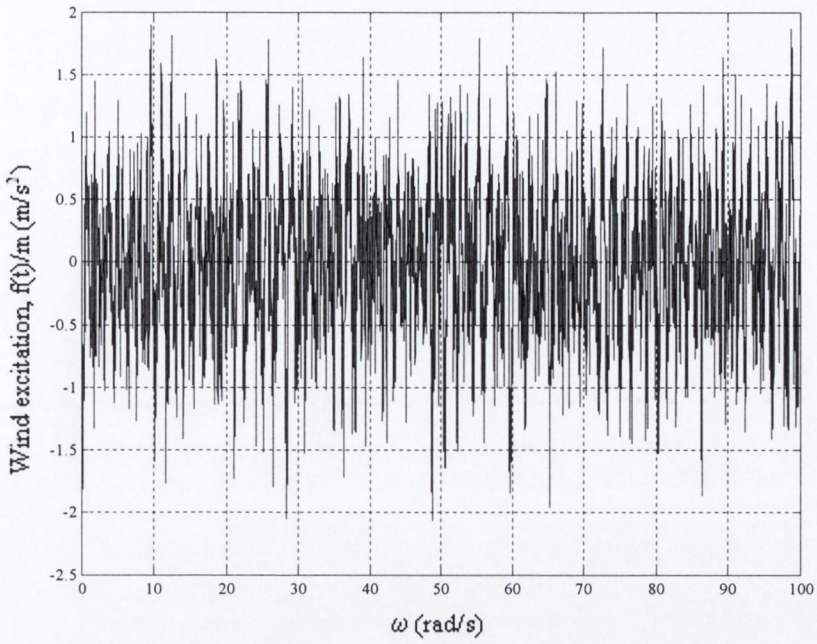

Figure 3.11 – Wind excitation with frequency close to the frequency matching a peak of the FRF of SDOF structure-TMD system with a low natural frequency

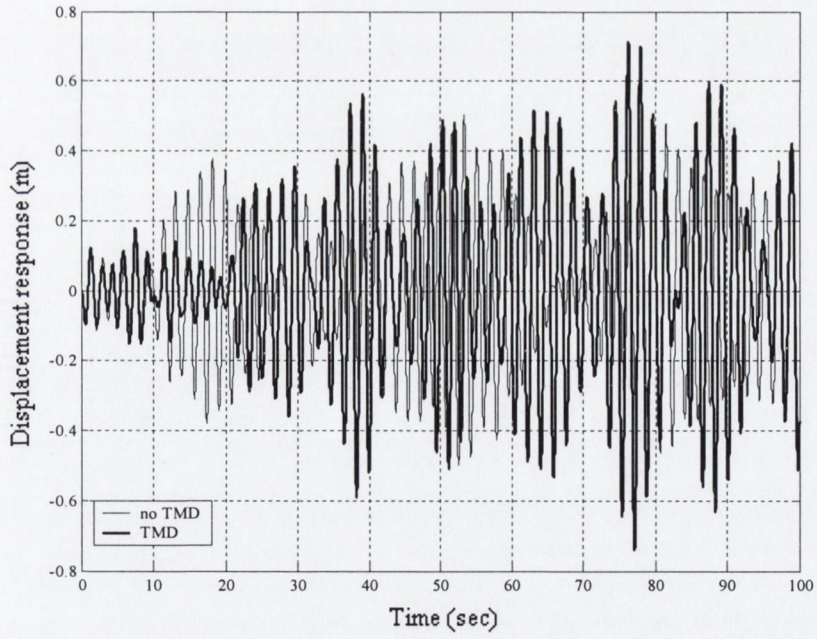

Figure 3.12 – Response of low frequency SDOF structure with and without TMD, under random wind excitation (loading spectrum peak close to resonant frequency of coupled structure-TMD system)

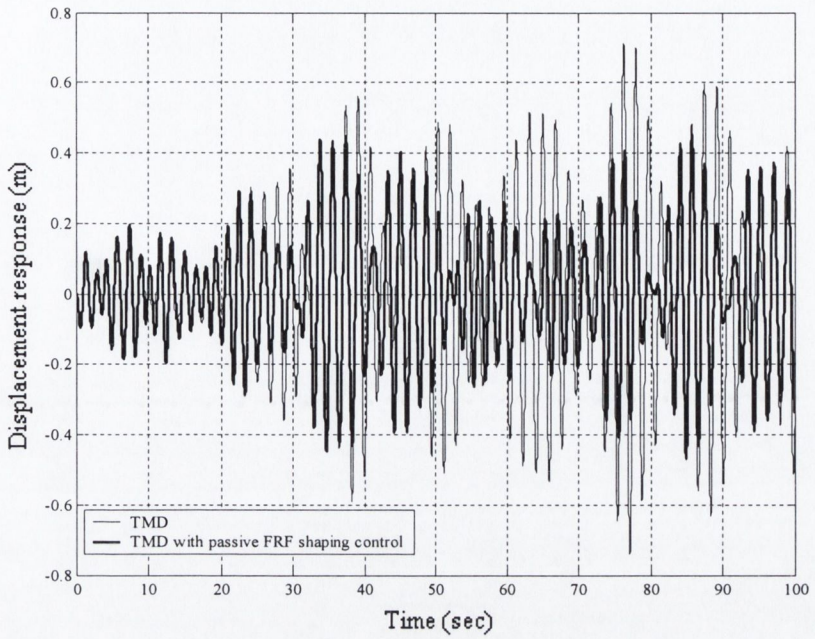

Figure 3.13 – Response of the structure with TMD and passive FRF control strategy, under random wind excitation (loading spectrum peak close to resonant frequency of coupled structure-TMD system)

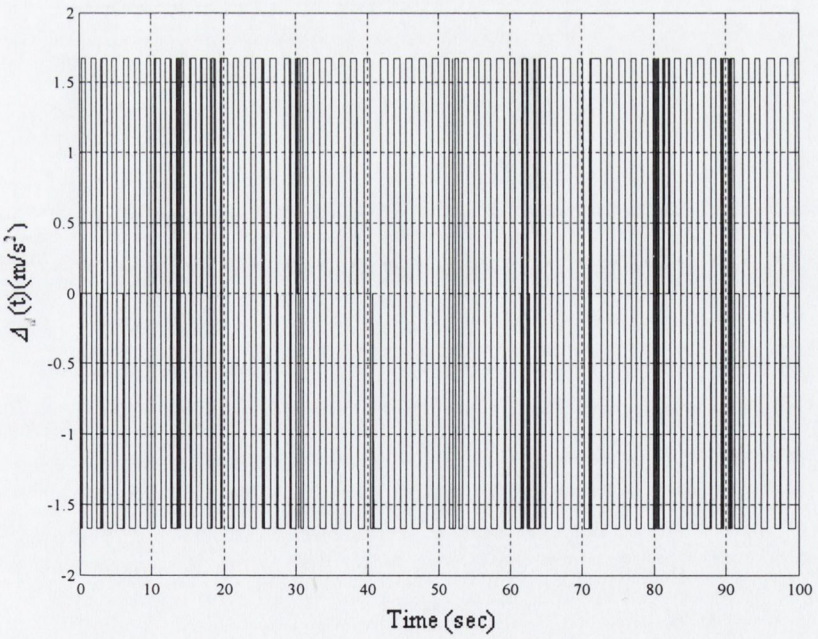

Figure 3.14 – Profile of the bang-bang control acceleration, applied to the TMD with passive FRF shaping, (loading spectrum peak close to resonant frequency of coupled structure-TMD system)

3.6 APPLICATION TO 76-STOREY BENCHMARK PROBLEM

3.6.1 Analytical model

In this section, the control scheme for a MDOF structure developed in Section 3.3.2 is applied to the 76-storey benchmark problem proposed by Yang et el. (2004). A 76 storey 306m office tower was proposed for the city of Melbourne, Australia. However, it was not built due an economic decline. Yang et al. (2004) developed the structural model as basis for the evaluation of different structural control methods. It is available to researchers worldwide who wish to compare their control techniques to others using a realistic model. MATLAB programs for calculating the properties and the response of the uncontrolled tower were provided by Prof. Satish Nagarajaiah of Rice University, Houston, Texas.

The first five natural frequencies of the primary structure are 0.16Hz, 0.765Hz, 1.992Hz, 3.79Hz and 6.395Hz. A stiffness uncertainty of ±15% is considered in order to determine the efficiency of the controller. For the +15% and -15% case, the fundamental frequencies are 1.72Hz and 1.48Hz respectively. As 76 DOFs result in large computational effort, the state order reduction method [e.g. Davison (1966)] has been used to derive reduced order models for the building with and without TMD. This is achieved by retaining the eigenvalues and eigenvectors of selected modes of the 76-storey model. The wind force data acting on the model was determined from wind-tunnel tests of a scaled model. Details of the 76 storey model and the wind force data can be found on the Smart Structures Technology Laboratory website (http://www.cee.uiuc.edu/sstl/default.html). An ATMD, with a mass of 500tons, is added to the building, giving a mass ratio $\alpha = 0.327\%$, with respect to the total mass of the building. The damping ratio of the ATMD is chosen to be 7%. Active control is applied to the TMD using the bang-bang control with minimax shaping of the FRF developed in Sections 3.3 and 3.4.

3.6.2 Performance criteria

A set of non-dimensional performance criteria was developed by Yang et al. (2004) and is useful for comparing different structural control methods applied to the benchmark problem. The criterion examines the RMS and peak accelerations and displacements of selected modes of the structure. Reducing the accelerations in a structure alleviates the discomfort of occupants, but the frequency dependence of human perception to acceleration must also be considered. The displacements in a structure may also need to be reduced to limit the inter-storey drift. The first evaluation criterion considered here is the ability of the control scheme to reduce the maximum floor RMS acceleration.

$$J_1 = max(\sigma_{\ddot{x}1}, \sigma_{\ddot{x}30}, \sigma_{\ddot{x}50}, \sigma_{\ddot{x}55}, \sigma_{\ddot{x}60}, \sigma_{\ddot{x}65}, \sigma_{\ddot{x}70}, \sigma_{\ddot{x}75}) / \sigma_{\ddot{x}75o} \tag{3.37}$$

where $\sigma_{\ddot{x}i}$ is the RMS acceleration of the i^{th} floor and $\sigma_{\ddot{x}75o}$ is the RMS acceleration of the 75^{th} floor without control. Only the accelerations up to the 75^{th} floor are considered as the 76^{th} floor is not occupied. The second criterion is the average reduction in the RMS floor acceleration above the 49^{th} floor

$$J_2 = \sum_i (\sigma_{\ddot{x}i} / \sigma_{\ddot{x}io}), for \quad i = 50,55,60,65,70,75 \tag{3.38}$$

where $\sigma_{\ddot{x}io}$ is the RMS acceleration of the i^{th} floor without control. The third criterion is the ability of the controller to reduce the top floor RMS displacements

$$J_3 = \sigma_{x76} / \sigma_{x76o} \tag{3.39}$$

where σ_{x76} and σ_{x76o} are the RMS displacements of the 76^{th} DOF of the structure with and without control, respectively. The fourth criterion is the average reduction in the RMS displacements of selected floors above the 49^{th} floor. Here the 76^{th} DOF is included as it is important to reduce the top floor displacement.

$$J_4 = \sum_i (\sigma_{xi} / \sigma_{xio}), for \quad i = 50,55,60,65,70,75,76 \tag{3.40}$$

Constraints are placed on actuator capacity in the control design. The RMS control force, σ_u and the actuator stroke, σ_{xm} cannot exceed 100kN and 30cm respectively. In addition to this constraint, the RMS control effort requirements of the control design are evaluated as

$$J_5 = \sigma_{xm} / \sigma_{x76o} \tag{3.41}$$

$$J_6 = \sigma_p = \left\{ \frac{1}{T} \int_0^T [\dot{x}_m(t) u(t)]^2 \, dt \right\}^{1/2} \tag{3.42}$$

where $\dot{x}_m(t)$ is the actuator velocity, T is the total integration time and σ_p denotes the RMS control power. Equivalent performance criteria defined in terms of peak displacements and accelerations are also given by

$$J_7 = max(\ddot{x}_{p1}, \ddot{x}_{p30}, \ddot{x}_{p50}, \ddot{x}_{p55}, \ddot{x}_{p60}, \ddot{x}_{p65}, \ddot{x}_{p70}, \ddot{x}_{p75}) / \ddot{x}_{p75o} \tag{3.43}$$

$$J_8 = \sum_i (\ddot{x}_{pi} / \ddot{x}_{pio}), for \quad i = 50,55,60,65,70,75 \tag{3.44}$$

$$J_9 = x_{p76} / x_{p76o} \tag{3.45}$$

$$J_{10} = \sum_i (x_{pxi} / x_{pio}), for \quad i = 50,55,60,65,70.75,76 \tag{3.46}$$

where x_{pi} and x_{pio} are the peak displacements of the i^{th} DOF of the structure with control and without control, respectively, and $\ddot{x}_{pi}$ and $\ddot{x}_{pio}$ are the peak accelerations of the i^{th} DOF of the structure with control and without control, respectively. The peak constraints on actuator capacity are defined as 300kN for the max actuator control force, $\max|u(t)|$, and 95cm for the maximum actuator stroke, $\max|x_m(t)|$. In addition to these constraints, the peak control effort requirements of the control design are evaluated as

$$J_{11} = x_{pm} / x_{p76o} \tag{3.47}$$

$$J_{12} = P_{max} = max\,|\,\dot{x}_m(t)u(t)\,| \tag{3.48}$$

where x_{pm} is the peak actuator stroke and P_{max} is the peak control power. Better control system performance is indicated by lower J_1 to J_{12} values. For J_1 to J_4 and J_7 to J_{10}, the performance criteria relate to the RMS and peak response of the structure respectively, values less than 1.0 indicate reductions in the response of the structure.

3.6.3 Numerical simulation

The bang-bang control law with minimax shaping of the FRF is applied to the 76-storey benchmark problem. Figure 3.15 shows the reduction in the acceleration response at the 75th DOF for the ATMD with minimax shaping of the FRF compared to the uncontrolled case. The reduction in the response compared to the uncontrolled case is confirmed. Figure 3.16 shows the control time history of the ATMD for minimax shaping of the FRF.

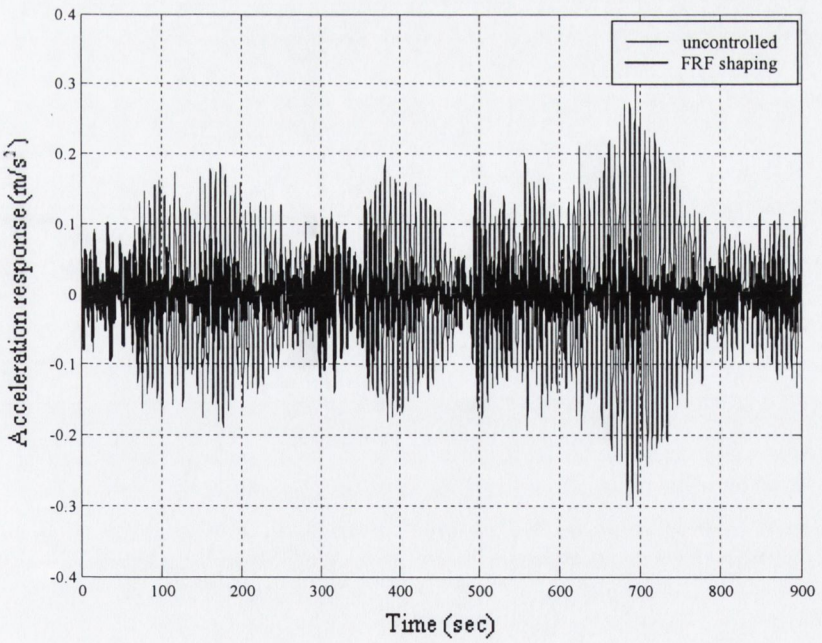

Figure 3.15 – Comparison of the acceleration response of the 75th floor for 0% uncertainty for the ATMD with minimax shaping of the FRF versus the uncontrolled system

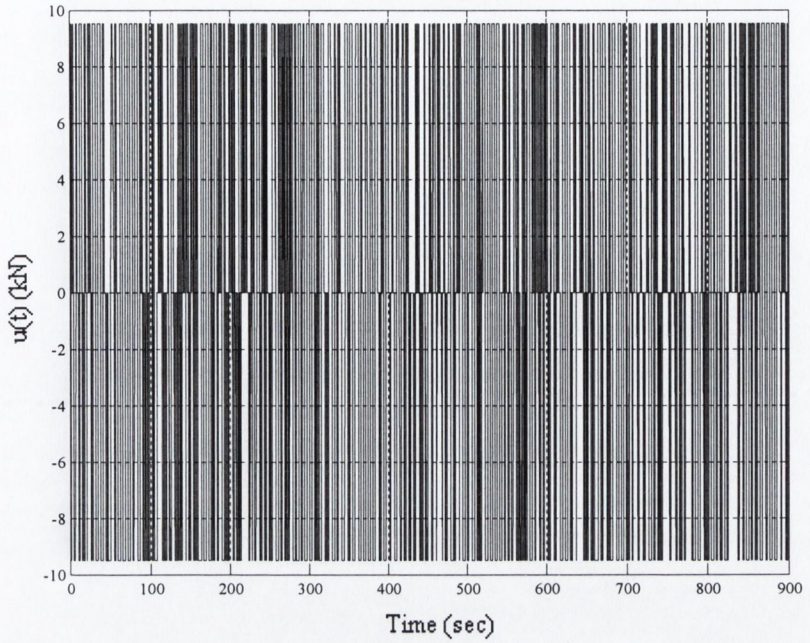

Figure 3.16 – Control force applied to the ATMD with minimax shaping of the FRF for 0% uncertainty in the stiffness

The computed responses with 0 and ±15% stiffness uncertainty are presented in terms of peak and RMS displacements and accelerations, and the performance criteria are obtained. The values of η, γ and $\ddot{x}_{max}$ for 0% and ±15% uncertainty in the stiffness are given in Table 3.4. The ATMD with bang-bang (B-B) control and minimax shaping of the FRF is compared to the uncontrolled structure and the ATMD with LQR developed by Yang at al. (2004).

	$\ddot{x}_{max}$	η	γ
0%	0.01	1900	0.9935
+15%	0.01	2200	0.9935
-15%	0.01	700	0.9935

Table 3.4 – Bang-bang control values for benchmark problem

Tables 3.5 and 3.6 present the peak and RMS displacements and accelerations of the structure, with 0% stiffness uncertainty. Each control method achieves similar acceleration and displacement response reductions, approximately 50% and 30% lower than the uncontrolled case, respectively. The proposed control method reduces the peak displacement response the most, e.g. approximately 22cm versus 23cm at the

76th floor for the ATMD with LQR. However, there is more variation in the values of the acceleration response with the proposed control strategy and the ATMD with LQR achieves slightly better reductions.

	Uncontrolled		ATMD with LQR		ATMD with B-B and minimax FRF	
Floor no.	x (cm)	$\ddot{x}$ (cm/s^2)	x (cm)	$\ddot{x}$ (cm/s^2	x (cm)	$\ddot{x}$ (cm/s^2)
1	0.05	0.22	0.04	0.23	0.04	0.25
30	6.84	7.14	5.14	3.37	4.91	3.74
50	16.59	14.96	12.22	6.73	11.63	7.54
55	19.41	17.48	14.22	8.05	13.52	8.77
60	22.34	19.95	16.27	8.93	15.47	10.10
65	25.35	22.58	18.36	10.05	17.45	11.15
70	28.41	26.04	20.48	10.67	19.45	12.19
75	31.59	30.33	22.67	11.56	21.52	13.80
76	32.30	31.17	23.15	15.89	21.98	15.86
TMD	-	-	74.27	72.74	83.48	86.70

Table 3.5 – Comparison of peak response for 0% uncertainty in the stiffness

	Uncontrolled		ATMD with LQR		ATMD with B-B and minimax FRF	
Floor no.	σ (cm)	$\ddot{\sigma}$ (cm/s^2)	σ (cm)	$\ddot{\sigma}$ (cm/s^2	σ (cm)	$\ddot{\sigma}$ (cm/s^2)
1	0.02	0.06	0.01	0.06	0.01	0.06
30	2.15	2.02	1.26	0.89	1.21	0.95
50	5.22	4.78	3.04	2.03	2.91	1.93
55	6.11	5.59	3.55	2.41	3.4	2.23
60	7.02	6.42	4.08	2.81	3.91	2.55
65	7.97	7.31	4.62	3.16	4.42	2.90
70	8.92	8.18	5.17	3.38	4.95	3.18
75	9.92	9.14	5.74	3.34	5.49	3.46
76	10.14	9.35	5.86	4.70	5.61	4.15
TMD	-	-	23.03	22.40	29.69	29.52

Table 3.6 – Comparison of RMS response for 0% uncertainty in the stiffness

Tables 3.7 and 3.8 present the peak displacement and acceleration responses for ±15% uncertainty in the stiffness. For +15% stiffness uncertainty, there is similar reduction in the displacement response compared to the uncontrolled structure for each case.

For the proposed method, the reduction in the acceleration response is slightly greater. For -15% stiffness uncertainty, there is a decrease in the peak displacement response but a slight increase in the peak acceleration response.

	Uncontrolled		ATMD with LQR		ATMD with B-B and minimax FRF	
Floor no.	x (cm)	$\ddot{x}$ (cm/s^2)	x (cm)	$\ddot{x}$ (cm/s^2	x (cm)	$\ddot{x}$ (cm/s^2)
1	0.04	0.22	0.03	0.23	0.03	0.29
30	5.52	4.78	4.35	3.36	4.44	3.78
50	13.37	11.28	10.35	6.63	10.55	6.77
55	15.63	12.85	12.04	8.00	12.28	7.25
60	17.94	14.91	13.78	9.13	14.05	8.04
65	20.32	16.87	15.55	10.09	15.85	9.47
70	22.72	18.98	17.34	11.58	17.67	10.56
75	25.20	21.75	19.19	12.46	19.55	14.03
76	25.76	21.6	19.6	15.86	19.97	14.43
Md	-	-	59.83	60.87	68.92	88.78

Table 3.7 – Comparison of peak response for +15% uncertainty in the stiffness

	Uncontrolled		ATMD with LQR		ATMD with B-B and minimax FRF	
Floor no.	x (cm)	$\ddot{x}$ (cm/s^2)	x (cm)	$\ddot{x}$ (cm/s^2	x (cm)	$\ddot{x}$ (cm/s^2)
1	0.06	0.22	0.04	0.22	0.05	0.24
30	7.69	6.01	5.54	3.64	5.86	4.52
50	18.34	12.83	13.12	7.87	13.89	8.89
55	21.37	14.41	15.27	9.9	16.16	10.16
60	24.49	15.97	17.47	11.13	18.49	11.08
65	27.68	17.4	19.72	12.63	20.86	13.37
70	30.9	19.86	21.99	14.01	23.25	15.3
75	34.24	23.09	24.34	14.8	25.73	17.15
76	34.99	22.8	24.87	18.76	26.28	17.79
Md	-	-	91.6	79.06	83.42	63.02

Table 3.8 – Comparison of peak response for -15% uncertainty in the stiffness

Compared to the ATMD with LQR, for 0% uncertainty in the stiffness, similar reductions are observed to that of the SAIVS-TMD with EMD/HT. For +15% uncertainty in the stiffness, the peak displacements are increased by 2% (Table 3.7). The peak acceleration increases at the 75th DOF by 12% but decreases at the higher

DOFs, by between 8 to 12%. For -15% uncertainty in the stiffness, the peak displacements are increased by 6% and the peak accelerations are increased by between 2 and 15% except for a decrease of 5% at the 76th DOF (Table 3.8). The proposed control strategy, on average, achieves similar reductions compared to the ATMD with LQR where it is more advantageous in some cases and less advantageous in others. Compared to the uncontrolled case, the response of the structure is always reduced, achieving reductions up to 57% in some cases.

Table 3.9 details the performance criteria used to compare the controlled response with that of the uncontrolled structure at 0% stiffness uncertainty, for the ATMD with LQR, and the ATMD with bang-bang control and minimax shaping of the FRF. Table 3.10 and 3.11 present equivalent results for ±15% stiffness uncertainty. It is shown in Tables 3.9 to 3.11 that the value of the actuator stroke and maximum actuator power are within the design constraints given in Section 3.6.2. Compared to the ATMD with LQR, for 0% stiffness uncertainty, the ATMD with minimax shaping of the FRF achieves greater response reduction in all cases except for the performance criteria based on the peak accelerations; however, the increase is not significant. For ±15% uncertainty in the stiffness, the proposed control method achieves slightly greater reduction in the response criteria. For 0% and +15% uncertainty in the stiffness there is no improvement in the performance measures J_6 and J_{12} compared to the ATMD with LQR. For -15%, J_6 and J_{12} are slightly better than the ATMD with LQR.

Criteria	ATMD with LQR	ATMD with B-B and minimax FRF
Peak Responses		
J_1	0.369	0.379
J_2	0.417	0.392
J_3	0.578	0.554
J_4	0.580	0.555
J_5	2.271	2.928
J_6	11.99	25.746
σ_u (kN)	34.07	81.38
σ_{xm} (cm)	23.03	29.685
RMS Responses		
J_7	0.381	0.455
J_8	0.432	0.464
J_9	0.717	0.681
J_{10}	0.725	0.688
J_{11}	2.300	2.585
J_{12}	71.96	81.076
max|$u(t)$| (kN)	118.24	96.52
max|x_m| (cm)	74.29	83.481

Table 3.9 – Comparison of Performance Criteria for 0% Uncertainty in the Stiffness

Criteria	ATMD with LQR	ATMD with B-B and minimax FRF
Peak Responses		
J_1	0.365	0.378
J_2	0.409	0.410
J_3	0.487	0.506
J_4	0.489	0.507
J_5	1.812	2.583
J_6	8.463	44.374
σ_u (kN)	28.29	96.029
σ_{xm} (cm)	18.37	22.136
RMS Responses		
J_7	0.411	0.463
J_8	0.443	0.427
J_9	0.607	0.618
J_{10}	0.614	0.625
J_{11}	1.852	2.134
J_{12}	52.680	137.98
max|$u(t)$| (kN)	105.58	111.76
max|x_m| (cm)	59.83	56.222

Table 3.10 – Comparison of Performance Criteria for +15% Uncertainty in the Stiffness

Criteria	ATMD with LQR	ATMD with B-B and minimax FRF
Peak Responses		
J_1	0.387	0.530
J_2	0.438	0.532
J_3	0.711	0.743
J_4	0.712	0.746
J_5	2.709	2.944
J_6	16.610	9.037
σ_u (kN)	44.32	32.269
σ_{xm} (cm)	27.46	29.848
RMS Responses		
J_7	0.488	0.566
J_8	0.539	0.578
J_9	0.770	0.814
J_{10}	0.779	0.822
J_{11}	2.836	2.583
J_{12}	118.33	27.39
max$\|u(t)\|$ (kN)	164.33	35.56
max$\|x_m\|$ (cm)	91.60	83.421

Table 3.11 – Comparison of performance criteria for -15% uncertainty in the stiffness

3.7 CONCLUSION

A control strategy incorporating bang-bang control and the minimax principle for shaping the FRF of ATMDs has been proposed. The simulated results prove that the control law is very effective in controlling structures under resonant and non-resonant excitations. Bang-bang control with minimax shaping of the FRF was compared to another conventional method, the LQC with minimax shaping of the FRF. The control strategy proposed herein provided reduced control forces and increased performance. The proposed control strategy was also applied to a low frequency coupled SDOF-TMD structure subjected to random excitations. With the addition of the control force using the bang-bang control law and FRF shaping, the response was considerably reduced. Finally, the control strategy was applied to the 76-storey model proposed by Yang et al. (2004) and the results were compared to the uncontrolled model and an ATMD with LQR proposed by Yang et al. (2004). It is observed that the ATMD with bang-bang control and online shaping of the FRF achieved slightly greater reductions in the vibration than the ATMD with LQR and

the average power consumption and the peak power consumption are similar to that of the ATMD with LQR.

CHAPTER 4

CONTROL STRATEGY USING BANG-BANG AND ONLINE SHAPING OF FRF WITH SAIVS-TMD

4.1 INTRODUCTION

The addition of the control force based on the bang-bang control scheme can be effective in reducing the response of the structure at relatively low control force values. However, the control effort could be further reduced if Den Hartog's minimax principle was applied to a VSTMD with bang-bang control. By retuning the VSTMD in real time, the external excitation would no longer match a peak of the FRF of the coupled structure-VSTMD system allowing the response to be decreased to a desired level with smaller values of the control force.

4.2 SEMI-ACTIVE CONTROL WITH TMD

A semiactive variable stiffness device (SAIVS) has been developed by Nagarajaiah [U.S. Patent No. 6,098,969 (2000)]. Nagarajaiah and Varadarajan (2000) continued this research by developing a SAIVS-TMD. The advantage of this device is that it can be retuned in real time and therefore mistuning due to changes in the structural properties can be avoided. The instantaneous frequency is obtained using the Empirical Mode Decomposition/Hilbert Transform (EMD/HT), based on the displacement at the top floor, of the structure under consideration. Using the EMD/HT, the dominant instantaneous frequency is identified and the SAIVS-TMD is retuned in real time in order to reduce the vibrations in the structure at this frequency. A linear electromechanical actuator/controller is used to change the stiffness of the SAIVS-TMD.

An alternative technique to the control of the SAIVS-TMD proposed by Varadarajan and Nagarajaiah (2004) is presented in this chapter. The control scheme involves a combination of controlling the response of the structure using bang-bang control with a control force applied to the SAIVS-TMD and the use of the principle of minimizing

the maximum value of the FRF for a coupled structure SAIVS-TMD system. In addition to the control force applied to the SAIVS-TMD, the control strategy incorporates the minimax principle, such that the corresponding FRF for the coupled structure SAIVS-TMD system is shaped by tuning the SAIVS-TMD, which results in the magnitude of the peaks of the FRF being equal. Once the control is applied, the TMD will retune in real time in order to achieve the minimax principle for the desired level of control. Three expressions for the tuning parameter derived from the equations of motion taking into account the bang-bang control law are obtained; for positive control, negative control and no control. The advantage of the proposed control strategy compared to the tuning of the SAIVS-TMD using the EMD/HT is that at any one time, only three states of the SAIVS-TMD are considered, which eliminates the online calculation of the instantaneous frequency in the structure using the EMD/HT. The control law, with the three states of the SAIVS-TMD, is applied based on the acceleration response of the structure and therefore the computational effort is considerably reduced. Also, as the control law is based on the fundamental mode of the structure only, all other modes in the control scheme can be ignored, further reducing the computational effort.

The performance of an ATMD with bang-bang control and minimax shaping of the FRF was obtained in Chapter 3. In this case, the TMD was not retuned in real-time, but its FRF was shaped for the case when no control force was applied, i.e. for a passive TMD. This approach will be known as *passive shaping of the FRF* from this point forward. The SAIVS-TMD developed by Nagarajaiah and Varadarajan (2000) with bang-bang control and minimax shaping of the FRF in real-time, described in Section 1.3, will be known as *online shaping of the FRF* from this point forward.

The SAIVS-TMD with bang-bang control and online shaping of the FRF is applied to a SDOF system subjected to harmonic and random excitations. The results are compared to those presented in Chapter 3 for an ATMD with bang-bang control and passive shaping of the FRF. The control strategy is then applied to the 76-storey benchmark problem and its performance compared to the ATMD with LQR, the SAIVS-TMD with EMD/HT and the SAIVS-TMD with bang-bang control and passive shaping of the FRF.

4.3 SHAPING OF THE FRF: MINIMAX PRINCIPLE, FOR THE SAIVS-TMD CONTROL SYSTEM

When the bang-bang control strategy is applied to a structure, the two peaks of the close loop FRF move further apart or closer together depending on the direction (positive or negative) of the control force; and one peak of the FRF increases while the other decreases. Therefore, the value of the tuning parameter given by Eq (3.34) will not apply for active control systems and can only be employed with passive mass dampers.

This feature of the behaviour is modelled by including the bang-bang control force in the equations of motion of the structure-TMD system. As the control effort is of a typical bang-bang type with $\Delta_d(t)$ switching between positive and negative values, two different values of the control force must be added to the equations of motion, resulting in two different values of the tuning. Assuming that the value of the tuning parameter is calculated for the extreme condition, i.e. $\ddot{x}_{max} = \ddot{x}_s$, for a positive value of the control force, $\Delta_d(t) = \eta \ddot{x}_{max}$, the augmented equations of motion are

$$\ddot{x}_s(t)(1+\alpha\eta) + \omega_n^2 x_s(t) - 2\zeta_n \omega_n \alpha \gamma^{1/2} \dot{x}_d(t) - \omega_n^2 \alpha\gamma x_d(t) = f(t) \tag{4.1}$$

$$\ddot{x}_s(t)(1-\eta) + \ddot{x}_d(t) + 2\zeta_n \omega_n \gamma^{1/2} \dot{x}_d(t) + \omega_n^2 \gamma x_d(t) = 0 \tag{4.2}$$

To obtain the transfer function of the response $x_s(t)$, a harmonic input of unit amplitude $f(t) = e^{i\omega t}$ is considered. The normalised transfer function for x_s with respect to the static displacement, x_{st} ($=1/\omega_n^2$) is given by

$$\left|\frac{x_s}{x_{st}}\right| = \sqrt{\frac{(2\zeta_n)^2(\Omega\sqrt{\gamma})^2 + (\gamma - \Omega^2)^2}{(2\zeta_n)^2(\Omega\sqrt{\gamma}(1-\Omega^2(1+\alpha)))^2 + (\gamma(1-\Omega^2(1+\alpha)) - \Omega^2 + \Omega^4(1+\alpha\eta))^2}} \tag{4.3}$$

where Ω ($=\omega/\omega_n$) is the non-dimensional frequency ratio. The expression for $|x_s/x_{st}|$ becomes independent of ζ_n if

$$\frac{(\Omega\sqrt{\gamma})^2}{(\Omega\sqrt{\gamma}(1-\Omega^2(1+\alpha)))^2} = \frac{(\gamma-\Omega^2)^2}{(\gamma(1-\Omega^2(1+\alpha))-\Omega^2+\Omega^4(1+\alpha\eta))^2} \tag{4.4}$$

leading to the following bi-quadratic equation

$$\Omega^4 - \frac{2(\gamma(1+\alpha)+1)}{2+\alpha(\eta+1)}\Omega^2 + \frac{2\gamma}{2+\alpha(\eta+1)} = 0 \tag{4.5}$$

Ignoring the trivial solution of $\Omega = 0$, two solutions, Ω_1^2 and Ω_2^2 of Eq (4.5) exist. However, Eq (4.5) is difficult to solve. As it is known, from the theory of fixed points (Den Hartog, 1956), that Eq (4.3) is independent of damping, it can also be observed that if ζ_n equals ∞, Eq (4.3) can be reduced to a simpler form

$$\left|\frac{x_s}{x_{st}}\right| = \frac{1}{1-\Omega^2(1+\alpha)} \tag{4.6}$$

Considering $\Omega_1 = \Omega_2$, substituting Ω_1 and Ω_2 into Eq (4.6) and equating the two resulting expressions yields

$$\frac{1}{1-\Omega_1^2(1+\alpha)} = \frac{1}{1-\Omega_2^2(1+\alpha)} \tag{4.7}$$

However, Den Hartog (1956) explains that this is not quite correct as Eq (4.7) is not really represented by the curve $\zeta_n = \infty$ but rather by a curve which is negative for values of Ω larger than $1/\sqrt{1+\alpha}$. In other words, if $\Omega^2(1+\alpha)$ is less than or greater than one, the amplitude of the transfer function will be positive or negative, respectively. Therefore the two fixed points of the transfer function, independent of damping, lie on different sides of this value of Ω and therefore Eq (4.7) must be corrected by a minus sign on one side or the other

$$\frac{1}{1-\Omega_1^2(1+\alpha)} = -\frac{1}{1-\Omega_2^2(1+\alpha)} \tag{4.8}$$

This leads to

$$\Omega_1^2+\Omega_2^2 = \frac{2}{1+\alpha} \tag{4.9}$$

It is also known that for a quadratic equation, the negative coefficient of the middle term is equal to the sum of the roots, therefore from Eq (4.5)

$$\Omega_1^2 + \Omega_2^2 = \frac{2(\gamma(1+\alpha)+1)}{2+\alpha(\eta+1)} \tag{4.10}$$

Now, it is no longer necessary to solve the complicated quadratic equation given in Eq (4.5), but rather by equating, Eqs (4.9) and (4.10), the tuning parameter, γ, is found to be

$$\gamma = \frac{1+\alpha\eta}{(1+\alpha)^2} \tag{4.11}$$

It is interesting to note that when η equals 0, the result is the same as that given in Eq (3.34). Similarly for $\Delta_d(t)=-\eta\ddot{x}_{max}$, γ is found to be

$$\gamma = \frac{1-\alpha\eta}{(1+\alpha)^2} \tag{4.12}$$

Two different values of the tuning parameter can now be obtained depending on whether the control force is positive or negative, for a given value of $\ddot{x}_{max}$. When there is no control force, the expression obtained in Eq (3.34) applied. This allows for the online tuning of the TMD by shaping the FRF using the minimax principle.

4.4 NUMERICAL EXAMPLE

4.4.1 SDOF SAIVS-TMD model subjected to harmonic excitations

The SAIVS-TMD developed by Nagarajaiah and Varadarajan (2000), is employed to tune the TMD using the minimax principle. When no control force is applied, the SAIVS-TMD does not retune in real time, but acts as a passive TMD tuned using the minimax principle according to Eq. (3.34). When the bang-bang control force given by Eq (3.34) is applied, the SAIVS-TMD is retuned in real time according to the expression given in Eqs (4.11) and (4.12).

A SAIVS-TMD with a mass ratio of 2% and a damping ratio of 1% is applied to the SDOF system considered in Section 3.4.1. Figure 4.1 shows the FRF obtained when a control value of $\Delta_d(t)=\eta \ddot{x}_{max}$ is applied to the TMD, with η and $\ddot{x}_{max}$ values of 0.2 and 1, respectively. The effect of the control force is to cause the first peak of the FRF to move down and the second peak to move up. Figure 4.2 shows that when the online control strategy is applied, with a value of γ equal to 0.965, calculated from Eq (4.11), the two peaks are once again equal. Figure 4.3 shows that as η increases, the peaks of the FRF are shifted closer together. The four curves correspond to the values given in Table 4.1. Similar plots for $\Delta_d(t)=-\eta \ddot{x}_{max}$ are shown in Figure 4.4. Here, the curves shift further apart from the case, η=0. The four curves correspond to the values given in Table 4.2. Therefore, for positive $\Delta_d(t)$, as η increases, the peaks of the FRF are shifted closer together and for negative $\Delta_d(t)$, as η increases, the peaks of the FRF move further apart. The greatest control effect is achieved with large η values to minimise the required control force while maximising η, $\ddot{x}_{max}$ must be reduced. It is important to note that for smaller $\ddot{x}_{max}$ values, faster switching between the positive and negative control force values is required. Hence, the online requirements to calculate the value of the control force must be taken into account before deciding on the value of $\ddot{x}_{max}$.

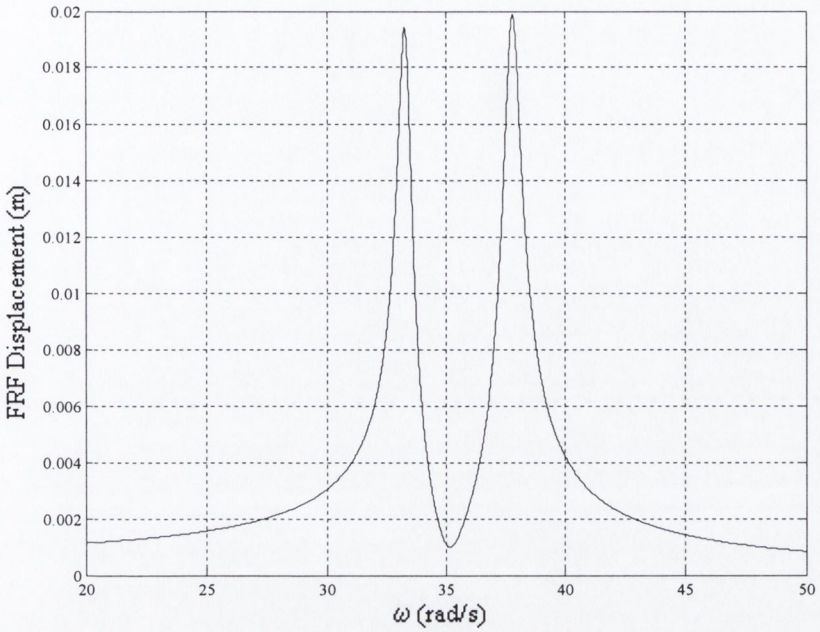

Figure 4.1 – Displacement transfer function of SDOF system with TMD, $\gamma = 0.96$, $\eta = 0.2$, $\ddot{x}_{max} = 1$

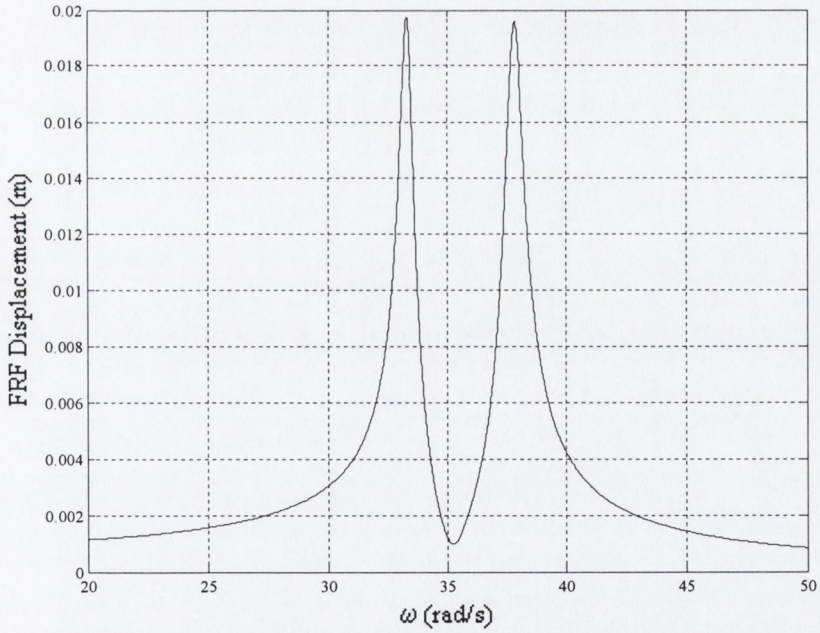

Figure 4.2 - Transfer function of SDOF system with TMD, $\gamma = 0.965$, $\eta = 0.2$, $\ddot{x}_{max} = 1$

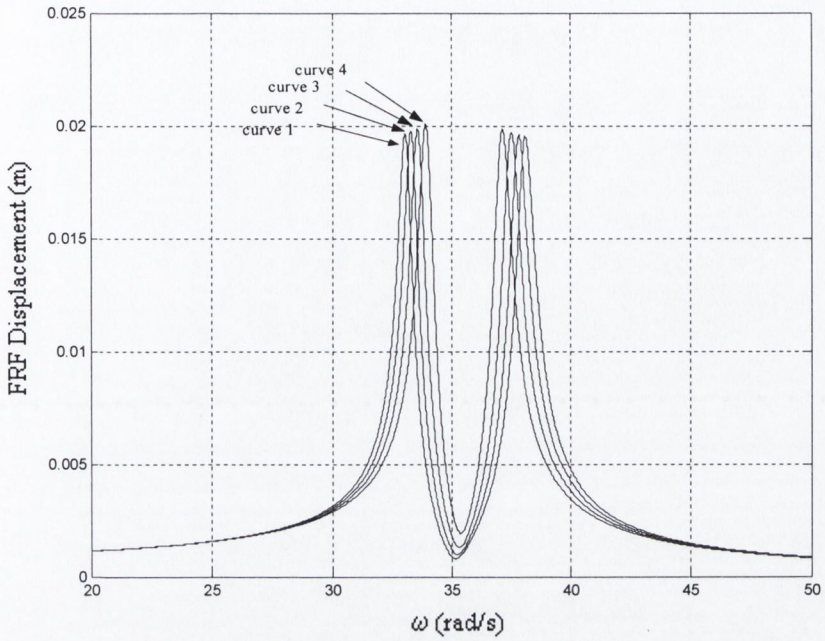

Figure 4.3 – FRF for increasing values of η and with the TMD tuned according to the online FRF shaping where $\Delta_d(t)=\eta\,\ddot{x}_{max}$

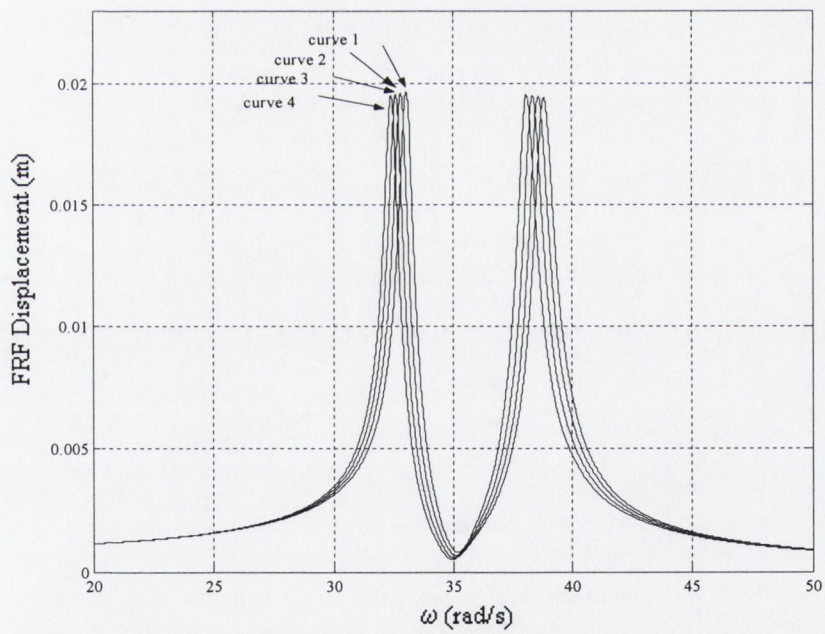

Figure 4.4 - FRF for increasing values of η and with the TMD tuned according to the online FRF shaping where $\Delta_d(t)=-\eta\,\ddot{x}_{max}$

	η	$\ddot{x}_{max}$	γ
Curve 1	0	1	0.961
Curve 2	0.2	1	**0.965**
Curve 3	0.4	1	0.9689
Curve 4	0.6	1	0.9727

Table 4.1 - Values of η, $\ddot{x}_{max}$ and γ corresponding to the curves in Figure 4.3

	η	$\ddot{x}_{max}$	γ
Curve 1	0	1	0.961
Curve 2	0.2	1	0.9573
Curve 3	0.4	1	0.9535
Curve 4	0.6	1	0.9496

Table 4.2- Values of η, $\ddot{x}_{max}$ and γ corresponding to the curves in Figure 4.4

As obtained in Chapter 3, when a harmonic excitation with frequency equal to the natural frequency of the structure is applied, the structural response is reduced considerably by a passive TMD and the application of a control force to the TMD is not required. However, the frequency of a non-resonant excitation may match the frequency of a peak in the transfer function of the response of the coupled structure-TMD system (in this case, at $\omega = 33.04$rad/s), and the response of the structure will be increased. Accordingly, the SAIVS-TMD with bang-bang control and online shaping of the FRF is employed. For increasing values of η, the corresponding values of γ_1 and γ_2, (where γ_1 and γ_2, correspond to $\Delta_d(t)=\eta\ddot{x}_{max}$ and $\Delta_d(t)=-\eta\ddot{x}_{max}$ respectively), the response of the coupled structure-TMD system and the values of the control accelerations are given in Tables 4.3, 4.4 and 4.5 for three different values of $\ddot{x}_{max}$.

γ_1	γ_2	η	x(mm)	$\ddot{x}$ (m/s^2)	Δ_d(m/s^2)	$\ddot{x}_{max}$ (m/s^2)
0.961	0.961	0	20.48	22.3	0	1
0.971	0.952	0.5	20.23	21.93	0.5	1
0.980	0.942	1	19.69	21.50	1	1
0.990	0.932	1.5	18.90	20.64	1.5	1
1.000	0.923	2	17.88	19.65	2	1
1.009	0.913	2.5	16.80	18.24	2.5	1
1.019	0.903	3	15.20	16.44	3	1
1.028	0.894	3.5	13.12	14.10	3.5	1
1.038	0.884	4	10.26	10.95	4	1
1.048	0.875	4.5	7.24	7.62	4.5	1
1.057	0.865	5	4.18	4.29	5	1

Table 4.3 - Response of coupled structure-ATMD system to harmonic excitation of amplitude 1m/s at non-resonant frequency, ω = 33.04 rad/s, with bang-bang control and online FRF shaping, for $\ddot{x}_{max}$ = 1m/s^2

η	γ_1	γ_2	x(m)	$\ddot{x}$ (m/s^2)	Δ_d(m/s^2)	$\ddot{x}_{max}$ (m/s^2)
0	0.961	0.961	20.48	22.33	0	0.5
1	0.980	0.942	20.25	21.80	0.5	0.5
2	1.000	0.923	19.69	21.24	1	0.5
3	1.019	0.903	18.68	20.04	1.5	0.5
4	1.038	0.884	16.75	18.20	2	0.5
5	1.057	0.865	14.92	15.90	2.5	0.5
6	1.077	0.846	12.00	12.71	3	0.5
7	1.096	0.827	8.30	8.70	3.5	0.5
8	1.115	0.807	4.66	4.69	4	0.5

Table 4.4 - Response of coupled structure-ATMD system to harmonic excitation of amplitude 1m/s at non-resonant frequency, ω = 33.04 rad/s, with bang-bang control and online FRF shaping, for $\ddot{x}_{max}$ = 0.5m/s^2

η	γ_1	γ_2	$\ddot{x}$ (m/s^2)	x(m)	Δ_d(m/s^2)	$\ddot{x}_{max}$ (m/s^2)
0	0.961	0.961	22.33	20.48	0	0.1
2	0.999	0.923	22	20.25	0.2	0.1
4	1.038	0.884	21.2	19.5	0.4	0.1
6	1.077	0.846	19.6	18.5	0.6	0.1
8	1.115	0.807	16.5	15.8	0.8	0.1
10	1.153	0.769	12.4	12	1	0.1
12	1.192	0.73	8	8	1.2	0.1
14	1.23	0.692	4.7	4.6	1.4	0.1

Table 4.5 - Response of coupled structure-ATMD system to harmonic excitation of amplitude 1m/s at non-resonant frequency, ω = 33.04 rad/s, with bang-bang control and online FRF shaping, for $\ddot{x}_{max}$ = 0.1m/s^2

For $\ddot{x}_{max}$ = 1m/s^2, the value of Δ_d equals 5m/s^2 and the percentage reduction in structural response is 80%. This value of the control acceleration is similar to that for the ATMD with bang-bang control and passive shaping of the FRF observed in Table 3.1, but the reduction in the response is smaller. It is shown in Table 3.1 that the value of Δ_d to achieve similar response reduction to that given in Table 4.5 is 4.95m/s^2, therefore when $\ddot{x}_{max}$ = 1m/s^2 the control strategy with online shaping of the FRF has no advantage to passive shaping of the FRF. However, as $\ddot{x}_{max}$ decreases, so does the required value of Δ_d. When $\ddot{x}_{max}$ = 0.5m/s^2 and $\ddot{x}_{max}$ = 0.1m/s^2, the value of Δ_d is obtained as 4m/s^2 and 1.4m/s^2, respectively, for similar values in response reduction. For the latter of the $\ddot{x}_{max}$ values, the value of Δ_d is now approximately one quarter of the value of Δ_d given in Table 3.1 and Table 4.5, for similar response reduction. Even though online shaping of the FRF does not have the ability to reduce the structural response to the level given in Table 3.1, the reduction in the response is still considerable and the online control strategy achieves greater reduction in the control effort. Therefore as long as the control actuator can allow for fast switching, $\ddot{x}_{max}$ may be small and this will lead to lower values in the control force.

4.4.2 Random excitation

A random excitation with a frequency equal to that at which a peak occurs in the transfer function, given in Figure 3.8, is applied to a coupled structure SDOF-TMD system with a low natural frequency. The control strategy with online shaping of the FRF is now considered. Figure 4.5 shows that the addition of the SAIVS-TMD with bang-bang control and online shaping of the FRF reduces the peak displacement response of the structure to 0.466m, a similar reduction to the ATMD with bang-bang control and passive shaping of the FRF, observed in Figure 3.10. The magnitude of the control acceleration to achieve the response reduction obtained in Figure 4.5 is given in Figure 4.6 to be 0.7275m/s^2. This is half the value given in Figure 3.11, which achieves the same response reduction using the bang-bang control strategy with passive shaping of the FRF. It is also observed from Figure 4.6 that the average switching time of the actuator is 1.2 times per second.

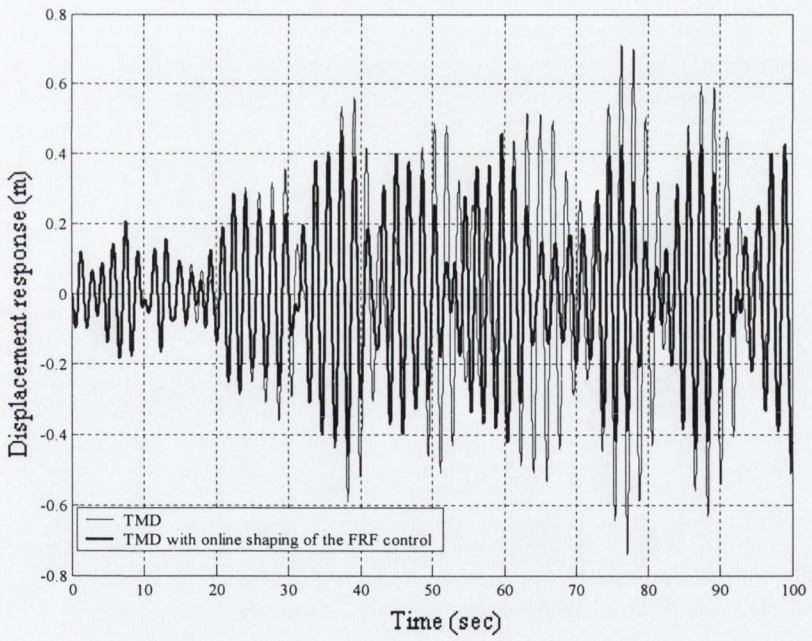

Figure 4.5 - Response of the structure with TMD and online FRF control strategy under random wind excitation (loading spectrum peak close to resonant frequency of coupled structure-TMD system)

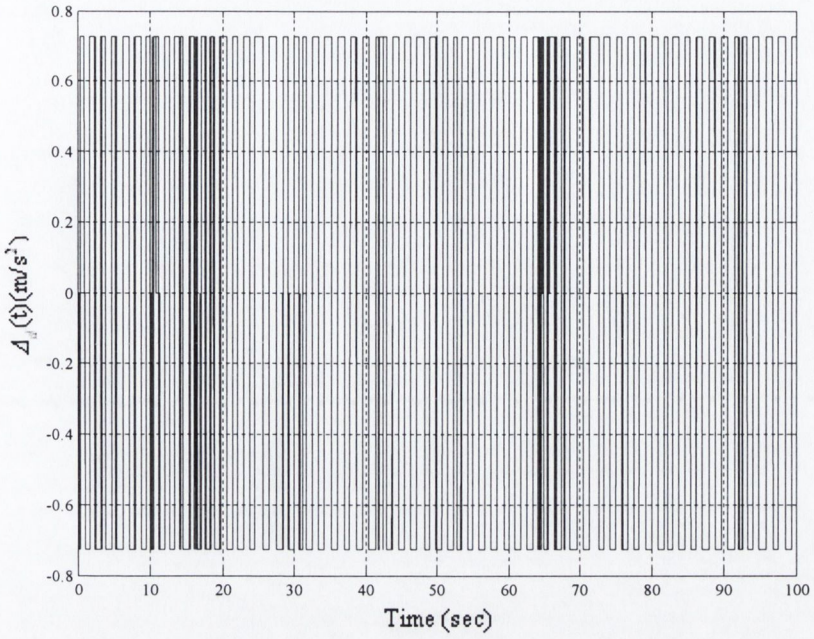

Figure 4.6 – Profile of the bang-bang control force applied to the TMD with online FRF shaping (loading spectrum peak close to resonant frequency of coupled structure-TMD system)

4.5 APPLICATION TO 76-STOREY BENCHMARK PROBLEM

The new control strategy with online shaping of the FRF is now applied to the 76-storey benchmark problem. Figure 4.7 compares the acceleration response at the 75th DOF for the uncontrolled case with that achieved using the SAIVS-TMD with bang-bang control and online shaping of the FRF. The reduction in the response compared to the uncontrolled case is confirmed. Figure 4.8 shows the control time history of the SAIVS-TMD with bang-bang control and online shaping of the FRF. The required control is a small fraction of that for the ATMD with bang-bang control and passive shaping of the FRF shown in Figure 3.13. The average switching time of the actuator is observed in Figure 4.8 to be 0.15 times per second.

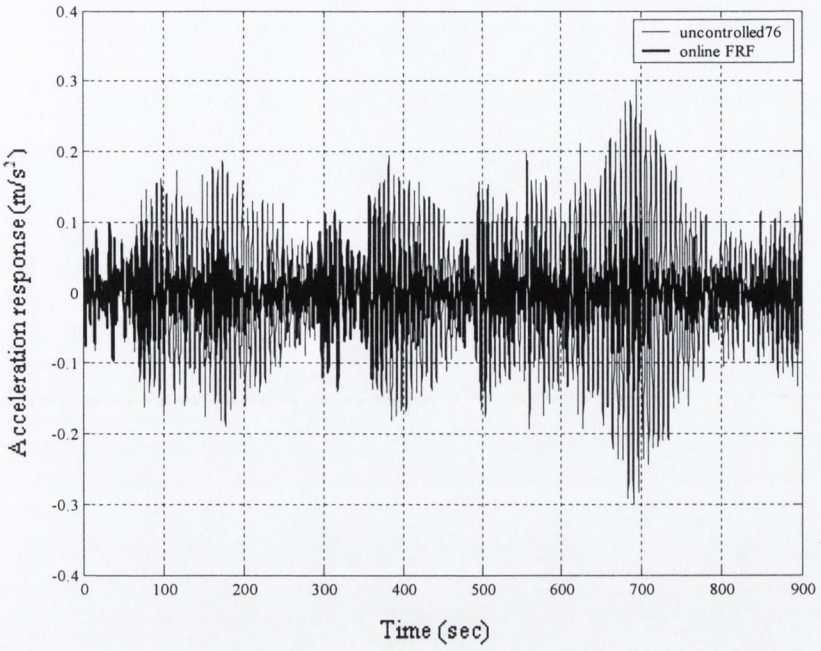

Figure 4.7 – Comparison of the acceleration response of the 75th floor with 0% uncertainty for the SAIVS-TMD with bang-bang control and online shaping of the FRF

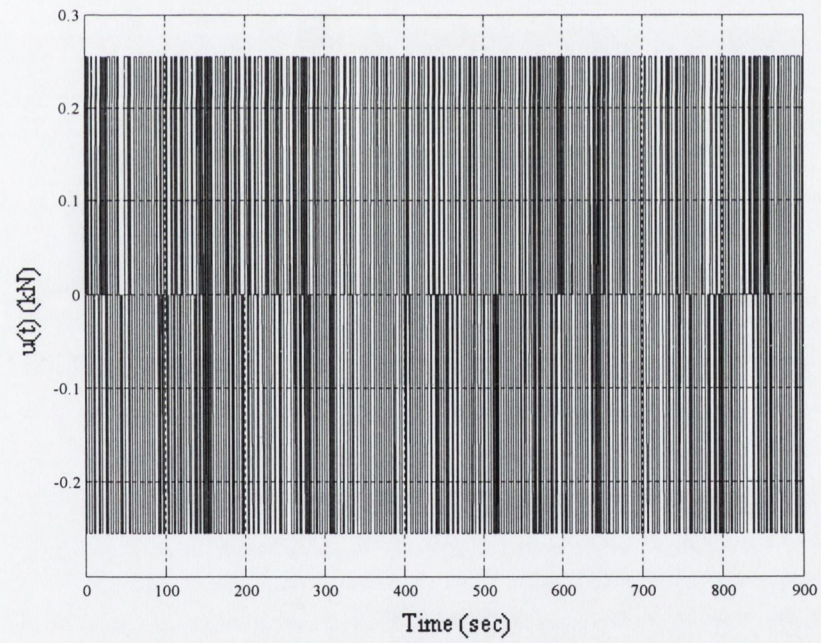

Figure 4.8 – Control force applied to the SAIVS-TMD with bang-bang control and online shaping of the FRF for 0% uncertainty in the stiffness

It was shown in Chapter 3 that the ATMD with LQR and the ATMD with bang-bang control and passive shaping of the FRF reduce the response of the uncontrolled structure considerably. In this section, SAIVS-TMD with bang-bang control and

online shaping of the FRF is compared with the ATMD and LQR, the ATMD with bang-bang control and passive shaping of the FRF and with the SAIVS-TMD with EMD/HT. The values of η, γ_1, γ_2, and $\ddot{x}_{max}$ for 0% and ±15% uncertainty in the stiffness are given in Table 4.6.

	$\ddot{x}_{max}$	η	γ_2	γ_1
0%	0.01	51	1.159	0.828
+15%	0.01	10	1.026	0.961
-15%	0.01	60	1.188	0.799

Table 4.6 – Bang-bang control values for benchmark problem with online shaping of the FRF

Figures 4.9 and 4.10 illustrate the peak displacements and accelerations of the structure, respectively, for 0% stiffness uncertainty. It is clear from Figure 4.9 that the peak displacement response of the proposed method achieves similar reduction compared to the ATMD with bang-bang control and passive shaping of the FRF, and higher reduction as compared to the other two methods. Greater response reduction is achieved at the higher DOFs. It is observed from Figure 4.10, that the peak acceleration response of the proposed method achieves higher reduction compared to the ATMD with bang-bang control and passive shaping of the FRF, similar reduction compared to the SAIVS-TMD with EMD/HT and less reduction compared to the ATMD with LQR.

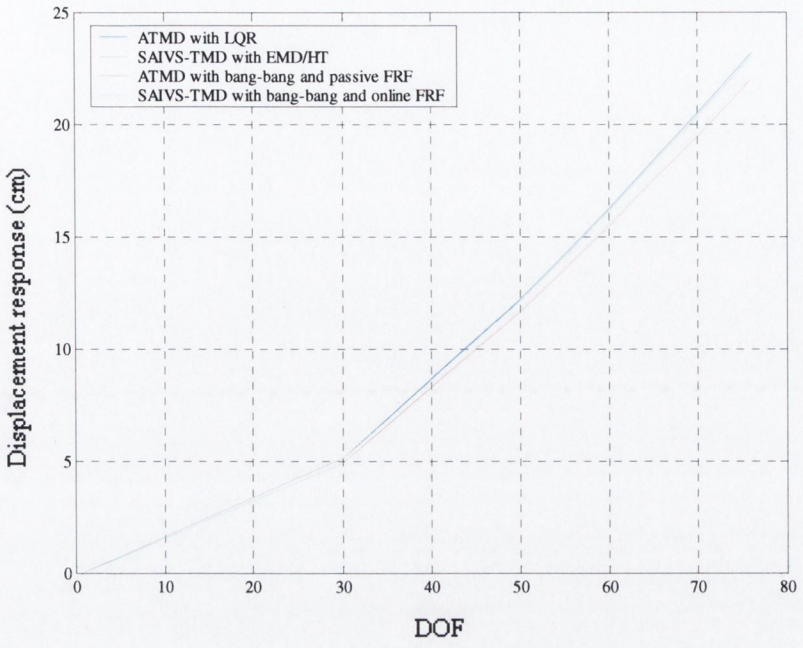

Figure 4.9 – Comparison of peak displacements for 0% uncertainty in the stiffness

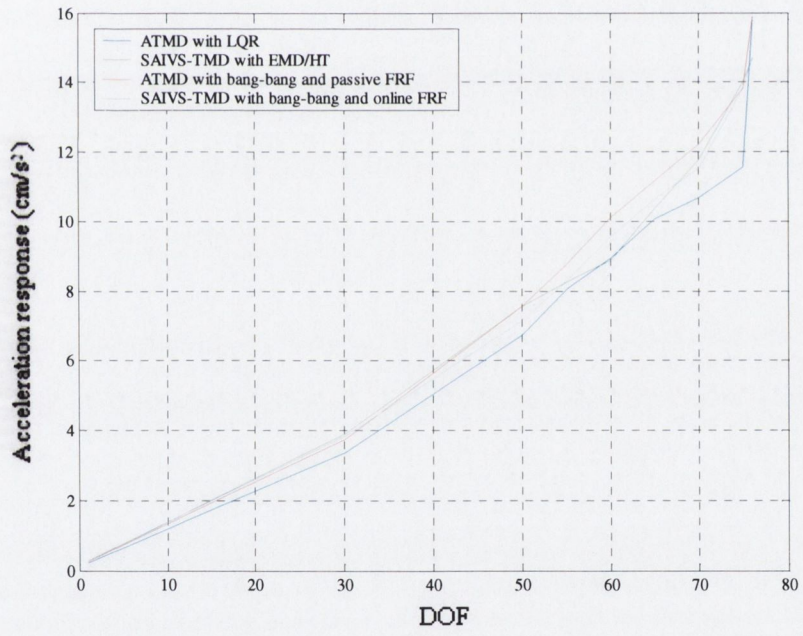

Figure 4.10 – Comparison of peak accelerations for 0% uncertainty in the stiffness

Figures 4.11 and 4.12 illustrate the RMS displacements and accelerations of the structure, respectively, for 0% stiffness uncertainty. It is clear from Figure 4.11 that the maximum reduction in the RMS displacement occurs for the ATMD with bang-bang control and passive shaping of the FRF and the other three methods achieve similar response reduction. It is shown in Figure 4.12 that the maximum reduction in

the RMS acceleration response also occurs for the ATMD with bang-bang control and passive shaping of the FRF. The ATMD with LQR achieves the next best reduction in the peak acceleration response, and the proposed method and the SAIVS-TMD with EMD/HT achieve similar results.

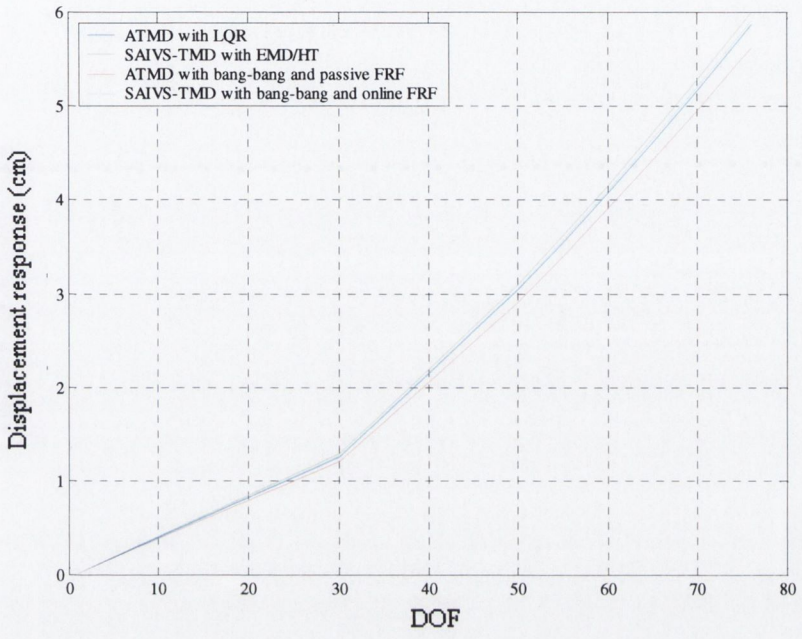

Figure 4.11 – Comparison of RMS displacements for 0% uncertainty in the stiffness

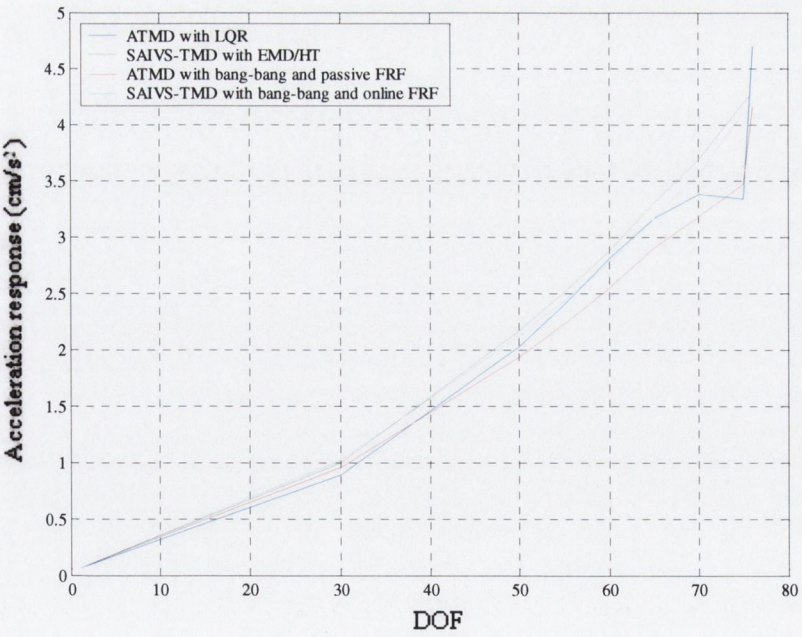

Figure 4.12 – Comparison of RMS accelerations for 0% uncertainty in the stiffness

Figures 4.13 and 4.14 illustrate the peak displacements and accelerations of the structure, respectively, for +15% stiffness uncertainty. Figure 4.13, shows there is little difference in the peak displacement responses, whereas the greatest reduction for the peak acceleration responses occurs for the ATMD with bang-bang control and passive shaping of the FRF. The ATMD with LQR achieves the next best reduction in the peak acceleration response, and the proposed method and the SAIVS-TMD with EMD/HT achieve similar results.

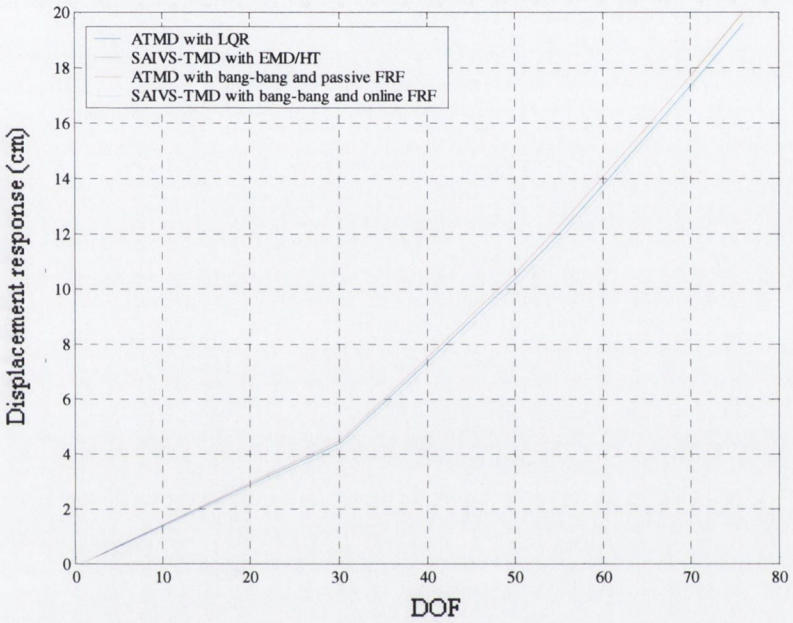

Figure 4.13 – Comparison of peak displacements for +15% uncertainty in the stiffness

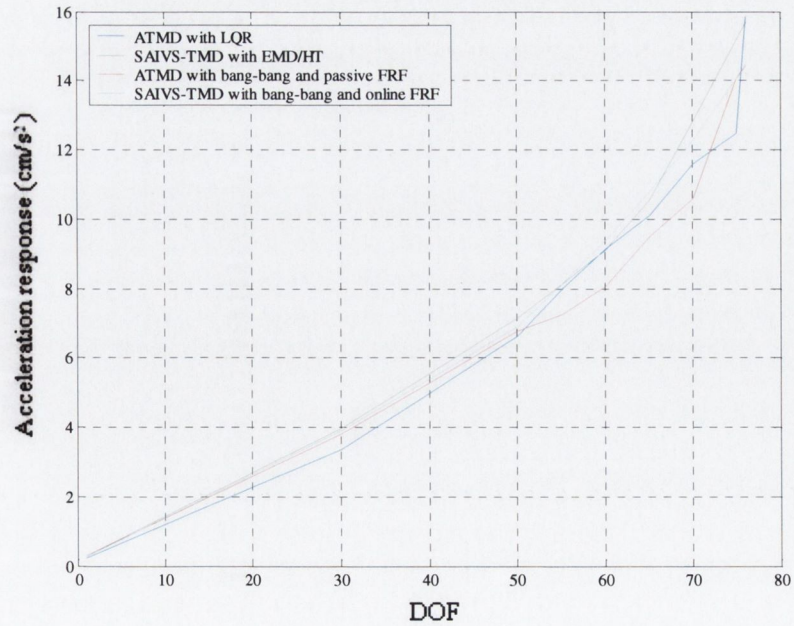

Figure 4.14 – Comparison of peak accelerations for +15% uncertainty in the stiffness

Figures 4.15 and 4.16 illustrate the peak displacements and accelerations of the structure, respectively, for -15% stiffness uncertainty. It is clear that the ATMD with LQR achieves the greatest reduction in the peak displacement and acceleration response and the other three methods achieve similar results. On average, the performance of the SAIVS-TMD with bang-bang control and online shaping of the FRF is more or less the same as that of the ATMD with bang-bang control and passive shaping of the FRF.

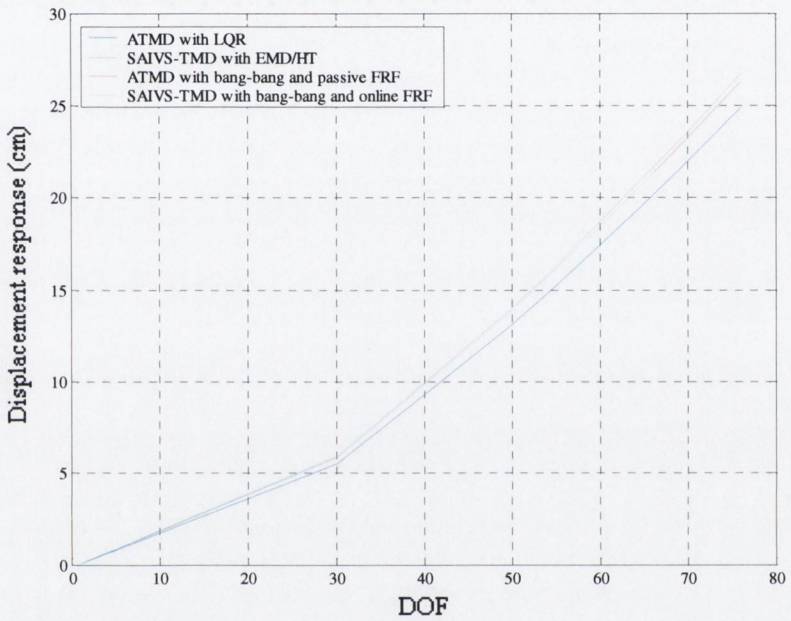

Figure 4.15 – Comparison of peak displacements for -15% uncertainty in the stiffness

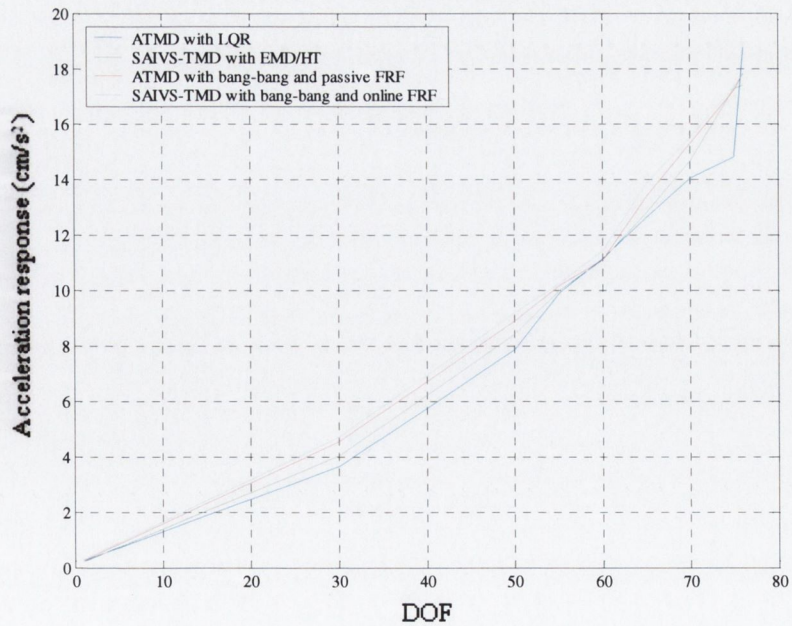

Figure 4.16 – Comparison of peak accelerations for -15% uncertainty in the stiffness

The performance criteria for each control strategy are shown in Tables 4.7, 4.8 and 4.9. The values of J_6 for the SAIVS-TMD with bang-bang control and online shaping of the FRF do not include the power required to change the stiffness of the SAIVS-TMD between the three states of the control law. However, this value is described by Varadarajan and Nagarajaiah (2004) to be nominal and therefore is indicated by the figure ε, i.e. small number. It is shown in Tables 4.7 to 4.9 that the value of the actuator stroke and maximum actuator power are within the design constraints given in Section 3.5.2. Table 4.7, details the performance criteria used to compare the controlled response with that of the uncontrolled structure at 0% stiffness uncertainty, for the ATMD with LQR, the SAIVS-TMD with EMD/HT, the ATMD with bang-bang control and passive shaping of the FRF, and the SAIVS-TMD with bang-bang control and online shaping of the FRF. Tables 4.8 and 4.9 present equivalent results for ±15% stiffness uncertainty. Values of the performance criterion, J_1 to J_4 and J_7 to J_{10} for the SAIVS-TMD with bang-bang control and online shaping of the FRF are slightly higher than those for the ATMD with LQR or the ATMD with bang-bang control and passive shaping of the FRF, but similar to those for the SAIVS-TMD with EMD/HT. Of greater significance is that with the proposed control strategy (for 0% and ±15% uncertainty in the stiffness), the performance measures J_6 and J_{12}, relating to the average power consumption and peak power, are only a fraction of that with the ATMD with LQR or the ATMD with bang-bang control and passive shaping of the FRF, even with the nominal addition of the control force required to change the stiffness of the SAIVS-TMD. Hence, in terms of response reduction, it is seen from the comparison of the performance criteria that the required level of control is only a small fraction of that required with either the ATMD with bang-bang control with passive shaping of the FRF or the ATMD with LQR. If a VSTMD that did not require an electromechanical force to change the stiffness could be developed, the performance measure J_6 would now be considerably smaller than that for the SAIVS-TMD with EMD/HT and the performance measure J_{12} would be the same, except for +15% uncertainty in the stiffness where it would be reduced. This is examined further in following chapters.

Criteria	ATMD with LQR	SAIVS-TMD EMD/HT	ATMD with B-B and passive FRF	SAIVS-TMD with B-B and Online FRF
Peak Responses				
J_1	0.369	0.458	0.379	0.449
J_2	0.417	0.452	0.392	0.439
J_3	0.578	0.591	0.554	0.583
J_4	0.580	0.592	0.555	0.584
J_5	2.271	2.206	2.928	2.433
J_6	11.99	2.378	$25.746 + \varepsilon$	$0.590 + \varepsilon$
σ_u (kN)	34.07	-	81.38	2.318
σ_{xm} (cm)	23.03	-	29.685	24.665
RMS Responses				
J_7	0.381	0.462	0.455	0.456
J_8	0.432	0.465	0.464	0.464
J_9	0.717	0.712	0.681	0.688
J_{10}	0.725	0.721	0.688	0.695
J_{11}	2.300	2.105	2.585	2.380
J_{12}	71.96	2.274	$81.076 + \varepsilon$	$2.318 + \varepsilon$
max|$u(t)$| (kN)	118.24	-	96.52	2.591
max|x_m| (cm)	74.29	-	83.481	76.886

Table 4.7 – Comparison of performance criteria for 0% uncertainty in the stiffness

Criteria	ATMD with LQR	SAIVS-TMD EMD/HT	ATMD with B-B and passive FRF	SAIVS-TMD with B-B and Online FRF
Peak Responses				
J_1	0.365	0.458	0.378	0.464
J_2	0.409	0.448	0.410	0.455
J_3	0.487	0.506	0.506	0.520
J_4	0.489	0.507	0.507	0.521
J_5	1.812	1.788	2.583	1.433
J_6	8.463	2.079	$44.374 + \varepsilon$	$0.075 + \varepsilon$
σ_u (kN)	28.29	-	96.029	0.457
σ_{xm} (cm)	18.37	-	22.136	14.531
RMS Responses				
J_7	0.411	0.500	0.463	0.463
J_8	0.443	0.476	0.427	0.468
J_9	0.607	0.619	0.618	0.605
J_{10}	0.614	0.627	0.625	0.606
J_{11}	1.852	1.814	2.134	1.382
J_{12}	52.680	2.107	$137.98 + \varepsilon$	$0.24 + \varepsilon$
max|$u(t)$| (kN)	105.58	-	111.76	0.508
max|x_m| (cm)	59.83	-	56.222	44.630

Table 4.8 – Comparison of performance criteria for 15% uncertainty in the stiffness

Criteria	ATMD with LQR	SAIVS-TMD EMD/HT	ATMD with B-B and passive FRF	SAIVS-TMD with B-B and Online FRF
Peak Responses				
J_1	0.387	0.504	0.530	0.547
J_2	0.438	0.495	0.532	0.540
J_3	0.711	0.737	0.743	0.752
J_4	0.712	0.738	0.746	0.754
J_5	2.709	2.441	2.944	2.496
J_6	16.610	2.464	$9.037 + \varepsilon$	$0.66 + \varepsilon$
σ_u (kN)	44.32	-	32.269	2.79
σ_{xm} (cm)	27.46	-	29.848	25.310
RMS Responses				
J_7	0.488	0.569	0.566	0.570
J_8	0.539	0.564	0.578	0.590
J_9	0.770	0.827	0.814	0.811
J_{10}	0.779	0.835	0.822	0.820
J_{11}	2.836	2.553	2.583	2.498
J_{12}	118.33	2.594	$27.39 + \varepsilon$	$2.472 + \varepsilon$
$\max\|u(t)\|$ (kN)	164.33	-	35.56	3.048
$\max\|x_m\|$ (cm)	91.60	-	83.421	80.678

Table 4.9 – Comparison of performance criteria for -15% uncertainty in the stiffness

4.6 CONCLUSION

The bang-bang control law obtained in Chapter 3 has been applied to the SAIVS-TMD, developed by Varadarajan and Nagarajaiah (2005), which was retuned in real time according to the minimax principle taking into account the level of control required. The simulated results show that online shaping of the FRF achieves the same reduction as the ATMD with bang-bang control and passive shaping of the FRF, but with much less control effort. The control strategy was also applied to the 76-storey model proposed by Yang et al. (2004) for comparison with other structural control methods. It was observed that the proposed control strategy achieves similar response reductions to the ATMD with LQR, the SAIVS-TMD with EMD/HT and the ATMD with bang-bang control and minimax shaping of the FRF, with low values of control force.

CHAPTER 5

CHARACTERISATION OF SOLENOID BASED VSTMD AND EXPERIMENTAL VALIDATION

5.1 INTRODUCTION

It was shown in Chapter 4 how the SAIVS-TMD with bang-bang control was effective in controlling the vibrations in a structure. This type of stiffness device uses an electromechanical actuator to change the stiffness of the TMD. If a VSTMD that did not require a force to change its mechanical properties was available, the total control force required in the control strategy would be reduced. In this chapter, a solenoid based VSTMD is introduced and described. Detailed descriptions of the experimental set-up, the test model and the instruments used in characterising the damper are provided, along with the corresponding test results. The VSTMD is employed in a series of tests on a model SDOF structure. The VSTMD is first tuned to the structure using the minimax principle when no current is applied, as described in Chapter 3. The VSTMD is then deliberately mistuned and it is shown how the addition of current through the solenoid can retune the VSTMD.

5.2 VARIABLE STIFFNESS TUNED MASS DAMPER

The TMD stiffness can be varied due to the presence of a solenoid through which the mass of the TMD passes. When current is supplied to the solenoid, a magnetic field is created. Depending on the level of current supplied, the magnetic field resists the motion of the mass, effectively providing additional stiffness to the TMD. The stiffness and damping of the VSTMD are characterised for different levels of current. When no current is supplied to the solenoid, the VSTMD acts as a passive device and this is also subjected to experimental analysis.

A TMD is shown in Figure 5.1. The mass is connected to a spring, which is attached to the structure. The mass of the TMD consists of a bar with two weights on either end attached to small wheels so that is free to move.

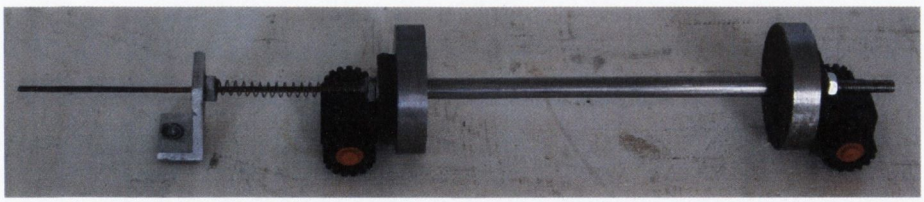

Figure 5.1 Tuned mass damper

The bar of the TMD is placed through a solenoid as shown in Figure 5.2. A solenoid can be described as a tightly wound helical coil of wire. When a current is applied to the solenoid, a magnetic field is created. This magnetic field is the sum of the fields produced by the individual turns that make up the solenoid, therefore the more turns in the solenoid, the stronger the magnetic field will become.

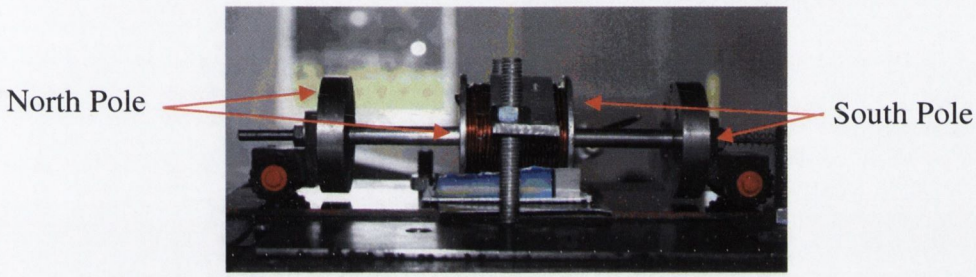

Figure 5.2 – TMD and solenoid

Figure 5.3 shows the magnetic field for a solenoid. The spacing of the lines at the centre of the solenoid, such as P_1, indicates that the field inside the coil is strong and uniform over the cross section of the coil. The lines of the external field, such as P_2, are far apart, indicating that they are weak over the cross section of the coil. As the bar of the VSTMD passes through the centre of the solenoid, i.e. the strong part of the magnetic field, the weakness of the external field is not relevant.

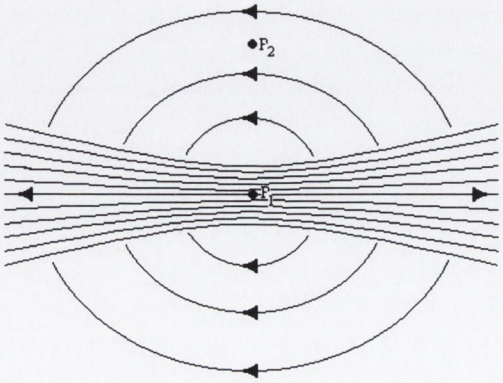

Figure 5.3 – Magnetic field for a solenoid

From Amperes law, the magnetic field, B, can be related to the net current i, by the following equation

$$B = \mu_0 in \tag{5.1}$$

where μ_0 is a constant called the permeability constant and n is the number of turns per unit length of the solenoid. Therefore the strength of the magnetic field is dependent on two factors; the current passing through the solenoid and the number of turns in the solenoid. When current is applied to the solenoid and the magnetic field is created, the bar passing through the centre of the solenoid becomes magnetised, along with the weights attached to each end of the bar and the metal ends of the solenoid itself. In effect, a north and south pole are created at either side of the solenoid and a north and south pole are created at the two weights attached to the bar, as indicated in Figure 5.2. Figure 5.2 also shows the resting position of the bar, which is at the centre of the solenoid. If the bar is pushed from left to right, the pole of the weight on the left side of the bar moves towards the same orientation pole on the end of the left side of the solenoid; therefore they will repel each other. The closer this weight moves toward the solenoid, the stronger the repelling force. Because of this, the resting position of the bar will always be at the centre of the solenoid. The higher the current, the higher the magnetic field and the faster the bar will return to this position. This force effectively provides an additional resistance to the displacement of the bar, which increases the stiffness of the VSTMD. Further research into the physics of solenoids and electromagnets could be carried out. As the solenoid is in parallel with the mechanical spring, this additional stiffness is added to the stiffness of the spring to determine the total stiffness of the TMD. A sequence of the TMD movement during vibration is shown in Figure 5.4

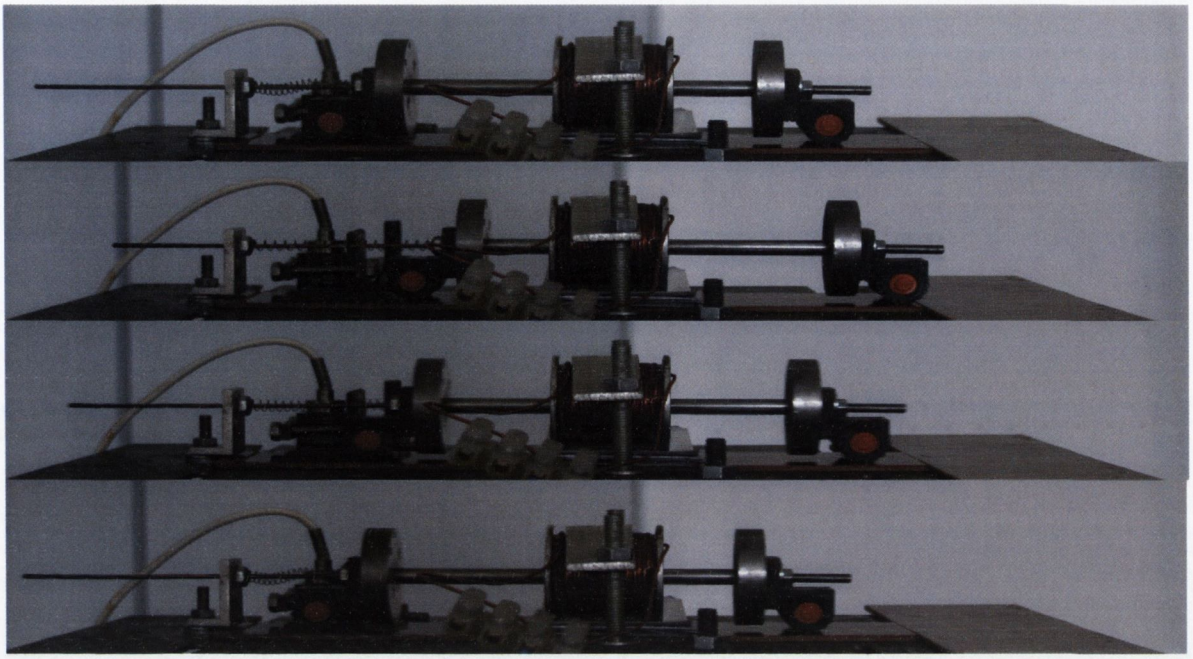

Figure 5.4 – Moving VSTMD

The VSTMD is first characterised using a static force deformation test. A linear variable differential transducer (LDVT) is placed at one end of the VSTMD and a force measured by a load cell is applied to the other end, for different levels of current passing through the solenoid. The force applied to the VSTMD and the resulting displacement is recorded, and a force deformation graph is plotted. From this graph, the stiffness of the VSTMD is calculated.

To determine whether the stiffness of the VSTMD varies with excitation frequency, the VSTMD is placed on a shaking platform which is caused to oscillate at frequencies between 0 and 7Hz. The acceleration of the TMD is recorded using an accelerometer. From this acceleration, the force and displacement are found from the following two equations

$$F_i = m\ddot{x}_i \tag{5.2}$$

$$x_{i+1} = \dot{x}_i t + \frac{1}{2}\ddot{x}_i t^2 \tag{5.3}$$

where F_i is the force, m is the mass of the TMD, t is the time at which the response is recorded, x_i, $\dot{x}_i$ and $\ddot{x}_i$ are the displacement, velocity and acceleration of the TMD

respectively at time instant t. The dynamic stiffness, k can be found from Hooke's law

$$k = \frac{F_i}{x_i} \tag{5.4}$$

and therefore graphs of frequency against stiffness can be plotted for different levels of current applied to the solenoid.

5.3 INSTRUMENTATION AND APPARATUS

5.3.1 Experimental set-up

The experimental set up for tests on the SDOF-VSTMD model is shown in Figure 5.5. The same set up is used in the VSTMD characterisation tests, except that the damper is attached to the shaking platform rather than the roof of the SDOF model. The VSTMD or the SDOF-VSTMD model is placed on a shaking platform, which is caused to oscillate at a specified frequency and amplitude by an actuator.

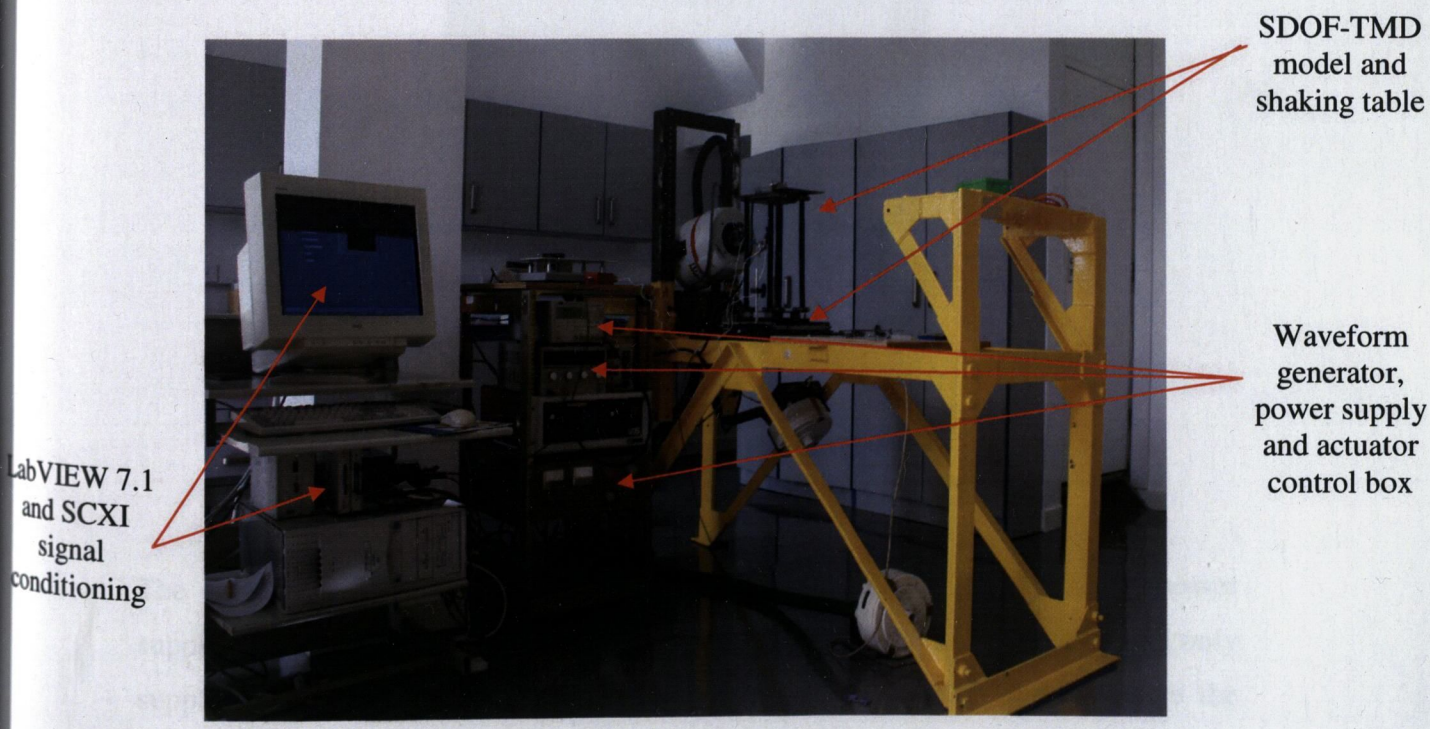

Figure 5.5 – Experimental set-up

The actuator is controlled using a waveform generator connected to the control box of the actuator, as shown in Figure 5.6. The waveform generator is a TTi TGA1241 signal channel arbitrary with 40MHz clock speed and 12bit vertical resolution. It is capable of producing multiple waveforms including sine, square, triangle, ramp and pulse. The control box contains an electromagnet and a transformer and is connected to a magnetron (actuator), which is in turn connected to the shaking table. When the input frequency is applied, the electromagnet controls the speed and amplitude at which the shaking table moves in and out.

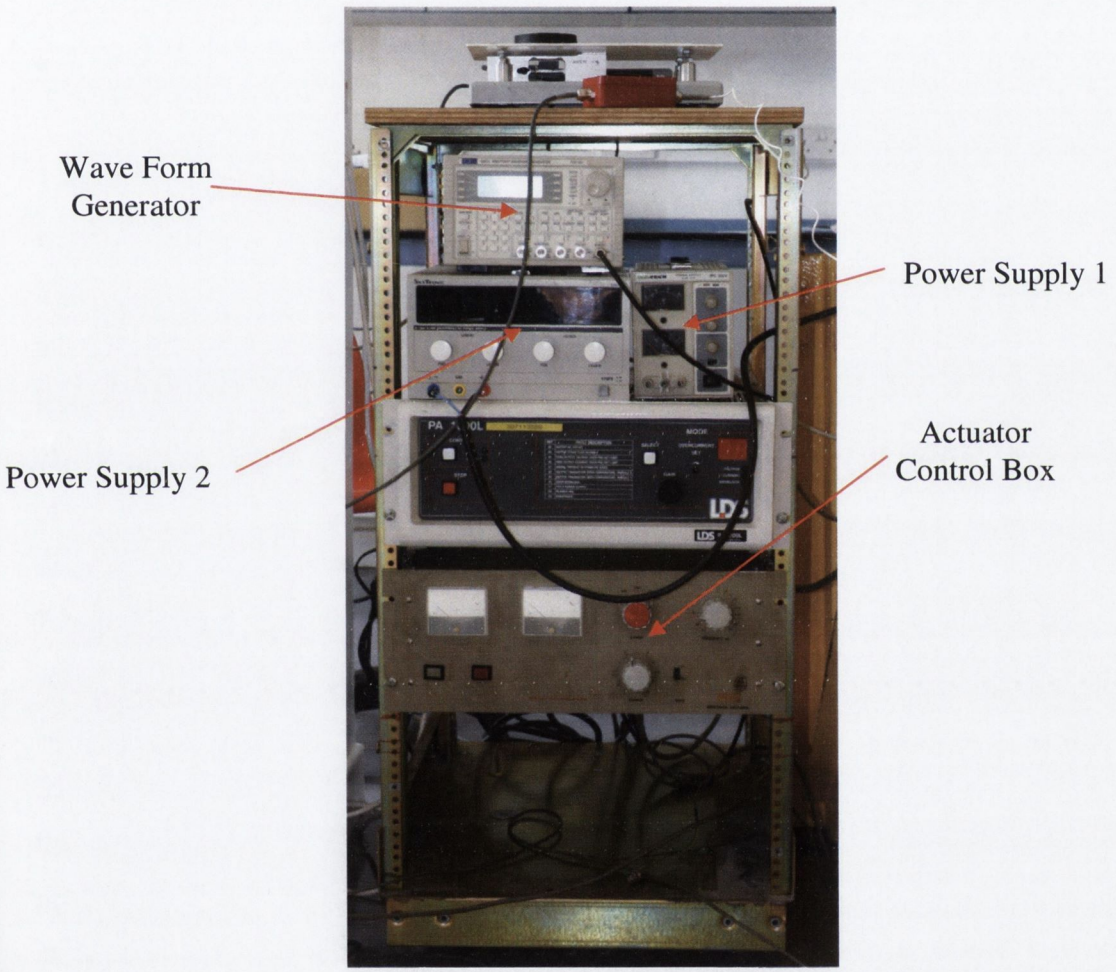

Figure 5.6 – Waveform generator, actuator control box and power supplies

The power supply applied to the solenoid is also shown in Figure 5.6; two power supplies were required, as the first only supplied current of 0-2A and the second only supplied current of more than 2A. Two accelerometers are used to measure the acceleration of the system. Accelerometers were preferred over linear variable differential transducers (LVDTs), as LVDTs limit the response amplitude. The first is

a ±2g Entran accelerometer, model - EGCS-A2-2, placed at the top of the structure with dimensions 1.5cm by 1.5cm by 1.5cm and a sensitivity of 2.43V/g. The second is a ±5g RDP accelerometer, model - JTF/F482-02, placed at the base of the structure with dimensions 2.5cm by 1cm by 2cm. A transducer amplifier, type S7DC, is employed to increase the sensitivity of this accelerometer to 1V/g. The response of the system, in the form of volts from the accelerometers, is sent to the computer via the signal conditioning box, otherwise known as signal condition and extended instrumentation, or SCXI, and a Data Acquisition card (DAQcard). A software program, LabVIEW 7.1 is then employed to write the data to a file.

5.3.2 SDOF-VSTMD experimental model

The SDOF model shown in Figure 5.7 (a) and (b) was investigated in the laboratory experiments, in which m_D, k_D amd c_D are the mass, stiffness and damping of the VSTMD, respectively and m_s, k_s and c_s are the mass stiffness and damping of the model structure, respectively. The SDOF model consists of 4 steel columns of fixed length 350mm, and a cross sectional area of 2.5mm by 25mm. The Young's modulus of the steel is 210kN/mm^2 and the top mass of the structure is 5kg. The TMD consists of a bar with two attached weights at the end. The length of the bar is 110mm with a diameter of 6mm and the circular weights have a diameter of 45mm and a width of 7.5mm. The total mass of the TMD is 165g, giving a mass ratio of $\alpha = 0.032$. The solenoid of the model VSTMD consists of a cylinder of length 50mm and a hollow section of diameter 7mm to allow the bar to pass through the solenoid without any friction. Two hundred and eighty turns of 1mm thick copper wire are placed around the cylinder and the ends of the copper wire are attached to the power supply to provide a current to the solenoid. The model is placed on the shaking platform, which is driven by an actuator controlled using a wave generator. The wave generator is programmed to produce a sine sweep from 0Hz to 7Hz, and the natural frequency of the structure can be obtained from the observed FRF. The accelerations are measured using two accelerometers placed at the top and the base of the structure.

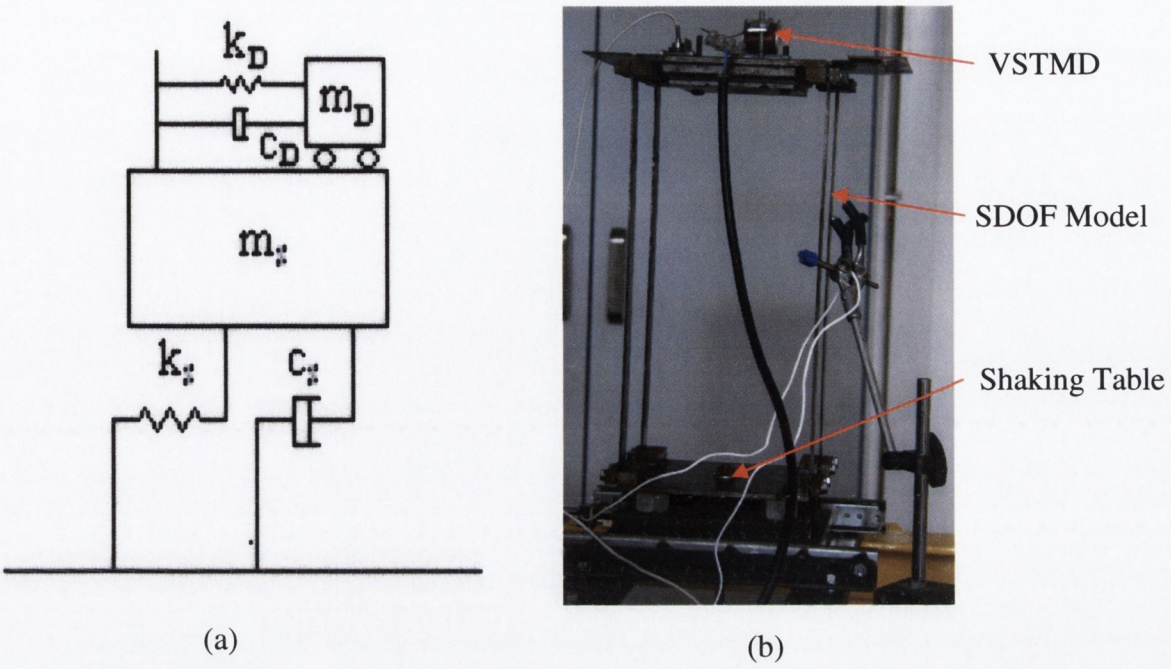

Figure 5.7 – SDOF structure

5.3.3 SCXI chassis, modules and terminal blocks

National Instruments SCXI is a high-performance signal conditioning and switching platform for measurement and automation systems. SCXI provides a single, integrated platform for a wide range of signal conditioning and switching needs, e.g. measure sensors or raw signals, generate voltages or currents, monitor digital lines, or route signals with switching. The SCXI box allows for the acquisition of analogue signals from thermocouples, resistive temperature devices (RTDs), strain gauges, voltage sources and current sources. Digital signals can also be acquired and generated for communication and control. The SCXI system consists of multi-channel signal conditioning modules installed in one or more chassis slots. Depending on the application requirement, the modules can perform analogue input, analogue output, digital I/O, and switching.

The SCXI chassis houses the SCXI modules, supplying power and controlling the data and control lines of the SCXI bus. The SCXI chassis is an aluminium box that contains an analogue bus, a digital bus and a chassis controller that regulates bus operation as shown in Figure 5.8. The chassis communicates with the DAQcard by transferring analogue signals along the analogue bus, which is connected from the

modules to the DAQcard. The digital bus controls chassis operation and is manipulated when the digital lines of the DAQcard communicate with the SCXI chassis controller. The SCXI chassis used for the experiments is the four slot SCXI-1000. It is powered with standard AC power and emits a low noise environment for signal conditioning and power and control circuitry for the modules.

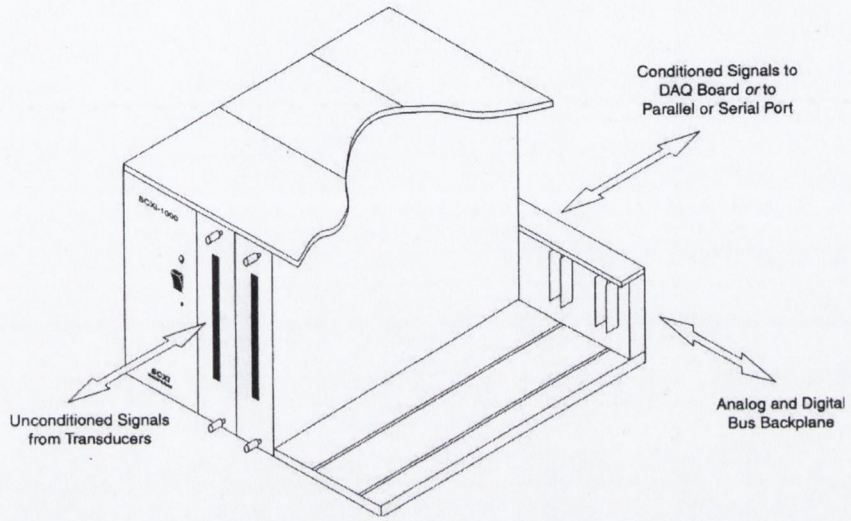

Figure 5.8 – SCXI Chassis

There are a number of different SCXI input and output modules that perform various operations. Analogue input modules can multiplex, amplify, filter and isolate voltage and current signals. The output modules allow the design of custom circuits such as signal conditioning and filtering networks to particular specifications. The modules can operate in parallel or multiplex mode. For example, if a module contains four input channels in parallel mode, these four channels are connected directly to four data acquisition board channels. In multiplexed mode, all four channels are multiplexed into a single data acquisition board channel. The advantage of multiplexing is that thousands of signals can be passed to the card through a signal module, allowing for extensive analysis to be carried out. However, the disadvantage is that there is now a limit on the scan rate of the number of signals to be acquired and if high scan rate is required, multiplex mode must be applied. As less than 4 channels are required for the experiment, the SCXI chassis is programmed in parallel mode.

For the experiment, the SCXI-1121 module, as shown in Figure 5.9, is used for the input of the voltage signal from the accelerometers. The SCXI-1121 consists of four

input channels and four excitation channels. The module contains 49 jumpers, which are denoted by the letter W in Figure 5.10. Jumpers W32, W38 and W44 are dedicated for communication between the DAQ board and the SCXI bus. The jumper configuration for each input channel is the same, and if one is changed, they all must be changed. Each input channel has two gain stages. The gain jumpers for each input channel are given in Table 5.1 and the gain setting and jumper position is given in Table 5.2

Input Channel Number	First Gain Jumper	Second Gain Jumper
0	W3	W4
1	W19	W20
2	W29	W30
3	W41	W42

Table 5.1 – SCXI 1121 gain jumpers for each input channel

Gain	Setting	Jumper Position
First Stage	1	D
	10	C
	50	B
	100	A (factory setting)
Second Stage	1	A
	2	B
	5	C
	10	D(factory setting)
	20	E

Table 5.2 – SCXI 1121 gain setting and jumper position

In order to determine the overall gain, the setting at the first gain stage is multiplied by the setting at the second gain stage. The gain for each channel is currently set at the factory setting, which results in an overall gain of 1000. Two-stage filtering is also available for the SCXI-1121. The first filter stage is located in the isolated section of the input channel, whereas the second filter stage is located in the non-isolated section of the input channel. The module is configured in this fashion so that the noise generated by the isolation amplifier is eliminated, which results in a higher signal to noise ratio. Two filter bandwidths 4Hz and 10kHz are available. Both stages must be set to the same bandwidth. Table 5.3 shows the configuration of the

filter jumpers and it is illustrated in Figure 5.10 that the first and second filter setting for each channel of the SCXI 1121 module is 4Hz.

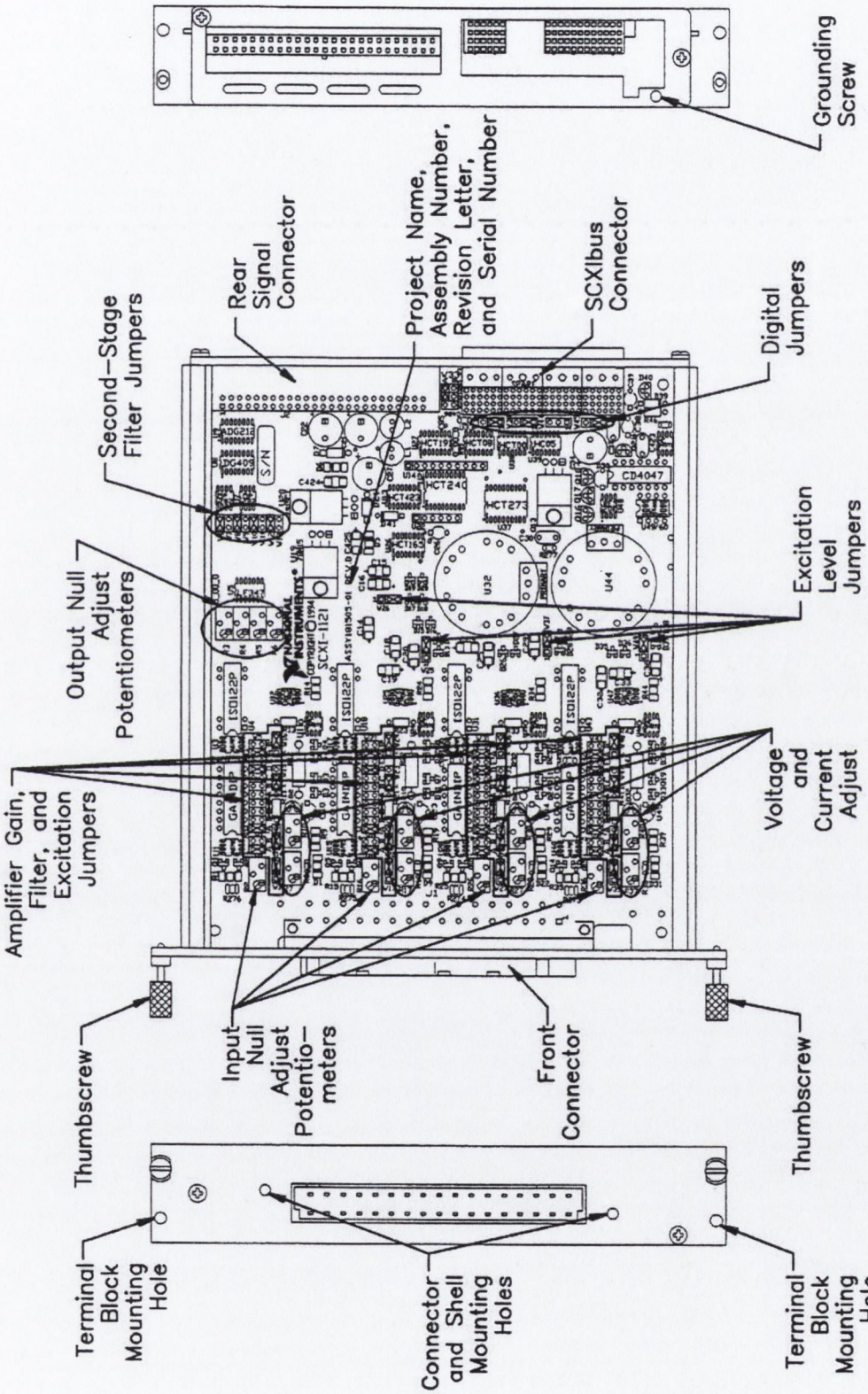

Figure 5.9 – SCXI 1121 module diagram

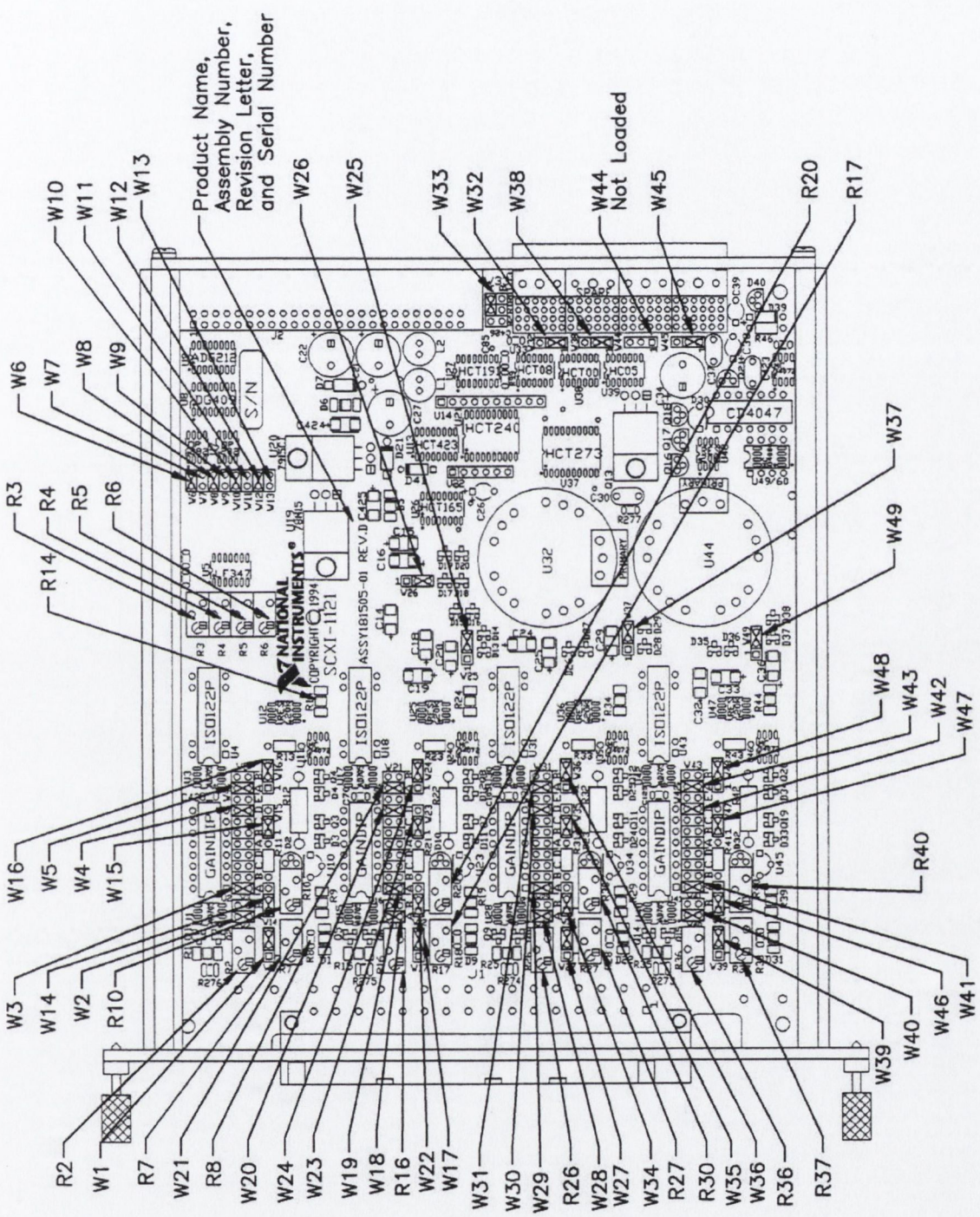

Figure 5.10 – SCXI 1121 jumper configuration

Input Channel	First Filter Jumper		Second Filter Jumper	
Number	4Hz (FS)	10kHz	4Hz (FS)	10kHz
0	W5-A	W5-B	W6	W7
1	W21-A	W21-B	W8	W9
2	W31-A	W31-B	W10	W11
3	W43-A	W43-B	W12	W13

Table 5.3 – SCXI 1121 filter settings and jumper position

For the experiments, the 1180 feedthrough panel is used to output a signal from LabVIEW 7.1 to the actuator via the control box. The module contains a front panel and a 50-pin cable assembly connected to the SCXI chassis as shown in Figure 5.11.

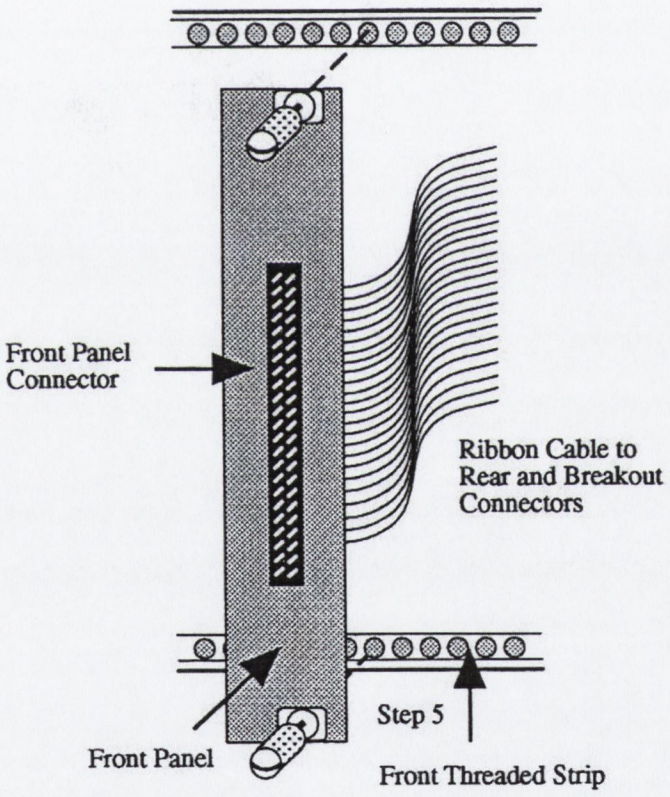

Figure 5.11 – SCXI 1180 feedthrough panel

SCXI terminal blocks are used to provide a quick and convenient method of connecting the input/output signals to the system and are attached directly to the front of the SCXI modules as shown in Figure 5.12. Terminal blocks can also provide additional signal conditioning.

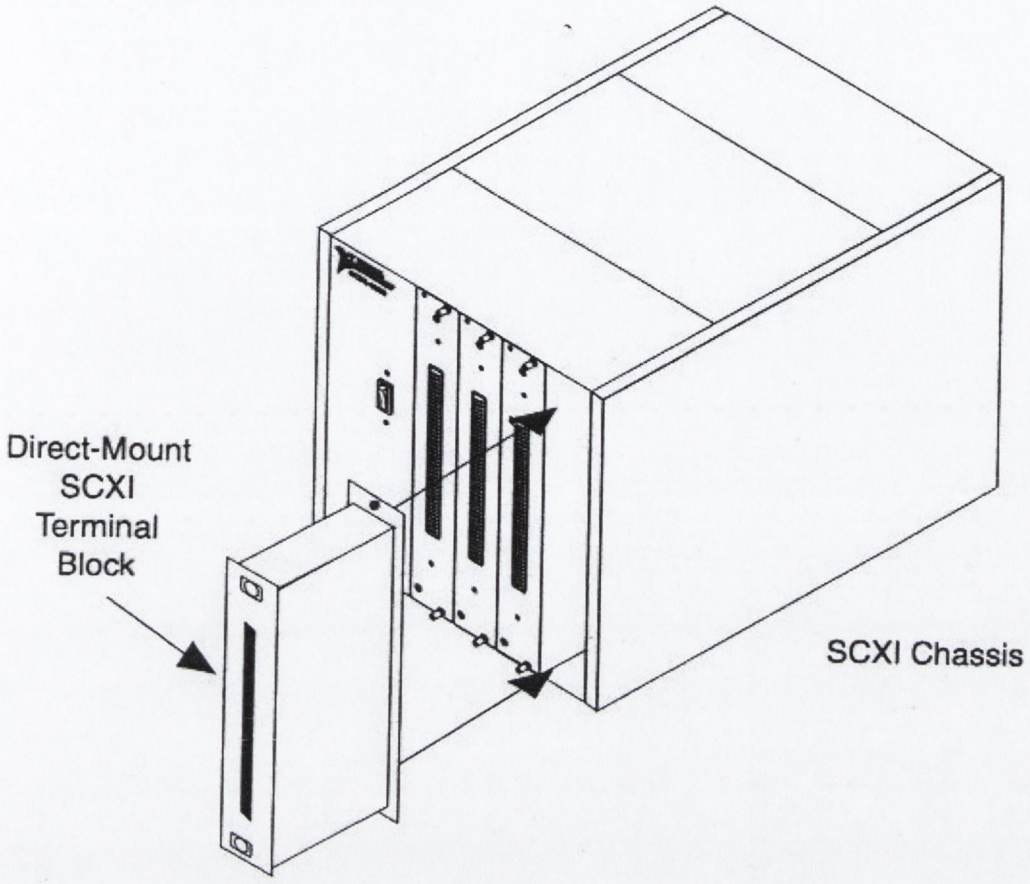

Figure 5.12 – SCXI terminal block set up

The 1321 terminal block is used for the SCXI 1121 chassis module. The terminal block has a removable cover for easy access and the configuration of the terminal block is shown in Figure 5.13. Each of the four channels denoted by Ch0 to Ch3 has two screw terminals for easy access to an external device such as an accelerometer, LVDT or strain gauge etc. For the experiment, Channel 1 and 2 are connected to the two accelerometers placed at the top and the base of the structure. The 1302 terminal block is attached to the 1180 feedthrough panel. Its configuration is similar to that of the 1321, with a number of screw terminals for easy access to the output channels.

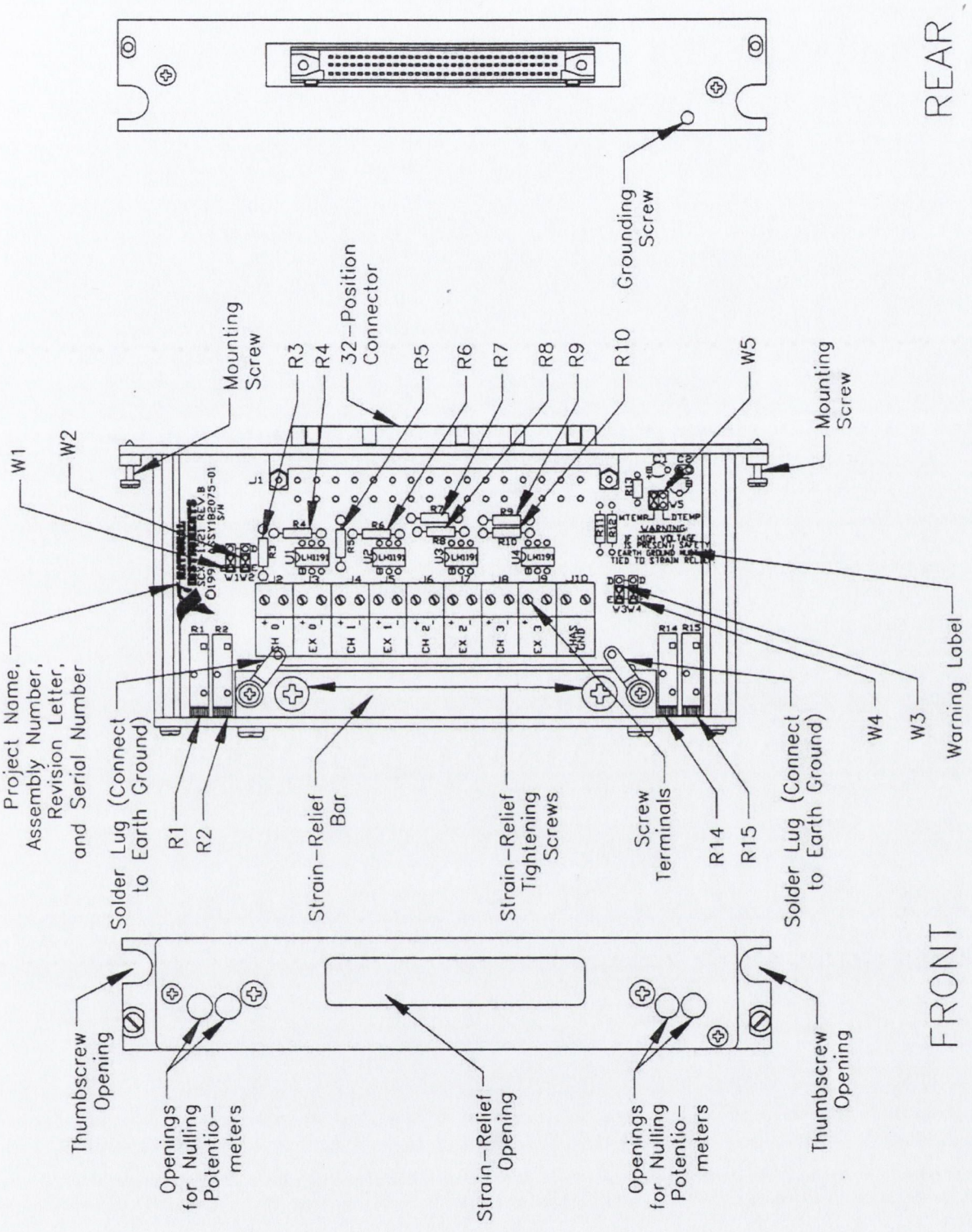

Figure 5.13 – SCXI 1321 terminal block

5.3.4 Data acquisition card

"Data acquisition is the process of gathering information in an automated fashion from analogue and digital measurement sources such as sensors and devices under test. Data acquisition uses a combination of PC-based measurement hardware and software to provide a flexible, user-defined measurement system" (www.ni.com). A national instruments data acquisition card (DAQcard), PCI-MIO-16E-1 is used to communicate between the software and the external voltage device. The DAQcard is placed in the computer, which is connected to an SCXI chassis as shown in Figure 5.14, which in turn is connected to the accelerometers, which record the response of the structure. This type of DAQcard is a multifunction analogue, digital and timing input/output card. The maximum speed of the card is 1.25Msamples per second ($1.25x10^6$ samples per second).

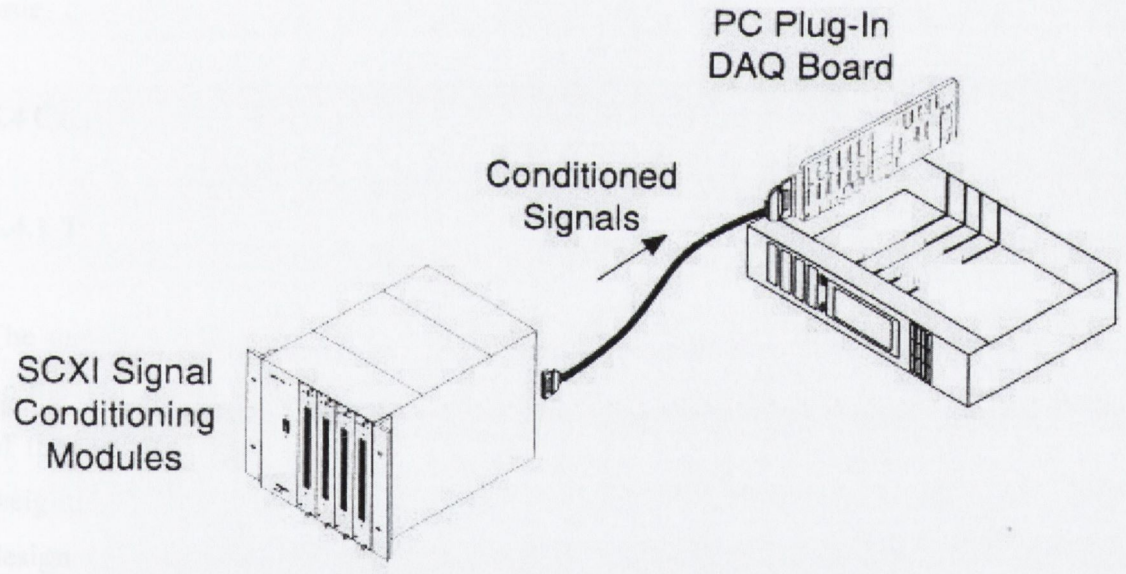

Figure 5.14 – DAQcard and SCXI chassis module

5.3.5 Labview 7.1

National Instruments LabVIEW is a software tool for designing test, measurement, and control systems. The LabVIEW environment interfaces with real world signals, analyzing data from external devices such as transducers, accelerometers, strain

gauges and many other voltage and current devices. LabVIEW can be used for test measurement and control of simple data acquisition programs or more complicated simulation and control systems. LabVIEW programs are called virtual instruments (VIs) because the user screen, otherwise known as the front panel, can be designed to look like an instrument, e.g. an oscilloscope depicting a waveform, and the underlying program, otherwise known as the block diagram, can perform many of the functions of instruments. The front panel contains knobs, push bottoms, graphs, controls and indicators; the data is entered on the front diagram, which instructs the block diagram. LabVIEW incorporates a hierarchical programming system. Each VI is made up of sub-Vis, which are in turn made up of more sub-VIs etc., so that a complicated application becomes a series of simpler sub-tasks. Debugging of the system is also easier as each sub VI can be executed by itself. Furthermore, many low level sub-VIs are common to a number of programs and therefore a set of standardized VIs can be developed. LabVIEW 7.1 itself has an extensive library of VIs for simple tasks in order to build many more complicated programs.

5.4 CHARACTERISATION OF VSTMD

5.4.1 Test set-up and execution

The mechanical spring was removed from the VSTMD, and the VSTMD was placed on the shaking platform, to which an excitation of 0-7Hz was applied. The response of the VSTMD was measured by an accelerometer attached to one of the circular weights. The circular weight with the attached accelerometer differed from that in the design specified in Section 5.3.2, so that the weight of the accelerometer was taken into account and the total mass of the VSTMD did not change. Static force deformation tests were first carried out for 0-6A of current passing through the solenoid. The dynamic response over the excitation frequency range was then recorded, again for 0-6A of current passing through the solenoid.

5.4.2 LabVIEW DAQ program

A simple program to acquire a waveform from an external voltage source was written in Labview 7.1 and the front and block diagrams are shown in Figures 5.15 and 5.16.

In the front diagram, the file name is specified, along with the maximum and minimum voltage input, the number of scans acquired and the rate at which they are acquired. The block diagram then takes the number of scans, outputs them to a graph in the front diagram and writes them to a text file for analysis.

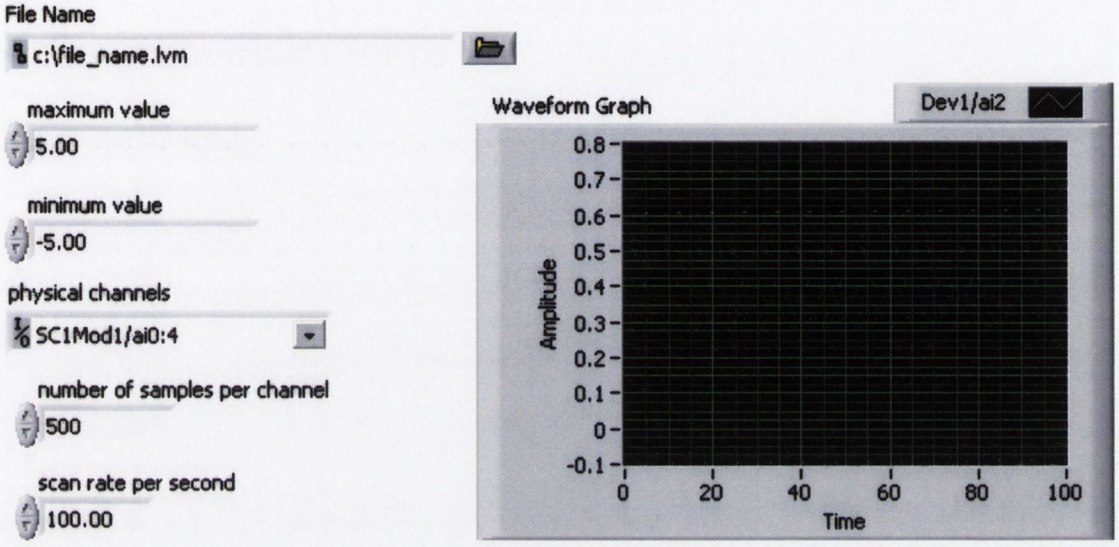

Figure 5.15 – Front diagram

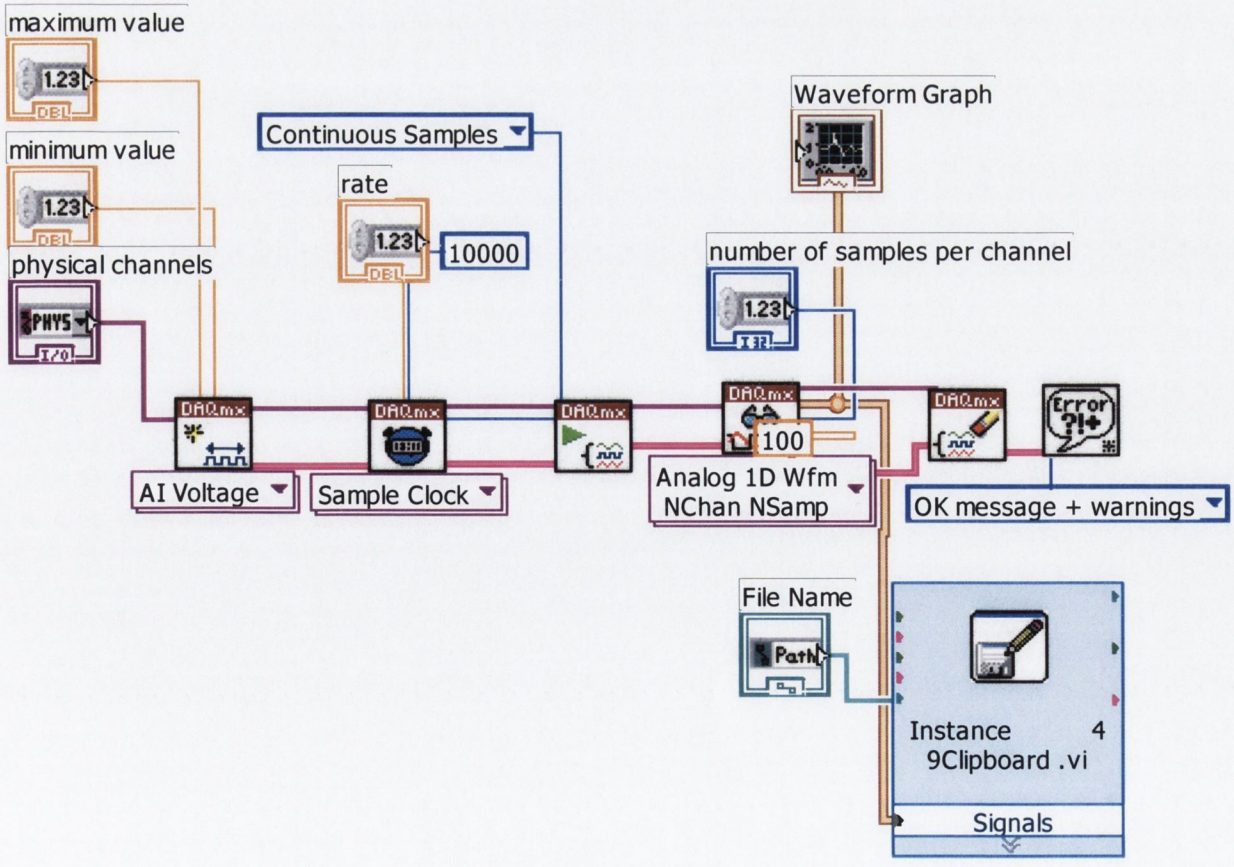

Figure 5.16 – Block diagram

5.4.3 Stiffness of VSTMD

5.4.3.1 Static response characterisation

A force was applied to one end of the VSTMD and the resulting displacement was measured. Figures 5.17 to 5.23 show the linear part of the cubic force-deformation graphs obtained for 0-6A of current passing through the solenoid.

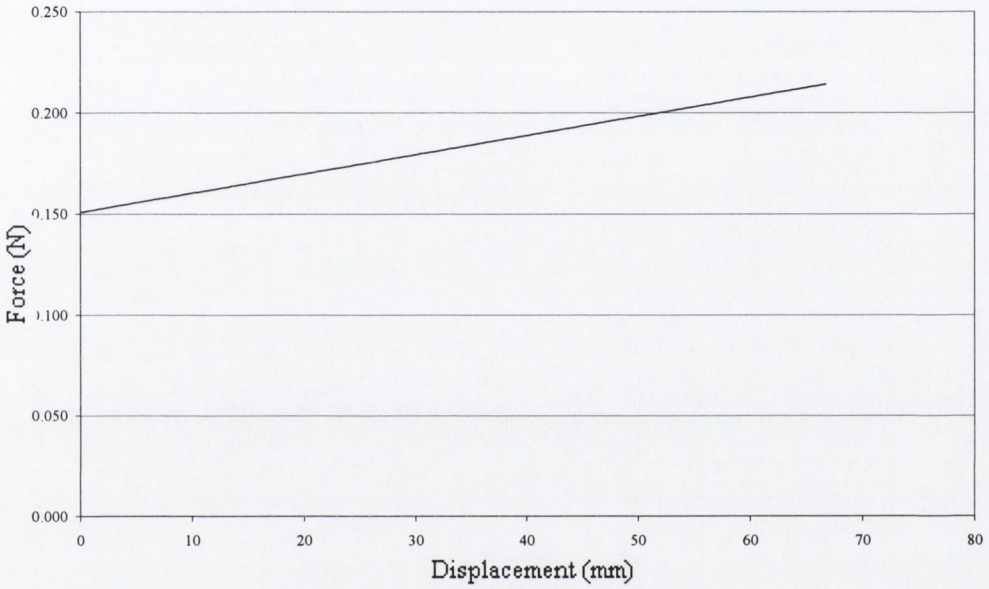

Figure 5.17 – Force deformation for 0A

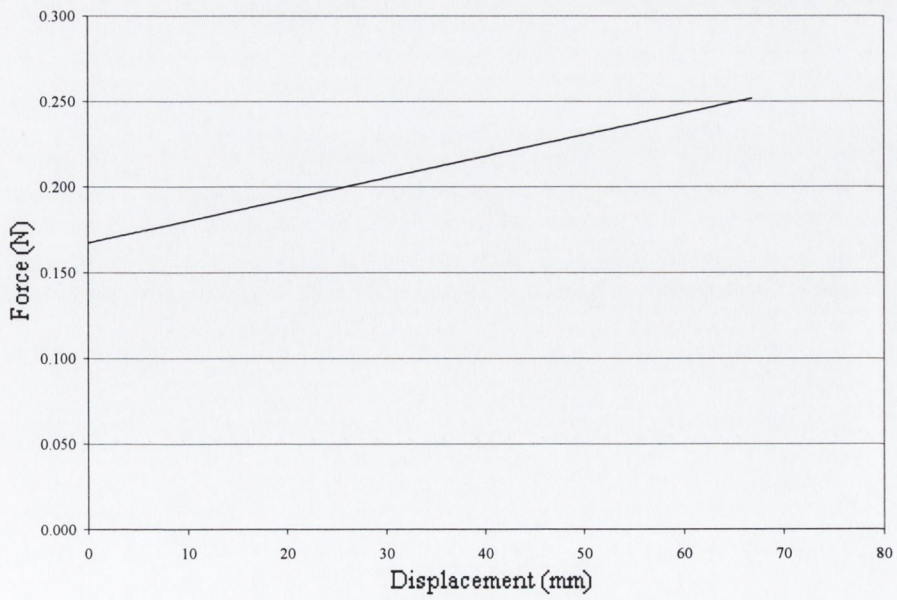

Figure 5.18 – Force deformation for 1A

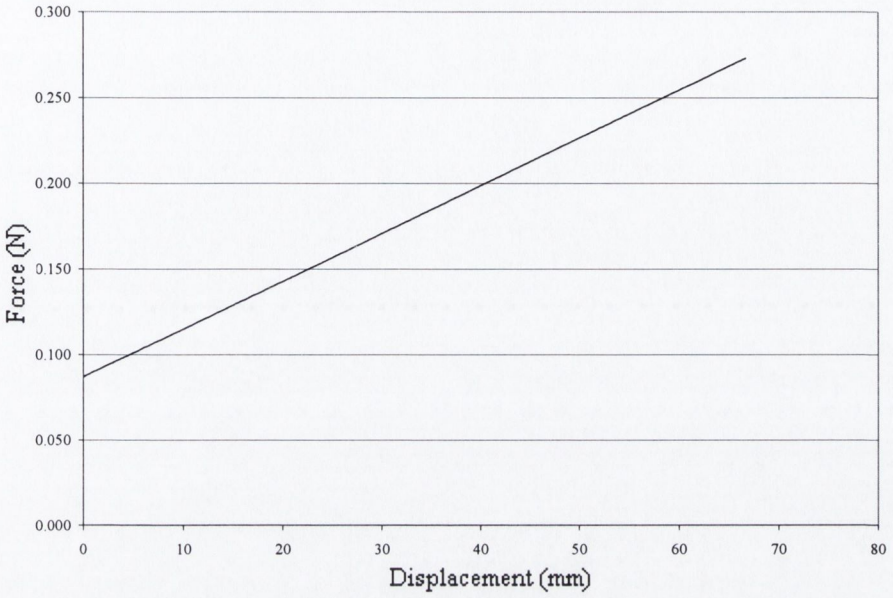

Figure 5.19 – Force deformation for 2A

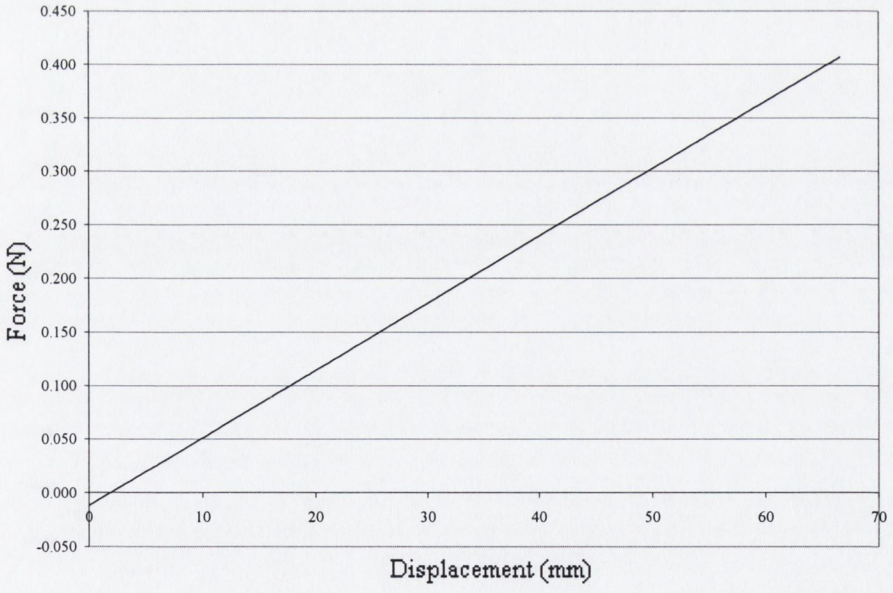

Figure 5.20 – Force deformation for 3A

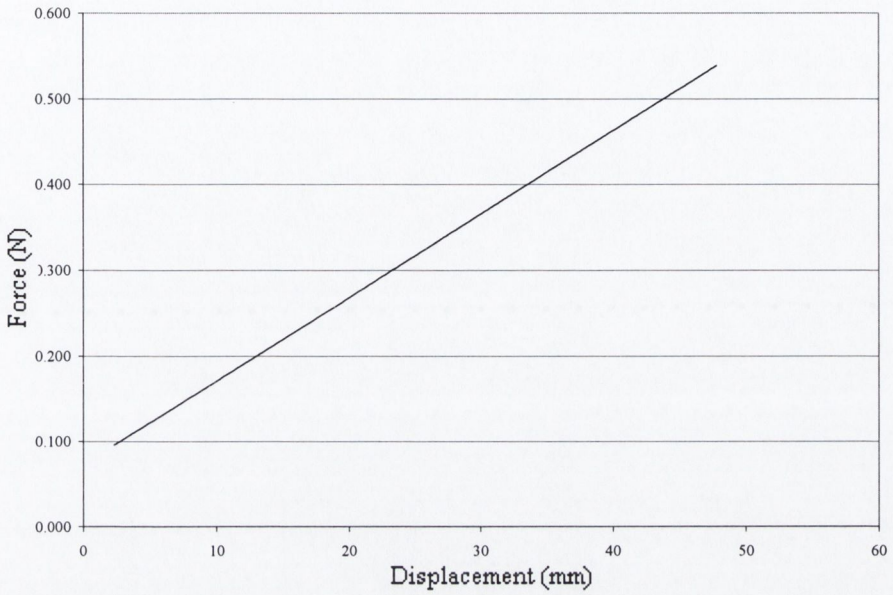

Figure 5.21 – Force deformation for 4A

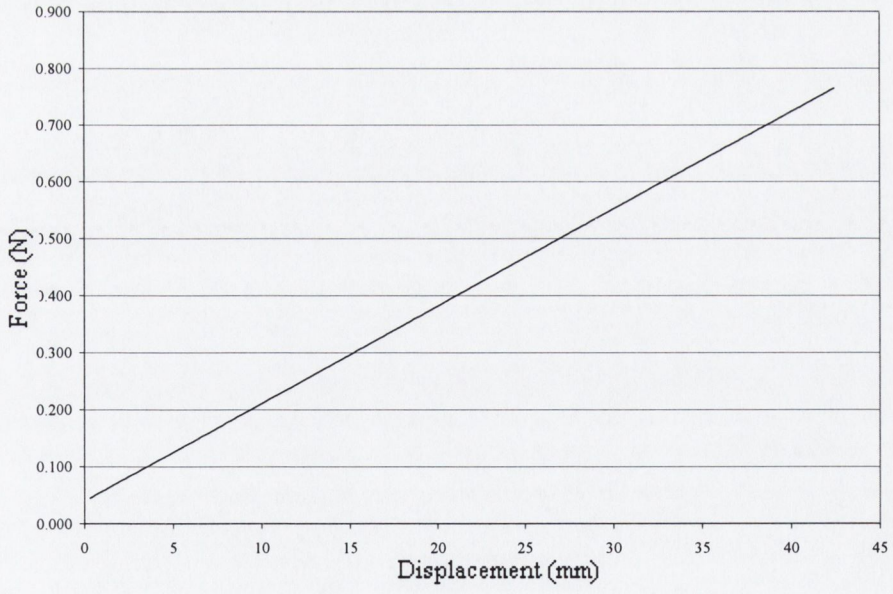

Figure 5.22 – Force deformation for 5A

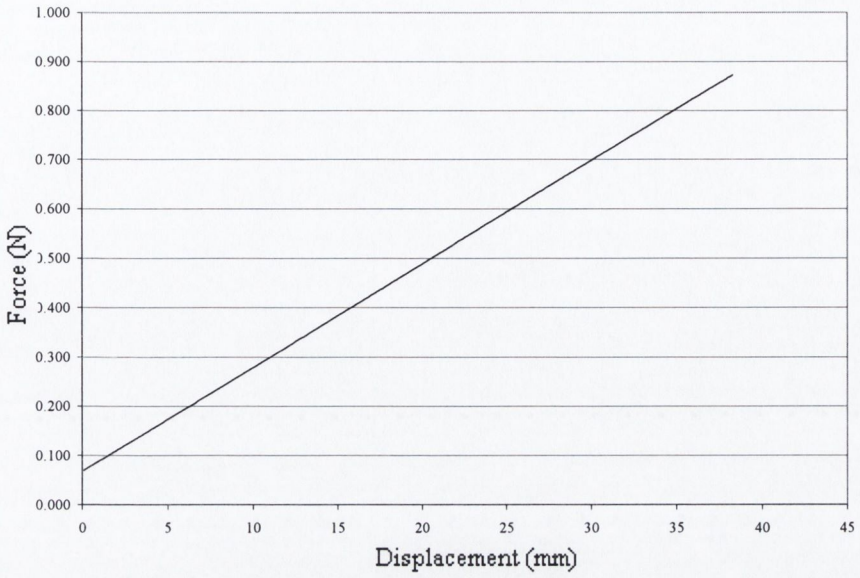

Figure 5.23 – Force deformation for 6A

The stiffness of the VSTMD is calculated from Eq (5.4). It would be expected that when no current passes through the solenoid, the VSTMD would have zero stiffness, however, friction effects and other external elements provide some stiffness to the VSTMD. The points at the start of the graph are ignored, as these include the friction required to initially push the VSTMD. The stiffness of the VSTMD with a current passing through the solenoid is compared to the stiffness of the VSTMD with no current passing through the solenoid. Table 5.4 presents the measured stiffness in each test, and the effective stiffness from 1 to 6A, removing the stiffness due to friction measured at 0A. It is observed in Table 5.4, that there is very little additional stiffness with 1A and 2A of current passing through the solenoid. The stiffness increases with current, achieving 19.5N/m with 6A of current. For current greater than 3A, a near linear trend is observed.

Current	Stiffness including friction (N/m)	Stiffness removing friction (N/m)
0A	3.21	-
1A	3.77	0.56
2A	4.09	0.88
3A	6.11	2.90
4A	11.3	8.09
5A	18.00	14.79
6A	22.70	19.49

Table 5.4 – Stiffness of VSTMD from static force deformation tests

5.4.3.2 Dynamic response characterisation

The VSTMD was placed on the shaking platform to which a frequency of 0 to 7Hz was applied. The force and displacement of the VSTMD were determined from the measured acceleration, using Eqs (5.2) and (5.3), and the stiffness was calculated from Eq (5.4). Figures 5.24 and 5.25 show the acceleration of the VSTMD for 0A and 6A of current passing through the solenoid. The acceleration of the shaking table is given in Figure 5.26, which remained the same for all tests.

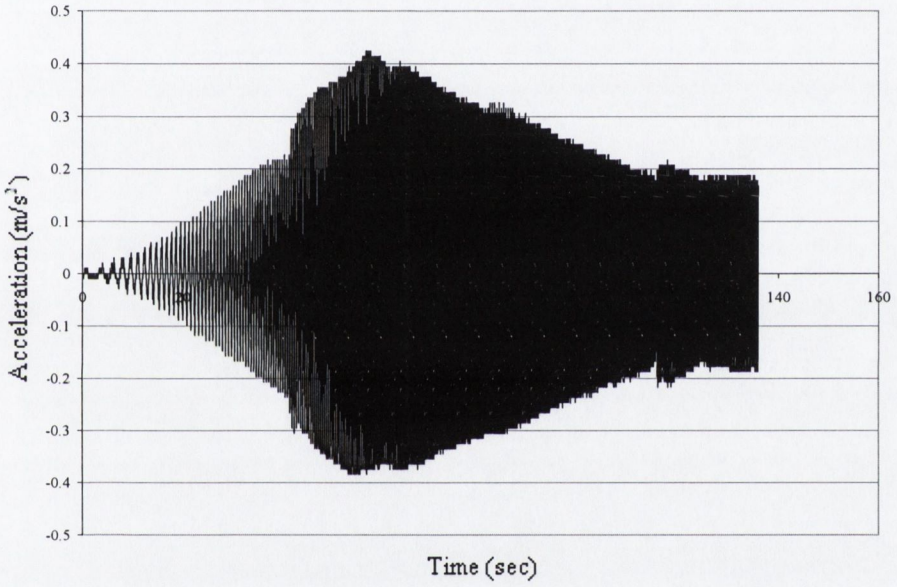

Figure 5.24 – Acceleration of VSTMD, 0A

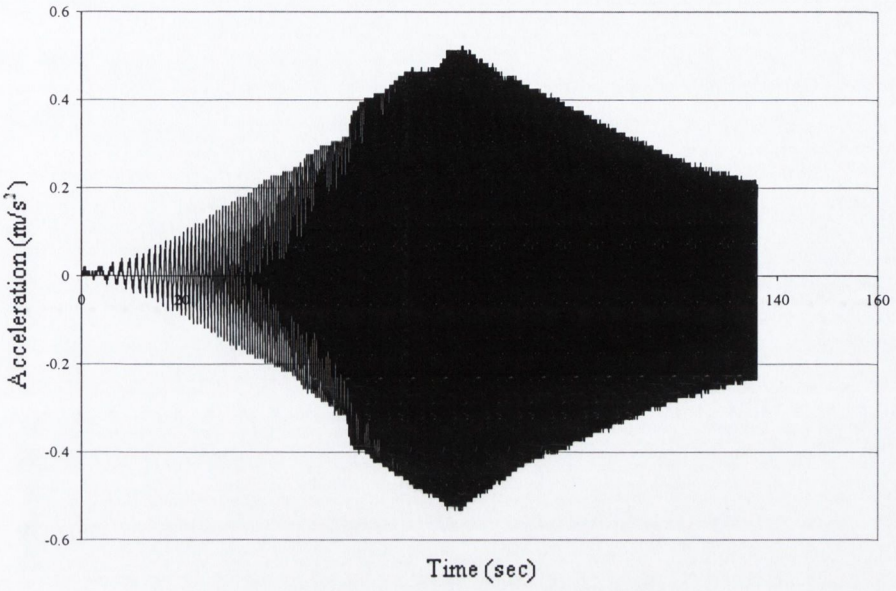

Figure 5.25 – Acceleration of VSTMD, 6A

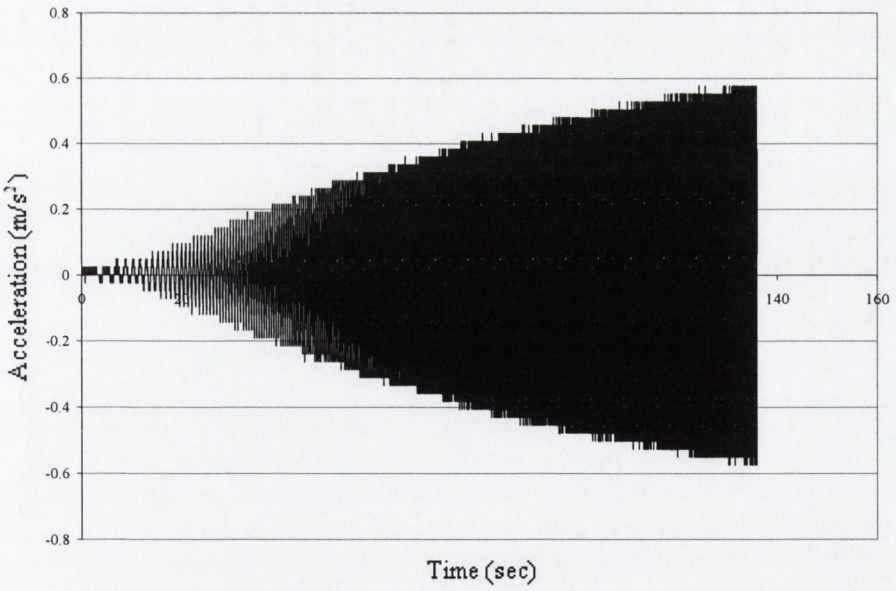

Figure 5.26 – Acceleration of shaking table

The stiffness of the VSTMD with current passing through the solenoid is compared to the stiffness of the VSTMD with no current passing through the solenoid, and the difference between the two is the additional stiffness of the VSTMD due to a particular level of current. Figures 5.27 to 5.33 show the variation in stiffness with input frequency for currents in the range 1 to 6A.

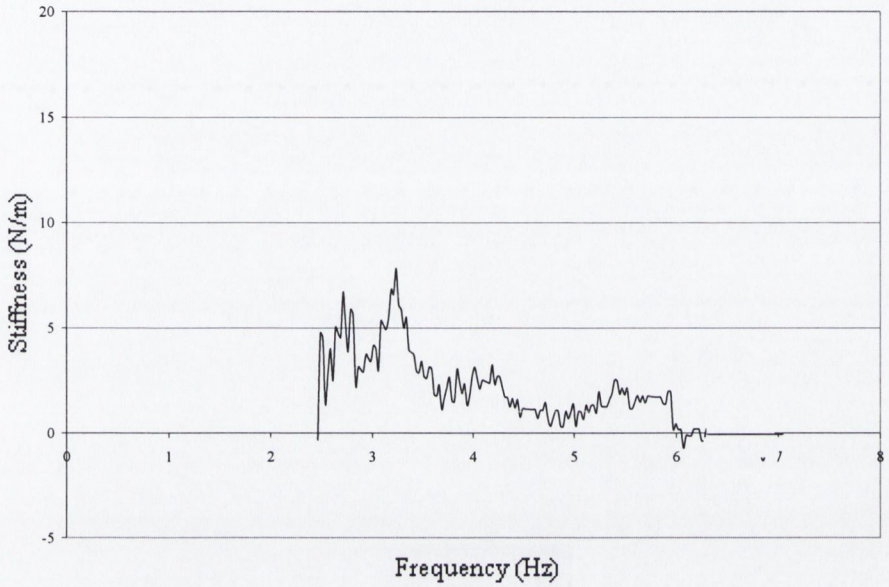

Figure 5.27 – Response of TMD with 1A

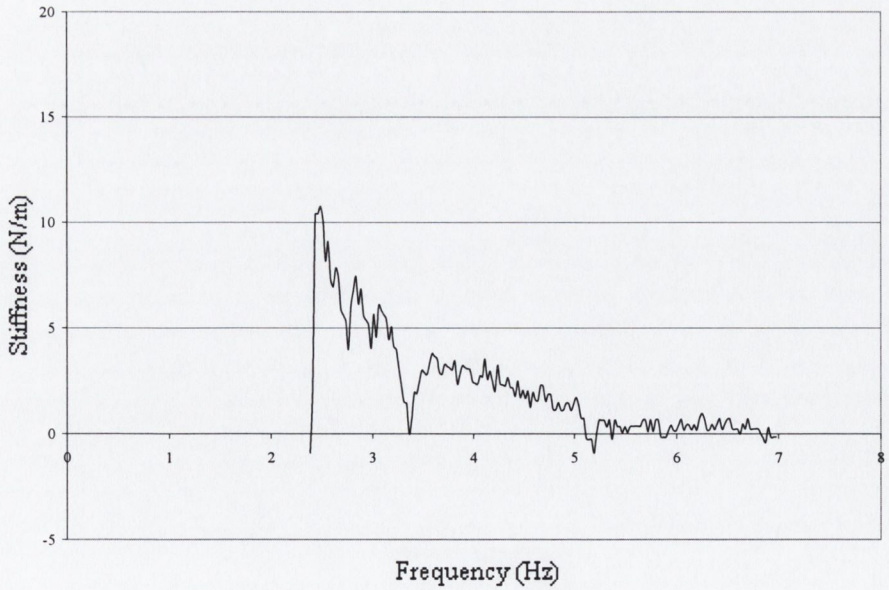

Figure 5.28 – Response of TMD with 2A

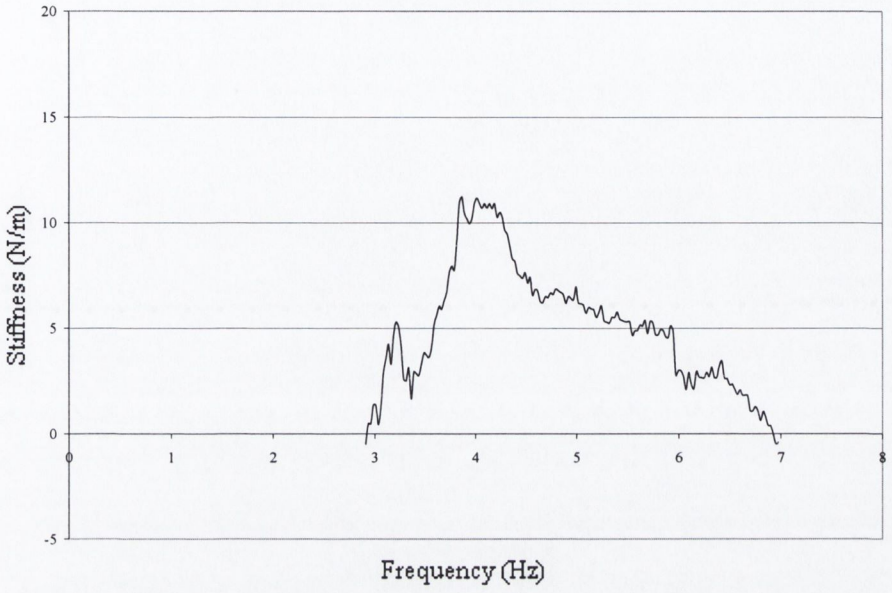

Figure 5.29 – Response of TMD with 3A

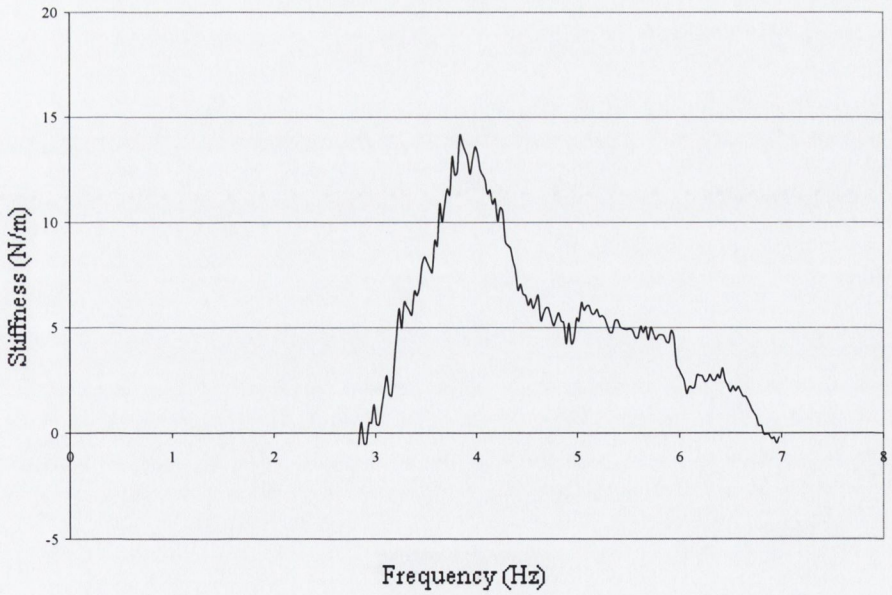

Figure 5.30 – Response of TMD with 4A

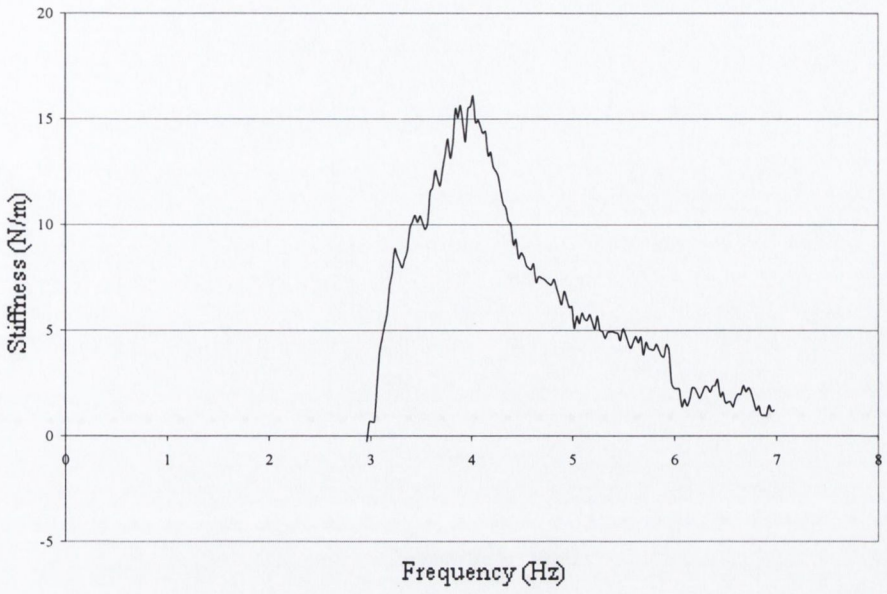

Figure 5.31 – Response of TMD with 5A

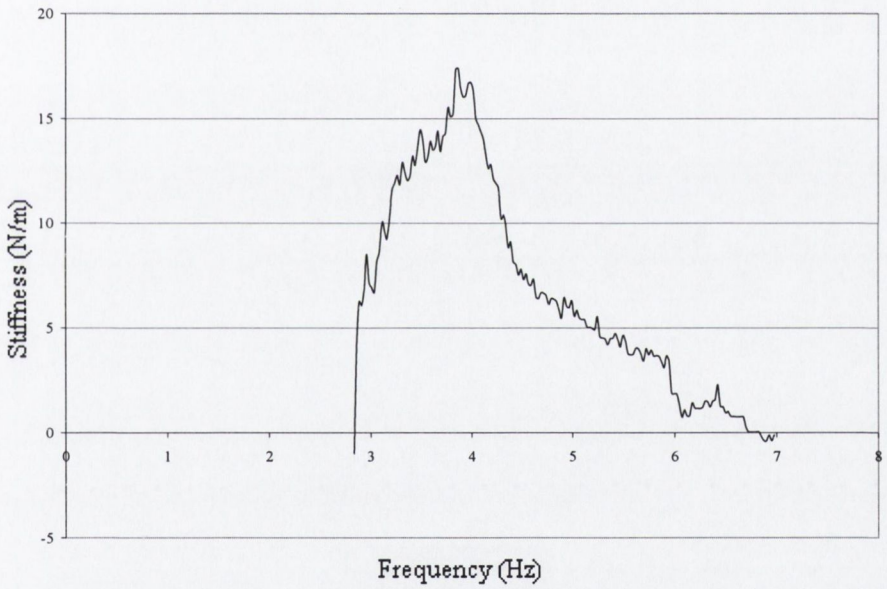

Figure 5.32 – Response of TMD with 6A

It is observed from these graphs, that the stiffness of the VSTMD only starts to increase above 2.5Hz. Below 2.5Hz, the computed stiffness is nearly zero and is not considered. Therefore, the prototype VSTMD would not be appropriate for structures with fundamental natural frequencies less than 2.5Hz. It is also observed that the stiffness of the VSTMD varies with excitation frequency. Apart from the graphs of 1 and 2A, the VSTMD reaches a peak in the stiffness at approximately 4Hz. As the magnetic field at 1 and 2A is not as strong as the field developed by 3A or more, influences such as friction and external elements will have been stronger in these

plots. This was also observed in the static force deformation tests. It is noted that the plots in Figures 5.27 and 5.28 are not as smooth, which also suggests friction interference.

The peak stiffness observed close to 4Hz increases with current: for 1A the peak stiffness is 7N/m and for 6A, the peak is 17N/m. Figure 5.33 shows the variation with current of the average stiffness of the VSTMD close to 4Hz. For currents greater than 3A, a near linear trend is again observed. From Figure 5.33, it is also observed that the stiffness of the VSTMD at higher values of the current is close to the values obtained in the static force deformation tests. In further testing, applying a current greater than 6A caused the solenoid to overheat. Further development of the solenoid could be carried out to develop a more efficient and elaborate design.

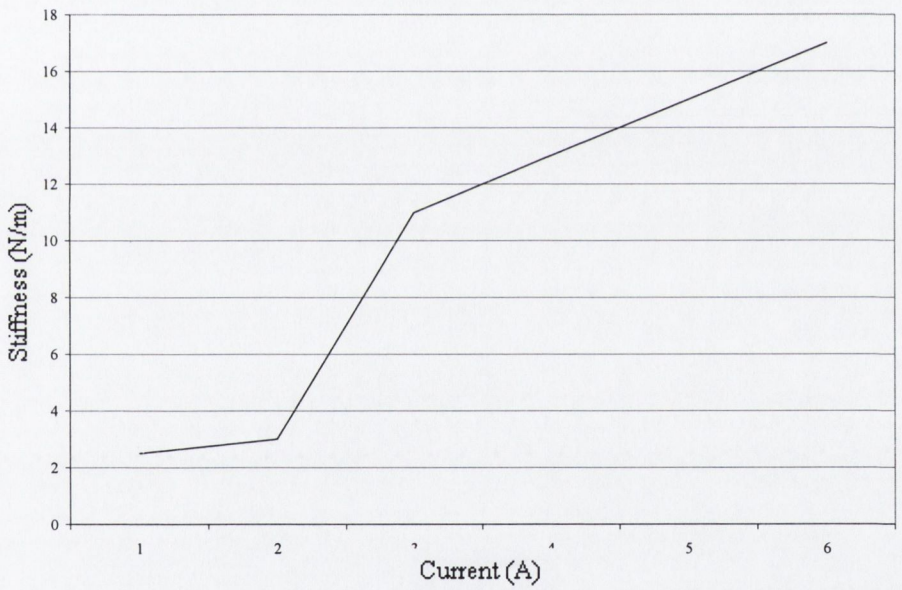

Figure 5.33 – Variation with current of average stiffness of VSTMD close to 4Hz

5.4.4 Damping of the VSTMD

To determine the effect of the solenoid current on the damping in the TMD, the logarithmic decrement method was applied to find the value of the damping ratio, ζ_d from free vibration decay curves. The spring was re-attached to the VSTMD and the VSTMD was compressed to a pre-determined point, and released so that it oscillated freely. The value of ζ_d at 0A is assumed to be zero, and the difference in damping

observed with other currents is the additional damping due to the VSTMD. Three tests were carried out at each level of current, and the average value obtained. Figure's 5.34 and 5.35 show the free vibration decay curve for the TMD with 0A and 6A. It is noted that the time of decay for 0A (1.25 seconds) is greater than that for 6A (1 second); this is caused by the friction in the TMD. When the magnetic field in the solenoid is strong, the mass of the TMD is pulled towards the centre of the solenoid. The force created by the magnetic field is stronger than the friction in the VSTMD and therefore for higher values of current passing through the solenoid, the free vibration curve decays quicker.

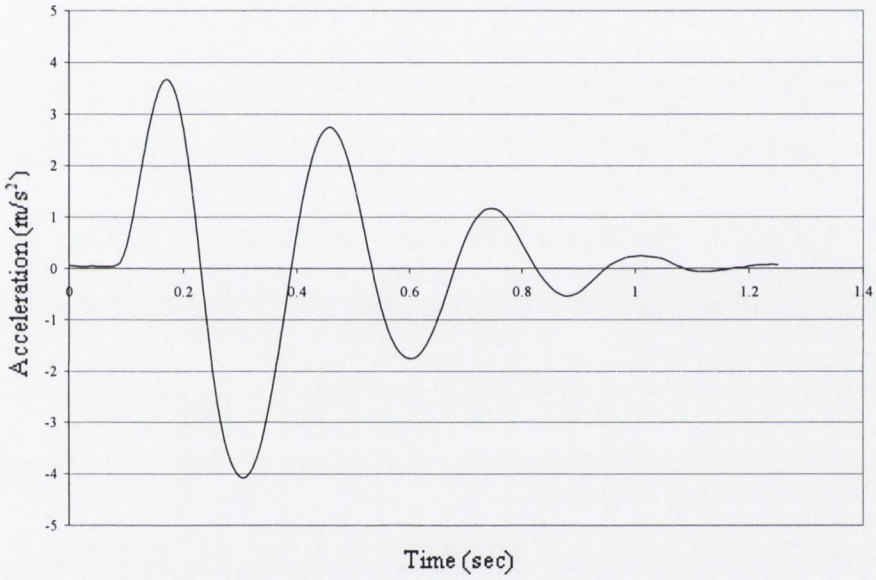

Figure 5.34 – Free vibration curve VSTMD with 0A

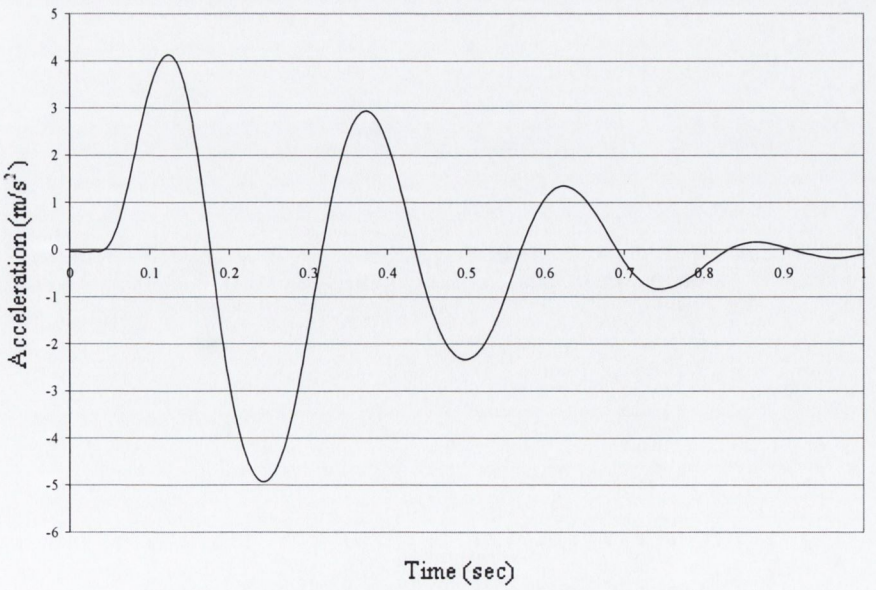

Figure 5.35 – Free vibration curve VSTMD with 6A

The value of the first peak is denoted by u_p and the next by u_q. The value for ζ_d is calculated from

$$\zeta_d = \frac{1}{2\pi} ln \left| \frac{u_q}{u_p} \right| \tag{5.5}$$

As the VSTMD is compressed and released manually, it is difficult to ensure this is carried out in the same way each time. Therefore, in each test, the second and third peaks of the graph are used in the calculations, as it is known that the VSTMD is oscillating freely at these points. The resulting ζ_d values are shown in Table 5.5; it is observed that the damping ratio is small at all levels of current, and that the variation with current shows no trend. Hence it may be assumed that the solenoid makes no significant contribution to the viscous damping in the VSTMD.

	1A	2A	3A	4A	5A	6A
ζ_d(%)	0.860	1.544	0.987	1.153	0.072	0.878

Table 5.5 – Values of damping ratio with additional current

5.5 EXPERIMENTAL ANALYSIS

5.5.1 Passive control of the structure

The SDOF structure was first tested without the VSTMD to determine the natural frequency of the structure. It is clear from the FRF shown in Figure 5.36 that this natural frequency ω_n is equal to 3.71Hz. The TMD is first tuned to the structure using the formula given in Eq (3.30) and the value of the tuning parameter is obtained using the minimax principle. From this, it is determined that the value of stiffness required in the VSTMD is 84N/m. The closest spring stiffness available was 80N/m and therefore this was employed in the VSTMD. The FRF of the acceleration response of the structure with this TMD is shown in Figure 5.37. The FRF has two peaks and is only slightly mistuned from the minimax principle, due to the use of an 80N/m spring. However, the response of the structure has reduced by 60% compared to Figure 5.36, and therefore it is not necessary to change the stiffness of the VSTMD to reduce the

response further. The FRF of the acceleration of the VSTMD with 0A, is shown in Figure 5.38.

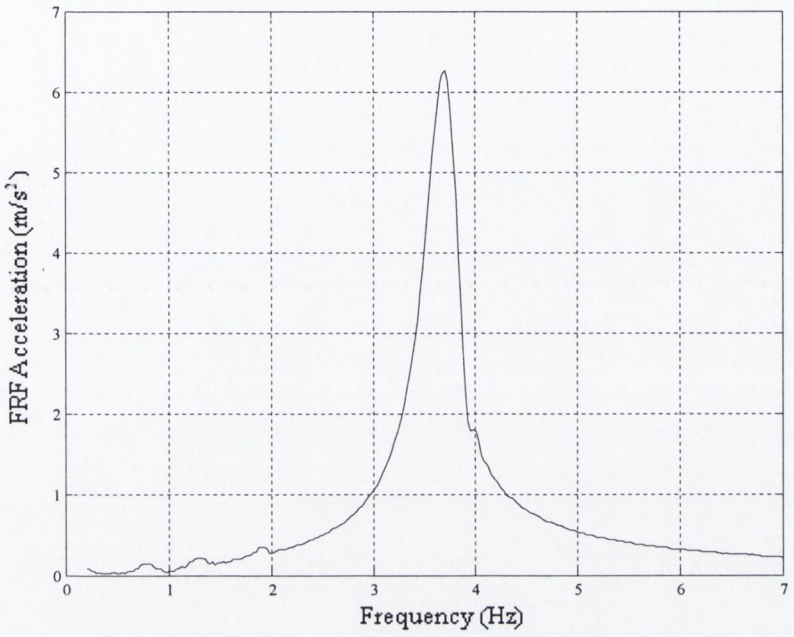

Figure 5.36 – FRF of SDOF structure with no TMD

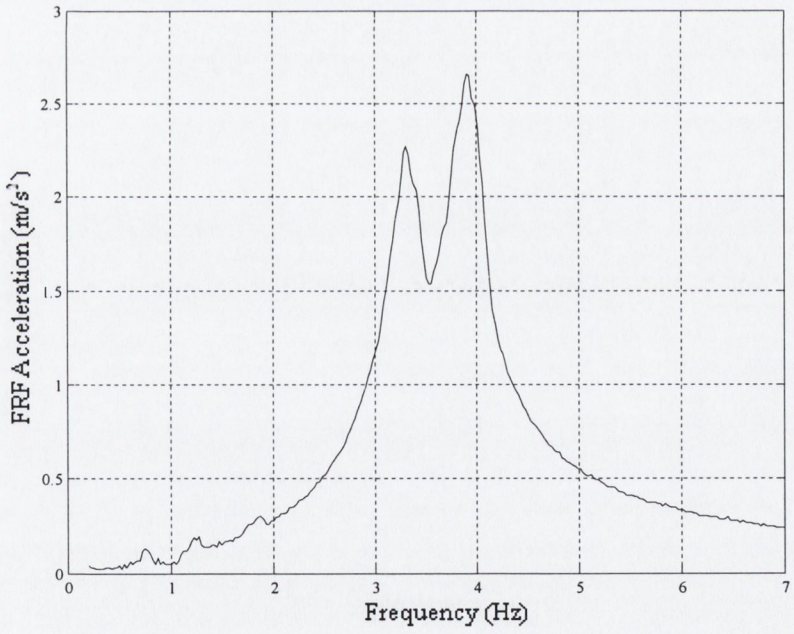

Figure 5.37 – FRF of SDOF structure with tuned TMD

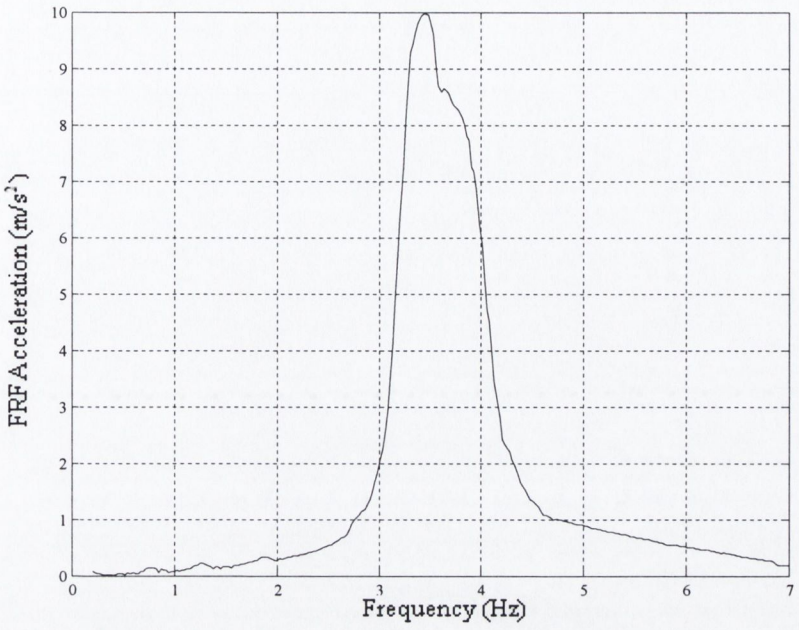

Figure 5.38 – FRF for acceleration of VSTMD with 0A

A spring of stiffness 60N/m was employed to deliberately mistune the VSTMD, allowing the effects of the addition of current to the solenoid to be studied. This spring was approximately 10mm shorter than the 80N/m spring it replaced. Due to limitations on the travel of the VSTMD, this meant that the amplitude of the base excitation had to be reduced. The response of the structure, without the VSTMD, to this reduced amplitude excitation is shown in Figure 5.39. Figure 5.40 shows how the addition of the mistuned VSTMD resulted in one peak in the FRF at 3.83Hz, and the response of the structure being reduced by only 30% (as compared to 60% with the tuned damper). Figures 5.41 and 5.42 show that the addition of the VSTMD with 1A or 2A did not reduce the response of the structure any further, as the peaks of the response are close to that in Figure 5.40. This agrees with the results of the VSTMD characterisation described earlier, when currents of 1A or 2A had little or no stiffness. Figure 5.43 shows that when 3A was passed through the solenoid, the peak of the response shifted to 3.88Hz and the response of the structure reduced by 41%. With currents of 4A and 5A passing through the solenoid, Figures 5.44 and 5.45 show a second peak beginning to form between 3.4 and 3.7Hz, with peak response reductions of 46% and 53%, respectively. Figure 5.46 shows that with 6A of current passing through the solenoid, two peaks form in the FRF (at 3.5Hz and 3.96Hz) and the response of the structure is reduced by 58%, which is approximately the same

reduction observed with the tuned VSTMD. In the static force-deformation tests, the addition of a current of 6A increased the stiffness of the VSTMD by 19.49N/m, which when added to the spring stiffness of 60N/m suggests a tuned TMD stiffness of 80N/m. Similarly, in the dynamic force-deformation tests, the addition of a current of 6A increased the stiffness of the VSTMD by a maximum of 17N/m at 4Hz, which again suggests tuning of the TMD to the natural frequency of the structure.

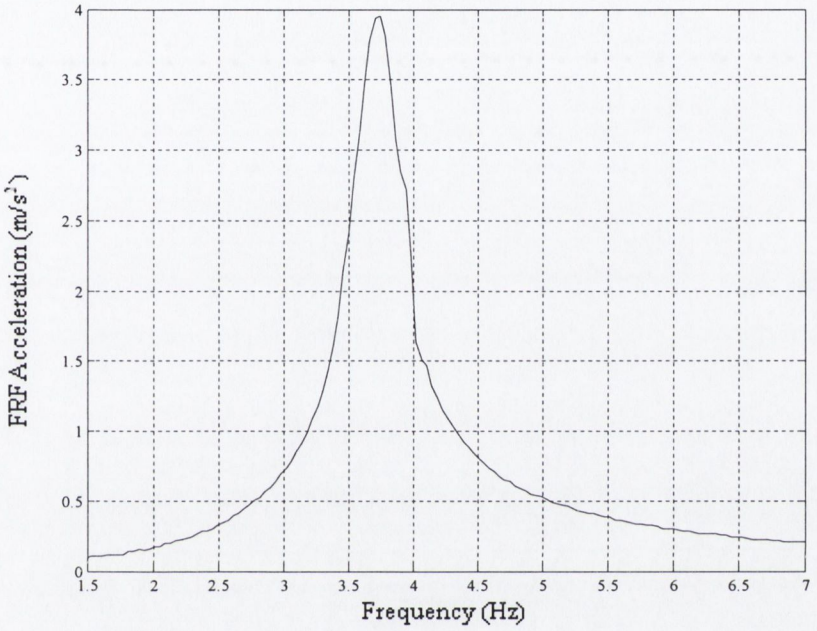

Figure 5.39 – FRF of SDOF structure without TMD

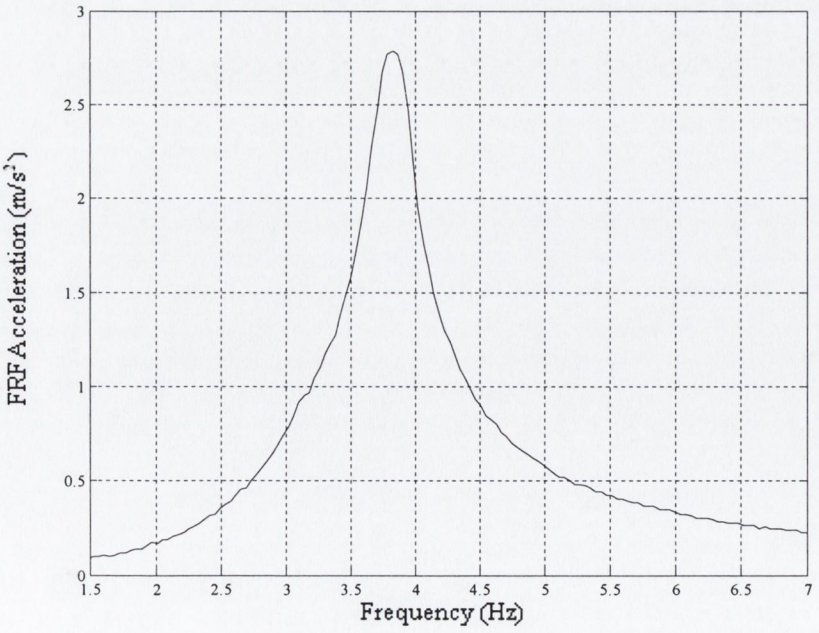

Figure 5.40 – FRF of SDOF structure with mistuned TMD

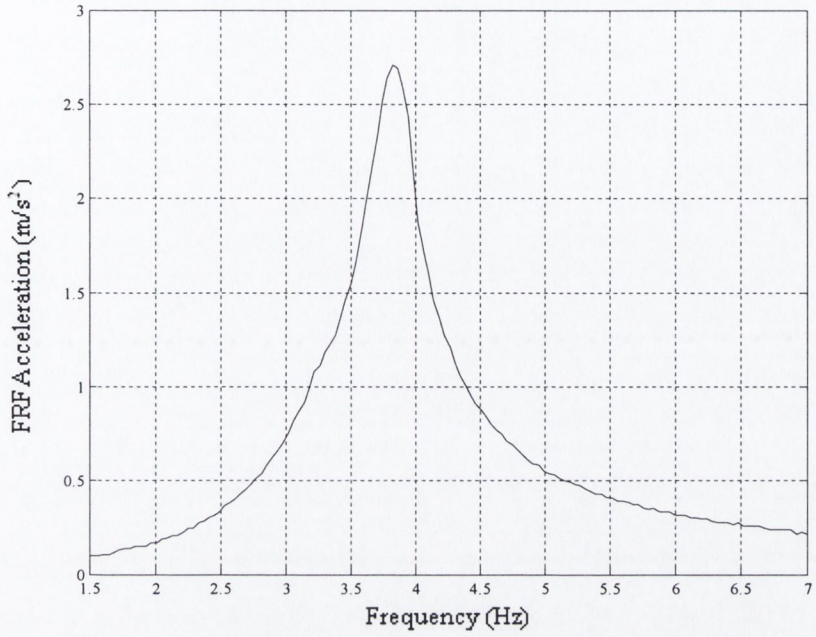

Figure 5.41 – FRF of SDOF structure with mistuned TMD and 1A

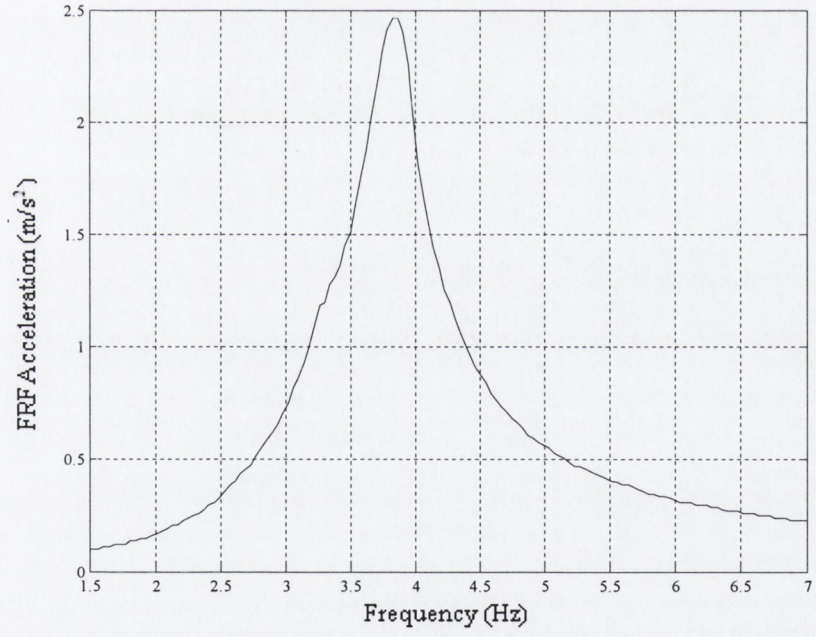

Figure 5.42 – FRF of SDOF structure with mistuned TMD and 2A

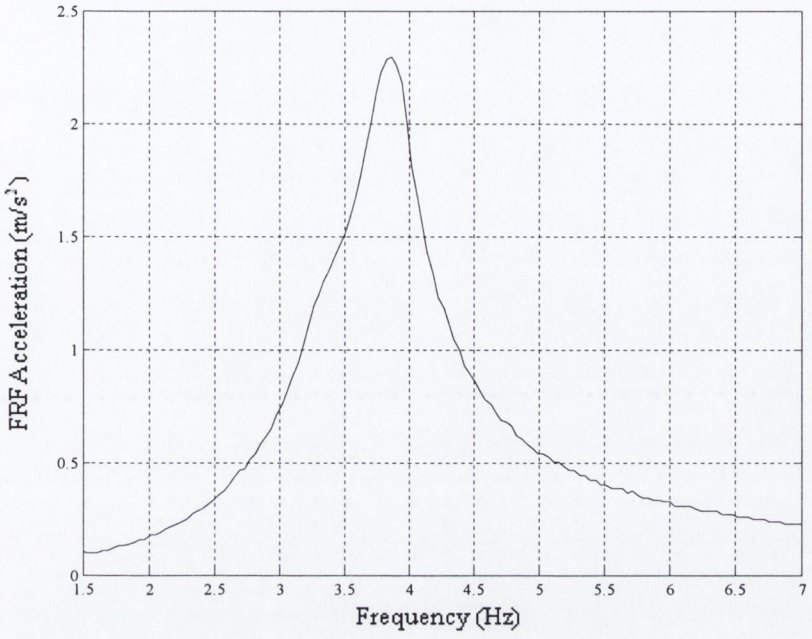

Figure 5.43 – FRF of SDOF structure with mistuned TMD and 3A

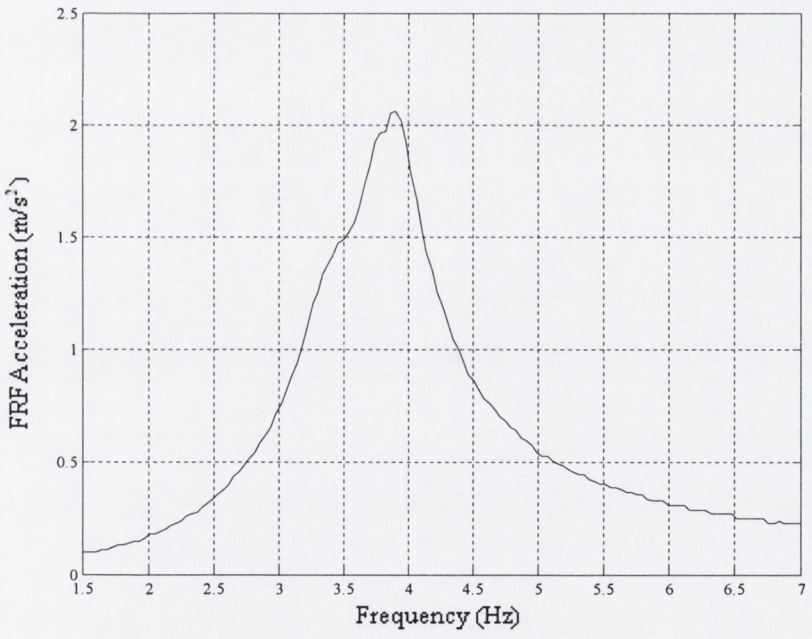

Figure 5.44 – FRF of SDOF structure with mistuned TMD and 4A

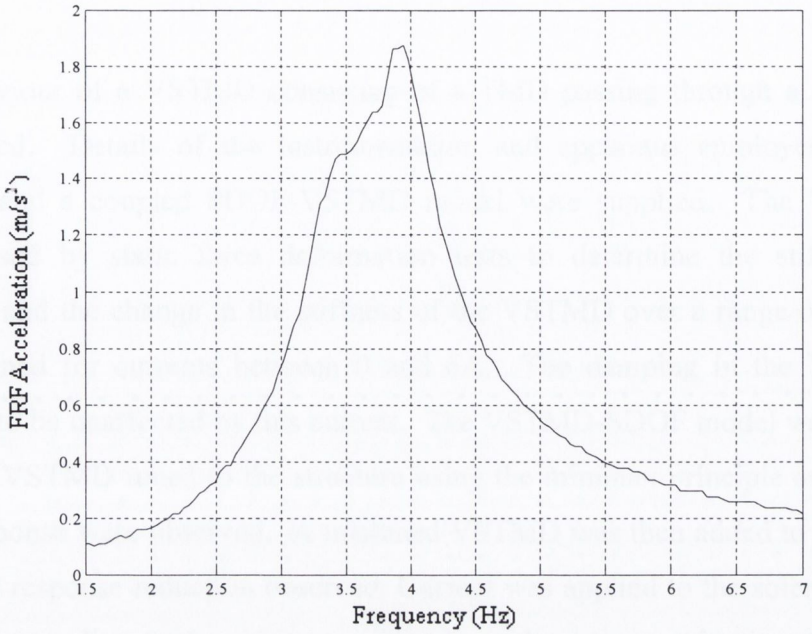

Figure 5.45 – FRF of SDOF structure with mistuned TMD and 5A

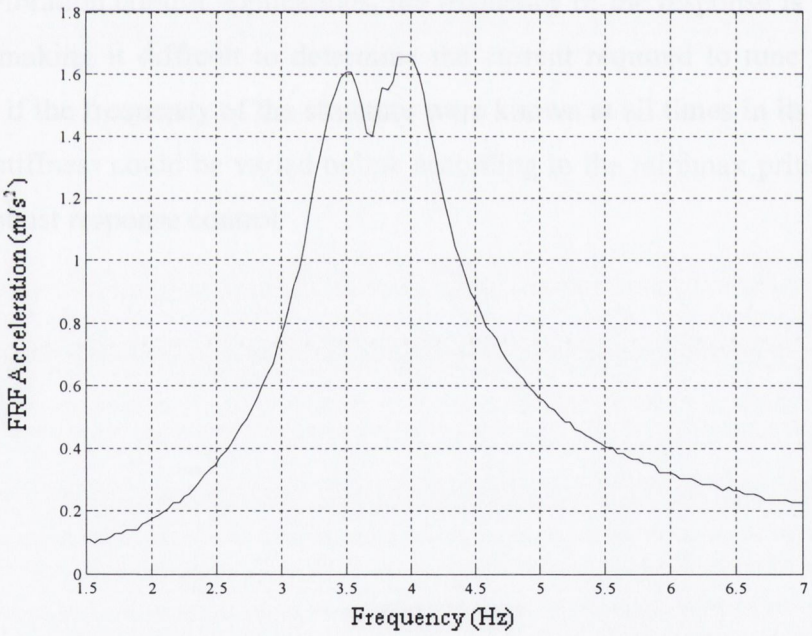

Figure 5.46 – FRF of SDOF structure with mistuned TMD and 6A

5.6 CONCLUSION

The behaviour of a VSTMD consisting of a TMD passing through a solenoid was investigated. Details of the instrumentation and apparatus employed to test the VSTMD and a coupled SDOF-VSTMD model were supplied. The VSTMD was characterised by static force deformation tests to determine the stiffness of the VSTMD, and the change in the stiffness of the VSTMD over a range of frequencies was obtained for currents between 0 and 6A. The damping in the VSTMD was observed to be unaffected by this current. The VSTMD-SDOF model was tested with a passive VSTMD tuned to the structure using the minimax principle and reductions in the response were observed. A mistuned VSTMD was then added to the structure, and lower response reduction observed. Current was applied to the solenoid to retune the TMD according to the minimax principle, and response reduction similar to that achieved by the tuned TMD was observed.

In many vibration control applications, the frequency of the response is not known in advance, making it difficult to determine the current required to tune the VSTMD. However, if the frequency of the structure were known at all times in its response, the VSTMD stiffness could be varied online according to the minimax principle, leading to more robust response control

CHAPTER 6

EXPERIMENTAL RESULTS FOR ONLINE VSTMD

6.1 INTRODUCTION

An online VSTMD is now investigated in this chapter, where the VSTMD is retuned in real time. A VSTMD was introduced in Chapter 5. The VSTMD was tested offline, i.e. the frequency response of the structure was known in advance and the VSTMD was tuned accordingly and experimentally tested leading to reduction in vibration of the structure. A real time wavelet based algorithm is used to detect the dominant frequency from the structural response and the VSTMD is appropriately tuned.

6.2 VSTMD BASED ON AMPLITUDE RESPONSE

6.2.1 Principle

The response of the model structure is measured at interval time steps. Based on this response, a current is applied to the solenoid, which ensures that the VSTMD obtains the stiffness required to retune it according to the minimax principle. A sine sweep base excitation from 0 to 7Hz and a random white noise excitation are applied. Figure 6.1 shows the time history of the acceleration response of the model structure with no TMD, under a sine sweep excitation of 0 to 7Hz.

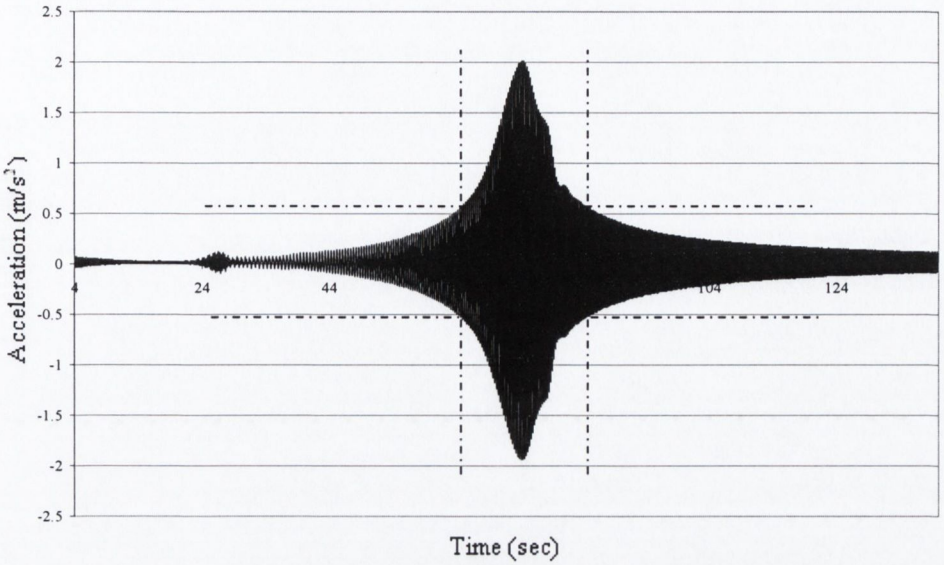

Figure 6.1 – Time history of model structure with no TMD

It can be observed from the FRF of the structure with no TMD, given in Figure 5.19, that the resonant condition of the response of the structure lies between 3.25 and 4.25Hz. From Figure 6.1, it is shown that this region occurs between 65 and 85 seconds of the response. The response before and after these points is small, hence control is only required when the response is greater than $0.55m/s^2$ or less than $-0.55m/s^2$, as shown in Figure 6.1. The mistuned TMD, described in Section 5.5.1 is now added to the structure and the resulting time history of the acceleration response is shown in Figure 6.2.

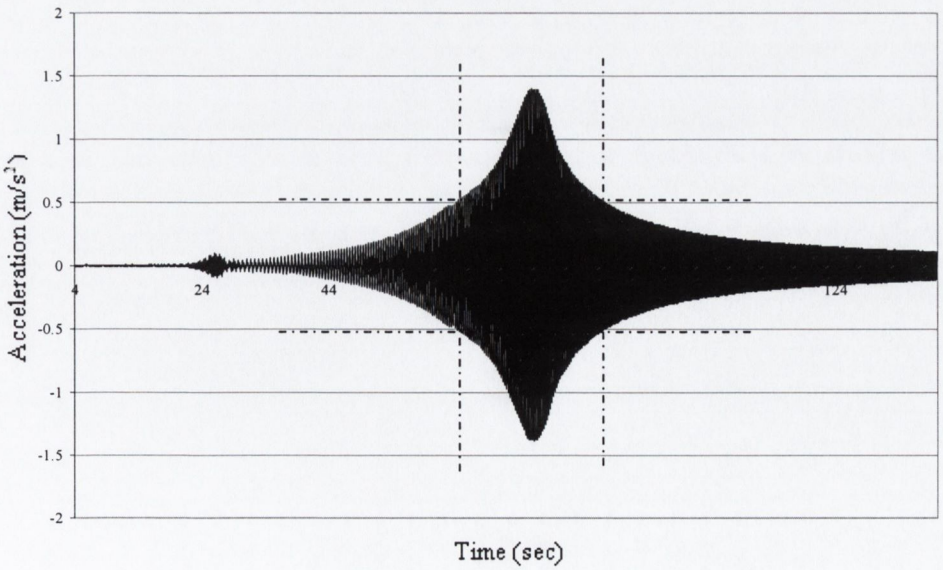

Figure 6.2 – Time history of model structure with mistuned TMD

The peak acceleration response of the structure is reduced by approximately 30%. The FRF in Figure 5.40, shows that the resonant response occurs between 3.25 and 4.25Hz, while Figure 6.2 shows that the response before 65 seconds and after 85 seconds is the same as that given for Figure 6.1 for the structure with no TMD. Therefore, it is still only necessary to retune the TMD between these times, i.e. when the response is greater than $0.55m/s^2$ or less than $-0.55m/s^2$.

6.2.2 LabVIEW program

The LabVIEW program that tunes the VSTMD when the response is above or below certain limits is presented in Figures 6.3, 6.4, 6.5 and 6.6. The program obtains the response of the structure using the acquire waveform program given in Chapter 5. However, instead of acquiring a finite number of samples, the program is now placed in a while loop, so that the response is obtained until the program is told to stop. For each time step, the results are appended to a file.

When the response over the time step is obtained, the output section of the program compares the response to two defined parameters. In this case, (as shown in Figure 6.2) these two parameters are accelerations of $0.55m/s^2$ and $-0.55m/s^2$. The LabVIEW input from the accelerometers is measured in volts, and the accelerometer measuring the response of the structure is calibrated so that $1V=0.412m/s^2$. In Figures 6.4, 6.5 and 6.6, therefore the two defined parameters for comparison are 0.136V and –0.136V.

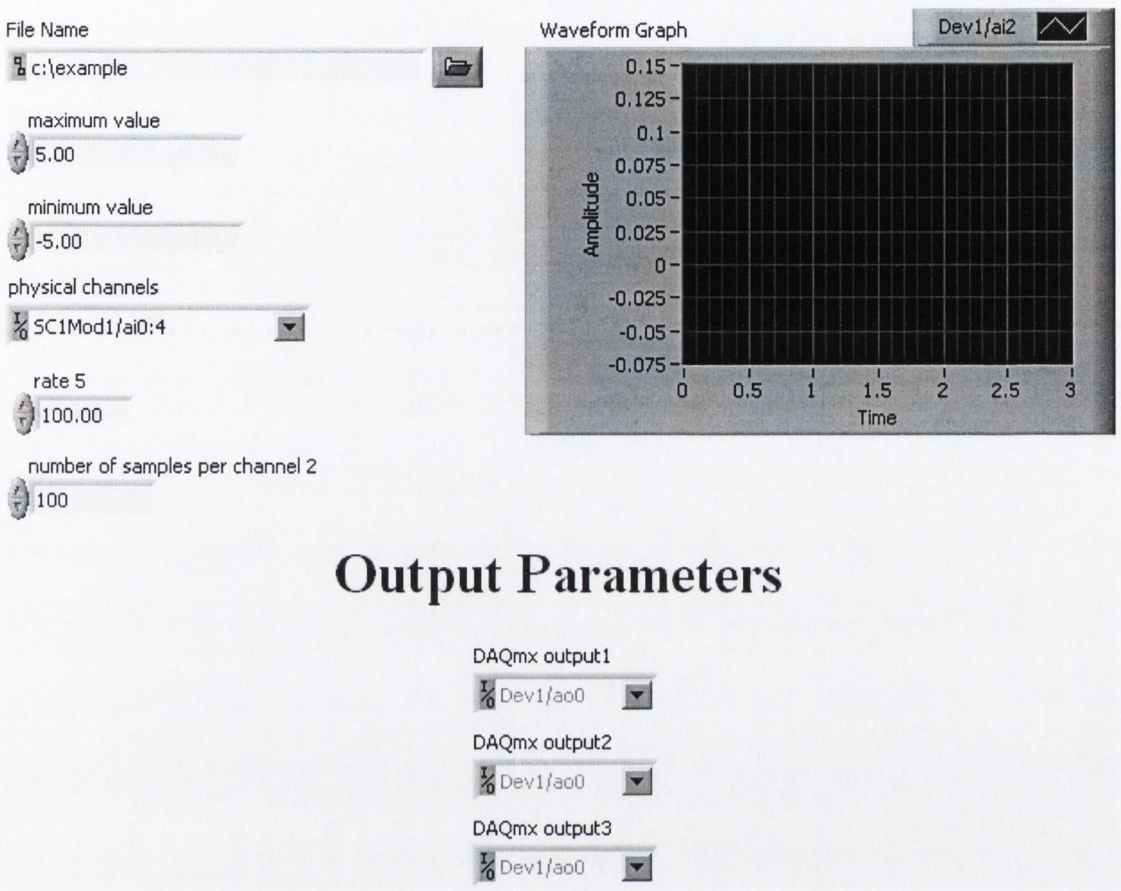

Figure 6.3 – Front diagram of LabVIEW program for the VSTMD based on the amplitude response

Figures 6.4, 6.5 and 6.6 show how the response is compared to the two defined parameters using two *if* structure's, one placed inside another. If the response is greater than the first value, the true statement of the first *if* structure is executed, as shown in Figure 6.4. Another *if* structure is placed inside the false statement of the first *if,* structure, as shown in Figure 6.5. The program compares the response to the second defined parameter, if the response is less than this value, the true statement of the second *if* structure is executed. Figure 6.6 shows that the false statement of the second *if* structure is executed if the response is neither greater than the first parameter nor less than the second.

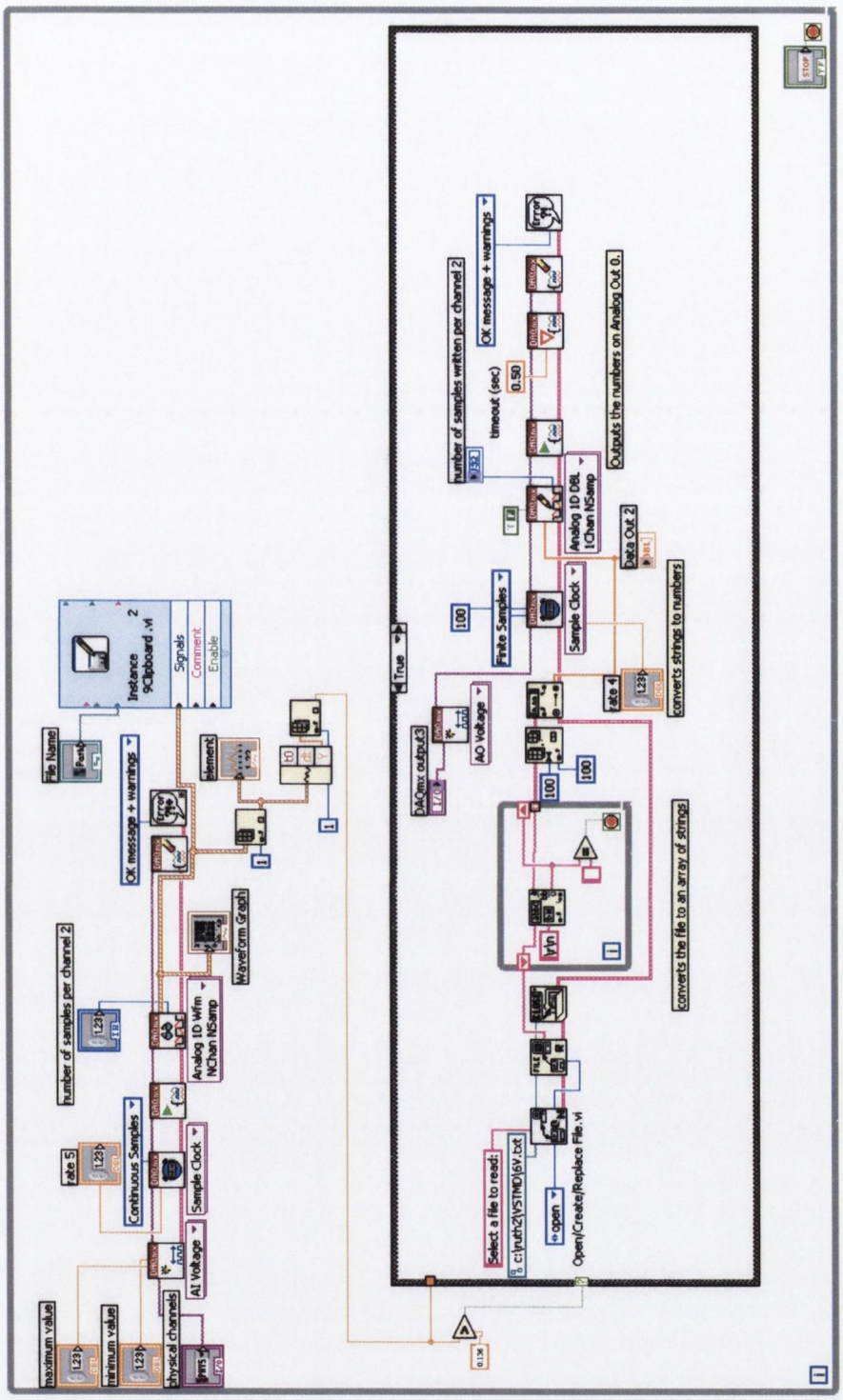

Figure 6.4 – Block diagram of LabVIEW program for the VSTMD based on the amplitude response, true statement of first if structure

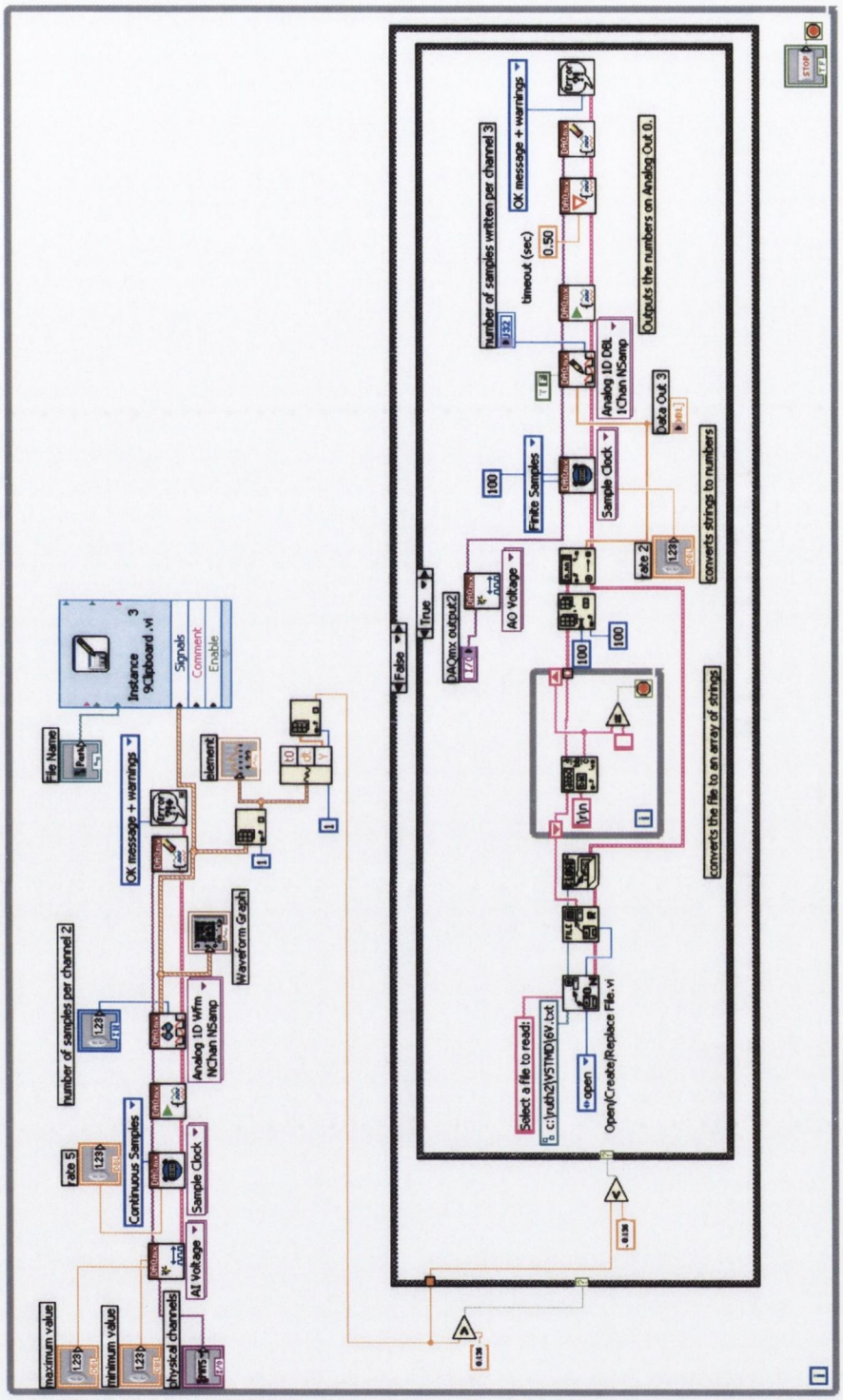

Figure 6.5– Block diagram of LabVIEW program for the VSTMD based on the amplitude response, false statement of first if structure and true statement of second if structure

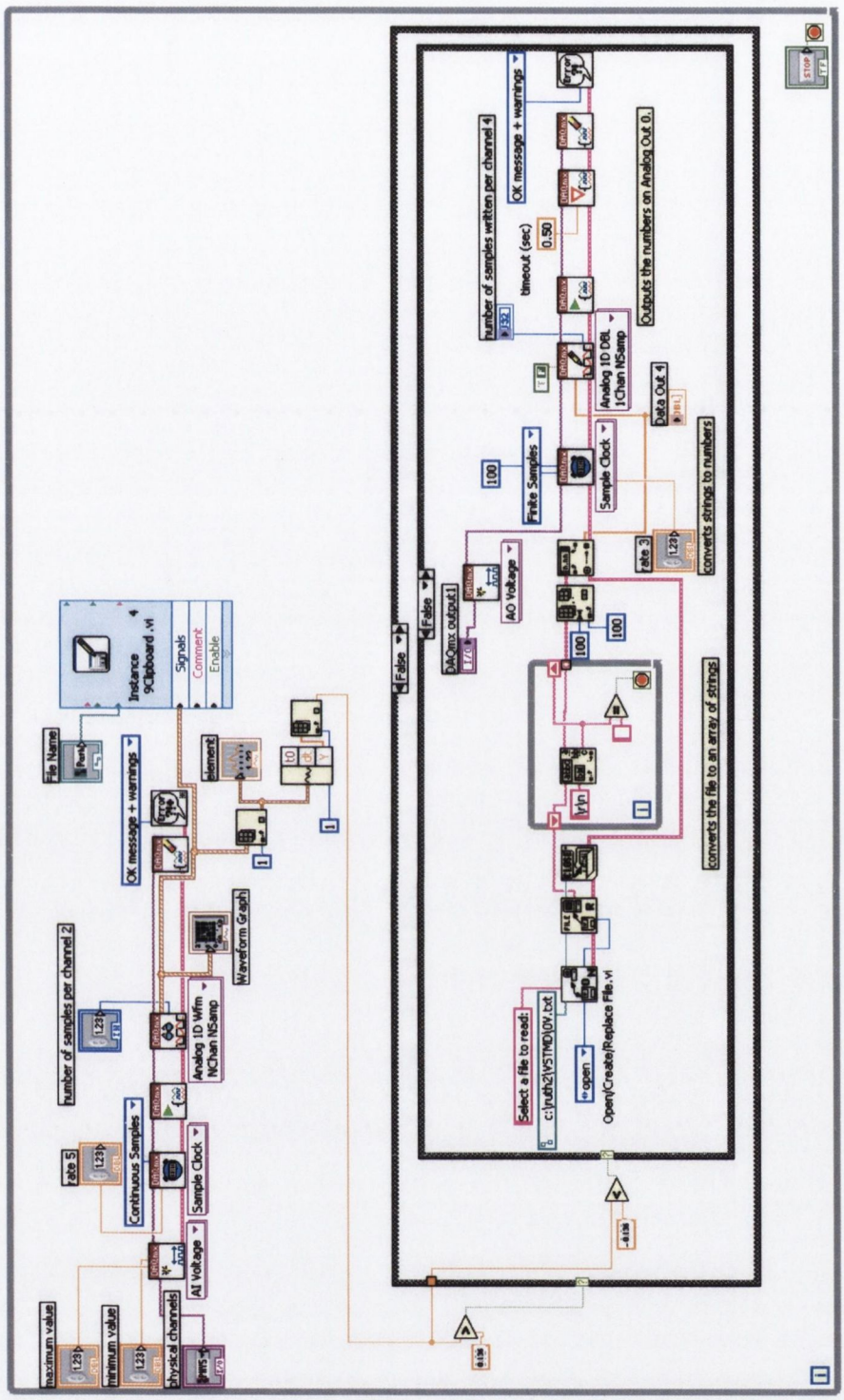

Figure 6.6– Block diagram of LabVIEW program for the VSTMD based on the amplitude response, false statement of first if structure and false statement of second if structure

The executed output program, is shown in each of the statements in the two *if* structures, in Figures 6.4, 6.5 and 6.6. The program reads a value from a text file, converts this value to a numerical value in LabVIEW and outputs this value as a voltage to one of the two output channels. The output channel is specified in the front diagram, as shown in Figure 6.3. The system is set up so that the output voltage is sent from channel 0 to the solenoid, and the solenoid is calibrated so that 1V = 1A. Effectively therefore, a current is sent to the solenoid. It was shown in Chapter 5 that to tune the VSTMD to the structure using the minimax principle, 6A passing through the solenoid is required. Two text files are written, one for 0A and one for 6A, if the response is within the defined limits, 6A passes through the solenoid, otherwise 0A passes through the solenoid.

6.2.3 Results

The LabVIEW program described above is employed to tune the VSTMD to the model structure when the response is greater than $0.55m/s^2$ (0.136V) or less than $-0.55m/s^2$ (-0.136V). The time history of the resulting acceleration response is shown in Figure 6.7, and the corresonding FRF is shown in Figure 6.8

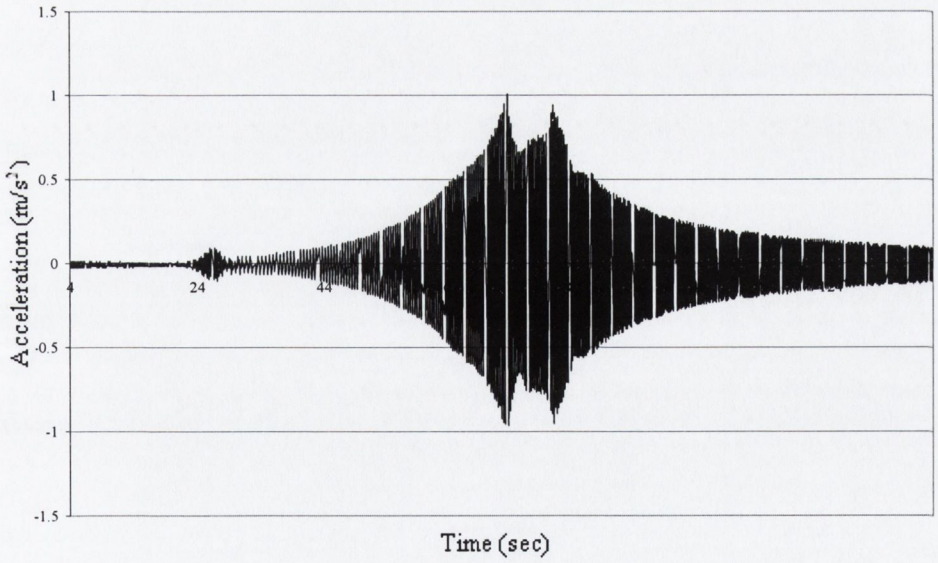

Figure 6.7 – Time history of structure with VSTMD based on amplitude response

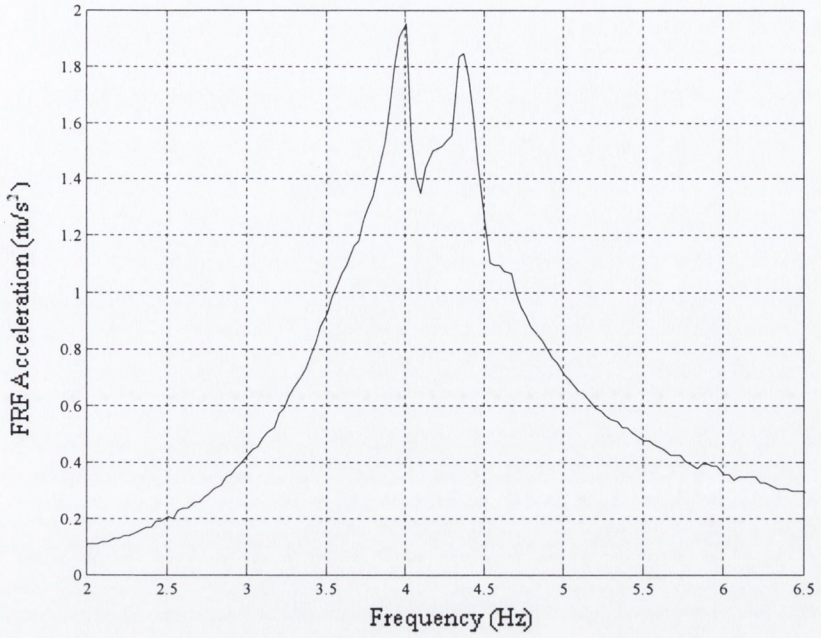

Figure 6.8 – FRF of structure with VSTMD based on amplitude response

Compared to the structure without a TMD, the maximum response of the structure is reduced by approximately 50%. There are now also two peaks in the FRF of the structure, of near equal magnitude, which indicates that the TMD is tuned to the minimax principle. Therefore by only tuning the VSTMD when the response is close to the resonant condition, the response of the structure can be reduced. However, in most applications, the resonant amplitude of the response will not be known in advance, hence this approach may be difficult to apply. Therefore, if the local frequency of the response at each time step could be calculated, the VSTMD could be retuned online based on this value, leading to a more efficient design.

6.3 VSTMD USING WAVELET ANALYSIS

6.3.1 Wavelet analysis

Wavelet analysis is employed to transfer a time history of the response of the structure into the time-frequency domain, allowing the local frequency content associated with the mode of vibration of the response to be identified. The advantage of the wavelet transform is that it is capable of retaining both time and frequency details of the vibrating signal (Chakraborty and Basu, 2005).

If $f(t)$ is a square function that can be integrated in $L^2(R)$, i.e.

$$\int f^2(t)dt < \infty \tag{6.1}$$

the wavelet tranform of $f(t)$ can be converted into a two dimensional signal as a function of the parameters a and b (Basu, 2004), such that

$$W_\psi f(a,b) = \frac{1}{\sqrt{|a|}} \int f(t)\psi^* \left(\frac{t-b}{a} \right) dt \tag{6.2}$$

where ψ is known as the mother wavelet, and * denotes the complex conjugate. In Eq (6.2), a family of wavelet bases, $W_\psi f(a,b)$ are created by varying the parameters a and b for the desired time and frequency localisation. The scaling factor, a, dilates the wavelet basis and b localises the wavelet basis about $t=b$. The mother wavelet used in this study is a modified form of the Littlewood-Paley (L-P) basis function (Chakraborty and Basu, 2005) and is given by

$$\begin{aligned} \psi(\omega) &= \frac{1}{\sqrt{4\pi F_1(\sigma-1)}}, \quad F_1 \le \left| \frac{\omega}{2\pi} \right| \le \sigma F_1 \\ &= \quad 0 \quad , \ otherwise \end{aligned} \tag{6.3}$$

where the value of σ is chosen based on the frequency band desired for the analysis.

6.3.2 LabVIEW program

A program written in MATLAB, that determines the local frequency content of the response of the structure using wavelet analysis, is incorporated into LabVIEW to allow the VSTMD to be tuned based on the frequency response of the structure. A flow chart illustrating the methodology of the LabVIEW program is given in Figure 6.9.

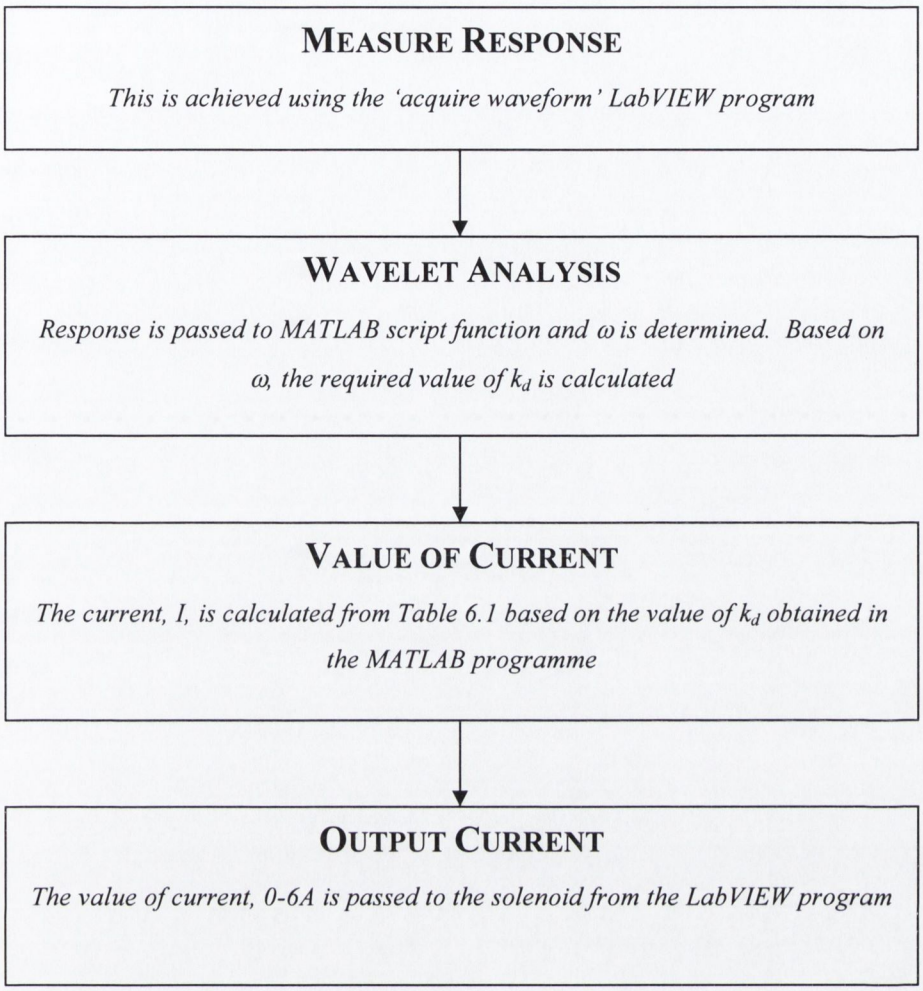

Figure 6.9 – Methodology used in LabVIEW program for online VSTMD based on frequency response

The front diagram of the LabVIEW program is given in Figure 6.10 and the block diagram is given in Figures 6.11 and 6.12. The LabVIEW program is an extension of the 'acquire waveform' program given in Section 5.4.2 placed inside a while loop, i.e. the program will continue to acquire samples until it is told to stop. The first set of acquired samples is placed in an array and passed into the MATLAB script function, as shown on the block diagram in Figures 6.11 and 6.12. Wavelet analysis is performed on the set of acquired data, using the MATLAB program 'find_kd', which is called using the MATLAB script function, and the frequency of the response ω, is obtained. The 'error out' box indicates if there is an error with the MATLAB program. Based on the frequency of response, the stiffness, k_d, required to tune the VSTMD according to the minimax principle is obtained. The value of the current, I, required to provide this stiffness in the damper is then calculated using Table 6.1,

which is based on the characterisation of the solenoid from Chapter 5. As the stiffness was characterised for real numbers of 0 to 6A, the value of the stiffness at intermediate points, (e.g. 3.5A) is not known. Therefore, a current value is selected if k_d occurs around the value obtained in the characterisation. For example, if k_d is greater than 1.89N/m, the value of the applied current will be 3A, while if k_d is less than 1.89N/m, the applied current will be 2A. The parameters ω, k_d and I, are displayed on the front panel to allow the program to be checked while it is running. The value of the current obtained using the MATLAB program is compared to values between 0 and 6A using a number of *if* structures placed inside each other. Two cases of the *if* structure are shown in Figures 6.11 and 6.12, for example. When the current equals 0, it is shown in Figure 6.11 that 0A is passed through the solenoid. When the current equals 5, it is shown in Figure 6.12, that 5A is passed through the solenoid. The output program is the same as that for the VSTMD based on the amplitude response.

Current	Characterised Stiffness (N/m)	Stiffness of VSTMD, k_d (N/m)
0A	0	$k_d<0.28$
1A	0.56	$0.28 < k_d < 0.72$
2A	0.88	$0.72 < k_d < 1.89$
3A	2.90	$1.89 < k_d < 5.5$
4A	8.09	$5.5 < k_d < 11.44$
5A	14.79	$11.44 < k_d < 17.14$
6A	19.49	$k_d > 17.14$

Table 6.1 – Values of current to be passed to the solenoid based on k_d

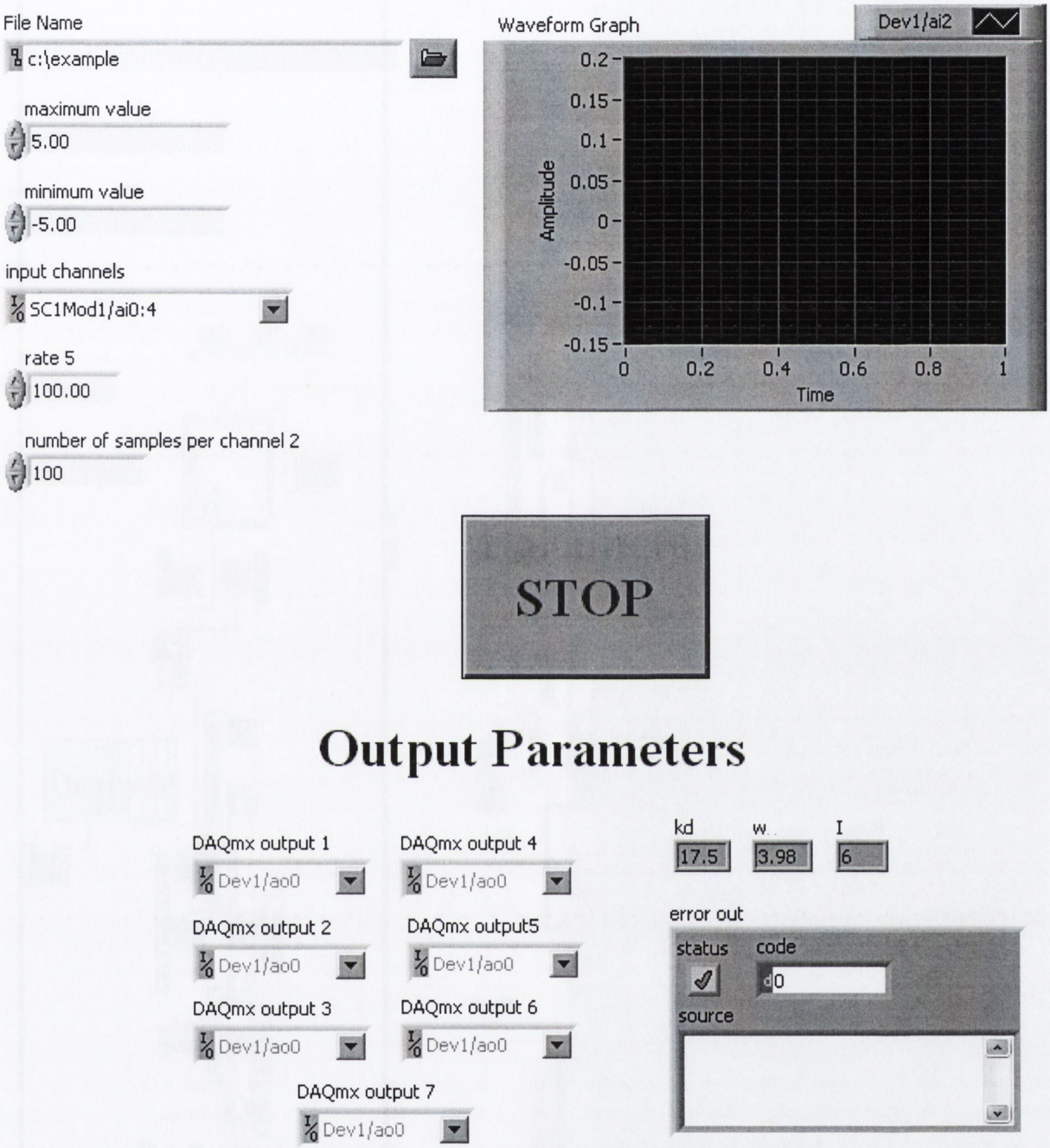

Figure 6.10 – Front diagram of LabVIEW program for the VSTMD using wavelet analysis

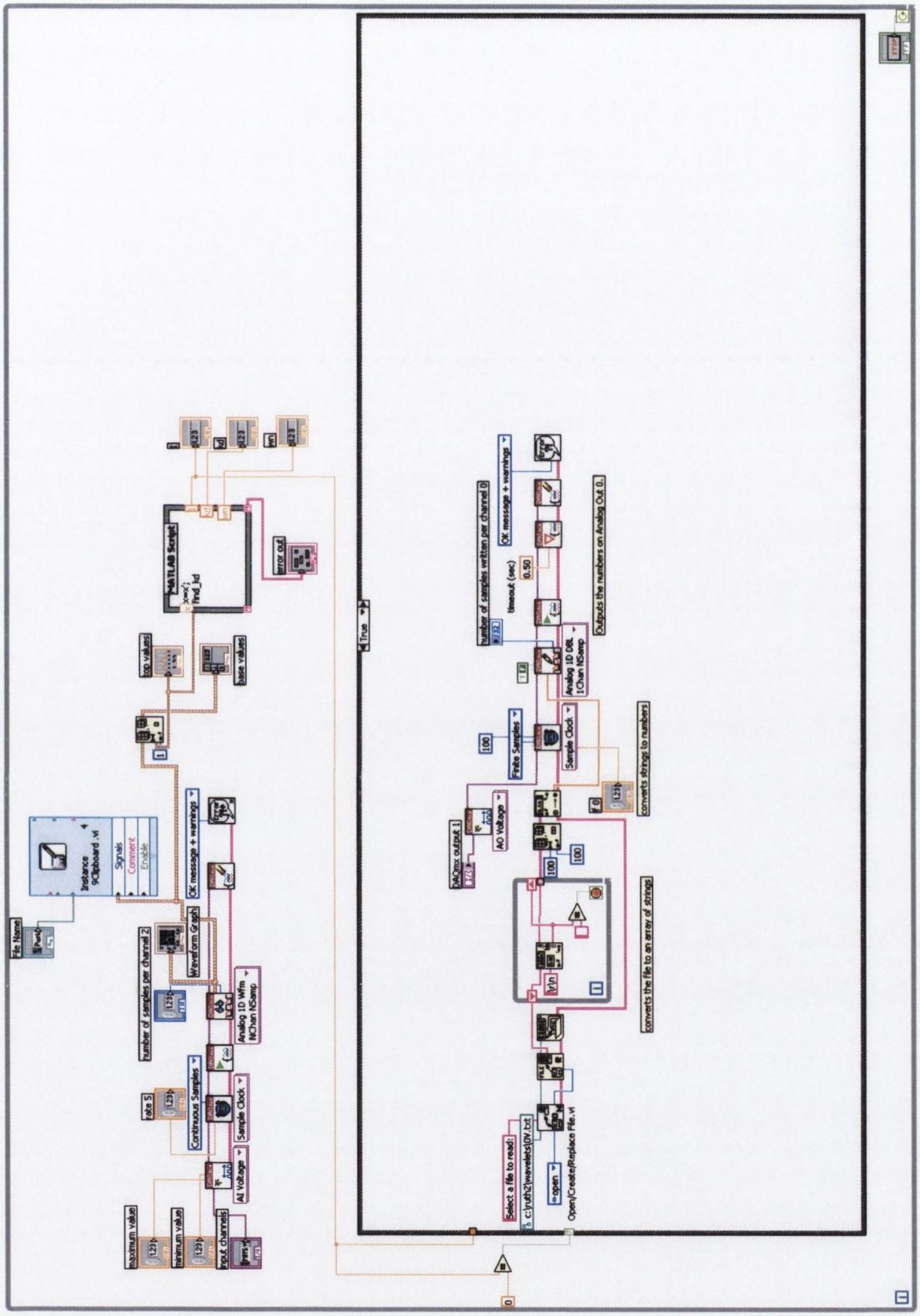

Figure 6.11– Block diagram of LabVIEW program for the VSTMD with wavelet analysis when current = 0A

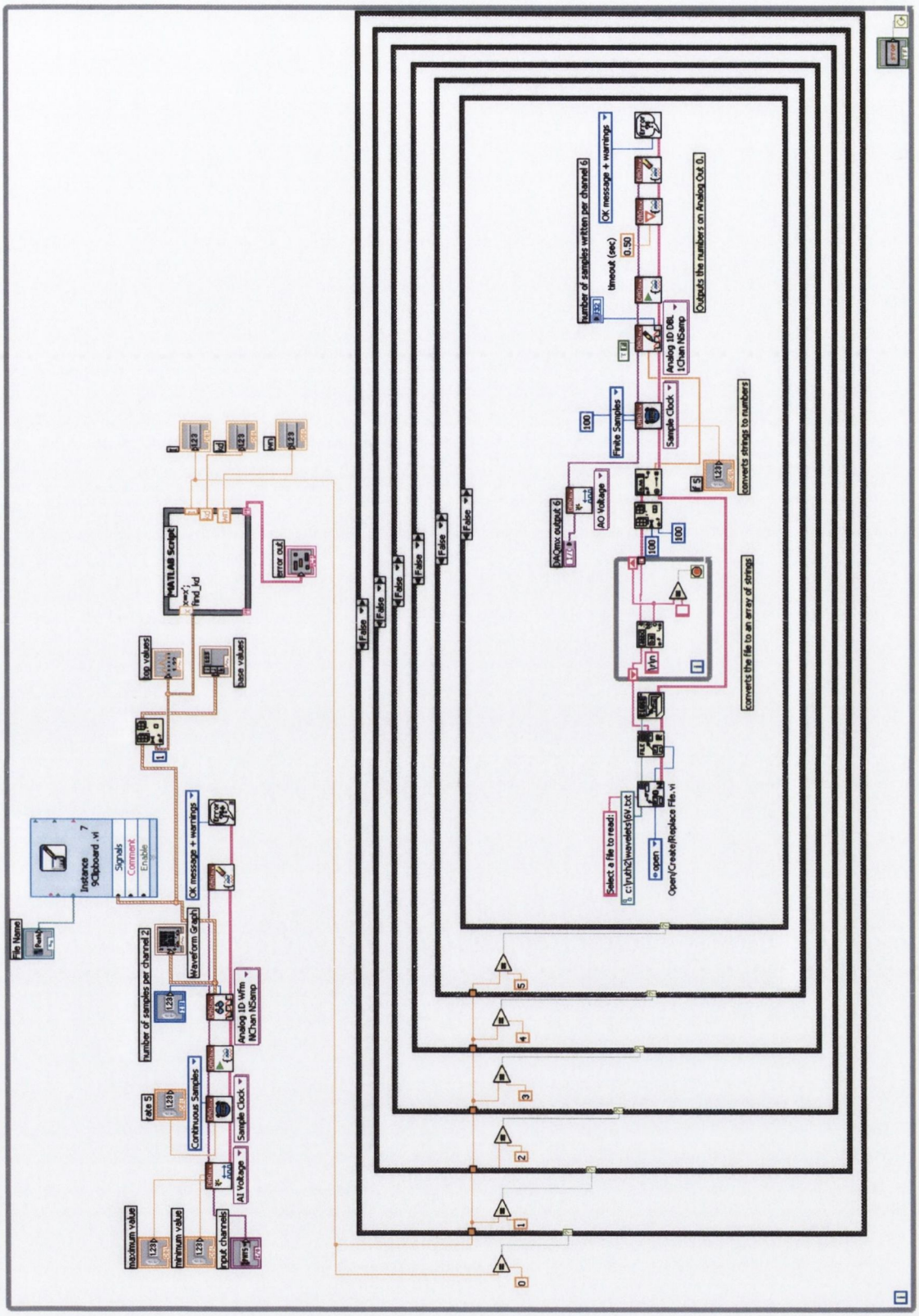

Figure 6.12– Block diagram of LabVIEW program for the VSTMD with wavelet analysis when current = 0A

6.3.3 Results

6.3.3.1 Sine sweep

A sine sweep of 0 to 7Hz is applied to the base of the structure and the VSTMD is retuned in real time using wavelet analysis. The smaller the frequency band of the mother wavelet function, the more accurate the results. As the resonant condition of the structure occurs between 3.25 and 4.25Hz, the mother wavelet function is designed to identify the frequency between these bands. The frequency of the response identified outside this range is not very accurate, but this response is small and does not need to be controlled. Figures 6.13 and 6.14 show the time history and the FRF of the response of the structure, respectively. The maximum response is nearly 20% lower than the VSTMD based on the amplitude response. The FRF has two peaks of nearly equal magnitude, indicating that the VSTMD is tuned to the structure using the minimax principle. The amplitude and the peaks of the response are similar to those observed when the mistuned TMD was retuned offline by passing 6A through the solenoid, shown in Figure 5.46.

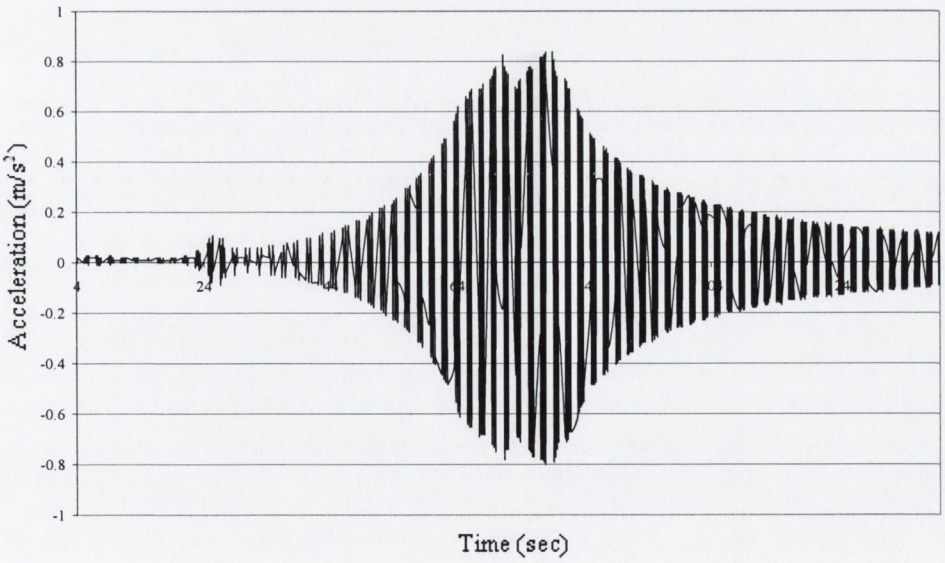

Figure 6.13 – Time history of structure with VSTMD tuned using wavelet analysis

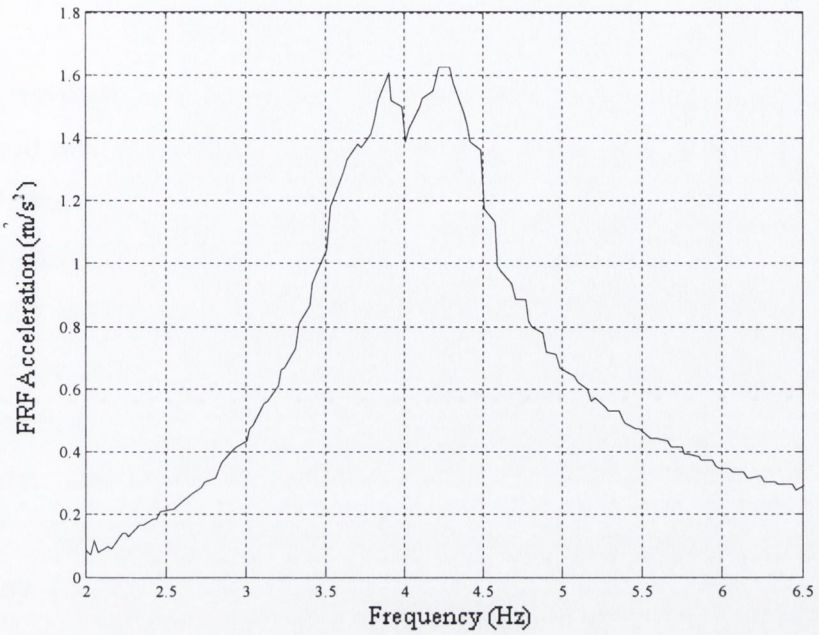

Figure 6.14 – FRF of structure with VSTMD using wavelet analysis

When the VSTMD changes its frequency according to the response of the structure, it is preferable to keep the sampling rate of the acquired data small, as this allows more rapid updating of the stiffness of the VSTMD. However, this can lead to problems in the accuracy of the acquired data. In the application described here, the data is collected at a rate of 100 samples per second. Although this allowed for relatively frequent tuning of the VSTMD, the number of samples acquired is small, risking inaccuracy in the results. However, increasing the sample rate leads to a delay in the switching of the VSTMD, causing instability in the structure. This is due to the constraints of the computer software in the lab. With a low sample rate, some data is left out of the acquired samples, but the accuracy of the wavelet analysis used to determine the stiffness of the VSTMD is much better, therefore a compromise is made and it is decided that faster switching of the VSTMD is more important. A number of sample rates were tested until the sample rate, which gave the best results for the model system was determined. Future work into the sampling rate could be examined.

6.3.3.2 Random excitation

A random excitation with predominant energy content in the frequency band 3 to 4Hz is applied to the structure. Three models are investigated, the structure without any TMD, the structure with the mistuned TMD and the structure with the VSTMD. Due to the low sampling rate, the excitation applied to the base is not identical in each test, although all excitations remain in the range of 3-4Hz, and the peak and RMS excitations are close. Figures 6.15, 6.17 and 6.19 show the base excitations for the model structure without any TMD, with the mistuned TMD and the VSTMD, respectively: the peak excitation accelerations are $0.837m/s^2$, $0.863m/s^2$ and $0.828m/s^2$. Figures 6.16, 6.18 and 6.20 show the response at the top of the structure without any TMD, with the mistuned TMD and with the VSTMD, respectively: the peak response accelerations are $1.600m/s^2$, $1.932m/s^2$ and $1.498m/s^2$. Compared to the model without any TMD, the peak response of model with the mistuned TMD is 17% greater, suggesting that the frequency of the base excitation matches that of a peak in the FRF of the coupled SDOF-TMD structure. When the VSTMD is applied, the peak response is reduced by 22% and 6% compared to the model with the mistuned TMD and without any TMD, respectively. Therefore, the problem of a mistuned TMD matching a peak in the FRF of the structure is avoided.

The RMS values were also examined. For the model structure without any TMD, with the mistuned TMD and the VSTMD, respectively: the RMS excitation accelerations at the base of the structure are $0.1208m/s^2$, $0.1206m/s^2$ and $0.1287m/s^2$, respectively, and at the top of the structure are $0.4816m/s^2$, $0.4016m/s^2$ and $0.4229m/s^2$, respectively. The RMS values for the base acceleration are similar in each case. In contrast to the peak accelerations, the RMS response of the structure with the mistuned TMD and the VSTMD are both less than structure without any TMD by 17% and 12%, respectively. However, the response of the structure with the VSTMD is slightly higher than that of the mistuned TMD, suggesting that for this case, online tuning of the TMD has no advantage in reducing the RMS response of the structure.

If the amplitude of the response is small, the VSTMD will have little interaction with the model structure. In this study, the amplitude was low because large jumps in

excitation caused instability in the TMD. This was a result of the limited travel of the TMD due to the length of the bar passing thorough the solenoid. This issue should be examined in further research where excitations of higher amplitude are employed to determine whether a greater reduction in response could be achieved with more interaction with the VSTMD. Further research should also be carried out into the sampling rate of the data and the switching rate of the VSTMD to create a more efficient design.

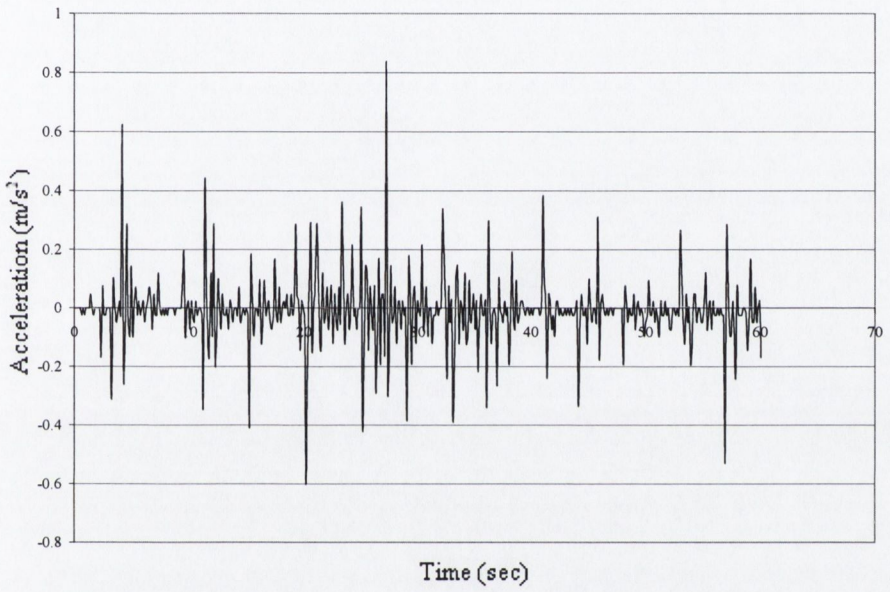

Figure 6.15 – Random excitation applied to structure without any TMD

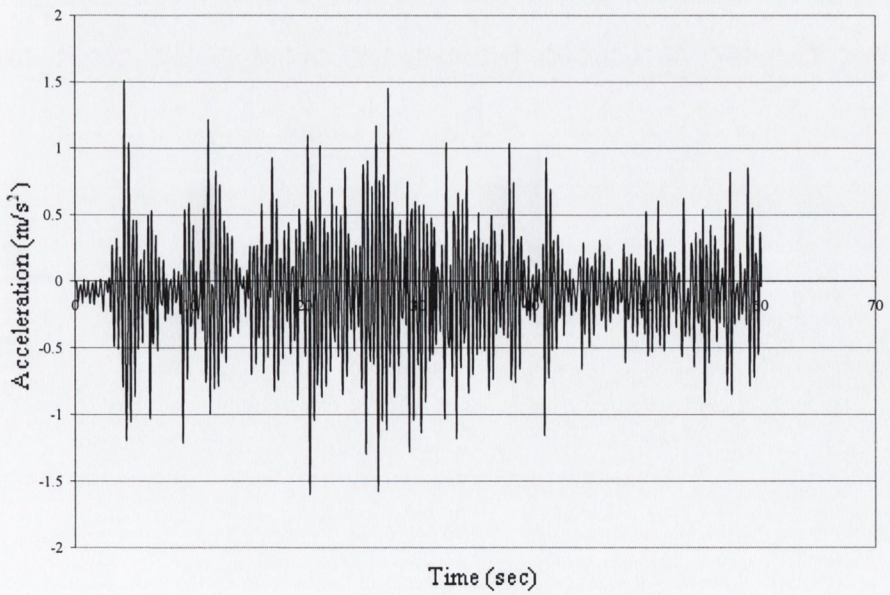

Figure 6.16 – Response of structure without any TMD with random excitation applied to the base

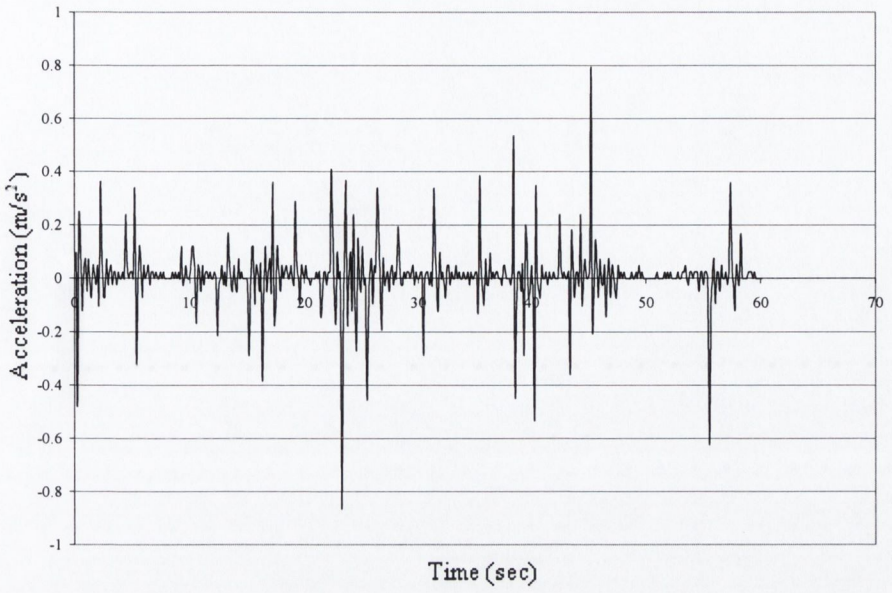

Figure 6.17 – Random excitation applied to structure with mis-tuned TMD

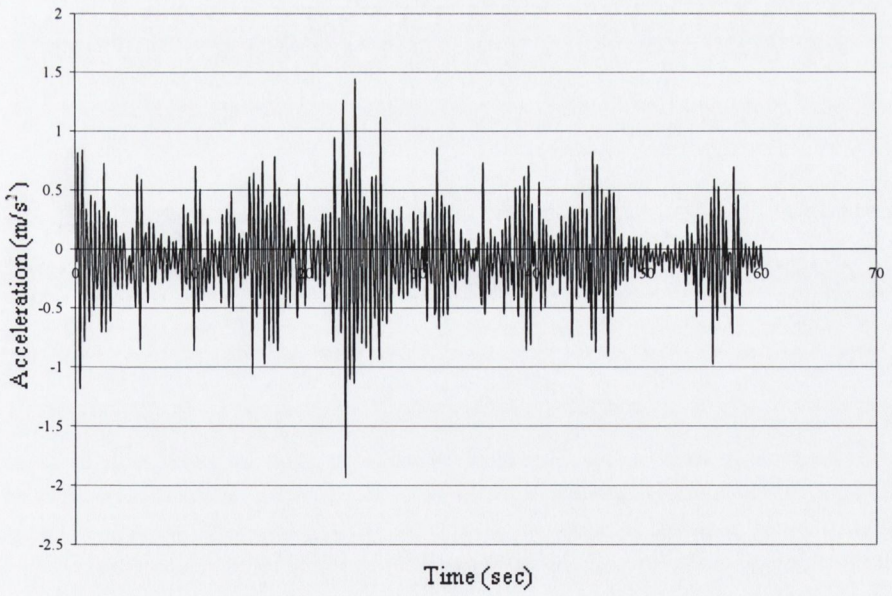

Figure 6.18 – Response of structure with mis-tuned with random excitation applied to the base

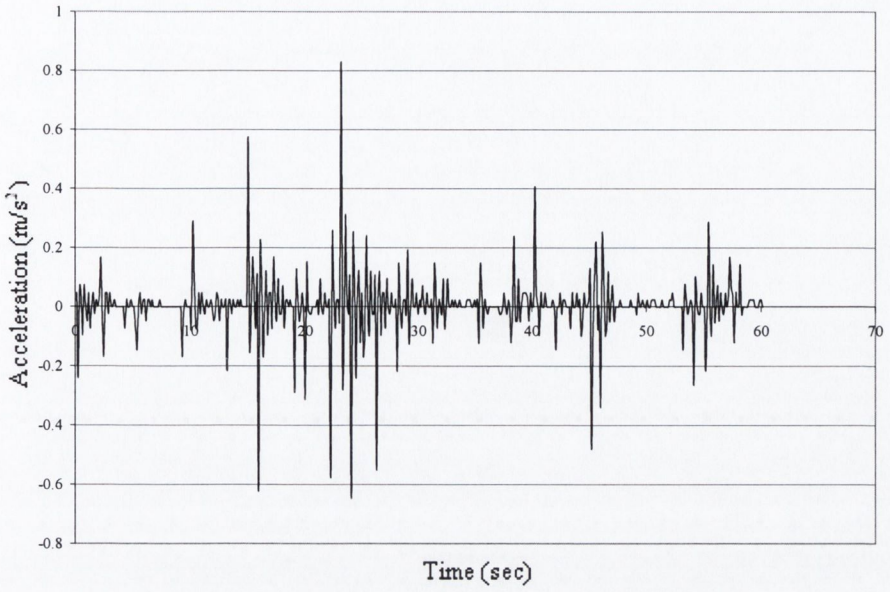

Figure 6.19 – Random excitation applied to structure with VSTMD

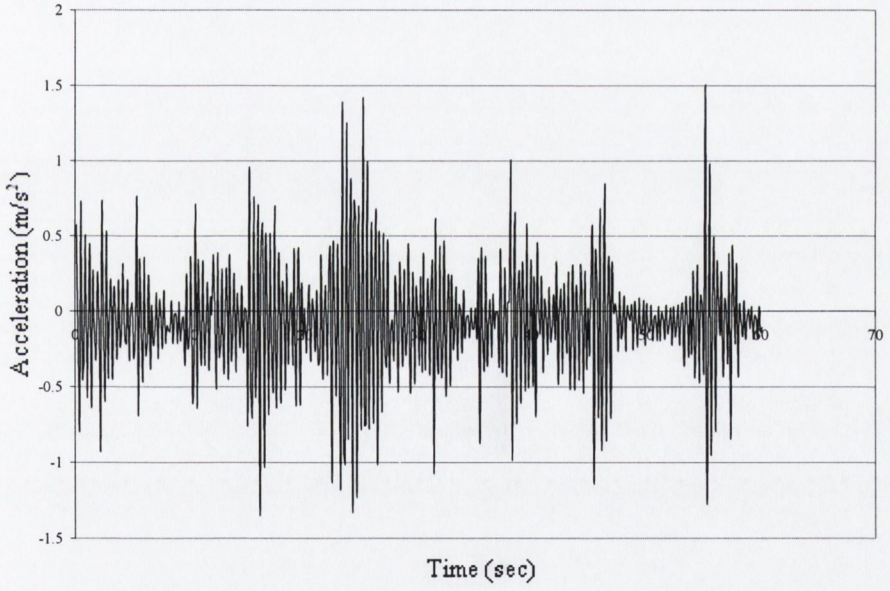

Figure 6.20 – Response of structure with VSTMD with random excitation applied to the base

6.4 CONCLUSION

A series of experiments investigating online control of the VSTMD were presented in this chapter. Two LabVIEW programs based on the amplitude and frequency response of the structure for online control of the VSTMD were created. The amplitude of the response was obtained using accelerometers and the local frequency content of the response of the structure was calculated using a wavelet analysis program in MATLAB. A sine sweep of 0 to 7Hz and a random excitation were

applied to the structure. It was shown that online control of the VSTMD successfully retuned the TMD in real time according to the minimax principle, leading to significantly reduced vibration response.

CHAPTER 7

ATMD - PASSIVE FRF AND VSTMD – ONLINE FRF APPLIED TO WTTS WITH MTMDS

7.1 INTRODUCTION

In this chapter, the ATMD with passive shaping of the FRF and the VSTMD with online shaping of the FRF are incorporated into the WTT with MTMDs. The WTT, with the MTMD configuration obtained in Chapter 2 is subjected to a wind excitation derived from the Davenport spectrum. The peak and RMS displacement and acceleration response of the structure are obtained. The control strategy for ATMDs with passive shaping of the FRF, developed in Chapter 3, is first applied to the WTT with MTMDs. The VSTMD developed in Chapter 5 and 6, and online shaping of the FRF, developed in Chapter 4, is then applied to the WTT with MTMDs. The stiffness of the structure is varied by ±15% and the performance of the MTMD configuration with the control strategy for passive and online shaping of the FRF are compared to that of the passive MTMD control strategy. Additional performance criteria based on modified values of the Yang performance criteria (2004) obtained in Chapter 2 are derived for the peak responses of the structure and the applied control force. Finally, the response of the WTT with the passive MTMD configuration and optimal damping is examined.

7.2 MTMD CONFIGURATION WITH ATMD

The MTMD configuration is applied to the WTT model described in Chapter 2. From Table 2.5, the optimal number and location of the MTMDs is 7 TMDs placed at the 20^{th}, 19^{th}, 18^{th}, 17^{th}, 12^{th}, 15^{th} and 16^{th} DOF. The tuning parameter for each TMD is, 1, 0.885, 1.11, 0.81, 0.99, 1.16 and 0.865, respectively. The first four TMDs were placed in the structure using the SSA when the CI was based on the RMS displacement response of the structure. It was shown in Chapter 2 that the dominant mode of the displacement response of the structure is the fundamental mode of the structure and therefore these four TMDs are tuned to the fundamental mode. The last three TMDs were placed in the structure using the SSA when the CI was based on the

acceleration response of the structure. It was shown that the dominant mode of the acceleration response of a WTT is the second mode and therefore these three TMDs are tuned to the second mode of the structure

It was shown in Chapter 3 that for a MDOF structure, if the fundamental mode only is considered, the bang-bang control law remains the same and can be applied to a single TMD tuned to the fundamental mode of the structure. For the 20 DOF structure investigated in Chapter 2, if the second mode of the structure is considered, the maximum value of the mode shape occurs at the 12th DOF, close to the centre of the structure, such that

$$x_{12} = \phi_{12,2} v_{12} \tag{7.1}$$

If $\phi_{12,2}$ is normalised such that $\phi_{12,2}$ = 1, then the amplitude of the second mode response gives the response of the structure at the 12th DOF. Therefore the control law obtained in Chapter 3 will also apply for a TMD tuned to the second mode, except in this case the value of $\ddot{x}_{max}$ is not the maximum acceleration at the top of the structure, but it is the maximum acceleration at the 12th DOF.

The control is applied to two of the TMDs in the MTMD configuration; the first TMD (tuned to the first mode of vibration) and the fifth TMD (tuned to the second mode of vibration). These TMDs are chosen because they are the first two TMDs placed to control the displacement and acceleration response respectively, and their tuning parameters are close/equal to 1. These TMDs are tuned according to the minimax principle. It is assumed that each TMD is placed in the structure on its own and the other modes will not have an effect on the tuning of the TMD. Both the ATMD control strategy with passive shaping of the FRF and the VSTMD control strategy with online shaping of the FRF is applied. The remaining five TMDs in the WTT remain as passive TMDs tuned to the structure according to the MTMD configuration developed in Chapter 2.

7.3 OPTIMAL DAMPING RATIO

Optimal tuning of the TMD was examined in section 3.3 of Chapter 3. Optimal damping in the TMD is now considered. It was shown in Figure 3.3 that there must be some level of damping for which the peaks of the FRF are a minimum. Based on the optimal value of the tuning parameter, obtained in Chapter 3, these two peaks will have the same magnitude and is given by (Den Hartog, 1956)

$$R = \sqrt{1 + \frac{2}{\mu}} \tag{7.2}$$

This value of the amplitude and the value of the optimum tuning parameter are used to obtain the transfer function of the system, which is differentiated with respect to frequency ratio, with the resulting slope being equated to zero to identify the first peak of the FRF (Den Hartog, 1956), which leads to the result

$$\zeta_d = \sqrt{\frac{\mu\left(3 - \sqrt{\frac{\mu}{\mu+2}}\right)}{8(1+\mu)^3}} \tag{7.3}$$

Similarly, for the second peak of the FRF, the value of the damping ratio is obtained as

$$\zeta_d = \sqrt{\frac{\mu\left(3 + \sqrt{\frac{\mu}{\mu+2}}\right)}{8(1+\mu)^3}} \tag{7.4}$$

The optimum damping ratio is now defined as the average of the two values that render the two peaks on the FRF maxima (Den Harotg, 1956), such that

$$\zeta_{opt} = \sqrt{\frac{3\mu}{8(1+\mu)}} \tag{7.5}$$

As it is not envisaged to change the damping ratio of the TMD in real time, this value of optimal damping is applied to the TMD with bang-bang control for both passive shaping of the FRF and online shaping of the FRF.

7.4 PERFORMANCE CRITERIA

Based on the performance criteria proposed by Yang et al (2004), for the benchmark problem on the response control of tall buildings, a non-dimensional set of criteria for the RMS response of a structure was obtained in Chapter 2, where the first 5 evaluation criteria are given in Eqs (2.27) to (2.31). Additional criteria are now specified for average power consumption, peak responses, peak TMD stroke and peak control power for a n-DOF system. The average power consumption $\bar{\sigma}_p$ is given by the performance criteria,

$$\bar{J}_6 = \bar{\sigma}_p = \left\{ \frac{1}{T} \int_0^T [\dot{x}_m(t) u(t)]^2 \, dt \right\}^{1/2} \tag{7.6}$$

where $\dot{x}_m(t)$ is the actuator velocity and $u(t)$ is the control force of the actuator. The ability of the controller to reduce the maximum peak acceleration of the structure is represented by

$$\bar{J}_7 = \frac{max(\ddot{x}_{p1}, \ddot{x}_{p2}, \ldots, \ddot{x}_{pn})}{max(\ddot{x}_{p1o}, \ddot{x}_{p2o}, \ldots, \ddot{x}_{pno})} \tag{7.7}$$

where $\ddot{x}_{pi}$ and $\ddot{x}_{pio}$ are the peak accelerations at the i^{th} DOF of the controlled structure and the uncontrolled structure respectively. The performance of the controller in reducing the average peak acceleration of the structure is measured by

$$\bar{J}_8 = \sum_i (\ddot{x}_{pi} / \ddot{x}_{pio}), for \quad i = 1,2,\ldots,n \tag{7.8}$$

The reduction in the maximum peak displacement is given by

$$\bar{J}_9 = \frac{max(x_{p1}, x_{p2}, \ldots, x_{pn})}{max(x_{p1o}, x_{p2o}, \ldots, x_{pno})} \tag{7.9}$$

where x_{pi} and x_{pio} are the peak displacement of the i^{th} DOF of the controlled structure and the uncontrolled structure respectively. The average reduction in peak displacement is given by

$$\bar{J}_{10} = \sum_i (x_{pxi} / x_{pio}), for \quad i = 1,2\ldots,n \tag{7.10}$$

The control effort of the TMD stroke is given by

$$\bar{J}_{11} = \frac{\max(x_{pm1}, x_{pm2}, \ldots, x_{pmi})}{\max(x_{p1o}, x_{p2o}, \ldots, x_{pno})} \tag{7.11}$$

where x_{pmi} is the maximum peak displacement of the i^{th} TMD. Finally the peak power consumption is given by

$$\bar{J}_{12} = \bar{P}_{max} = max\,|\,\dot{x}_m(t)u(t)\,| \tag{7.12}$$

7.5 NUMERICAL RESULTS

7.5.1 Random excitation

A random excitation is generated from the Davenport spectrum and applied to the WTT. The time history of the excitation acceleration (obtained my multiplying the inverse of the mass matrix by the force vector) are generated for 20 DOFs. The excitation at the 20th and 12th DOF are shown in Figures 7.1 and 7.2. The amplitude of the Fourier transform of the excitation at the 20th and 12th DOF, where the dominant modes of vibration for the displacement and acceleration response of the structure are maxima, are shown in Figures 7.3 and 7.4, respectively.

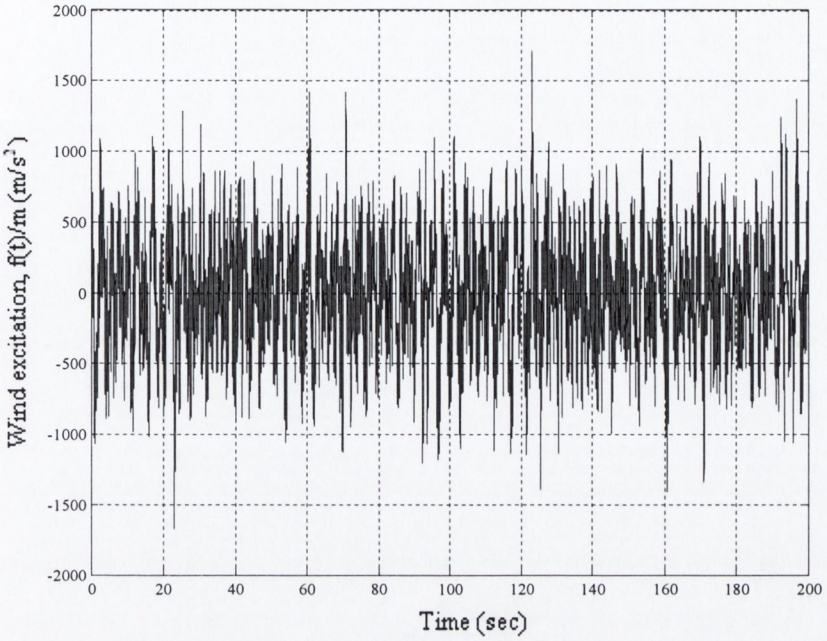

Figure 7.1 – Random excitation at the 20th DOF applied to WTT

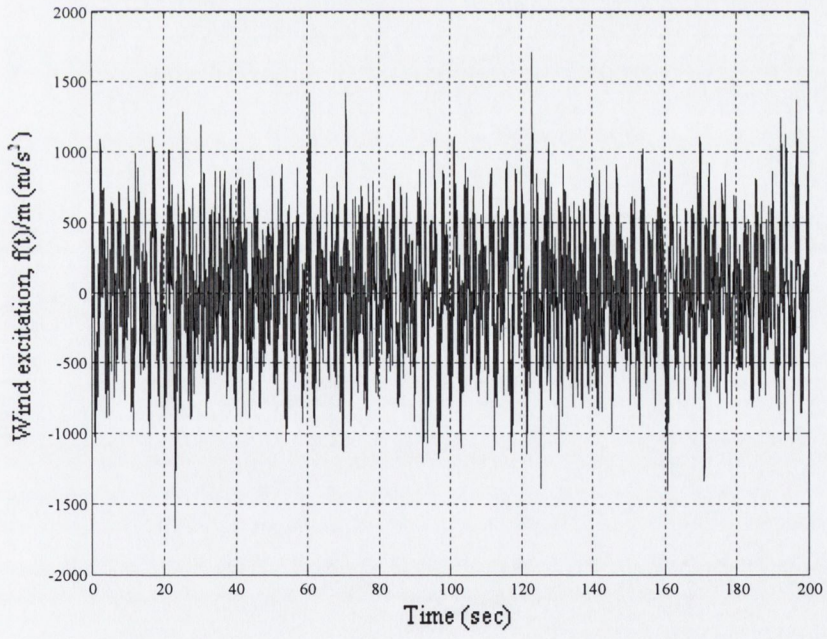

Figure 7.2 - Random excitation at the 12th DOF applied to WTT

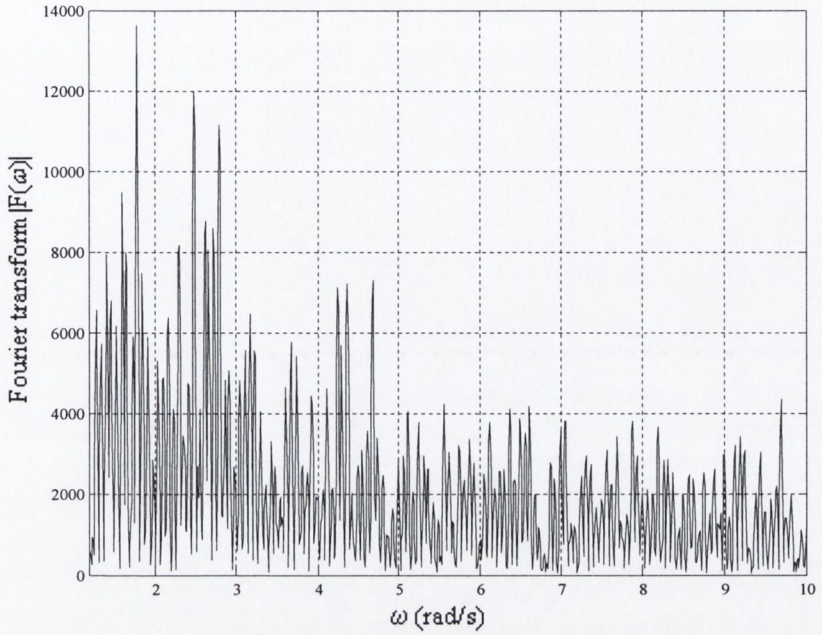

Figure 7.3 – Fourier transform of random excitation at 20th DOF

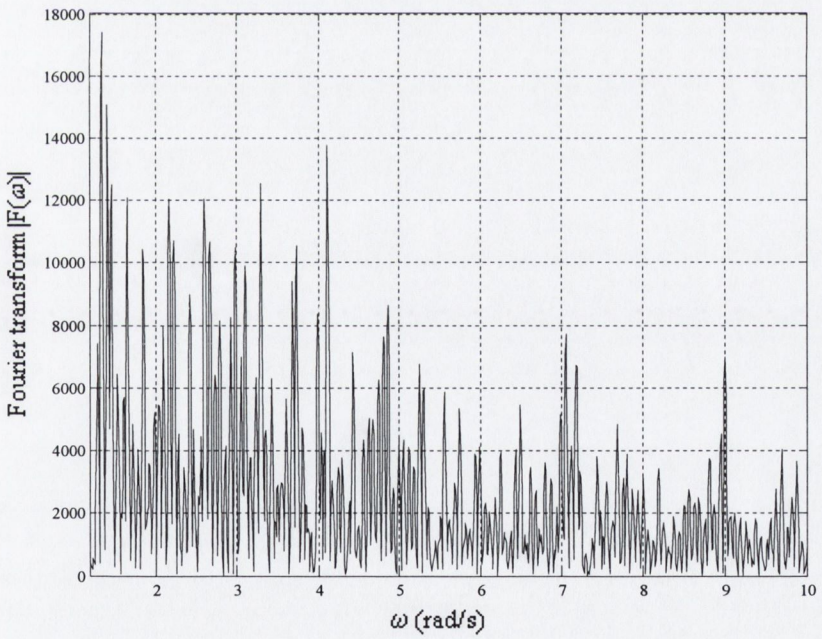

Figure 7.4 - Fourier transform of random excitation at 12th DOF

7.5.2 Passive MTMDs

Tables 7.1, 7.2 and 7.3 present the response of the structure with no TMDs, a single TMD applied at the 20th DOF and the MTMD configuration given in Table 2.5, respectively. In all subsequent tables in this chapter, the degrees of freedom beyond 20 represent the DOFs for the additional TMDs in the MTMD system.

DOF	x_p (cm)	$\ddot{x}_p$ (cm/s^2)	σ (cm)	$\ddot{\sigma}$ (cm/s^2)
1	0.005	28.476	0.002	7.357
2	0.019	73.609	0.007	20.131
3	0.043	119.410	0.016	31.934
4	0.075	150.220	0.028	42.040
5	0.115	191.160	0.044	49.758
6	0.164	209.270	0.063	54.852
7	0.221	223.170	0.085	58.276
8	0.285	220.450	0.111	60.287
9	0.357	226.200	0.140	61.018
10	0.436	225.810	0.172	60.542
11	0.519	205.160	0.208	59.570
12	0.610	189.990	0.246	59.448
13	0.708	203.990	0.287	60.872
14	0.810	221.330	0.331	62.542
15	0.921	238.320	0.378	63.750
16	1.036	241.910	0.427	63.489
17	1.153	220.470	0.478	60.587
18	1.273	203.750	0.532	51.602
19	1.396	127.070	0.586	32.712
20	1.530	74.556	0.641	21.882

Table 7.1 – Response of WTT with no TMDs

Comparing Table 7.1 and Table 7.2, shows that the addition of a TMD at the 20th DOF increases the peak response of the structure, on an average, by 18% but reduces the RMS displacement, on an average by 23%. In contrast, the addition of one TMD has little effect on the acceleration response. This is expected, as the TMD is tuned to the fundamental mode of vibration, whereas the acceleration response depends more strongly on the second mode of vibration. When the MTMD configuration is added, it is shown in Table 7.3 that the peak displacement response of the structure is reduced by between 12 and 20%, the RMS displacement is now reduced on average by 34%, the peak acceleration response is now reduced by up to 39% at the centre of

the structure and the RMS acceleration response is reduced by up to 45% at the centre of the structure. Therefore MTMDs do not significantly change the peak displacement response compared to the WTT with one TMD but considerable reductions in the RMS displacement, the peak acceleration and the RMS acceleration response are observed.

DOF	x_p (cm)	$\ddot{x}_p$ (cm/s^2)	σ (cm)	$\ddot{\sigma}$ (cm/s^2)
1	0.006	27.159	0.001	7.359
2	0.023	73.664	0.006	20.131
3	0.051	119.150	0.012	31.937
4	0.089	150.750	0.022	42.041
5	0.138	192.060	0.034	49.755
6	0.196	208.650	0.049	54.834
7	0.264	222.680	0.066	58.254
8	0.340	219.940	0.085	60.255
9	0.424	227.390	0.107	60.968
10	0.515	225.570	0.131	60.465
11	0.614	205.920	0.157	59.468
12	0.722	182.980	0.185	59.311
13	0.839	204.360	0.216	60.693
14	0.964	222.150	0.248	62.315
15	1.092	242.060	0.283	63.480
16	1.224	251.160	0.319	63.145
17	1.360	225.030	0.357	60.139
18	1.499	204.150	0.396	50.971
19	1.642	131.530	0.436	31.477
20	1.806	77.607	0.478	19.591
21	14.651	353.120	5.753	124.090

Table 7.2 – Response of WTT with one TMD

DOF	x_p (cm)	$\ddot{x}_p$ (cm/s^2)	σ (cm)	$\ddot{\sigma}$ (cm/s^2)
1	0.004	27.265	0.001	7.372
2	0.015	80.898	0.004	19.872
3	0.034	119.400	0.010	31.078
4	0.061	144.460	0.018	40.143
5	0.094	162.320	0.028	46.388
6	0.134	169.820	0.041	49.421
7	0.180	174.080	0.055	50.042
8	0.234	158.850	0.072	48.553
9	0.293	152.660	0.091	45.195
10	0.360	155.660	0.113	40.020
11	0.434	128.590	0.137	34.464
12	0.517	117.420	0.162	32.111
13	0.607	124.330	0.190	35.291
14	0.702	150.040	0.220	41.174
15	0.803	160.680	0.251	47.728
16	0.906	174.780	0.284	52.701
17	1.011	208.180	0.318	54.281
18	1.118	191.730	0.354	48.770
19	1.224	123.980	0.390	31.097
20	1.334	50.740	0.427	13.195
21	12.735	294.140	3.978	89.251
22	16.557	406.670	6.560	128.710
23	10.997	392.220	4.429	120.040
24	19.393	450.310	6.722	132.520
25	0.305	358.410	0.088	113.000
26	0.225	363.180	0.063	105.460
27	0.366	458.070	0.114	138.070

Table 7.3 – Response of WTT with passive MTMD configuration

The performance criteria for the WTT with one TMD and the WTT with the MTMD configuration are presented in Tables 7.4 and 7.5, respectively. The lower the performance criteria values are, the better the performance of the control strategy. With one TMD, the only observed reduction is in the RMS displacement criteria, the other criteria vary marginally around 1. With the MTMD configuration, the RMS displacement criteria are further reduced and the RMS displacement, the peak acceleration and the RMS acceleration criteria are all reduced below 1.

J_1	0.996	J_7	1.038
J_2	0.994	J_8	1.005
J_3	0.744	J_9	1.181
J_4	0.750	J_{10}	1.183
J_5	8.968	J_{11}	9.578
J_6	0.000	J_{12}	0.000

Table 7.4 – Performance criteria for response of WTT with one TMD

J_1	0.851	J_7	0.861
J_2	0.782	J_8	0.772
J_3	0.665	J_9	0.872
J_4	0.662	J_{10}	0.862
J_5	6.201	J_{11}	8.326
J_6	0.000	J_{12}	0.000

Table 7.5 – Performance criteria for response of WTT with passive MTMD configuration

7.5.3 Bang-bang control strategy with ATMDs and MTMD configuration

The condition of the minimax principle for a MDOF structure is a difficult and a complex problem to solve. It is therefore simplified by assuming that when the TMD is tuned to the minimax principle, only one TMD is placed in the structure. It is observed from the MTMD configuration obtained in Chapter 2 that the first TMD placed in the structure at the 20th DOF (tuned to the first mode of vibration) and the fifth TMD placed in the structure at the 12th DOF (tuned to the second mode of vibration) both have tuning parameters close or equal to 1. Therefore, the control strategy is applied to these two TMDs, as applying it to any other TMD would considerably alter their optimum tuning parameter.

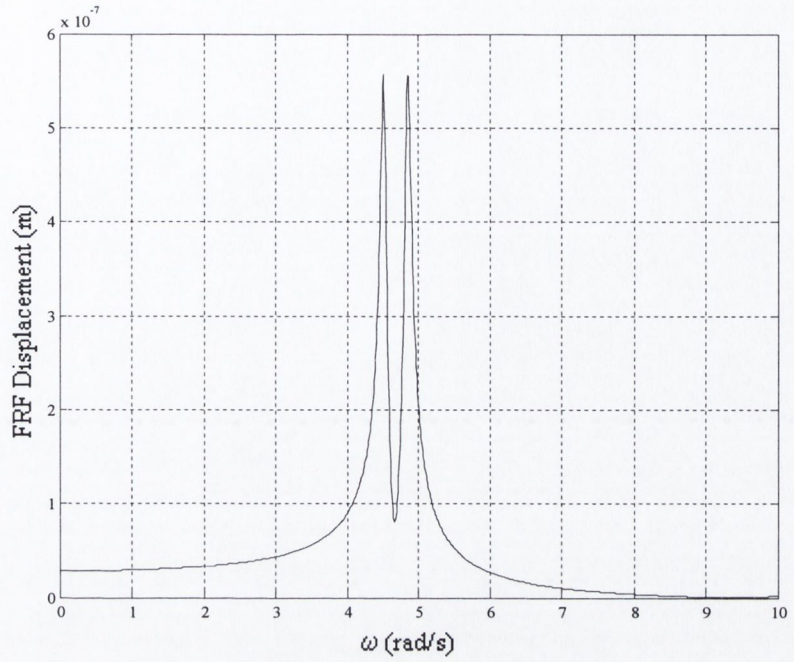

Figure 7.5 – FRF of WTT with TMD at 20th DOF tuned to the minimax principle

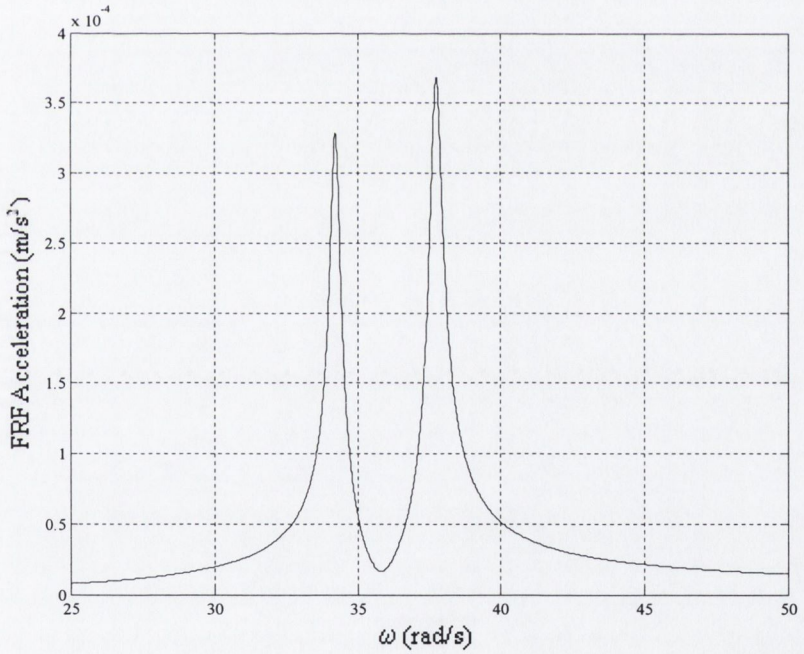

Figure 7.6 – FRF of WTT with TMD at 12th DOF tuned to the minimax principle

The FRF for the WTT with the first TMD tuned to the minimax principle is shown in Figure 7.5, in which it is observed that the two peaks are equal. The FRF for the WTT with the fifth TMD tuned to the minimax principle is shown in Figure 7.6. Although in this case, the two peaks are not equal, as the magnitude of the

acceleration response is very small, they are close together. The difference in their magnitudes arises because the equation for the minimax principle is obtained by assuming that only one mode of vibration affects the response. However, the fundamental mode of vibration will have a non-negligible effect when the second mode dominates. As the control strategy has been developed for the case of one TMD in the structure, the FRFs in Figures 7.5 and 7.6 show the responses of the WTT with only the first and fifth TMD respectively.

The bang-bang control strategy with passive shaping of the FRF is applied to the two chosen TMDs. The five other TMDs in the structure remain as passive TMDs tuned according to the MTMD configuration obtained in Chapter 2. The optimum values of η, γ and $\ddot{x}_{max}$ for two chosen TMDs are shown in Table 7.6.

	η	γ	$\ddot{x}_{max}$
1st TMD	12	0.9913	0.01
5th TMD	20	0.9913	0.01

Table 7.6 – Values of η, γ and $\ddot{x}_{max}$ for WTT with active MTMDs and bang-bang control with passive shaping of the FRF

The response of the structure is presented in Table 7.7. Compared to the WTT with the MTMD passive configuration, the peak displacement response is reduced on average by 10% and the RMS displacement response is reduced on an average by 5.5%. The peak acceleration response is reduced at most degrees of freedom, by a maximum of 6%, with more reductions than increases. The RMS acceleration response is reduced by a maximum of 2%. The corresponding performance criteria are presented in Table 7.8. Compared to Table 7.5, there are improvements in all performance criteria. The greatest reduction is observed for the peak displacement response. The values of the performance measures J_6 and J_{12} shown are the greater of those obtained in the two actuators; in this case the actuator placed at the 12th DOF to control the acceleration response.

DOF	x_p (cm)	$\ddot{x}_p$ (cm/s^2)	σ (cm)	$\ddot{\sigma}$ (cm/s^2)
1	0.003	26.718	0.001	7.304
2	0.013	79.383	0.004	19.608
3	0.030	117.770	0.010	30.511
4	0.053	146.990	0.017	39.268
5	0.083	165.660	0.027	45.342
6	0.118	160.900	0.038	48.397
7	0.160	163.430	0.052	49.243
8	0.208	153.340	0.068	48.118
9	0.263	150.550	0.086	45.057
10	0.325	151.470	0.107	39.946
11	0.392	134.200	0.129	34.244
12	0.465	112.380	0.153	31.880
13	0.542	123.150	0.179	35.292
14	0.623	153.050	0.207	41.245
15	0.708	155.400	0.237	47.465
16	0.798	169.530	0.268	51.940
17	0.895	195.910	0.300	53.119
18	0.994	186.730	0.333	47.678
19	1.093	123.500	0.367	30.475
20	1.195	52.654	0.402	12.802
21	5.128	138.460	1.851	42.270
22	16.303	402.550	6.589	129.200
23	11.413	406.220	4.426	119.470
24	19.320	435.150	6.491	127.970
25	0.280	383.240	0.082	106.670
26	0.262	415.670	0.064	104.180
27	0.363	470.200	0.122	148.780

Table 7.7 – Response of WTT with active MTMDs and bang-bang control with passive shaping of the FRF

J_1	0.833	J_7	0.810
J_2	0.772	J_8	0.758
J_3	0.627	J_9	0.781
J_4	0.624	J_{10}	0.768
J_5	2.885	J_{11}	3.353
J_6	1.28E-04	J_{12}	4.50E-04

Table 7.8 – Performance criteria for response of WTT with active MTMDs and bang-bang control with passive shaping of the FRF

7.5.4 Bang-bang control strategy with VSTMDs and MTMD configuration

The VSTMD with online shaping of the FRF, proposed in Chapter 4, using bang-bang control with VSTMDs and online shaping of the FRF, is now applied to the two chosen TMDs. The first and fifth TMDs in the structure are retuned in real time according to the minimax principle, and a control force is applied. The values of η, γ_1, γ_2 and $\ddot{x}_{max}$ for these TMDs are shown in Table 7.9.

	η	γ_1	γ_2	$\ddot{x}_{max}$
1st TMD	80	1.3402	0.6424	0.001
5th TMD	30	1.1222	0.8604	0.005

Table 7.9 – Values of η, γ_1, γ_2 and $\ddot{x}_{max}$ for WTT with VS MTMDs with bang-bang control and online shaping of the FRF

The response of the structure is presented in Table 7.10. Compared to the passive MTMD configuration, the peak displacement response of the structure is reduced on average by 10% and the RMS displacement response is reduced on average by 4.5%. The peak acceleration is reduced at most degrees of freedom, by a maximum of 4%, with more reductions than increases. The RMS acceleration response reduces on average by 1%. The greatest reduction is observed in the peak displacement response. The performance criteria are shown in Table 7.11. Compared to the passive control strategy, the reductions in the peak displacement and peak acceleration responses are not as large, and the difference in the RMS displacement and acceleration is marginal. In contrast, the performance measures J_6 and J_{12}, given for the higher of the two actuators (that at the 12th DOF controlling the acceleration response), are now reduced by 25%. Indeed, even to achieve the same reduction in response as bang-bang control with passive shaping of the FRF, the control forces with bang-bang control and online shaping of the FRF are still significantly lower.

DOF	x_p (cm)	$\ddot{x}_p$ (cm/s^2)	σ (cm)	$\ddot{\sigma}$ (cm/s^2)
1	0.003	27.564	0.001	7.336
2	0.014	80.624	0.004	19.717
3	0.031	119.600	0.010	30.731
4	0.054	145.620	0.017	39.593
5	0.084	165.070	0.027	45.722
6	0.120	166.250	0.039	48.744
7	0.162	170.340	0.053	49.492
8	0.210	156.270	0.069	48.216
9	0.264	150.140	0.087	45.018
10	0.323	154.390	0.108	39.877
11	0.388	127.440	0.130	34.225
12	0.461	111.360	0.155	31.848
13	0.542	123.320	0.181	35.171
14	0.630	156.080	0.210	41.116
15	0.723	157.980	0.240	47.480
16	0.821	170.070	0.271	52.153
17	0.921	200.670	0.304	53.517
18	1.024	189.030	0.338	48.071
19	1.129	122.060	0.372	30.707
20	1.235	51.690	0.407	12.852
21	8.718	257.870	2.637	62.391
22	16.063	393.360	6.569	128.810
23	11.133	399.510	4.431	119.840
24	19.541	445.590	6.589	129.840
25	0.373	510.050	0.085	110.890
26	0.252	413.430	0.064	105.140
27	0.379	483.930	0.119	143.980

Table 7.10 – Response of WTT with VS MTMDs and bang-bang control with online shaping of the FRF

J_1	0.839	J_7	0.830
J_2	0.775	J_8	0.764
J_3	0.635	J_9	0.807
J_4	0.632	J_{10}	0.783
J_5	4.111	J_{11}	5.700
J_6	9.55E-05	J_{12}	3.34E-04

Table 7.11 – Performance criteria for response of WTT with VS MTMDs and bang-bang control with online shaping of the FRF

A comparison of the performance criteria, J_1 to J_4 and J_6 to J_{10} for each of the control methods is illustrated in Figure 7.7. It is observed that the control strategies with

MTMDs perform better than one TMD only. Even thought the passive MTMD configuration achieves similar results to the active control strategies when the structural properties are known, the advantage of the active control strategies will be shown in the next section when the stiffness of the structure is varied.

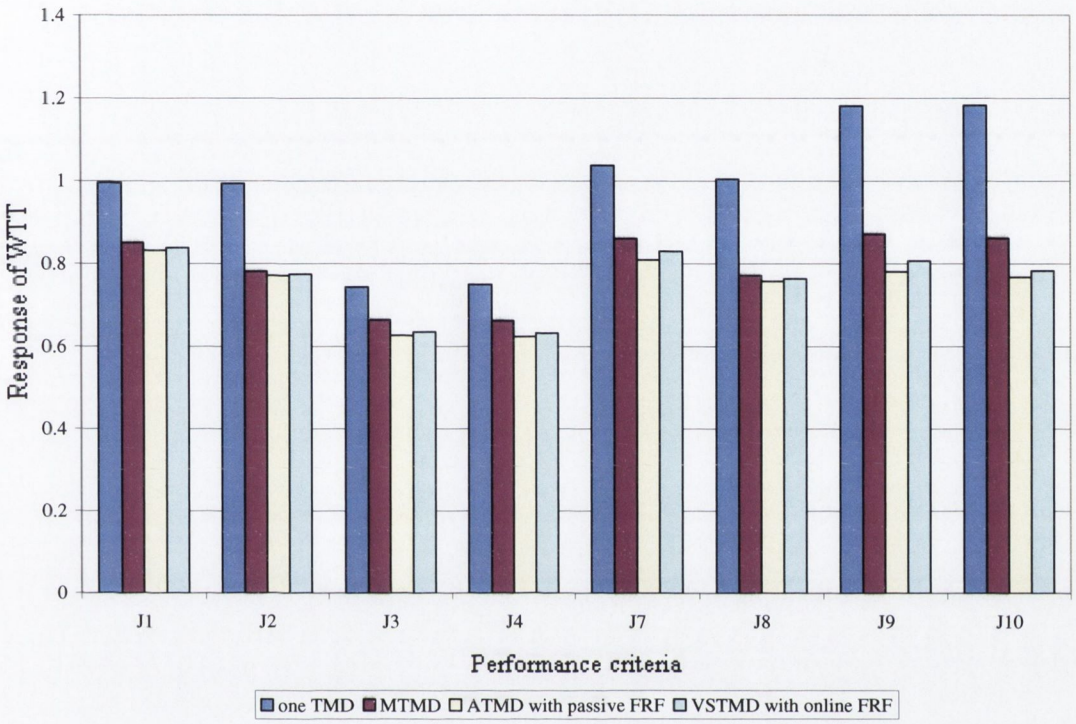

Figure 7.7 – Comparison of performance criteria for control strategies

7.5.5 Variation in the stiffness of the WTT by ±15%

In order to investigate the robustness of the specified control strategies, a variation in the stiffness of the structure of ±15% is introduced. All values are compared to the response of the uncontrolled structure with 0% variation in the stiffness.

7.5.5.1 Variation in the stiffness by +15%

Tables 7.12 and 7.13 show the response of the structure with one TMD and the MTMD configuration for +15% variation in the stiffness. With one TMD, the peak response of the structure is increased on an average by 34% and the RMS displacement response is increased on an average by 36%. The peak acceleration is

reduced at most degrees of freedom, by a maximum of 16%, with more reductions than increases and the RMS acceleration is reduced at most degrees of freedom, by a maximum of 12%, with more reductions than increases. This response is reflected in the performance criteria presented in Table 7.13 when, compared to the uncontrolled structure, the peak and RMS displacement criteria are increased and the peak and RMS acceleration criteria are reduced. It is observed in Table 7.14 when the MTMD configuration is introduced, compared to the uncontrolled structure, the peak response of the structure is reduced on an average by 31%, the RMS displacement response is reduced on an average by 37%, the peak acceleration response is reduced by between 4 and 41% and the RMS acceleration response is reduced by between 9 and 46%. Table 7.15 presents the resulting performance criteria, which are significantly reduced with the MTMD configuration.

DOF	x_p (cm)	$\ddot{x}_p$ (cm/s^2)	σ (cm)	$\ddot{\sigma}$ (cm/s^2)
1	0.006	36.826	0.002	7.906
2	0.026	93.202	0.009	21.168
3	0.057	137.770	0.021	32.829
4	0.101	167.740	0.037	42.111
5	0.155	181.660	0.058	48.145
6	0.220	189.440	0.084	51.092
7	0.295	193.020	0.114	52.518
8	0.379	201.990	0.149	52.964
9	0.476	202.500	0.188	53.958
10	0.584	181.320	0.232	54.568
11	0.699	178.490	0.281	55.452
12	0.823	183.420	0.333	55.447
13	0.953	194.880	0.390	55.672
14	1.090	218.080	0.450	55.940
15	1.231	199.370	0.514	56.228
16	1.380	202.800	0.582	57.297
17	1.532	207.670	0.652	57.798
18	1.687	181.080	0.725	50.927
19	1.842	141.730	0.799	34.948
20	2.001	69.063	0.875	21.639
21	14.328	320.600	5.096	100.500

Table 7.12 – Response of WTT with one TMD and +15% variation in the stiffness

J_1	0.907	J_7	0.901
J_2	0.935	J_8	0.935
J_3	1.364	J_9	1.308
J_4	1.359	J_{10}	1.331
J_5	7.944	J_{11}	9.367
J_6	0.000	J_{12}	0.000

Table 7.13 – Performance criteria for response of WTT with one TMD and +15% variation in the stiffness

DOF	x_p (cm)	$\ddot{x}_p$ (cm/s^2)	σ (cm)	$\ddot{\sigma}$ (cm/s^2)
1	0.003	24.015	0.001	6.508
2	0.013	70.064	0.004	18.038
3	0.029	107.130	0.010	28.477
4	0.051	144.450	0.017	36.389
5	0.079	158.880	0.027	42.125
6	0.112	171.920	0.039	45.459
7	0.150	162.160	0.053	46.113
8	0.193	160.450	0.069	44.787
9	0.242	145.550	0.088	41.743
10	0.295	138.040	0.108	37.105
11	0.353	120.550	0.131	33.135
12	0.416	119.960	0.156	31.621
13	0.485	131.510	0.182	33.263
14	0.561	141.550	0.211	38.202
15	0.642	163.520	0.241	44.189
16	0.726	180.540	0.272	49.441
17	0.812	196.560	0.305	50.479
18	0.899	171.970	0.339	44.624
19	0.986	113.800	0.374	29.712
20	1.078	52.229	0.409	13.896
21	9.909	259.960	2.914	70.719
22	14.757	348.360	5.646	112.570
23	12.412	378.680	4.574	123.190
24	15.827	358.700	5.391	110.550
25	0.248	391.250	0.076	106.040
26	0.287	484.870	0.085	141.300
27	0.252	330.900	0.066	90.648

Table 7.14 – Response of WTT with passive MTMDs and +15% variation in the stiffness

J_1	0.792	J_7	0.813
J_2	0.728	J_8	0.744
J_3	0.637	J_9	0.705
J_4	0.635	J_{10}	0.696
J_5	4.542	J_{11}	6.478
J_6	0.000	J_{12}	0.000

Table 7.15 – Performance criteria for response of WTT with passive MTMDs and +15% variation in the stiffness

The bang-bang control strategy with passive shaping of the FRF is applied to the two chosen TMDs. The values of η, γ and $\ddot{x}_{max}$ for each TMD are shown in Table 7.16.

	η	γ	$\ddot{x}_{max}$
1st TMD	10	0.9913	0.01
5th TMD	20	0.9913	0.01

Table 7.16 – Values of η, γ and $\ddot{x}_{max}$ for WTT with active MTMDs and bang-bang control with passive shaping of the FRF and +15% variation in the stiffness

Table 7.17 presents the response of the structure when the control strategy is applied. Compared to the WTT with the MTMD configuration, the peak displacement response is now reduced by between 2 and 6% and the RMS displacement response is reduced on an average by 7.5%. The peak acceleration response is reduced at most degrees of freedom, by a maximum of 7%, with more reductions than increases and the RMS acceleration response is reduced by up to 5%. Table 7.18 shows the corresponding performance criteria. It is observed that all the performance measures are reduced compared to the WTT with the passive MTMD configuration, with over 40% reduction in the peak displacement response.

DOF	x_p (cm)	$\ddot{x}_p$ (cm/s^2)	σ (cm)	$\ddot{\sigma}$ (cm/s^2)
1	0.003	23.963	0.001	6.484
2	0.013	70.276	0.004	17.908
3	0.028	107.740	0.009	28.149
4	0.049	145.350	0.016	35.868
5	0.076	163.340	0.025	41.544
6	0.108	173.190	0.036	44.919
7	0.146	159.900	0.049	45.701
8	0.188	159.070	0.064	44.510
9	0.234	146.840	0.081	41.512
10	0.286	146.550	0.100	36.765
11	0.342	112.740	0.120	32.518
12	0.404	111.100	0.143	30.819
13	0.469	138.100	0.167	32.676
14	0.538	149.200	0.193	37.952
15	0.611	164.500	0.221	43.914
16	0.686	177.580	0.250	48.874
17	0.763	195.150	0.280	49.749
18	0.841	172.100	0.311	43.934
19	0.922	117.590	0.343	29.219
20	1.006	48.525	0.375	13.188
21	12.043	301.130	3.989	97.287
22	14.676	344.480	5.648	111.980
23	11.955	363.060	4.334	116.580
24	15.685	369.490	5.416	110.420
25	0.312	469.030	0.076	104.240
26	0.293	501.600	0.087	143.900
27	0.274	365.390	0.066	90.637

Table 7.17 – Response of WTT with active MTMDs and bang-bang control and passive shaping of the FRF and +15% variation in the stiffness

J_1	0.780	J_7	0.807
J_2	0.719	J_8	0.746
J_3	0.585	J_9	0.658
J_4	0.583	J_{10}	0.661
J_5	8.805	J_{11}	10.254
J_6	1.23E-04	J_{12}	4.44E-04

Table 7.18 – Performance criteria for response of WTT with active MTMDs and bang-bang control and passive shaping of the FRF and +15% variation in the stiffness

The online control strategy using bang-bang control with VSTMDs and online shaping of the FRF is now applied to the WTT. Table 7.19 shows the value of η, γ_1, γ_2 and $\ddot{x}_{max}$ for the two chosen TMDs. The values of γ_1, γ_2 take into account the +15% variation in the stiffness.

	η	γ_1	γ_2	$\ddot{x}_{max}$
1st TMD	30	1.3197	1.0119	0.001
5th TMD	30	1.3197	1.0119	0.005

Table 7.19 – Values of η, γ_1, γ_2 and $\ddot{x}_{max}$ VS MTMDs with bang-bang control and online shaping of the FRF and +15% variation in the stiffness

Table 7.20 shows the response of the structure with the online control strategy. The peak displacement response is reduced by 4 to 13% and the RMS displacement response is reduced on an average by 15%. The peak acceleration response is reduced at most degrees of freedom, by a maximum of 9%, with more reductions than increases and the RMS acceleration response is reduced up to 10%. The performance criteria are shown in Table 7.21. Compared to the passive control strategy, all performance criteria except for the RMS displacement criteria are reduced. Now, nearly 50% reduction is observed in the peak displacement criteria. The performance measures J_6 and J_{12} are now significantly reduced by 85%. Therefore, in addition to achieving greater response reduction, by the application of the VSTMD with online shaping of the FRF, the ability of the VSTMD to retune according to the minimax principle reduces the average control power and peak control power considerably more than was observed for the WTT with 0% uncertainty in its stiffness.

DOF	x_p (cm)	$\ddot{x}_p$ (cm/s^2)	σ (cm)	$\ddot{\sigma}$ (cm/s^2)
1	0.003	24.140	0.001	6.502
2	0.011	70.400	0.004	17.961
3	0.026	111.120	0.008	28.249
4	0.046	143.100	0.015	35.971
5	0.072	160.890	0.023	41.557
6	0.103	169.850	0.033	44.737
7	0.140	161.380	0.045	45.318
8	0.182	152.230	0.059	43.962
9	0.229	150.630	0.074	40.922
10	0.281	156.560	0.092	36.349
11	0.337	129.310	0.111	32.438
12	0.400	116.200	0.131	30.905
13	0.466	118.390	0.154	32.514
14	0.537	138.410	0.178	37.414
15	0.612	168.940	0.203	43.248
16	0.688	180.440	0.230	48.406
17	0.767	191.040	0.257	49.513
18	0.847	167.950	0.286	43.814
19	0.935	114.910	0.315	29.000
20	1.030	47.933	0.345	12.375
21	11.367	335.370	3.727	97.741
22	14.943	345.360	5.640	111.950
23	11.065	333.920	3.658	99.691
24	15.473	343.700	5.331	108.530
25	0.287	509.450	0.078	121.460
26	0.250	442.360	0.075	120.640
27	0.227	338.270	0.066	91.022

Table 7.20 – Response of WTT with VS MTMDs and bang-bang control and online shaping of the FRF and +15% variation in the stiffness

J_1	0.777	J_7	0.790
J_2	0.714	J_8	0.744
J_3	0.537	J_9	0.673
J_4	0.536	J_{10}	0.661
J_5	5.809	J_{11}	7.431
J_6	1.85E-05	J_{12}	6.97E-05

Table 7.21 – Performance criteria for response of WTT with VS MTMDs and bang-bang control and online shaping of the FRF and +15% variation in the stiffness

A comparison of the performance criteria, J_1 to J_4 and J_6 to J_{10} for each of the control methods is illustrated in Figure 7.8. It is observed that the active control strategies

perform better than the passive control strategies and generally the VSTMD with online shaping of the FRF performs better than the ATMD with passive shaping of the FRF.

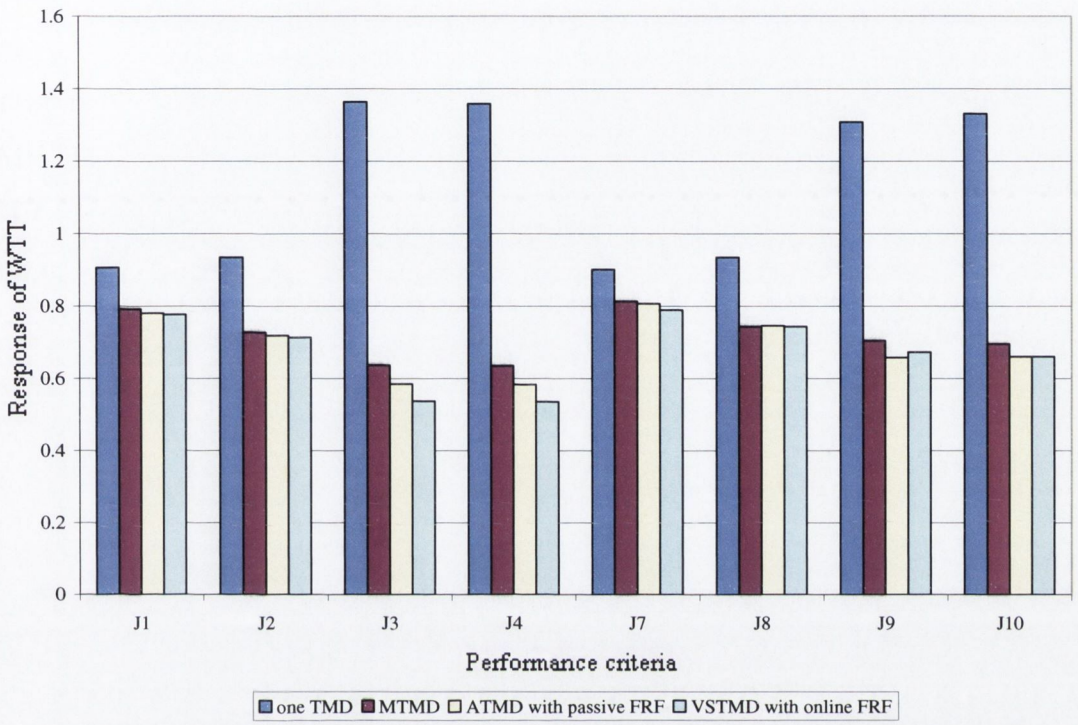

Figure 7.8 – Comparison of performance criteria for control strategies with +15% variation in the stiffness in the WTT

7.5.5.2 Variation in the stiffness by -15%

The stiffness of the WTT is now varied by –15%. Table 7.22 shows the response of the structure with one TMD. Compared to the uncontrolled structure, the peak displacement response of the structure is reduced by between 1 and 8% and the RMS displacement response is reduced on an average by 18%. The peak acceleration response is reduced at most degrees of freedom, by a maximum of 14%, with more reductions than increases and the RMS acceleration response is reduced at most degrees of freedom, by a maximum of 11%, with more reductions than increases. In the performance criteria in Table 7.23, small reductions are observed in the peak and RMS displacement response criteria, but the peak and RMS acceleration response do not change substantially. When the MTMD configuration is applied to the structure,

it is observed in Table 7.24 that the peak displacement response now increases by between 6 and 17%, and the displacement response is greater than that of the uncontrolled structure and the RMS displacement response increases by between 6 and 10%. The peak acceleration response is reduced at most degrees of freedom, by a maximum of 29%, with more reductions than increases and the RMS acceleration response reduces by 7 to 52%. The performance criteria presented in Table 7.25 show reductions in the peak and RMS acceleration responses, but increases in the peak and RMS displacement responses. Therefore the MTMD configuration, designed for the WTT with 0% uncertainty in the stiffness, increases the displacement response of the structure when its stiffness is varied by -15%.

DOF	x_p (cm)	$\ddot{x}_p$ (cm/s^2)	σ (cm)	$\ddot{\sigma}$ (cm/s^2)
1	0.005	24.972	0.001	6.545
2	0.019	73.094	0.006	18.456
3	0.042	115.630	0.013	29.790
4	0.074	155.880	0.023	39.196
5	0.114	183.410	0.036	47.057
6	0.162	205.440	0.052	53.322
7	0.218	226.590	0.070	57.815
8	0.281	239.120	0.091	60.980
9	0.350	220.850	0.114	62.937
10	0.424	223.240	0.140	63.560
11	0.503	217.030	0.169	64.012
12	0.586	226.100	0.199	64.737
13	0.672	234.170	0.233	65.247
14	0.760	221.400	0.268	65.745
15	0.855	218.170	0.305	65.681
16	0.959	206.300	0.345	64.202
17	1.065	209.130	0.386	59.028
18	1.173	183.560	0.428	48.226
19	1.282	111.220	0.472	30.892
20	1.393	71.777	0.517	22.853
21	10.619	298.150	3.641	91.387

Table 7.22 – Response of WTT with one TMD and -15% variation in the stiffness

J_1	1.031	J_7	0.988
J_2	1.008	J_8	0.992
J_3	0.806	J_9	0.911
J_4	0.809	J_{10}	0.936
J_5	5.676	J_{11}	6.942
J_6	0.000	J_{12}	0.000

Table 7.23 – Performance criteria for response of WTT with one TMD and -15% variation in the stiffness

DOF	x_p (cm)	$\ddot{x}_p$ (cm/s^2)	σ (cm)	$\ddot{\sigma}$ (cm/s^2)
1	0.005	36.753	0.002	7.802
2	0.020	97.304	0.006	20.723
3	0.046	139.830	0.014	31.797
4	0.082	143.990	0.025	40.291
5	0.127	159.790	0.040	45.306
6	0.182	161.700	0.057	46.739
7	0.246	157.620	0.078	45.984
8	0.319	177.260	0.102	43.767
9	0.402	168.740	0.129	42.418
10	0.494	152.610	0.159	41.544
11	0.596	144.820	0.192	41.737
12	0.708	140.430	0.228	41.066
13	0.826	143.610	0.267	41.042
14	0.951	179.670	0.309	42.116
15	1.081	165.790	0.353	44.495
16	1.215	171.420	0.399	48.879
17	1.352	195.020	0.447	52.573
18	1.491	182.800	0.497	47.788
19	1.633	127.400	0.548	32.637
20	1.779	59.120	0.600	15.029
21	10.693	240.850	3.737	76.515
22	20.090	428.180	6.125	119.080
23	11.521	373.600	3.871	105.670
24	19.641	469.080	8.097	151.350
25	0.391	432.890	0.097	112.240
26	0.225	308.470	0.057	85.787
27	0.563	638.600	0.144	156.860

Table 7.24 – Response of WTT with passive MTMDs and -15% variation in the stiffness

J_1	0.825	J_7	0.806
J_2	0.787	J_8	0.808
J_3	0.936	J_9	1.163
J_4	0.931	J_{10}	1.161
J_5	8.793	J_{11}	10.116
J_6	0.000	J_{12}	0.000

Table 7.25 – Performance criteria for response of WTT with passive MTMDs and -15% variation in the stiffness

The ATMD with passive shaping of the FRF is now applied to the WTT. The values of η, γ and $\ddot{x}_{max}$ for the two controlled TMDs are shown in Table 7.26.

	η	γ	$\ddot{x}_{max}$
1st TMD	50	0.9913	0.01
5th TMD	20	0.9913	0.01

Table 7.26 – Values of η, γ and $\ddot{x}_{max}$ for active MTMDs with bang-bang control and passive shaping of the FRF and -15% variation in the stiffness

The response of the structure with MTMDs is shown in Table 7.27 and the performance criteria are shown in Table 7.28. It is observed in Table 7.27 that the peak displacement response is now reduced by between 2 and 7% and the RMS displacement response is reduced on an average by 12%. The peak acceleration response is reduced at some degrees of freedom, by a maximum of 16%, however, it is increased at others, also by a maximum of 16%, overall the peak acceleration response is increased and the RMS acceleration response is also increased up to 6%. These results suggest that applying control to the first TMD is effective in reducing the displacement response of the structure; however, it also increases the acceleration response. Further control applied to the fifth TMD does not reduce the acceleration response significantly. This is reflected in the performance criteria given in Table 7.28; it is observed that the acceleration performance criteria are increased compared to the MTMD configuration, but the displacement criteria are reduced. However, the peak displacement criteria is still greater than 1, therefore no reduction compared to the uncontrolled structure is acheived.

DOF	x_p (cm)	$\ddot{x}_p$ (cm/s^2)	σ (cm)	$\ddot{\sigma}$ (cm/s^2)
1	0.005	37.724	0.001	7.951
2	0.019	99.757	0.005	21.402
3	0.043	144.810	0.012	33.371
4	0.075	152.680	0.022	42.776
5	0.117	170.900	0.035	48.379
6	0.168	173.440	0.050	49.738
7	0.229	169.200	0.068	48.127
8	0.298	178.940	0.089	44.604
9	0.376	167.780	0.112	42.158
10	0.462	150.950	0.139	41.065
11	0.557	155.690	0.168	41.618
12	0.662	145.000	0.199	41.028
13	0.773	147.360	0.234	40.410
14	0.894	171.990	0.270	40.975
15	1.021	155.910	0.309	44.295
16	1.153	199.190	0.350	50.657
17	1.292	212.330	0.392	55.606
18	1.437	198.920	0.436	50.553
19	1.585	135.520	0.481	33.686
20	1.735	49.611	0.527	13.804
21	28.130	671.040	10.183	223.830
22	17.057	394.860	4.796	95.182
23	11.379	357.220	3.920	108.950
24	18.719	465.040	6.338	124.080
25	0.426	488.100	0.106	127.460
26	0.198	330.120	0.053	85.566
27	0.403	515.640	0.111	127.400

Table 7.27 – Response of WTT with active MTMDs and bang-bang control and passive shaping of the FRF and -15% variation in the stiffness

J_1	0.872	J_7	0.878
J_2	0.806	J_8	0.840
J_3	0.821	J_9	1.134
J_4	0.816	J_{10}	1.105
J_5	15.874	J_{11}	18.390
J_6	1.64E-04	J_{12}	5.80E-04

Table 7.28 – Performance criteria for response of WTT with active MTMDs and bang-bang control and passive shaping of the FRF and -15% variation in the stiffness

The VSTMD with online shaping of the FRF is now applied and the values of η, γ_1, γ_2 and $\ddot{x}_{max}$ determined for a -15% variation in the stiffness are shown in Table 7.29

	η	γ_1	γ_2	$\ddot{x}_{max}$
1st TMD	50	1.037	0.663	0.005
5th TMD	20	0.9248	0.7752	0.005

Table 7.29 – Values of η, γ_1, γ_2 and $\ddot{x}_{max}$ for VS MTMDs with bang-bang control and online shaping of the FRF and -15% variation in the stiffness

The response of the structure with MTMDs is shown in Table 7.30 and the performance criteria are given in Table 7.31. Compared to the MTMD configuration, the peak displacement response is now reduced on an average by 22% and the RMS displacement response is reduced on an average by 26%. The peak acceleration response is reduced at most degrees of freedom, by a maximum of 13% with more reductions than increases and the RMS acceleration is reduced by up to 19%. It is shown in the performance criteria in Table 7.31 that the peak displacement criteria are now reduced below 1 and the RMS displacement criteria are significantly reduced compared to those for the ATMD with passive shaping of the FRF. The peak and RMS acceleration criteria are also reduced compared to the ATMD with passive shaping of the FRF, but are increased compared to the MTMD configuration without control. One possible reason for this is that the fifth TMD is tuned according the minimax principle assuming it is the only mode in the structure, this is not true and therefore the magnitudes of the peaks of the FRF are not equal, as observed in Figure 7.5. However, there is still some reduction in the response compared to the uncontrolled structure. The performance measures J_6 and J_{12} are reduced by 54% compared to the passive strategy, therefore once again, the ability of the VSTMD to retune according to the minimax principle reduces the control power required to be applied to the TMD and also considerably reduces the displacement response of the structure.

DOF	x_p (cm)	$\ddot{x}_p$ (cm/s^2)	σ (cm)	$\ddot{\sigma}$ (cm/s^2)
1	0.004	36.690	0.001	7.824
2	0.016	98.893	0.005	20.826
3	0.036	142.570	0.010	32.050
4	0.063	148.020	0.018	40.701
5	0.097	160.030	0.029	45.825
6	0.139	168.370	0.042	47.243
7	0.187	159.750	0.057	46.288
8	0.242	180.310	0.074	43.523
9	0.304	171.650	0.094	41.197
10	0.373	143.890	0.116	39.225
11	0.450	143.540	0.140	38.665
12	0.535	133.290	0.166	37.653
13	0.627	139.230	0.195	37.771
14	0.726	161.560	0.225	39.531
15	0.829	158.790	0.258	43.093
16	0.936	198.390	0.292	48.621
17	1.046	206.930	0.327	52.833
18	1.158	187.950	0.363	47.965
19	1.271	132.980	0.401	32.202
20	1.386	51.165	0.439	12.092
21	33.226	777.980	9.719	181.930
22	12.371	314.460	4.864	97.055
23	11.494	361.030	3.930	107.710
24	14.695	400.720	4.616	96.101
25	0.411	468.490	0.106	117.320
26	0.185	309.790	0.051	83.177
27	0.367	455.390	0.097	116.200

Table 7.30 – Response of WTT with VS MTMDs and bang-bang control and online shaping of the FRF and -15% variation in the stiffness

J_1	0.829	J_7	0.855
J_2	0.768	J_8	0.814
J_3	0.684	J_9	0.906
J_4	0.680	J_{10}	0.893
J_5	15.151	J_{11}	21.722
J_6	7.53E-05	J_{12}	2.67E-04

Table 7.31 – Performance criteria for response of WTT with VS MTMDs and bang-bang control and online shaping of the FRF and -15% variation in the stiffness

A comparison of the performance criteria, J_1 to J_4 and J_6 to J_{10} for each of the control methods is illustrated in Figure 7.9. It is observed that the passive MTMD

configuration and the ATMD with passive shaping of the FRF increases the response in some cases compared to the WTT with one TMD. However, in all cases, the VSTMD with online shaping of the FRF achieves the greatest response reduction, with the exception of J_7.

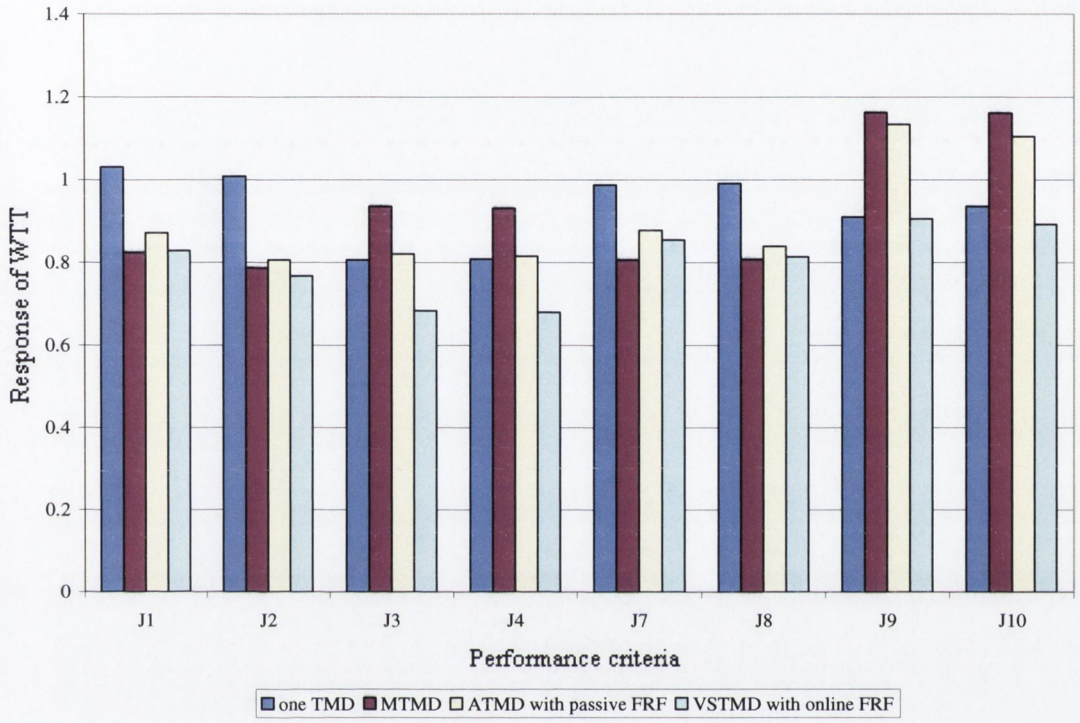

Figure 7.9 – Comparison of performance criteria for control strategies with -15% variation in the stiffness of the WTT

7.5.6 Application of optimal damping

To investigate whether employing optimal damping would be advantageous in the WTT, the value for optimal damping obtained in section 7.3 is applied to the first and fifth TMDs of the MTMD configuration, with these two dampers tuned using the minimax principle. The resulting response is presented in Table 7.32 and the corresponding performance criteria are shown in Table 7.33. Compared to the passive MTMD configuration without optimal damping, the peak displacement response is reduced on an average by 10% and the RMS displacement response is reduced on an average by 6%. The peak acceleration response is reduced at most degrees of freedom, by a maximum of 3% with more reductions than increases and the RMS

acceleration response is reduced up to 5%. All of the performance criteria shown in Table 7.33 are reduced. The response reduction is similar to that achieved with the ATMD and passive shaping of the FRF and the VSTMD and online shaping of the FRF.

DOF	x_p (cm)	$\ddot{x}_p$ (cm/s^2)	σ (cm)	$\ddot{\sigma}$ (cm/s^2)
1	0.004	27.091	0.001	7.351
2	0.014	80.471	0.004	19.796
3	0.031	119.430	0.009	30.926
4	0.055	145.810	0.017	39.905
5	0.085	164.390	0.026	46.108
6	0.121	167.250	0.038	49.145
7	0.163	170.580	0.051	49.804
8	0.211	154.250	0.067	48.344
9	0.264	155.380	0.085	44.947
10	0.322	151.250	0.105	39.581
11	0.387	126.410	0.127	33.732
12	0.457	121.020	0.151	31.229
13	0.538	125.180	0.177	34.606
14	0.624	151.050	0.204	40.752
15	0.715	156.780	0.233	47.427
16	0.808	178.550	0.264	52.378
17	0.903	202.950	0.296	53.907
18	1.000	189.170	0.329	48.412
19	1.098	123.850	0.363	30.783
20	1.198	51.141	0.397	12.534
21	7.943	190.790	2.583	58.393
22	16.484	401.910	6.256	122.510
23	11.088	394.140	4.004	109.950
24	19.408	447.740	6.518	128.750
25	0.204	283.520	0.058	75.563
26	0.189	334.590	0.055	95.420
27	0.299	392.030	0.095	118.490

Table 7.32 – Response of WTT with passive MTMDs and optimal damping

J_1	0.846	J_7	0.839
J_2	0.775	J_8	0.768
J_3	0.618	J_9	0.783
J_4	0.616	J_{10}	0.771
J_5	4.027	J_{11}	5.193
J_6	0.000	J_{12}	0.000

Table 7.33 – Performance criteria for response of WTT with passive MTMDs and optimal damping

Optimal damping is now applied to the structure with passive MTMDs and ±15% variation in the stiffness of the WTT. Tables 7.34 and 7.35 show the response of the structure and the performance criteria, respectively.

DOF	x_p (cm)	$\ddot{x}_p$ (cm/s^2)	σ (cm)	$\ddot{\sigma}$ (cm/s^2)
1	0.003	24.115	0.001	6.496
2	0.013	69.362	0.004	17.973
3	0.028	107.020	0.009	28.333
4	0.049	144.290	0.016	36.153
5	0.076	157.690	0.025	41.821
6	0.108	170.760	0.036	45.108
7	0.145	158.700	0.049	45.721
8	0.187	157.560	0.064	44.334
9	0.233	145.620	0.081	41.135
10	0.284	139.690	0.100	36.191
11	0.340	118.500	0.121	31.842
12	0.399	109.040	0.144	30.136
13	0.468	129.310	0.169	31.956
14	0.545	141.900	0.195	37.269
15	0.626	162.770	0.223	43.519
16	0.710	181.540	0.252	48.893
17	0.796	194.240	0.283	49.993
18	0.883	170.100	0.314	44.226
19	0.972	111.770	0.346	29.357
20	1.061	50.363	0.379	13.049
21	6.515	184.140	2.103	52.843
22	14.660	345.290	5.579	111.030
23	11.949	364.880	4.195	113.800
24	15.925	354.720	5.345	109.390
25	0.177	273.300	0.050	72.907
26	0.229	431.750	0.073	122.960
27	0.227	317.050	0.062	85.983

Table 7.34 – Response of WTT with passive MTMDs and optimal damping and +15% variation in the stiffness

J_1	0.784	J_7	0.803
J_2	0.716	J_8	0.736
J_3	0.591	J_9	0.694
J_4	0.588	J_{10}	0.679
J_5	3.278	J_{11}	4.259
J_6	0.000	J_{12}	0.000

Table 7.35 – Performance criteria for response of WTT with passive MTMDs and optimal damping and +15% variation in the stiffness

Due to the addition of optimal damping, to the first and fifth TMDs of the MTMD configuration, compared to the WTT and MTMDs without optimal damping, the peak displacement response is reduced by between 1 and 3%, the RMS displacement response is reduced on an average by 7%, the peak acceleration response is reduced up to 9% and the RMS acceleration response is reduced up to 6%. Compared to the two other control strategies, (i) ATMDs with passive shaping of the FRF and (ii) VSTMDs with online shaping of the FRF, the passive MTMD configuration with optimal damping to the first and fifth TMD achieves slightly higher values in the performance criteria but still adequate reduction.

Tables 7.36 and 7.37 show the response of the structure and the performance criteria for -15% variation in the stiffness. Due to the addition of optimal damping, the peak displacement response is reduced on an average by 5%, the RMS displacement response is reduced on an average by 4.5%, the peak acceleration response is reduced up to 14% and the RMS acceleration response is reduced up to 7%. Compared to the ATMD with passive shaping of the FRF, the peak displacement performance criteria is not as good but optimal damping achieves greater reductions in the acceleration performance criteria, and in the RMS displacement criteria. However, the peak displacement performance criteria here is still greater than 1, therefore no reduction compared to the uncontrolled structure is acheived. Compared to the VSTMD with online shaping of the FEF, optimal damping achieves greater reductions in the acceleration performance criteria, but it was seen that the online control strategy successfully reduced the displacement response.

DOF	x_p (cm)	$\ddot{x}_p$ (cm/s^2)	σ (cm)	$\ddot{\sigma}$ (cm/s^2)
1	0.005	36.891	0.001	7.770
2	0.019	97.494	0.006	20.593
3	0.043	140.150	0.014	31.505
4	0.077	144.830	0.024	39.800
5	0.120	160.770	0.038	44.626
6	0.172	157.730	0.054	45.886
7	0.233	154.080	0.074	44.982
8	0.304	175.820	0.097	42.532
9	0.382	169.240	0.123	40.742
10	0.469	142.860	0.152	39.221
11	0.565	140.760	0.183	38.866
12	0.670	135.010	0.218	37.929
13	0.783	131.790	0.255	38.103
14	0.901	173.110	0.295	39.713
15	1.025	160.370	0.338	42.714
16	1.153	172.320	0.382	47.596
17	1.283	192.510	0.428	51.644
18	1.416	180.300	0.476	47.180
19	1.550	125.180	0.525	32.309
20	1.688	50.622	0.575	13.918
21	7.434	172.850	2.676	53.249
22	18.139	402.530	5.802	112.570
23	11.335	352.650	3.790	103.650
24	19.576	446.640	7.794	146.120
25	0.284	315.270	0.067	78.018
26	0.206	291.540	0.050	79.644
27	0.485	536.560	0.117	132.330

Table 7.36 – Response of WTT with passive MTMDs and optimal damping and -15% variation in the stiffness

J_1	0.810	J_7	0.796
J_2	0.761	J_8	0.791
J_3	0.896	J_9	1.104
J_4	0.890	J_{10}	1.101
J_5	12.150	J_{11}	12.798
J_6	0.000	J_{12}	0.000

Table 7.37 – Performance criteria for response of WTT with passive MTMDs and optimal damping and -15% variation in the stiffness

Therefore, for -15% variation in the stiffness, when the ATMD with passive shaping of the FRF and the VSTMD with online shaping of the FRF are applied to the first and fifth TMD of the MTMD configuration, the acceleration response is not adequately reduced. This is possibly due to the assumption that the fifth TMD is tuned according to the minimax principle when there are no other degrees of freedom in the structure. However, with the addition of optimal damping to the first and fifth TMD in the passive MTMD configuration, the acceleration response is reduced. Future work could include the combination of optimal damping with the ATMD and the VSTMD with passive and online shaping of the FRF, respectively, in order to further reduce the response of the structure.

7.6 CONCLUSION

A set of random excitations was generated from the Davenport spectrum for a 20 DOF model and applied to a 20 DOF WTT. In order to examine the robustness of the control strategies, a variation in the stiffness of the structure by ±15% was introduced. Passive MTMDs were applied to the structure and the response was obtained. It was observed that for 0% uncertainty in the stiffness, the response reduction was considerable; however, it was not as good for ±15% variation in the stiffness. The ATMD with passive shaping of the FRF, obtained in Chapter 3 and the VSTMD with online shaping of the FRF, obtained in Chapter 4 were then applied to a WTT with MTMDs. The VSTMD that was developed in Chapters 5 and 6 was used for the control strategy with online shaping of the FRF. It was observed that similar response reduction was seen for 0% uncertainty in the stiffness and the control strategy with online shaping of the FRF had lower control force than the control strategy with passive shaping of the FRF. However, for ±15% variation in the stiffness, the control strategy with online shaping of the FRF proved the most efficient, reducing both the control effort and the response of the structure. Finally, optimal damping in the structure was examined for the passive MTMDs in order to determine its effectiveness for future design. It was observed that the response of the structure was decreased and therefore applications of optimal damping to the ATMD with passive shaping of the FRF and the VSTMD with online shaping of the FRF could be employed to further reduce the response of the WTT.

CHAPTER 8

CONCLUSIONS AND DISCUSSION

The study in this thesis focuses on the vibration control of tall and flexible structures, such as WTTs. Single and multiple TMDs with passive, active and semi-active control strategies for SDOF and MDOF structures have been examined. Two control strategies using bang-bang control with minimax shaping of the FRF have been proposed. The first control strategy employs ATMDs with passive shaping of the FRF and the second employs semi-active TMDs with online shaping of the FRF. A semi-active TMD in the form of a prototype VSTMD has been developed, characterised and tested experimentally. The VSTMD is capable of retuning in real time according to the minimax principle, based on the response of the structure. The control strategies were incorporated into the MTMD configuration for a WTT and the results were compared with the use of passive MTMDs in the WTT. Finally, optimal damping in the passive MTMD configuration has been investigated.

A procedure using SSA for identifying the optimal number, location and tuning parameters for MTMDs placed in a WTT has been presented. The procedure was investigated for both base and wind excitations, represented by four PSDFs; based excited white noise, the Kanai-Tajimi spectrum, wind excited white noise and the Harris spectrum. A CI based on the TMD displacement and acceleration response was defined and the optimum location, number and tuning parameter of MTMDs in the WTT for each of the PSDFs were determined. A generalised configuration for the MTMDs was subsequently obtained and shown to achieve response reductions similar to the individual optimum MTMD configurations when subjected to all of the above mentioned PSDFs. To determine the robustness of the design, the MTMD configuration was applied to a WTT with ±15% variation in the stiffness. It was observed that the response was considerably reduced in all cases. The potential for extending the outlined optimisation procedure to other areas of design is obvious, particularly in the context of performance based design. Here, specific objectives are defined for the response of a structure at different levels of base and wind excitation. These specific objectives may be used to define CIs on which the SSA is based and may include either deformation or force-based parameters.

ATMDs were introduced with the objective of reducing the number of MTMDs in the structure while achieving similar response reductions. An ATMD requires an external power source provided by an electromechanical actuator and a control strategy to drive the actuator. The principle advantage of the ATMD is that the control strategy is based on the response of the structure, thereby accounting for variations in the stiffness. A control strategy incorporating bang-bang control and the passive minimax principle for shaping the FRF has been proposed. Simulated results demonstrated that the control law can be very effective in controlling structures under resonant and non-resonant excitations, particularly in the case when there is a chance of the response being increased by the addition of a passive TMD. As the control force is applied to the TMD, the normal requirement of imposing a force on the structure, e.g. by reacting against a bracing system, is eliminated. This is useful in situations where bracing systems cannot be utilised, e.g. in WTTs or in chimneys. In addition, the control force requirements for coupled structure-ATMD systems are considerably less than those required when control forces are applied to the structure alone.

Bang-bang control with minimax shaping of the FRF was compared to another conventional method, the LQC with minimax shaping of the FRF. It was seen that the force required for the LQC with minimax shaping of the FRF was larger than that of bang-bang control with minimax shaping of the FRF, and a desired reduction in the overall response of the structure was not achieved. The control strategy proposed herein can provide reduced control forces and increased performance, enhancing safety and providing a more economic design.

The proposed control strategy was also applied to a low frequency coupled SDOF-TMD structure subjected to two random excitations, (i) with energy at the resonant frequency of the structure and (ii) with energy at the frequency for which a peak occurs in the FRF of the response of the coupled structure-TMD system. As was seen for the harmonic loading conditions, the TMD reduces the response of the structure under random excitation with energy at the resonant frequency and additional control force is not required. However, the response of the structure increases when the excitation frequency equals that at which a peak occurs in the FRF of the response of the coupled structure-TMD system. Under these conditions, the addition of the

control force using the bang-bang control law and FRF shaping, leads to a considerably reduced response.

The control strategy was then applied to the 76-storey benchmark model proposed by Yang et al. (2004) for comparison with other structural methods. To assess the robustness of the controller, a stiffness uncertainty of ±15% was applied to the model. The performance criteria developed by Yang et al. (2004) were obtained and the results were compared to the uncontrolled model and the ATMD with LQR proposed by Yang et al. (2004). It was observed that the ATMD with bang-bang control and passive shaping of the FRF achieved slightly greater reductions in the vibration than the ATMD with LQR, and that the average power consumption and the peak power consumption were similar to those of the ATMD with LQR.

An extension to the bang-bang control strategy proposed for the ATMD has been examined further, in which the ATMD is replaced with a SAIVS-TMD, developed by Varadarajan and Nagarajaiah (2004). The bang-bang control law obtained for the ATMD was applied to the SAIVS-TMD, which is retuned in real time according to the minimax principle, taking into account the level of control required. When no control was applied, the SAIVS-TMD acted as a passive damper tuned to the minimax principle by passive shaping of the FRF. The proposed control strategy was examined under harmonic and random excitations and compared to the ATMD with bang-bang control and passive shaping of the FRF. The simulated results showed that online shaping of the FRF achieved the same reduction as the ATMD with bang-bang control and passive shaping of the FRF, but with much less control effort. The semi-active damper has the capability of changing its mechanical properties and therefore the control force applied to the TMD was significantly reduced.

The control strategy was also applied to the 76-storey benchmark model proposed by Yang et al. (2004). The results were compared to the uncontrolled model, the ATMD with LQR, the SAIVS-TMD with EMD/HT and the ATMD with bang-bang control and passive shaping of the FRF. It was observed that the proposed control strategy achieved similar reductions to the other three methods, but more importantly the control effort was considerably reduced compared to the ATMD with LQR or bang-bang control and passive shaping of the FRF. As the amount of control energy to

change the stiffness of the SAIVS-TMD is nominal, the performance of the SAIVS-TMD with bang-bang control and online shaping of the FRF achieved comparable performance with the SAIVS-TMD with EMD/HT. The advantage of the proposed control strategy is that at any one time, only three states of the SAIVS-TMD are considered, which eliminates the online calculation of the instantaneous frequency of the structure required with EMD/HT, reducing the computational effort. In addition, as the control law is based on the fundamental mode of the structure only, all other modes in the control scheme can be ignored, further reducing the computational effort.

The behaviour of a VSTMD consisting of a TMD passing through a solenoid was experimentally investigated. When current is applied to the solenoid, a magnetic field is created and additional stiffness is supplied to the TMD, hence by varying the current in the solenoid, a VSTMD is created. Details of the instrumentation and apparatus employed to test the VSTMD and a coupled SDOF-VSTMD model were supplied. This solenoid based damper does not require any electro-mechanical actuator to change the stiffness and hence the force requirement would be very low.

The VSTMD was characterised by static force deformation tests that determine the stiffness of the VSTMD. The change in the stiffness of the VSTMD over a range of frequencies was obtained for different levels of applied current, between 0 and 6A. A small stiffness was observed at 0A due to friction in the VSTMD and other external elements. For small magnitudes of current passing through the solenoid, the stiffness of the VSTMD changed insignificantly. For current greater that a threshold (3A for the developed damper), a near linear current-stiffness trend was observed in the static force deformation tests. In the dynamic tests, the stiffness of the VSTMD was observed to be frequency dependent and for current greater than a threshold, a near linear trend of increasing stiffness with current was observed. The damping in the VSTMD was insignificant.

The VSTMD model was first tested experimentally with a passive TMD (no applied current) tuned to the structure using the minimax principle. Considerable reduction in the response was observed. When a mistuned TMD was added to the structure, the reduction in the response was not as large and only one peak was observed in the

FRF. When the stiffness of the TMD was varied, two peaks were observed for a certain level of current passing through the solenoid, which tuned the TMD with this level of current to the structure according to the minimax principle. This showed that by increasing the current passing through the solenoid, the stiffness of the VSTMD could be varied so that the VSTMD was tuned to the structure according to the minimax principle.

Online control of the VSTMD, which was characterised and tested offline was investigated further. Two LabVIEW programs were created to implement online control based on the amplitude and frequency response of the structure. The amplitude of the response of the model structure was obtained using accelerometers, and the local frequency content of the response of the structure was calculated using a wavelet analysis program in MATLAB. A sine sweep of 0 to 7Hz was applied to the structure with the mistuned TMD. It was shown that online control of the structure using the VSTMD, retuned the mistuned TMD according to the minimax principle and a significant response reduction was observed. This response reduction was similar to what would have been for the structure with a perfectly passively tuned TMD. When a random excitation, with a dominant frequency of 3 to 4Hz was applied to the structure, the response of the structure with the mistuned TMD increased. However, by applying the VSTMD, the response of the structure reduced. Further research in this area could be carried out, to investigate the relationship between the sampling rate of the acquired data and the switching time of the VSTMD.

A set of random excitations were derived from the Davenport spectrum for a 20 DOF model and applied to the 20 DOF WTT. Passive MTMDs were applied to the structure and it was observed that the response reduction was considerable. However, when a variation in the stiffness of the structure by ±15% was applied, the passive MTMD design was not as effective. The AMTD with passive shaping of the FRF and the VSTMD with online shaping of the FRF were then incorporated into the MTMD configuration for the WTT. For no change in the stiffness of the structure, similar response reduction using the two proposed control strategies compared to the passive MTMD configuration was achieved. However, for ±15% variation in the stiffness of the WTT, the control strategy with online shaping of the FRF was the most effective, as for this control strategy, the TMD changes it's mechanical properties depending on

the response of the structure, so that the TMD is tuned according to the minimax principle. This was particularly obvious for the -15% variation in the stiffness of the structure. Finally, optimal damping in the WTT was examined with passive MTMDs in order to determine its effectiveness for future design. Response reduction in the structure was achieved and therefore applications of optimal damping to the active control strategies could be examined in the future to further reduce the response of the WTT.

In conclusion, the research described in this thesis has shown how single and multiple passive, active and semi-active TMDs can be effective in tall structures. Passive MTMDs were placed in a WTT model and it was shown that they were effective at reducing the vibrations in a structure if the properties of the structure were previously known. Both ATMDs and VSTMDs with passive and online shaping of the FRF improved on the passive MTMD configuration as the force applied to the TMD was based on information about the response of the structure, thereby accounting for variations in the stiffness of the structure. As the semi-active TMD has the capability of retuning the mechanical properties of the TMD in real time, the control effort was considerably reduced. A prototype VSTMD that does not require an electromechanical actuator to change its mechanical properties was developed and tested in the laboratory. The VSTMD was capable of retuning the TMD online according to the minimax principle, based on the response of the structure, and the vibrations in the structure were considerably reduced. Finally, the active and semi-active control strategies were incorporated in the MTMD configuration for a WTT. The active control strategies improved the passive MTMD configuration as the variation in the stiffness of the structure was now taken into account. With variations in the stiffness (particularly with -15%), the VSTMD achieved considerable response reductions compared to the other two control strategies. Optimal damping in the passive MTMDs was also examined and shown to provide further reductions in the response for the passive MTMD control strategy. This could be incorporated for both ATMDs with passive shaping of the FRF and VSTMDs with online shaping of the FRF

Future research following on from this thesis could be carried out in several different areas as follows:

(i) It was seen that optimal damping in the passive MTMD configuration improved the response of the structure. Optimal damping could be incorporated into the active control strategies for ATMDs with passive shaping of the FRF and VSTMDs with online shaping of the FRF, to determine if the response of the structure could be further reduced.

(ii) The minimax principle could be examined further to incorporate multiple modes of vibration in the structure.

(iii) Further research into an improved design for the solenoid of the VSTMD could be carried out. A rudimentary approach to the design of the solenoid developed in the laboratory was taken, and the optimum physical properties and dimensions of the solenoid require further investigation.

(iv) A compromise between the number of acquired sample points and the online time window for retuning of the VSTMD was attempted in this thesis. Further research into the application of the LabVIEW control software should be carried out on this topic.

(v) Research into the understanding of the physics of solenoids and electromagnets could be carried out, in order to understand the way the stiffness of the VSTMD is obtained.

REFERENCES

1. Abe, M. and Fujino, Y. (1995). "Dynamic characterization of multiple tuned mass dampers and some design formula's". *Earthquake Engineering and Structural Dynamics,* 23: 813-835
2. Abe, M. and Igusa, T. (1995). "Tuned mass dampers for structures with closely spaced natural frequencies". *Earthquake Engineering and Structural Dynamics.* 24: 247-261
3. Abe, M., Kimura, S. and Fujino, Y. (1996). "Control laws for semi-active tuned liquid column damper with variable orifice openings". *Proceedings of Second International Workshop on Structural Control, Hong Kong*, 5–10.
4. Aiken, I.D. and Kelly, J.M. (1990). "Earthquake simulator testing and alaytical studies of two energy-absorbing systems for multi-storey structures", *Report No. UCB/EERC-90/03,* University of California, Berkley, CA
5. Akbay, Z. and Aktan, H.M. (1991). "Actively regulated friction slip braces". *Proceedings of Sixth Canadian Conference on Earthquake Engineering, Toronto, Canada*, 367–74.
6. Akbay, Z. and Aktan, H.M. (1992). "Improving seismic performance of buildings by actively regulated friction slip braces". *Proceedings of 63rd Shock and Vibration Symposium, Las Cruces, NM*, 152–60.
7. Aldawod, M., Samali, B., Naghdy, F., and Kwok, K. (2001) "Active control of along wind response of tall building using a fuzzy controller". *Engineering Structures*, 23: 1512–1522
8. Alspaugh, D.W. (1978). "Analysis of Coulomb friction vibration dampers". *Journal of Sound and Vibration,* 57(1): 65-78
9. Arima, F., Miyazaki, M., Tanaka, H. and Yamazaki, Y. (1988). "A study on buildings with large damping using viscous damping walls". *Ninth World Conference Earthquake Engineering., Tokyo, V,* 821-826
10. Assawinchaichote, W., Nguang, S.K. and Shi, P. (2004). "H_∞ output feedback control design for uncertain fuzzy singularly perturbed systems: an LMI approach". *Automatica*, 40(12): 2147-2152

11. Balendra, T., Sam. M.T. and Liaw, C.Y. (!991). "Design of earthquake-resistant steel frames with knee bracing". *Journal of Constructional Steel Research,* 18(3): 193-208

12. Balendra, T., Wang, C. and Yan, N. (2001). "Control of wind-excited towers by active tuned liquid column damper" *Engineering Structures*, 23: 1054–1067

13. Balendra, T., Wang, C.M. and Cheong, H.F. (1995). "Effectiveness of tuned liquid column dampers for vibration control of towers". *Engineering Structures,* 17(9): 668-675

14. Bansal, R. and Basar, T. (1987). "Solutions to a class of linear-quadratic-Gaussian (LQG) stochastic team problems with nonclassical information". *Systems & Control Letters,* 9(2): 125-130

15. Bartera, F. and Giacchetti, R. (2004). "Steel dissipating braces for upgrading existing building frames". *Journal of Constructional Steel Research,* 60(3-5): 751-769

16. Basu, B. (2004). "NDT for identification of stiffness degradation in railway bridges by wavelet analysis". *7th International Conf. Railway Engineering*, London, UK

17. Bazeos, N., Hatzigeorgiou, G., Hondros, I., Karamaneas, H., Karabalis, D. and Beskos, D. (2002). "Static, seismic and stability analyses of a prototype wind turbine steel tower". *Engineering Structures*, 24: 1015–1025

18. Berman, N. and Shaked, U. (2005). "H_∞-like control for nonlinear stochastic systems". *Systems & Control Letters, In Press, Corrected Proof, Available online 10 October 2005*

19. Bressan, A. and Piccoli, B. (1995). "A Baire category approach to the bang-bang property." *Journal of Differential Equations*, 116: 318-337

20. Burton, S.A. and Makris, N. (1996). "Structural control with electrorheological dampers: viscoplastic behavior and anticipation". *Proceedings of Structures Congress XIV, Chicago, IL*, 1261–8.

21. Burton, S.A., Makris, N., Antsaklis, P.J. and Zhang, J. (1997). "Nonparametric models for characterization and response control of a controllable fluid damper". *Proceedings of Structures Congress XV, Portland, OR*, 1363–7.

22. Burton, S.A., Makris, N., Konstantopoulos, I. and Antsaklis, P.J. (1996). "Modeling the response of ER damper: phenomenology and emulation". *Journal of Engineering Mechanics*, 122(9):897–906.

23. Caldwell, D.B. (1986). "Viscoelastic damping devices proving effective in tall buildings", *AISC Engineering Journal*, 23(4): 148-150

24. Carlson, J.D. and Spencer, B.F. (1996a). "Magneto-rheological fluid dampers for semi-active seismic control". *Proceedings of Third International Conference on Motion and Vibration Control, Vol. III, Chiba, Japan*, 35–40.

25. Carlson, J.D. and Spencer, B.F. Jr. (1996b). "Magneto-rheological fluid dampers: scalability and design issues for application to dynamic hazard mitigation". *Proceedings of Second International Workshop on Structural Control, Hong Kong,* 99–109.

26. Carlson, J.D., Catanzarite, D.M. and St.Clair, K.A. (1995). "Commercial magnetorheological fluid devices". *Proceedings of the 5th International Conference on ER Fluids and Associated Technology*, U. Sheffield, UK

27. Cerf, R. (1994). "Oriented measures with continuous densities and the bang-bang principle." *Journal of Functional Analysis*; 126: 476-505

28. Chakraborty, A. and Basu, B. (2005). "Identification of fundamental mode of a bridge using continous wavelet transform". *Proceedings of the SECED Young Engineers Conference,* University of Bath, Bath UK

29. Chang, C.C., Yu, L. (1998). "A Simple Optimal Pole Location Technique for Structural Control." *Engineering Structures,* 20(9): 792-804

30. Chang, K. and Zhu, Z. (2001). "Discrete-Time Sliding Mode Controller Design with Weak Pseudo Sliding Condition". *Journal of Mathematical Analysis and Applications,* 258(2): 536-555

31. Chase, G.J., Breneman, E.S., Smith, A.H. (1999). "Robust H-infinity Static Output Feedback Control with Actuator Simulation." *Journal of Engineering Mechanics, ASCE*, 125(2): 225-233

32. Chen, S.H. and Chou, J.H. (2004). "Robust stability analysis for discrete-time LQG system under finite wordlength effects, noise uncertainties and time-varying

structured parameter perturbations". *Mathematics and Computers in Simulation,* 66(1): 21-32

33. Cheng F.Y. and Jiang H. (1998). "Hybrid control of seismic structures with optimal placement of control devices". *Journal of Aerospace Engineering, ASCE*, 11(2): 52-58
34. Cho, K., Cermak, J., La, M. and Nielsen, E. (1998). „Viscoelastic damping for wind-excited motion of a five-story building frame". *Journal of Wind Engineering and Industrial Aerodynamics*, 77: 269-281
35. Choi, C. and Kim, J.S. (1996). "Robust control of positioning systems with a multi-step bang-bang actuator". *Mechatronics*, 6(8): 867-880
36. Clough, R. and Penzien, J. (1993) "Dynamics of Structures", *McGraw-Hill*
37. Colajanni, P. and Papia, M. (1995). "Seismic response of braced frames with and without friction dampers". *Engineering Structures,* 17(2): 129-140
38. Csaba, G. (1998). "Forced response analysis in time and frequency domains of a tuned bladed disk with friction dampers". *Journal of Sound and Vibration,* 214(3): 395-412
39. Davison, E.J. (1966). "A method for simplifying linear dynamic systems." *IEEE Trans. Autom. Control,* AC-11(1): 93-101
40. Den Hartog, J. P. (1956). "Mechanical Vibrations", *McGraw-Hill*
41. Dowdell, D.J. and Cherry, S. (1994a). "Semi-active friction dampers for seismic response control of structures". *Proceedings of Fifth U.S. National Conference on Earthquake Engineering, Vol. II, Chicago, IL* 819–28.
42. Dowdell, D.J. and Cherry, S. (1994b). "Structural control using semi-active friction dampers". *Proceedings of First World Conference on Structural Control, Los Angeles, CA,* FA1-59–FA1-68.
43. Dowell, E.H. (1983). "The behavior of a linear, damped modal system with a non-linear spring-mass-dry friction damper system attached". *Journal of Sound and Vibration,* 89(1): 65-84
44. Dowell, E.H. and Schwartz, H.B. (1983a). "Forced response of a cantilever beam with a dry friction damper attached, part I: Theory". *Journal of Sound and Vibration,* 91(2): 255-267

45. Dowell, E.H. and Schwartz, H.B. (1983b). "Forced response of a cantilever beam with a dry friction damper attached, part II: Experiment". *Journal of Sound and Vibration,* 91(2): 269-291

46. Dyke, S.J. and Spencer, B.F. (1997). "A comparison of semi-active control strategies for the MR damper". *Proceedings of International Conference on Intelligent Information Systems, Bahamas*

47. Dyke, S.J. and Spencer, B.F. Jr. (1996). "Seismic response control using multiple MR dampers". *Proceedings of Second International Workshop on Structural Control, Hong Kong*, 163–73.

48. Dyke, S.J., Spencer, B.F. Jr, Sain, M.K. and Carlson, J.D. (1996a). "Experimental verification of semi-active structural control strategies using acceleration feedback". *Proceedings of Third International Conference on Motion and Vibration Control, Vol. III, Chiba, Japan*, 291–6.

49. Dyke, S.J., Spencer, B.F. Jr, Sain, M.K. and Carlson, J.D. (1997a). "On the efficacy of magnetorheological dampers for seismic response reduction." *Proceedings of 1997 ASME Design Engineering Technical Conferences, Sacramento, CA*

50. Dyke, S.J., Spencer, B.F. Jr, Sain, M.K. and Carlson, J.D. (1997b). "An experimental study of magnetorheological dampers for seismic hazard mitigation". *Proceedings of Structures Congress XV, Portland, OR*, 1358–62.

51. Dyke, S.J., Spencer, B.F., Sain, M.K. and Carlson, J.D. (1996b). "Modeling and control of magnetorheological dampers for seismic response reduction". *Smart Materials and Structures*, 5: 565–75.

52. Ehrgott, R.C. and Masri, S.F. (1992b). "Modeling the oscillatory dynamic behavior of electrorheological materials in shear". *Smart Materials and Structures*, 1(4):275–85.

53. Ehrgott, R.C. and Masri, S.F. (1993). "Structural control applications of an electrorheological device". *Proceedings of International Workshop on Structural Control, Honolulu, HI*, 115–29.

54. Ehrgott, R.C., and Masri, S.F. (1992a). "Use of electro-rheological materials in intelligent systems". *Proceedings of U.S.–Italy–Japan Workshop/Symposium on Structural Control and Intelligent Systems, Italy*, 87–100.

55. Ekelund, T. (2000). "Yaw control for reduction of structural dynamic loads in wind turbines". *Journal of Wind Engineering and Industrial Aerodynamics*, 85: 241-262

56. Feigin, M.I. (1961). "On the evaluation of optimal parameters of a dry-friction damper". *Journal of Applied Mathematics and Mechanics,* 25(4): 1196-1200

57. Feng, M.Q. (1993). "Application of hybrid sliding isolation system to buildings". *Journal of Engineering Mechanics*, 119(10):2090–108.

58. Feng, M.Q., Shinozuka, M. and Fujii, S. (1992). "Experimental and analytical study of a hybrid isolation system using friction controllable sliding bearings". *Report No. NCEER 92-0009, National Center for Earthquake Engineering Research, Buffalo, NY.*

59. Feng, M.Q., Shinozuka, M. and Fujii, S. (1993). "Friction controllable sliding isolation system". *Journal of Engineering Mechanics*, 119(9):1845–64.

60. Feng, Q. and Shinozuka, M. (1990). "Use of a variable damper for hybrid control of bridge response under earthquake". *Proceedings of U.S. National Workshop on Structural Control Research, Los Angeles, CA,* 107–12.

61. Fuglsang P, Madsen H. (1999). "Optimization method for wind turbine rotors". *Journal of Wind Engineering and Industrial Aerodynamics*, 80: 191-206

62. Fujita, T., Shimazaki, M., Yutaka, H., Aizawa, S., Higashino, M. and Haniuda, N. (1994). "Semiactive seismic isolation system using controllable friction damper". *Bulletin of Earthquake Resistant Structure Research Center, No. 27*, 21–31.

63. Gao, H., Kwok, K.C.S. and Samali, B. (1997). "Optimization of tuned liquid column dampers". *Engineering Structures,* 19(6): 476-486

64. Gao, H., Kwok, K.C.S. and Samali, B. (1999). "Characteristics of multiple tuned liquid column dampers in suppressing structural vibration". *Engineering Structures,* 21(4): 316-331

65. Garcia, D.L. and Soong, T. (2002). "Efficiency of a simple approach to damper allocation in MDOF structures". *Journal of Structural Control*, 9: 19-30

66. Gavin, H.P. (1996). "High force electrorheological damper designs". *Proceedings of Second International Workshop on Structural Control, Hong Kong,* 186–97

67. Gavin, H.P. (1997). "ER material models and vibration control". *Proceedings of Eleventh VPI and SU Symposium on Structural Dynamics and Control, Blacksburg, VA,* 121–30

68. Gavin, H.P. and Hanson, R.D. (1994). "Characterization of an ER active member". *Proceedings of Structures Congress XII, Atlanta, GA*, 863–8.

69. Gavin, H.P., Hanson, R.D. and Filisko, F.E. (1996a). "Electrorheological dampers, part I: analysis and design". *Journal of Applied Mechanics*, 63:669–75.

70. Gavin, H.P., Hanson, R.D. and Filisko, F.E. (1996b). "Electrorheological dampers, part II: testing and modeling". *Journal of Applied Mechanics*, 63:676–82.

71. Gavin, H.P., Hanson, R.D. and McClamroch, N.H. (1996c). "Control of structures using electrorheological dampers". *Proceedings of Eleventh World Conference on Earthquake Engineering, Acapulco, Mexico*, Paper No. 272.

72. Gavin, H.P., Hose, Y.D., Hanson, R.D. (1994). "Design and control of electrorheological dampers". *Proceedings of First World Conference on Structural Control, Los Angeles, CA*, WP3-83–WP3- 92.

73. Gavin, H.P., Ortiz, D.S. and Hanson, R.D. (1993). "Testing and modeling of a proto-type ER damper for seismic structural response control". *Proceedings of International Workshop on Structural Control, Honolulu, HI*, 166–80.

74. Ghali, A. and Neville, A. (1997). "Structural Analysis, A Unified, Classical and Matrix Approach", *E and F.N. Spon*

75. Ghosh, A. and Basu, B. (2004). "Seismic vibration control of short period structures using the liquid column damper", *Engineering Structures,* 26(13): 1905-1913

76. Ghosh, A. and Basu, B. (2005). "Effect of soil interaction on the performance of liquid column dampers for seismic applications", *Earthquake Engineering & Structural Dynamics,* 34(11): 1375-1389

77. Glauser, G.J., Ahmadi, G. and Horta, L.G. (1997). "Integrated passive/active vibration absorber for multistory buildings". *Journal of Structural Engineering, ASCE*, 123(4): 499 – 504

78. Gordaninejad, F., Ray, A. and Bindu, R. (1994). "Vibration control of structures using hybrid ER/viscous fluid dampers". *Proceedings of First World Conference on Structural Control, Los Angeles, CA*, TA2-41–TA2-49.

79. Grimble, M.J. (1984). "Implicit and explicit LQG self-tuning controllers". *Automatica*, 20(5): 661-669

80. Grimble, M.J. (1990).. "LQG predictive optimal control for adaptive applications". *Automatica,* 26(6): 949-961

81. Haddad, W.M. and Tadmor, G. (1993). "Reduced order LQG controllers for linear time varying plants". *Systems & Control Letters,* 20(2): 87-97

82. Hakvoort, R.G., Schrama, R.J.P. and Van den Hof, P.M.J. (1994). "Approximate identification with closed-loop performance criterion and application to LQG feedback design". *Automatica,* 30(4): 679-690

83. Halevi, Y., Haddad, W.M. and Bernstein, D.S. (1993). "A riccati equation approach to the singular LQG problem". *Automatica,* 29(3): 773-778

84. Hansen, B.C., Gordaninejad, F., Saiidi, M. and Chang, F. (1997). "Control of bridges using magneto-rheological fluid dampers". *Proceedings of International Workshop on Health Monitoring, Stanford University, Palo Alto.*

85. Haroun, M.A., Pires, J.A. and Won, A.Y.J. (1994). "Active orifice control in hybrid liquid column dampers". *Proceedings of First World Conference on Structural Control, Los Angeles, CA*, FA1-69– FA1-78.

86. Herrmann, G., Spurgeon, S.K. and Edwards, C. (2003). "A model-based sliding mode control methodology applied to the HDA-plant". *Journal of Process Control,* 13(2): 129-138

87. Horr, A.M. and Schmidt, L.C. (1996). "Modelling of nonlinear damping characteristics of a viscoelastic structural damper". *Engineering Structures,* 18(2): 154-161

88. Hryniewicz, Z. (2004). "Dynamic analysis of system with deterministic and stochastic viscoelastic dampers". *Journal of Sound and Vibration,* 278(4-5): 1013-1023

89. Hsiao, F. and Chen, B. (1988). "LQG optimal and robust controller design for nonlinear stochastic systems: multivariable case". *Journal of the Franklin Institute,* 325(2): 189-206

90. Hsiao, F. and Hsieh, J. (1991). "Robust LQG optimal controller synthesis against noise spectral uncertainties and nonlinear time-varying unmodeled dynamics". *Systems & Control Letters,* 16(3): 167-178

91. Hwang, J.S., Kim, H. and Kim, J. (2005). "Estimation of the modal mass of a structure with a tuned-mass damper using H-infinity optimal model reduction". *Engineering Structures, In Press, Corrected Proof, Available online 24 August 2005*

92. Igusa, T. and Xu, K. (1993). "Vibration control using multiple tuned mass dampers". *Journal of Sound and Vibration,* 175: 491-503

93. Jangid, R. (1999). "Optimum multiple tuned mass dampers for base excited undamped system". *Earthquake Engineering and Structural Dynamics,* 28: 1041-1049

94. Jangid, R. and Datta, T. (1997). "Performance of multiple tuned mass dampers for torsionally coupled system". *Earthquake Engineering and Structural Dynamics,*.26: 307-317

95. Joshi, A. and Jangid, A. (1996). "Optimum parameters of multiple tuned mass dampers for base-excited damped systems". *Journal of Sound and Vibration,* 202: 657-667

96. Kalyanaraman, V., Mahadevan, K. and Thairani, V. (1998). "Core loaded earthquake resistant bracing system". *Journal of Constructional Steel Research,* 46(1-3): 437-439

97. Kameshki, E.S. and Saka, M.P. (2001). "Genetic algorithm based optimum bracing design of non-swaying tall plane frames". *Journal of Constructional Steel Research,* 57(10): 1081-1097

98. Kareem, A. (1994). "The next generation of tuned liquid dampers". *Proceedings of First World Conference on Structural Control, Los Angeles, CA,* FP5-19–FP5-28.

99. Kareem, A. and Kline, S. (1995). "Performance of multiple mass dampers under random loading". *Journal of Structural Engineering.* 121: 348-361

100. Kobori, T., Koshika, N., Yamada, N., and Ikeda, Y. (1991). ''Seismic response controlled structure with active mass driver system. Part 1: Design.'' *Earthquake Eng. Struct. Dyn.*, 20: 133–139.

101. Kobori, T., Takahashi, M., Nasu, T., Niwa, N. and Ogasawara, K. (1994). "Seismic response controlled structure with active variable stiffness system." *J. Struct. Eng,*120(4): 1291-1306

102. Kobori, T., Takahashi, M., Nasu, T., Niwa, N., and Ogasawara, K. (1993). "Seismic response controlled structure with active variable stiffness system". *Earthquake Engineering and Structural Dynamics,*22: 925–41.

103. Lavassas, I., Nikolaidis, G., Zervas, P., Efthimiou, E., Doudoumis, I. and Baniotopoulos C. (2003) "Analysis and design of the prototype of a steel 1-MW wind turbine tower". *Engineering Structures*, 25: 1097–1106

104. Lee, D.G., Hong, S. and Kim, J. (2002). "Efficient siesmic analysis of building structures with added viscoelastic dampers". *Engineering Structures,* 24(9): 1217-1227

105. Lee, H.H. and Tsai, C.S. (1994). "Analytical model of viscoelastic dampers for seismic mitigation of structures". *Computers & Structures*, 50(1): 111-121

106. Lee, J.H., Berger, E. and Kim, J.H. (2005). "Feasibility study of a tunable friction damper". *Journal of Sound and Vibration,* 283(3-5): 707-722

107. Levy, R., Marianchik, E., Rutenberg, A. and Segal, F. (2001). "A simple approach to the seismic design of friction damped braced medium-rise frames". *Engineering Structures,* 23(3): 250-259

108. Li, C. (2000). "Performance of multiple tuned mass dampers for attenuating undesirable oscillations of structures under the ground acceleration". *Earthquake Engineering and Structural Dynamics,* 29: 1045-1421

109. Li, C. (2002). "Optimum multiple tuned mass dampers for structures under the ground acceleration based on DDMF and ADMF". *Earthquake Engineering and Structural Dynamics,* 31: 897-919

110. Li, C. and Liu, Y. (2003). "Optimum multiple tuned mass dampers for structures under the ground acceleration based on the uniform distribution of system parameters". *Earthquake Engineering and Structural Dynamics,* 32: 671-690

111. Li, W.Q. and Tsai, C.S. (1994). "Seismic mitigation of structures by using viscoelastic dampers". *Nuclear Engineering and Design*, 147(3): 263-274

112. Liang, C. and Su, J. (2003). "A new approach to the design of a fuzzy sliding mode controller". *Fuzzy Sets and Systems,* 139(1): 111-124

113. Loh, C. and Ma, M. (1994) "Active-damping or active-stiffness control for seismic excited buildings". *Proceedings of First World Conference on Structural Control, Los Angeles, CA,* TA2-11–TA2-20.

114. López, I., Busturia, J.M. and Nijmeijer, H. (2004). "Energy dissipation of a friction damper". *Journal of Sound and Vibration,* 278(3): 539-561

115. Lou, J.Y.K., Lutes, L.D. and Li, J.J. (1994). "Active tuned liquid damper for structural control". *Proceedings of First World Conference on Structural Control, Los Angeles, CA,* TP1-70–TP1-79.

116. Maalawi, K and Negm, H. (2002). "Optimal frequency design of wind turbine blades". *Journal of Wind Engineering and Industrial Aerodynamics*, 90: 961–986

117. Madiwale, A.N., Haddad, W.M. and Bernstein, D.S. (1989). "Robust H_∞ control design for systems with structured parameter uncertainty". *Systems & Control Letters,* 12(5): 393-407

118. Mahmoodi, P. (1969). "Structural dampers", *ASCE Journal of the Structural Division*, 95(8), 1661-1672

119. Mahmoodi, P. and Keel, C.J. (1990). "Method of damped energy calculation for a multilayer viscoelastic (V.E.) damper". *Journal of Wind Engineering and Industrial Aerodynamics*, 36(2): 749-756

120. Mahmoodi, P., Robertson, L.E., Yontar, M., Moy, C. and Fled, I. (1987). "Performacne of viscoelastic dampers in world trade centre towers", *Dynamic of Structures, Structures Congress '87*, Orlando, FL

121. Makris, N. (1997). "Rigidity-plasticity-viscosity: can electrorheological dampers protect base-isolated structures from near-source ground motions?" *Earthquake Engineering and Structural Dynamics*, 26:571–91.

122. Makris, N. and McMahon, S. (1996a). "Seismic protection of bridges with fluid dampers and the issue of viscous heating". *Proceedings of Fourth U.S.–Japan Workshop on Earthquake Protective Systems for Bridges, Osaka, Japan,* 309–23.

123. Makris, N. and McMahon, S. (1996b). "Structural control with controllable fluid dampers: design and implementation issues". *Proceedings of Second International Workshop on Structural Control, Hong Kong*, 311–22.

124. Makris, N., Burton, S.A., Hill, D. and Jordan, M. (1996a). "Analysis and design of ER damper for seismic protection of structures". *Journal of Engineering Mechanics*, 122(10):1003–11.

125. Makris, N., Burton, S.A., Hill, D. and Jordan, M. (1996b). "An electrorheological damper with annular duct". *Proceedings of Structures Congress XIV, Chicago, IL*, 1197–204.

126. Makris, N., Hill, D., Burton, S. and Jordan, M. (1995). "Electrorheological fluid damper for seismic protection of structures". *Proceedings of Smart Structures and Materials, SPIE Vol. 2443, San Diego, CA*, 184–94.

127. Martinez-Rodrigo, M. and Romero, M.L. (2003). "An optimum retrofit strategy for moment resisting frames with nonlinear viscous dampers for seismic applications". *Engineering Structures,* 25(7): 913-925

128. McMahon, S. and Makris, N. (1997). "Large-scale ER-damper for seismic protection of bridges". *Proceedings of Structures Congress XV, Portland, OR*, 1451–5.

129. Meirovitch L. Dynamics and Control of Structures. John Wiley and Sons Inc., 1995

130. Min, K., Kim, H., Lee, S., Kim, H. and Ahn, S. (2005). "Performance evaluation of tuned liquid column dampers for response control of a 76-story benchmark building". *Engineering Structures,* 27(7): 1101-1112

131. Moghaddam, H.A. and Estekanchi, H.E. (1999). "Seismic behaviour of off centre bracing systems". *Journal of Constructional Steel Research,* 51(2): 177-196

132. Mohamed, and Magdi S. (1999). "H_∞-control design for systems with multiple delays". *Computers & Electrical Engineering*, 25(6): 451-475

133. Moore, J.B., Zhou, X.Y. and Lim, A.E.B. (1999). "Discrete time LQG controls with control dependent noise". *Systems & Control Letters,* 36(3): 199-206

134. Mualla, I.H. and Belev, B. (2002). "Performance of steel frames with a new friction damper device under earthquake excitation". *Engineering Structures,* 24(3): 365-371

135. Munshi, J.A. (1997). "Effect of viscoelastic dampers on hysteretic response of reinforced concrete elements". *Engineering Structures,* 19(11): 921-935

136. Munteanu, J., Cutululis, N.A., Bratcu, A.J. and Ceangă, E. (2005). "Optimization of variable speed wind power systems based on a LQG approach". *Control Engineering Practice*, 13(7): 903-912

137. Murtagh, P.J., Basu, B. and Broderick, B.M. (2004). "Mode acceleration approach for rotating wind turbine blades". *Proc. Institution Mechanical Engineers,* 218: Part K. Multi-body dynamics

138. Nacivet, S., Pierre, C., Thouverez, F. and Jezequel, L. (2003). "A dynamic Lagrangian frequency–time method for the vibration of dry-friction-damped systems". *Journal of Sound and Vibration,* 265(1): 201-219

139. Nagarajaiah, S. (1997). "Semi-active control of structures". *Proceedings of Structures Congress XV, ASCE, Portland, OR*, 1574–8.

140. Nagarajaiah, S. and Mate, D. (1998). "Semi-active control of continuously variable stiffness system." *Proc., 2nd World Conference on Structural Control*, Wiley, New York

141. Nagarajaiah, S. and Varadarajan, N. (2000) "Novel semi-active variable stiffness tuned mass damper with real time tuning capability." *Proc. 13th Engineering Mechanics Conference, ASCE,* Reston, Va

142. Nagarajaiah, S., Riley, M.A. and Reinhorn, A. (1993). "Control of sliding--isolated bridge with absolute acceleration feedback". *Journal of Engineering Mechanics, ASCE*, 119(11): 2317-2332

143. Nandy, U. and Sengupta, S.N. (1996). "Minimization of residual vibrations in lumped parameter positions-a non-time-optimal bang-bang control". *Journal of Sound and Vibration*, 196(3): 263-274

144. Nasu, T., Kobori, T., Takahashi, M., Niwa, N. and Ogasawara, K. (2001). "Active variable stiffness system with non-resonant control." *Earthquake Eng. Struct. Dyn.,* 30: 1597-1614

145. Nemir, D.C., Lin, Y. and Osegueda, R.A.. (1994). "Semiactive motion control using variable stiffness". *Journal of Structural Engineering,*120(4):1291–306.

146. Nims, D.K., Inaudi, J.A., Richter, P.J. and Kelly, J.M. (1993b). "Application of the energy dissipation restraint to buildings", *Proc. ATC 17-1 on Seismic Isolation, Energy Dissipation, and Active Control, 2*, 627-638

147. Nims, D.K., Richter, P.J. and Bachman, R.E. (1993a). "The use of the energy dissipating restraint for seismic hazard mitigation", *Earthquake Spectra*, 9(3): 467-489

148. Nise N.S. (1994). "Control Systems Engineering", *Bejamin/Cummings Publication Co*

149. Ostachowicz, W. (1989). "Forced vibrations of a beam including dry friction dampers". *Computers & Structures,* 33(3): 851-858

150. Pall, A.S. and Marsh, C. (1982). "Response of friction damped braced frames", *Journal of Structural Division, ASCE*, 108(ST6): 1313-1323

151. Pandya, J., Akbay, Z., Uras, M. and Aktan, H. (1996). "Experimental implementation of hybrid control". *Proceedings of Structures Congress XIV, Chicago, IL*, 1172–9.

152. Park, S.W. (2001). "Analytical modeling of viscoelastic dampers for structural and vibration control". *International Journal of Solids and Structures,* 38(44-45): 8065-8092

153. Perotti, F. De Amici, A. and Venturini, P. (1996). "Numerical analysis and design implications of the seismic behaviour of one-storey steel bracing systems". *Engineering Structures,* 18(2):162-178

154. Petersen, I.R. and Pota, H.R. (2003). "Minimax LQG optimal control of a flexible beam". *Control Engineering Practice,* 11(11): 1273-1287

155. Qu, W.L., Chen, Z.H. and Xu, Y.L. (2001).. "Dynamic analysis of wind-excited truss tower with friction dampers". *Computers & Structures,* 79(32): 2817-2831

156. Raftoyiannis, I.G. (2005). "The effect of semi-rigid joints and an elastic bracing system on the buckling load of simple rectangular steel frames". *Journal of Constructional Steel Research,* 61(9): 1205-1225

157. Ramar, K. and Appukuttan, K.K. (1991). "Pole assignment for multi-input multi-output systems using output feedback". *Automatica,* 27(6): 1061-1062

158. Rana, R. and Soong, T. (1998). "Parametric study and simplified design of tuned mass dampers". *Engineering Structures*, 20: 193-204

159. Ricciardelli F., Pizzimenti A.D. and Mattei M. (2003). "Passive and active mass damper control of the response of tall buildings to wind gustiness". *Engineering Structures*, 25: 1199–1209

160. Ricciardelli, F., Occhiuzzi, A. and Clemente, P. (2000). "Semi-active tuned mass damper control strategy for wind-excited structures". *Journal of Wind Engineering and Industrial Aerodynamics*, 88: 57-74

161. Ronold, K and Christensen, C. (2001). "Optimization of a design code for wind-turbine rotor blades in fatigue". *Engineering Structures*, 23: 993–1004

162. Ronold, K and Larsen G. (2000). "Reliability-based design of wind-turbine rotor blades against failure in ultimate loading". *Engineering Structures*, 22: 565–574

163. Samali B, and Kwok K. (1995). "Use of viscoelastic dampers in reducing wind and earthquake induced motion of building structures". *Engineering Structures*, 17(9): 639-654

164. Shen, K.L., Soong, T.T., Chang, K.C. and Lai, M.L. (1995). "Seismic behaviour of reinforced concrete frame with added viscoelastic dampers". *Engineering Structures,* 17(5): 372-380

165. Shkolnikov, I.A. and Shtessel, Y.B. (2002). "Tracking in a class of nonminimum-phase systems with nonlinear internal dynamics via sliding mode control using method of system center". *Automatica*, 38(5): 837-842

166. Shukla, A. and Datta, T. (1999). "Optimal use of viscoelastic dampers in building frames for seismic force". *Journal of Structural Engineering*, 125(4): 401-409

167. Shum, K.M. and Xu, Y.L. (2004). "Multiple tuned liquid column dampers for reducing coupled lateral and torsional vibration of structures". *Engineering Structures,* 26(6): 745-758

168. Slocum, A.H., Marsh, E.R. and Smith, D.H. (1994). "A new damper design for machine tool structures: the replicated internal viscous damper". *Precision Engineering,* 16(3): 174-183

169. Soong, T.T.. and Dargush, G.F. (1997). "Passive energy dissipation systems in structural engineering", *John Wiley and Sons Ltd.*

170. Spencer, B.F. Jr, Carlson, J.D., Sain, M.K. and Yang, G. (1997b). "On the current status of magnetorheological dampers: seismic protection of full-scale structures". *Proceedings of 1997 American Control Conference, Albuquerque, NM*, 458–62.

171. Spencer, B.F. Jr, Dyke, S.J., Sain, M.K. and Carlson, J.D. (1996) "Dynamical model of a magnetorheological damper". *Proceedings of Structures Congress XIV, ASCE, Chicago, IL*, 361–70.

172. Spencer, B.F., Dyke, S.J., Sain, M.K. and Carlson, J.D. (1997a). "Phenomenological model for magnetorheological dampers". *Journal of Engineering Mechanics,* 123(3):230–8.

173. Spencer, B.F., Suhardjo, J. and Sain, M.K. (1994). "Frequency Domain Optimal Control for Aseismic Protection". *Journal of Engineering Mechanics, ASCE*, 120(1): 135-159

174. Spencer, Jr. B.F. and Nagarajaiah, S. (2003). "State of the Art of Structural Control". *Journal of Structural Engineering, ASCE*, 129(7): 846-868

175. Spyrakos, C.C. and Ermopoulos, J. (2005). "Development of aluminum load-carrying space frame for building structures". *Engineering Structures,*27(13): 1942-1950

176. Sternad, M. and Söderström, T. (1988). "LQG-optimal feedforward regulators". *Automatica,* 24(4): 557-561

177. Su, J., Chen, T. and Wang, C.C. (2001). "Adaptive fuzzy sliding mode control with GA-based reaching laws". *Fuzzy Sets and Systems,* 120(1): 145-158

178. Suhardjo, J., Spencer, B.F. and Kareem, A. (1992) "Frequency Domain Optimal Control of Wind-Excited Buildings". *Journal of Engineering Mechanics, ASCE,* 118(12): 2463-2481

179. Suhardjo, J., Spencer, B.F., Kareem, A. (1992). "Frequency Domain Optimal Control of Wind-Excited Buildings." *Journal of Engineering Mechanics, ASCE*, 118(12): 2463-2481

180. Symans, M.D. and Constantinou, M.C. (1999). "Semi-active control systems for seoismic protection of structures: a state-of-the-art review" *Engineering Structures*, 21: 469-487

181. Tamura, Y., Fujii, K., Wakahara, T. and Kohsaka. (1995). "Effectiveness of tuned liquid dampers under wind excitation". *Engineering Structures*, 17(9): 609-621

182. Tezcan, S.S. and Uluca, O. (2003). "Reduction of earthquake response of plane frame buildings by viscoelastic dampers". *Engineering Structures,* 25(14): 1755-1761

183. Tsai, C.S. (1993). "Innovative design of viscoelastic dampers for seismic mitigation". *Nuclear Engineering and Design*, 139(2): 165-182

184. Tsai, C.S. and Lee, H.H. (1993). "Seismic mitigation of bridges by using viscoelastic dampers". *Computers & Structures,* 48(4): 719-727

185. Tsai, H. and Lin, G. (1993). "Optimum tuned mass dampers for minimising steady-state response of support excited and damped systems". *Earthquake Engineering and Structural Dynamics*. 22: 957-973.

186. Tzou, H and Schiff, A.J. (1987). "Development and evaluation of a pseudo-force approximation applied to nonlinear dynamic contacts and viscoelastic damping". *Computers & Structures,* 26(3): 481-493

187. Valásek, M. and Olgaç, N. (1999). "Pole placement for linear time-varying non-lexicographically fixed MIMO systems". *Automatica*, 35(1): 101-108

188. Varadarajan, N. and Nagarajaiah, S. (2004). "Wind response control of building with variable stiffness tuned mass damper using empirical mode decomposition Hilbert transform." *Journal of Engineering Mechanics,*130(4): 451-458

189. Varol, A., Ilkılıc, C. and Varol, Y. (2001). "Increasing the efficiency of wind turbines". *Journal of Wind Engineering and Industrial Aerodynamics*, 89: 809–815

190. Von Bokern, M.A., Paschall, R.N. and Welsh, B.M. (1992). "Modal control for an adaptive optics system using LQG compensation". *Computers & Electrical Engineering,* 18(6): 421-433

191. Whiteman, W.E. and Ferri, A.A. (1997). "Multi-mode analysis of beam-like structures subjected to displacement-dependent dry friction damping". *Journal of Sound and Vibration,* 207(3): 403-418

192. Winslow, W.M. (1949). "Induced fibration and suspensions", *Journal of Applied Physics*, 20: 1137-1140.

193. Won, A.Y.J, Pires, J.A. and Haroun, M.A. (1997). "Performance assessment of tuned liquid column dampers under random seismic loading". *International Journal of Non-Linear Mechanics*, 32(4): 745-758

194. Wu, J., Shih, M., Lin, Y. and Shen, Y. (2005). "Design guidelines for tuned liquid column damper for structures responding to wind". *Engineering Structures,* 27(13): 1893-1905

195. Wu, J.C., Yang, J.N. (1998). "Active Control of Transmission Tower under Stochastic Wind." *Journal of Structural Engineering, ASCE,* 124(11): 1302-1312

196. Wu, J.C., Yang, J.N., Schmitendorf, W.E. (1998). "Reduced-order H-infinity and LQR Control for Wind Excited Tall Buildings." *Engineering Structures*, 20(3): 222-236

197. Wu, Z., Soong, T.T. (1996). "Modified bang-bang control law for structural control implementation". *Journal of Engineering Mechanics*, 122(8): 771-777

198. Xu, K. and Igusa, T. (1992). "Dynamic characteristics of multiple substructures with closely spaced frequency". *Earthquake Engineering and Structural Dynamics*, 21: 1059-1070

199. Xu, Y. (1996). "Parametric study of active mass dampers for wind-excited tall buildings". *Engineering Structures,* 18(1): 64-76

200. Xu, Y.L., Kwok, K.C.S. and Samali, B. (1992). "The effect of tuned mass dampers and liquid dampers on cross-wind response of tall/slender structures". *Journal of Wind Engineering and Industrial Aerodynamics,* 40(1): 33-54

201. Xu, Z.D., Zhao, H.T. and Li. A.Q. (2004). "Optimal analysis and experimental study on structures with viscoelastic dampers". *Journal of Sound and Vibration,* 273(3): 607-618

202. Xue, S.D., Ko, J.M. and Xu, Y.L. (2000a). "Optimum parameters of tuned liquid column dampers for suppressing pitching vibration of an undamped structure". *Journal of Sound and Vibration,* 235(4): 639-653

203. Xue, S.D., Ko, J.M. and Xu, Y.L. (2000b). "Tuned liquid column damper for suppressing pitching motion of structures". *Engineering Structures,* 22(11): 1538-1551

204. Yamada, K. and Kobori, T. (1995). "Control algorithm for estimating future responses of active variable stiffness structure". *Earthquake Engineering and Structural Dynamics*, 24:1085–99.

205. Yamaguchi, H. and Harnpornchai, N. (1993). "Fundamental characteristics of multiple tuned mass dampers for surpressing harmonically forced oscillations". *Earthquake Engineering and Structural Dynamics*, 22: 51-62

206. Yang J. N.and Agrawal A.K. (2002). "Semi-active hybrid control systems for nonlinear buildings against near-field earthquakes". *Engineering Structures*, 24: 271–280

207. Yang, J.N., Agrawal, A.K., Samali, B. and Wu, J. (2004). "Benchmark problem for response control of wind-excited tall buildings." *Journal of Engineering Mechanics,* 130(4), 437 – 446

208. Yang, J.N., Li, Z. and Liu, S.C. (1992). "Stable controllers for instantaneous optimal control". *Journal of Engineering Mechanics, ASCE*, 118(8): 1612-1630

209. Yang, J.N., Wu, J.C. and Li, Z. (1996) "Control of seismic excited buildings using active variable stiffness systems". *Engineering Structures*, 18(8):589–96.

210. Yang, T.C. and Munro, N. (1991). "Power system stabilizer design based on the pole assignment technique for SIMO systems". *International Journal of Electrical Power & Energy Systems*, 13(6): 298-302

211. Yang, Y.N., Wu, J.C., Agrawal, A.K. (1995a). "Sliding Mode Control for Seismically Excited Linear Structures." *Journal of Engineering Mechanics*, ASCE, 121(12): 1386-1390

212. Yang, Y.N., Wu, J.C., Agrawal, A.K. (1995b). "Sliding Mode Control for Nonlinear and Hysteretic Structures." *Journal of Engineering Mechanics*, ASCE, 121(12): 1330-1339

213. Yang, Y.N., Wu, J.C., Reinhorn, A.M., Riley, M. (1995c). "Control of Sliding-Isolated Buildings Using Sliding-Mode Control." *Journal of Structural Engineering,* ASCE, 122(2): 179-186

214. Yang, Y.N., Wu, J.C., Reinhorn, A.M., Riley, M., Schmitendorf, W.E., Jabbari, F. (1996). "Experimental Verifications of H-infinity and Sliding Mode Control for

Seismically Excited Buildings." *Journal of Structural Engineering, ASCE*, 122(1): 69-75

215. Yu, W., Wang, G. and Chang, C. (2004). "Discrete sliding mode control with forgetting dynamic sliding surface". *Mechatronics*, 14(7): 737-755
216. Zhang, J. and Roschke, P. (1999). "Active control of a tall structure excited by wind". *Journal of Wind Engineering and Industrial Aerodynamics*, 83: 209-223
217. Zhang, R and Soong, T. (1992). "Seismic design of viscoelastic dampers for structural applications". *Journal of Structural Engineering*, 118(5):1375-1393
218. Zhang, W. and Xu, Y. (2001). "Closed form solution for along-wind response of actively controlled tall buildings with LQG controllers". *Journal of Wind Engineering and Industrial Aerodynamics*, 89: 785–807
219. Zhang, Y., Zhou, Z.W. and Guo, G.C. (2004). "Decoupling neighboring qubits in quantum computers through bang–bang pulse control." *Physics Letters A*, 327: 391–396

APPENDIX - PUBLICATIONS

ARTICLE IN PRESS

Available online at www.sciencedirect.com

SCIENCE DIRECT

ELSEVIER

Engineering Structures ▮ (▮▮▮▮) ▮▮▮–▮▮▮

ENGINEERING STRUCTURES

www.elsevier.com/locate/engstruct

Control strategy using bang–bang and minimax principle for FRF with ATMDs

R. Collins, B. Basu*, B. Broderick

Department of Civil, Structural and Environmental Engineering, Trinity College Dublin, Dublin 2, Ireland

Received 9 May 2005; received in revised form 19 August 2005; accepted 19 August 2005

Abstract

An active control strategy for vibration control of structures using ATMDs is proposed. The control strategy incorporates the minimax criteria for shaping the frequency response function (FRF) of the structure–TMD system and the bang–bang control law with a control force applied to a TMD. In the control scheme, the control law using bang–bang control is obtained by minimising the time derivative of a Lyapunov function of the open-loop structural system [Wu Z, Soong TT. Modified bang–bang control law for structural control implementation. Journal of Engineering Mechanics 1996;122(8):771–7] and is used to control the ATMD. In addition, the corresponding FRF for the coupled structure–ATMD system is reshaped by changing the tuning parameter of the TMD (when there is no control force applied), such that peaks in the FRF of the structure are equal in magnitude. When the active control is ineffective or is turned off, the damper system acts as a passive TMD. The proposed strategy is compared to another conventional control strategy, the Linear Quadratic Controller (LQC) applied to the structure–TMD system and the advantages are highlighted. The system is examined under harmonic and random excitations.

Keywords: Bang–bang control; Minimax principle; ATMD

Redacted

Redacted

Redacted

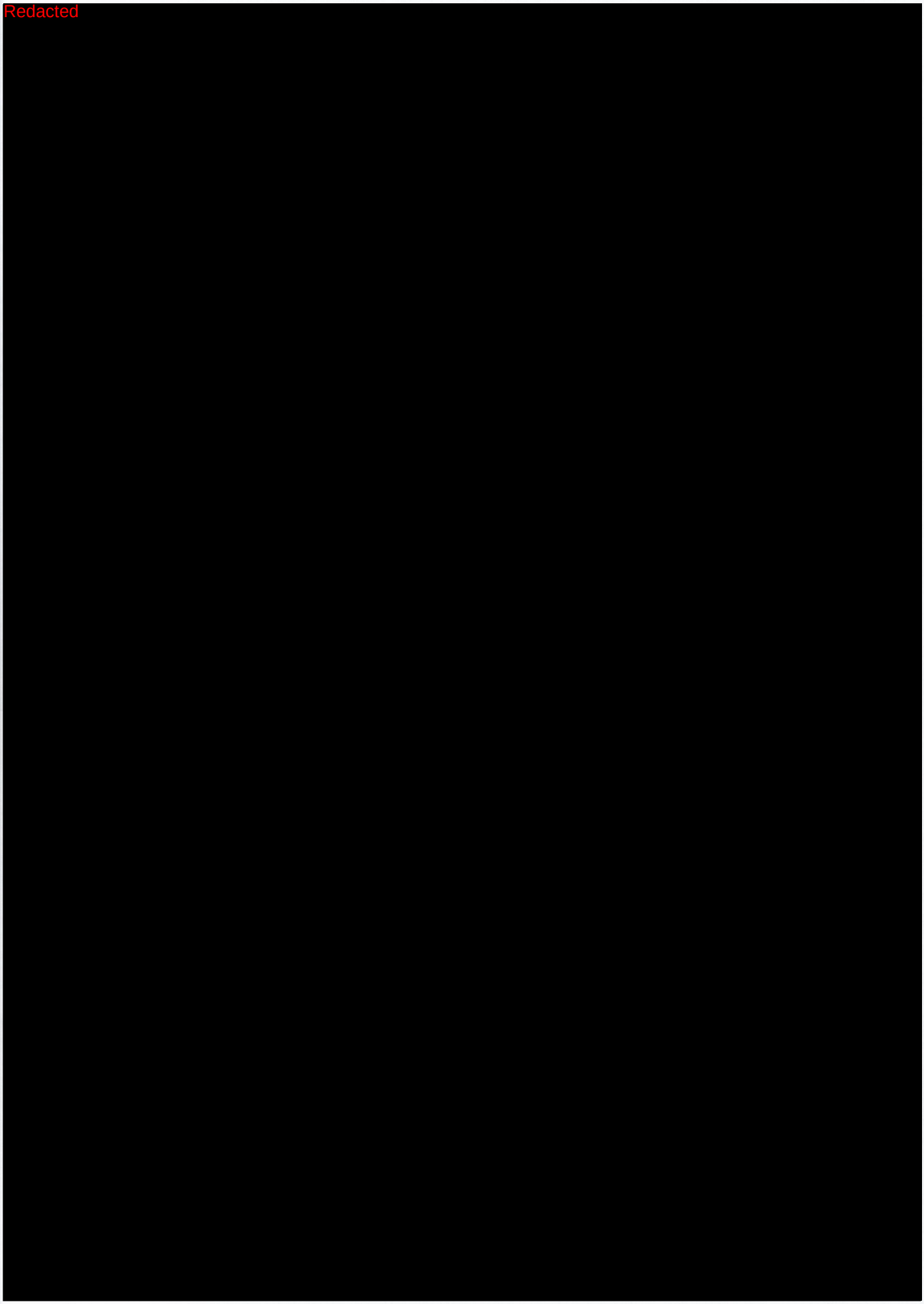
Redacted

Redacted

Redacted


Redacted

Proceedings of he
SECED Young Engineers Conference
21-22 March 2005, University of Bath, Bath, UK

OPTIMAL DESIGN OF MULTIPLE TUNED MASS DAMPERS (MTMDS) FOR WIND TURBINE TOWERS USING SSA

R.Collins[1], B.Basu[2] and B.Broderick[3]

[1,2,3]*Department of Civil, Structural and Environmental Engineering*
Trinity College Dublin, Dublin2, Ireland

A procedure to identify the optimal location and number of multiple tuned mass dampers (MTMDs) in a wind turbine tower, subjected to a stochastic excitation characterised by a power spectral density function (PSDF), is presented. The optimisation methodology employs the sequential search algorithm (SSA). The PSDFs applied to the structure represent wind and seismic excitations. The wind turbine tower is represented by a multi-degree-of-freedom (MDOF) model. Two variations of the model are considered: the tower is assumed to act as a cantilever, with an additional top mass representing the blades and nacelle of the turbine, and the nacelle and rotating blades are included as a separate DOF. Controllability indices (CIs) based on the rms acceleration and displacement response of the structure are determined. Using the SSA, configurations for the number and placement of the TMDs for the structure subjected to each PSDF are found and the optimal tuning parameters of each TMD placed in the structure are also obtained. To investigate the robustness of the design of the damper configuration when the applied loading varies from the assumed design loads, the structures whole damper configurations have been designed based on the PSDF of wind excitations and subjected to the PSDF for seismic excitations, and vice versa. Finally a general configuration is determined and subjected to all of the PSDFs to investigate the general performance of the dampers.

Keywords: *MTMD, Wind Turbine Tower, SSA*

1 Introduction

Many studies on the design of wind turbines have been carried out including those by Varol et al. [1], Bazeos et al. [2], and Lavassas et al. [3]. The majority of wind turbine towers incorporate one, two or three blades. The more blades there are, the larger the amount of power supplied. The blades can be modelled as slender prismatic beams, Baumgart [4] examined a model mounted on a rigid test stand and compared experimental and theoretical results. Murtagh et al [5] examined the displacement response of rotating wind turbine tower blades subjected to wind excitation.

One of the disadvantages of wind turbines is that they are unable to produce electricity when wind speeds are too low or too high, and current practice is to cease operation when wind speeds exceed a certain threshold. Wind turbines are also tall, slender structures and can be susceptible to vibration effects at the base, such as during earthquakes. Dampers can be used to control the associated structural vibrations, allowing wind turbines to operate at higher wind speeds and in earthquake regions.

Many studies have been carried out on the use of dampers in structures. Ricciardelli et al. [6] optimised the properties of the TMD based on the measured response of a wind-excited structure. Other studies have been carried out by Samali and Kwok [7], Tamura et al. [8], Zhang and Xu [9] and Balendra et al. [10].

In order to achieve the maximum reduction in vibrations, it is important to identify the optimum locations for the dampers. Zhang and Soong [11] suggested the use of a Sequential Search Algorithm (SSA) that determines the optimal location of viscoelastic (VE) dampers in a structure. A controllability index (CI), based on the response of the structure is defined. The response of the primary structure is calculated and the first damper placed where the CI is highest. The properties of the structure are altered by the presence of this additional damper, hence the response of the structure is recalculated. The next damper is then placed where the new CI is highest. The procedure is repeated until additional dampers cause insignificant changes to the response of

[1]Research Student, rucollin@tcd.ie
[2]Lecturer, basub@tcd.ie
[3]Lecturer, bbrodrck@tcd.ie

the structure. Garcia and Soong [12] developed a simplified version of the SSA, the Simplified Sequential Search Algorithm (SSSA), which provided further insight into the effectiveness of the SSA. Shukla and Datta [13] also examined the optimal locations of VE dampers in a structure. A CI was determined based on the root mean square (rms) of the displacement response and a similar sequential procedure was applied.

In this paper, a procedure to identify the optimal location and number of multiple tuned mass dampers (MTMDs) in a wind turbine tower, subjected to a stochastic excitation characterised by a power spectral density function (PSDF) is presented. The optimisation methodology employs the sequential search algorithm (SSA). The PSDFs applied to the structure represent wind and seismic excitations. The wind turbine tower is represented by a multi-degree-of-freedom (MDOF) model. Two variations of the model are considered: the tower is assumed to act as a cantilever, with an additional top mass representing the blades and nacelle of the turbine, and the nacelle and rotating blades are included as a separate DOF. Controllability indices (CIs) based on the rms acceleration and displacement responses of the structure are determined. The optimal tuning parameters for each TMD placed in the structure are obtained, and using the SSA, configurations for the number and placement of the TMDs in the structure subjected to each PSDF are found. To investigate the robustness of the design of the damper configuration when the applied loading varies from the assumed design loads, the structure with damper configurations designed based on the PSDF of wind excitations are subjected to the PSDF for seismic excitations, and vice versa. Finally, a general configuration is determined and subjected to each of the PSDFs to investigate the performance of the dampers.

2 Wind Turbine Model

2.1 Model 1

A wind turbine tower, assumed to be fixed into the ground and acting as a vertical cantilever is considered for analysis, as shown in Fig 1. The model is based on a wind turbine tower designed by Lavassas et al. [13] except that the rotors are lumped as a mass at the top of the tower in order to simplify the calculations. The mass of the tower is lumped at n nodes of interest, which leads to a discrete N-DOF system where the n^{th} mass, stiffness and damping values are designated by m_n, k_n and c_n. It can be assumed that the damping matrix, which is of Rayleigh type, is proportional to the mass and stiffness matrices.

When TMDs are added to any DOF of the structure, the augmented model (including the added TMD) represents an N+p DOF system (where p represents the number of additional TMDs), whose response is strongly dependent on the properties of the TMD. Each TMD is placed at a DOF, chosen based on the response of the structure and denoted by the position 'q'. The mass, stiffness and damping matrices will now change such that, m_{N+p} is placed at the position (N+p,q) and position (N+p,N+p); $-k_{N+p}$ and k_{N+p} are placed at the position (q,N+p) and (N+p,N+p) respectively; $-c_{N+p}$ and c_{N+p} are placed at the position (q,N+p) and (N+p,N+p) respectively for each addition of TMD.

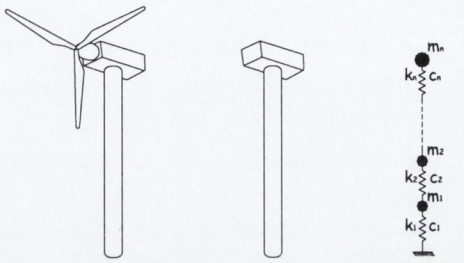

Figure 1: Wind turbine tower, simplified model and discretised model

2.2 Model 2

The tower is now modelled with three rotating blades, with each blade rotating at a frequency of 3.14rad/sec. The motion of the blades is assumed to be flapping, i.e. out of plane motion, and the natural frequency of the tower changes as a result of the rotating blades. The blades are modelled by a spring with an equivalent stiffness, which is coupled to the tower.

In order to replace the blades with a spring of equivalent stiffness, the natural frequency of the blades must first be calculated. This is obtained using a discretised method described in Murtagh et al [5]. The blade is separated into m nodes and the fundamental natural frequency, ω_B is calculated using a geometric stiffness matrix of the blade accounting for the axial forces arising in the blade due to its rotation.

Once the natural frequency of the blade is known, the natural frequency of the new system can be obtained. The blade is replaced by a spring of equivalent spring stiffness, K_s, and incorporated into the model. Assuming the blade acts like a SDOF system, the equivalent mass, M_s and damping C_s can also be obtained.

The mass, stiffness and damping matrices are obtained for the uncoupled system as calculated in section 2.1 and M_s, K_s and C_s are added to these. Once the blades have been added to the wind turbine tower, each additional damper can be added as described in section 2.1. Note that if the damper is to be placed at the N^{th} DOF of the uncoupled system, this will be the $N\text{-}1^{th}$ DOF of the coupled system.

3 Transfer Matrix and Stochastic Response

The transfer matrix is defined as the matrix that algebraically relates a system's output to its input. Here, the system input is the PSDF and the output includes the displacement, velocity or acceleration

response for which the transfer matrix is formulated. By employing a Laplace Transform, these inputs and outputs can be related in the frequency domain. For the model of the wind turbine tower considered, the theory of state space, modelled in the frequency domain, is used. A system can be represented in state space using the following equations [14].

$$[\dot{x}] = [A][x] + [B][\ddot{z}] \quad (1)$$

$$[y] = [C][x] + [D][\ddot{z}] \quad (2)$$

where [x] is the state vector, [y] is the output vector, $[\ddot{z}]$ is the input vector, [A] is the system matrix, [B] is the input matrix, [C] is the output matrix, [D] is the feed-forward matrix and the overdot implies differentiation with respect to time.

The vector, [x], is the relative displacement of the system with respect to the ground. From the state space equations, the transfer matrix, [H(iω)], is obtained by using the Laplace Transform. The resulting matrix is given in Eq. (3)

$$[H(i\omega)] = [C][(i\omega[I]-[A])]^{-1}[B] + [D] \quad (3)$$

The transfer matrix can also be expressed, as a function of the frequency ratio β, which is a ratio of the excitation frequency ω, to the fundamental natural frequency ω_n.

A relationship between the PSDFs of any input, F and any output, X at each point in the system can now be calculated using Eq. (4)

$$S_x(\beta) = H(\beta) S_F(\beta) H^*(\beta) \quad (4)$$

where, $H^*(\beta)$ is the complex conjugate of $H(\beta)$. PSDFs representing wind and base excitations are investigated. For the wind excitation, the PSDF is obtained from the along-wind excitation applied to the structure and the turbulence between two points, and is modelled by the Harris spectrum and wind excited white noise. For the base excitation the PSDF is modelled by the Kanai-Tajimi spectrum and base excited white noise.

The Harris Spectrum is calculated using the method given in Ref [10], where k_0=0.03, l_x=1200m, ω_1=2.9024rad/s, U_{10}=18m/s, α^p=0.23, ρ_0=1.2kg/m^3, A_0=114.258m^2 and C_0=1.2.

For the base excited system the Kanai Tajimi spectrum is given in Eq. (5)

$$S_{ii}(\omega) = S_0 \frac{1 + 4\zeta_g^2 (\frac{\omega}{\omega_g})^2}{[1 - (\frac{\omega}{\omega_g})^2]^2 + 4\zeta_g^2 (\frac{\omega}{\omega_g})^2} \quad (5)$$

In general, for firm ground conditions, values of 0.6 and 5π are assumed for ζ_g and ω_g, respectively [15]. For the numerical study considered in the following section, S_0 = 1cm^2/s^3 is assumed, without any loss of generality.

The rms value of the response variable considered is determined by taking the square root of the integral of Eq. (3).

4 MTMD Optimisation by SSA

4.1 Model 1

The approach described in the previous section is applied to a 20 DOF wind turbine model, comprising a steel tower of height, L=44.075m with a uniform annular cross-section with average outside and inside diameters of D=2.7m and d=2.69m, respectively. The mass of the tower is 47021.5kg, which is divided equally into 20 parts lumped at each degree of freedom. The mass of the nacelle and the rotor blades, 2766.42kg, is added to the mass at the top of the tower [3].

The fundamental natural frequency, ω_1 of the system, is found to be 2.68rad/sec or 0.43Hz. The second natural frequency is found at 26.14rad.sec or 4.16Hz, this is required to calculate the damping matrix. The modal damping of the structure is assumed to be 1% for the first and the second modes of vibration.

TMDs operate by reducing the response of a structure to imposed dynamic loading. A CI based on the relative acceleration and displacement response of the different degrees of freedom is employed to quantify the extent to which this is achieved using different numbers of MTMDs.

The PSDF modelled by the Harris spectrum was applied to the structure and the rms response calculated. The peak rms displacement response was found at the top of the structure at the 20th DOF, whereas the peak rms acceleration response was found at the centre of the structure at the 11th DOF.

The CI is based first on the rms displacement response. Following the SSA, the first TMD was placed where the rms displacement response of the primary structure was observed to be highest, i.e. the 20th DOF. The natural frequency of the TMD is determined by the natural frequency of the structure. This is achieved by letting k_D, the stiffness of the damper equal $\alpha_1 \omega_1^2 m_D$ where ω_1 is the fundamental natural frequency of the structure, m_D, the mass of the damper is 5% of the mass at the top of the structure and α_1, the tuning parameter, is the ratio of the frequency of the primary structure to the MTMD. A very low value of viscous damping in the TMD is assumed (1% in this case), to avoid an infinite value in the transfer matrix. This value of damping could be assumed to be still smaller as the reduction in the response is not dependent on this damping, but on the tuning parameter instead. It is expected that when α_1 is around 1 (but not exactly equal to 1) the maximum amount of energy in the structure will be dissipated.Fig 2 shows how the choice of α_1 influences the maximum rms

displacement response found at the 20th DOF. It is clear that the maximum decrease in the response of the structure occurs for $\alpha_1 = 0.88$. At this value, a reduction of 29.32% in the rms displacement response and 1.56% in the rms acceleration response is achieved. The next highest rms response in the modified structure was found at the 19th DOF, so a TMD was placed there. The procedure was repeated until the addition of another damper resulted in only an insignificant change in the structural response of the system. The results are shown in Table 1. The maximum displacement and acceleration responses are always found at the top and the centre of the structure respectively.

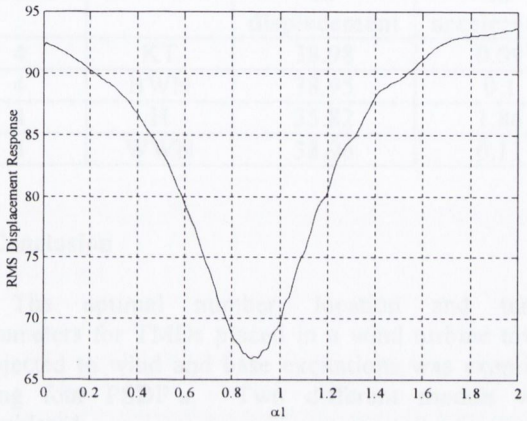

Figure 2: Generalised configuration with four TMDs is assumed

Table 1: Response of the structure subjected to each of the four PSDFs, when the CI is based on the rms displacement response

No. of TMDs	Pos. (DOF)	α	% reduction in disp.	% reduction in acc.
Harris Spectrum (H)				
1	20th	0.88	29.32	1.56
2	19th	0.67	36.44	1.99
3	18th	0.44	39.82	2.08
4	17th	0.7	41.62	2.2
Wind Excited White Noise (WWN)				
1	20th	0.91	30.18	0.09
2	19th	0.69	37.21	0.11
3	18th	0.45	41.1	0.11
4	17th	0.66	43.11	0.13
Kanai-Tajimi spectrum (KT)				
1	20th	0.9	29.85	0.08
2	19th	0.59	37.20	0.09
3	18th	0.45	41.02	0.09
4	17th	0.69	42.71	0.1
Base Excited White Noise (BWN)				
1	20th	0.91	30.17	0.09
2	19th	0.69	38.28	0.11
3	18th	0.445	41.97	0.11
4	17th	0.64	44.48	0.12

The CI was then based on the rms acceleration response of the structure and the procedure was repeated. The difference in the response of the structure was only marginal.

The procedure was repeated for the PSDF modelled by wind excited white noise, the Kanai-Tajimi spectrum and base excited white noise and the results are shown in Table 1. For each PSDF, the CI based on the rms displacement response of the system was taken. The tuning parameters for each method are very close to each other for each additional TMD, as is the reduction in rms displacement response. Therefore it is concluded that the SSA is an appropriate method to reduce the rms displacement response in a wind turbine tower, but not the rms acceleration response.

Table 2: Values of tuning parameter

	KT	BWN	H	WWN	Generalised
α_1	0.9	0.91	0.88	0.91	0.9
α_2	0.59	0.69	0.67	0.69	0.66
α_3	0.45	0.445	0.44	0.44	0.444
α_4	0.69	0.64	0.7	0.69	0.68

A generalised configuration obtained using the averages of the tuning parameters for the four PSDFs is shown in Table 2. The structure was then subjected to each PSDF using this generalised configuration and the considerable response reductions are shown in Table 3. Therefore it can be concluded that this generalised model is appropriate for most PSDFs.

Table 3: rms response reductions for each PSDF applied to model 1 when the generalised configuration is assumed

No. of TMDs	Spectrum	%reduction in displacement	%reduction in acceleration
4	KT	42.79	0.1
4	BWN	42.8	0.12
4	H	41.01	2.18
4	WWN	42.82	0.13

4.2 Model 2

The wind turbine tower now incorporates 3 rotating blades, rotating at a blade velocity, Ω of 3.14rad/s. The blade is modelled as a continuous prismatic beam of rectangular hollow cross-section of length, L_B=30m, depth, d=0.4m, breadth, b=2.4 m, thickness, t=0.01m, hub radius, R_H=2.5m, elastic modulus, E_B=65x10^{9}Nm^{-2}, density, ρ_B=2100 kgm^{-3} and mass per unit length, $\overline{m}_B$=116.76 kgm^{-1}.

As before, four PSDF's are considered. The natural frequency of the individual blades, ω_B, and the coupled tower-blade system ω_c are calculated to be 5.25rad/s and 2.46rad/s respectively. ω_c is very close to the natural frequency of the tower without the blades, ω_n which equals 2.54rad/s. Once ω_B is known the base shear is calculated and this equals the

equivalent spring stiffness K_s. From this M_s and C_s are known. These are added into the mass, stiffness and damping matrices to give the new parameters for the coupled system.

The generalised configuration calculated for model 1 was applied to model 2 and the response to each PSDF calculated, the results are shown in Table 4. Again the reduction in response is considerable, but slightly less than that for model 1.

Table 4: rms response reductions for each PSDF applied to model 2 when the generalised configuration obtained for model 1 is assumed

No. of TMDs	Spectrum	%reduction in displacement	%reduction in acceleration
4	KT	38.98	0.09
4	BWN	38.95	0.1
4	H	35.82	1.86
4	WWN	38.96	0.11

5 Conclusion

The optimal number, location and tuning parameters for TMDs placed in a wind turbine tower, subjected to wind and base excitations was examined using four PSDF's. Two different models were considered.

A CI based on the rms displacement response resulted in better reductions in the response of the structure than a CI based on the rms acceleration response. The optimal number and location of the TMDs did not change for each of the different PSDFs. A generalised configuration for the number, placement and tuning parameters of the TMDs was obtained and the results showed that the percentage reduction in response varied marginally.

It is clear that the use of TMDs is effective in reducing the vibrations in a wind turbine tower subjected to both wind and base excitations. Here, specific objectives are defined for the response of a structure for different excitations. These specific objectives may be used to define the controllability indices on which the SSA is based, and may include either deformation or force-based parameters.

References

[1] Varol A, Ilkılıc C, Varol Y., Increasing the efficiency of wind turbines, *Journal of Wind Engineering and Industrial Aerodynamics,* vol. 89, p. 809, 2001

[2] Bazeos N, Hatzigeorgiou G, Hondros I, Karamaneas H, Karabalis D, Beskos D. Static, seismic and stability analyses of a prototype wind turbine steel tower, *Engineering Structures*, vol. 24, p. 1015, 2002

[3] Lavassas I, Nikolaidis G, Zervas P, Efthimiou E, Doudoumis I, Baniotopoulos C, Analysis and design of the prototype of a steel 1-MW wind turbine tower, *Engineering Structures*, vol. 25, p. 1097, 2003

[4] Baumgart A., A Mathematical Model for Wind Turbine Blades, *Journal of Sound and Vibration*, vol. 251(1), p. 1, 2002

[5] Murtagh P J, Basu B, Broderick B M., Mode Acceleration Approach for Rotatin Wind Turbine Blades, *Proc. Institution Mechanical Engineers,* Vol 218 Part K. Multi-body dynamics, 2004

[6] Ricciardelli F, Occhiuzzi A, Clemente P. Semi-active Tuned Mass Damper control strategy for wind-excited structures, *Journal of Wind Engineering and Industrial Aerodynamics,* vol. 88, p. 57, 2000

[7] Tamura Y, Fujii K, Tamio, Wakahara T, Kohsaka. Effectiveness of tuned liquid dampers under wind excitation, *Engineering Structures*, Vol. 17, No. 9, p. 609, 1995

[9] Zhang W, Xu Y. Closed form solution for along-wind response of actively controlled tall buildings with LQG controllers, *Journal of Wind Engineering and Industrial Aerodynamics,* vol. 89, p.785, 2000

[10] Balendra T, Wang C, Yan N. Control of wind-excited towers by active tuned liquid column damper, *Engineering Structures*, vol. 23, p. 1054, 2001

[11] Zhang R and Soong T., Seismic design of viscoelastic dampers for structural applications, *Journal of Structural Engineering*, Vol 118, 1992

[12] Lopez Garcia D and Soong T., Efficiency of a simple approach to damper allocation in MDOF structures, *Journal of Structural Control*, Vol 9, p. 19, 2002

[13] Shukla A and Datta T., Optimal use of viscoelastic dampers in building frames for seismic force, *Journal of Structural Engineering,* 1999

[14] Norman S. Nise. Control Systems Engineering. Third Edition, 1994

[15] Clough R and Penzien J. Dynamics of Structures. Second Edition, 1993

ACADEMIC REVIEW

Dynamic response and vibration control of wind turbine towers

P.J. Murtagh, BE, MIEI, **R. Collins**, BA, BAI, **B. Basu**, BCEng, MTech, PhD, MIEI, and **B.M. Broderick**, BE, MEngSc, PhD, DIC, MIEI[1]

Department of Civil, Structural and Environmental Engineering, Trinity College Dublin.

Keywords:
Wind engineering, structural dynamics, wind turbine towers, power spectral density functions, tuned mass dampers.

Abstract

This paper addresses some of the design issues faced by structural/wind engineers tasked with ensuring the serviceability and survivability of wind turbine towers. The issues discussed include rotor blade and tower vibration coupling, as well as the suppression of vibrations caused by dynamic wind loading. Mathematical models are presented to investigate the response of rotor blades and coupled rotor blade/tower motion, subject to realistic random wind loading. The resultant vibrations are then mitigated by adding energy dampers to the system, and this paper investigates the optimal position of these dampers in order to minimise vibrations.

IRISH ENGINEERS JOURNAL vol. 58 : 07 September 2004: xx-xx

1. Introduction

Wind turbine towers are the means by which kinetic energy contained within the wind may be harnessed and transformed via mechanical energy, into electrical energy. The electricity thus created is fed into the national grid, being available to the consumer. Although wind turbine towers are commonplace throughout the landscape of mainland Europe, Irish people are only lately becoming aware of wind farms as their installation increases throughout the countryside.

It is in fact only within the last decade that wind turbines have become an economically viable option for widespread electrical energy production. Consequently, wind turbine technology has enjoyed considerable proliferation in the past ten years, particularly in Europe. As wind turbine towers are increasingly being placed in varying wind environments in different areas around the world, it is necessary that the structural/wind engineer has a comprehensive understanding of the behaviour of the structure under dynamic loading.

The recent success of wind turbines stems from the fact that units have now become more affordable, mainly due to improved mass production techniques, and from an increase in environmental awareness following Earth Summits, such as those in Rio de Janiero and Kyoto. The well-publicised Kyoto summit resulted in the formation of the Kyoto Protocol, which demanded that global production of greenhouse gases produced by developed countries be reduced by approximately 5% below 1990 levels by 2008-2012. The Irish Government acknowledges that in order to meet this target, it must foster renewable sources of energy and wind energy is abundantly available for this purpose.

The motivation behind this paper is to introduce various concepts and approaches concerned with characterising the dynamic behaviour of wind turbine towers. Wind turbine towers are complex structures, having many moving flexible parts which are easily affected by dynamic wind loading. This paper presents mathematical modelling techniques to predict some behavioural phenomena associated with wind turbine towers, as well as efforts to minimise the wind induced vibrations of the tower.

2. Theoretical considerations

The contemporary wind turbine tower, as seen about the Irish countryside and offshore along the southeast coast, has three flexible rotating blades, see Figure 1. The structure may be broadly separated into three components; the rotating blades, which collect the energy contained within the wind; the nacelle, which houses the mechanical and electrical equipment needed for electricity generation; and the tower, which supports the nacelle and rotor blades at a desired elevation above the ground, and transfers all gravity and environmental loadings to the foundation of the structure.

Figure 1: Three blade wind turbine tower.

Figure 2: Tapered rectangular hollow section wind turbine blade.

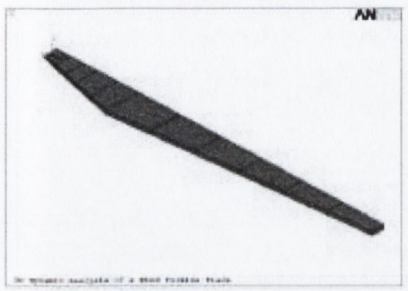

The geometry of the wind turbine rotor blade is actually quite complex. It usually will have a cross section similar to that of an aircraft wing, a so-called 'aerofoil', though the cross sectional shape will change along the length of the blade. A variety of materials have been employed to fabricate the rotor blades, including steel, a wood and epoxy mix, glass fibre reinforced epoxy, carbon fibre reinforced epoxy and glass fibre reinforced polyester.

The tower may be constructed from steel reinforced concrete, pre-stressed concrete, tapered tubular steel, or welded steel members arranged to form a lattice frame. Concrete towers have been used in Denmark but are very heavy in comparison to steel tubular or lattice towers. The steel shell towers, as used in Ireland, are constructed from curved steel plates which are welded together to form a conical section.

2.1 Structural Dynamics

The ultimate aim of any dynamic analysis is to estimate the response, for example, displacements, accelerations, shear forces and bending moments on a structure, subject to dynamic loading, termed a forced vibration analysis. The structure under forced vibration is subject to inertial forces, damping forces, elastic forces and applied environmental forces (such as wind or earthquake loading) and operational forces (such as those due to environmental mass eccentricities in the turbine). In order to predict the forced vibration response of any structural system, it is usually necessary to obtain the free vibration characteristics of that system, namely the natural frequencies and mode shapes.

2.1.1 Free vibrations of rotating blades

The blades are modelled as discrete multi-degree-of-freedom (MDOF) systems. In reality, blade geometry is usually complex with mass and stiffness varying along all major axes. The equation that represents free vibrational motion in the flapping direction for blades modelled as an undamped discrete system is

$$[M]\{\ddot{u}\}+[K]\{u\}=\{0\} \qquad (1)$$

where [M] and [K] denote the mass and stiffness matrices of the blade, and {u} and {ü} represent nodal displacement and acceleration response respectively. Due to the intricacy of blade geometry, the finite element method was employed to create a model with complex geometry, as presented in Figure 2. The blade was built using the software code ANSYS and consists of tapered beams of rectangular hollow cross section. The blade model was created using the beam element BEAM44, which has six degrees-of-freedom at each node and allows for different cross-sectional areas and moment of inertia at each node, facilitating tapered geometries. A unit load was placed at one node of the finite element model and a static analysis carried out to obtain the resulting displacements at each node of the model. If this is repeated for each node in turn the results may be cast within a matrix, known as the flexibility matrix, the inverse of which is the desired stiffness matrix of the system. This technique allows the formulation of the reduced stiffness matrix corresponding to certain nodes of interest and was used to transform the finite element model into a reduced order model. The mass matrix at the discrete nodes of interest, as in equation (1) may be formulated as a diagonal matrix with the i^{th} nodal mass m_i.

Although ANSYS has a modal analysis capability that yields the natural frequencies and mode shapes of the blade, the program does not have the capability of including centrifugal stiffening effects on the blades eigenproperties. Centrifugal stiffening, which occurs due to blade rotation, results in increased flexural stiffness. The eigenproperties of the rotating blade accounting for centrifugal stiffening may be obtained from

$$\mathrm{DET}\left|[K']-\omega_n{}^2[M]\right|=0 \qquad (2)$$

where, $[K'] = [K + K_G]$ represents the modified stiffness matrix due to the geometric stiffness accounting for the effect of centrifugal stiffening, ωn^2 are the desired natural frequencies. The geometric stiffness matrix, K_G, contains force contributions due to blade rotation which are always tensile, and contributions from the self-weight of the blade, which may be tensile or compressive, depending on blade position. The geometric stiffness matrix is obtainable as

Figure 3: Comparison of PSDFs as used in wind engineering.

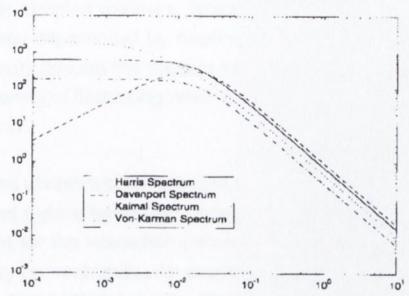

$$[K_G] = \begin{bmatrix} \frac{N_1}{l_1} & \frac{-N_1}{l_1} & \cdots & 0 \\ \frac{-N_1}{l_1} & \frac{N_1}{l_1}+\frac{N_2}{l_2} & \cdots & 0 \\ \vdots & \vdots & \ddots & \frac{-N_{m-1}}{l_{m-1}} \\ 0 & 0 & \frac{-N_{m-1}}{l_{m-1}} & \frac{N_{m-1}}{l_{m-1}}+\frac{N_m}{l_m} \end{bmatrix} \quad (3)$$

where N_i is the axial force at node 'i', l_i is the length of beam segment between the nodes 'i' and 'i+1', and 'm' is the total number of nodes. The axial force N_i can be expressed as

$$N_i = CT_i \pm G_i \quad (4)$$

in which CT_i and G_i are the axial forces at node 'i' due to centrifugal and gravity forces respectively, with the sign convention that tensile forces are positive and compressive forces are negative. The magnitude of the tensile centrifugal axial force, CT_i, may be obtained in discrete form (from the continuous form by Naguleswaran (1994)), as

$$CT_i = 0.5\Omega^2 \left(M_B L_B - m_i x_i\right) \quad (5)$$

where Ω is the blade rotational frequency, M_B is the total mass of the blade, L_B is the total length of the blade, m_i is the cumulative mass at node 'i' and x is the distance of node 'i' from the centre of rotation. The nodal axial force due to gravity (self-weight), G_i, may be obtained from geometry and depends on the angle of the blade to the horizontal.

2.2 Forced vibrations

Equation (6) describes forced vibration motion for a discrete damped system

$$[M]\{\ddot{u}\}+[C]\{\dot{u}\}+[K]\{u\}=\{P(t)\} \quad (6)$$

where [C] denotes the damping matrix,{P(t)} denotes a vector of nodal forces, and $\dot{u}$ denotes a vector of nodal velocities. In order to solve equation (6) for nodal displacement, the nodal loading vector containing wind loading information must first be derived. Wind is dynamic in both time and space, so engineers use a statistical approach based on random theory to characterise wind loading. Indeed, most wind engineering codes make use of a random theory representation of wind loading through use of the well known gust factor (ASCE 1998, CEN 2004). Using this statistical approach, a time-varying wind velocity time-history, V(t), can be divided into a mean component, $\overline{v}$ and a fluctuating component v'(t) as

Figure 4: Rotationally sampled spectrum showing distribution of energy.

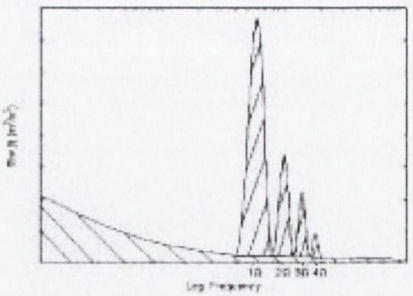

$$V(t) = \overline{v} + v'(t) \quad (7)$$

The fluctuating component is usually represented by a wind velocity power spectral density function (PSDF). This is fundamentally a measure of the kinetic energy within the fluctuating component of the wind, expressed as a function of frequency. Figure 3 illustrates four such PSDFs used in wind engineering, as suggested by von Kàrmàn (1948), Davenport (1961) and Harris (1971) and Kaimal *et al.* (1972).

Using a PSDF function, it is possible to generate a fluctuating wind velocity time history, which when added to the mean component, gives the total wind velocity at any time. This velocity may then be converted to a drag force, $F_d(t)$, using equation (8).

$$F_d(t) = 0.5\rho C_d A V^2(t) \quad (8)$$

where ρ is the density of air, C_d is a drag coefficient, and A is the area normal to the wind flow. Values of C_d may be sourced from European Committee for Standardization (CEN, 2004). Equation (8) may be used to create the force vector used in equation (6).

2.2.1 Forced vibrations of rotating blades

Because the turbine blades are rotating, they are subjected to a slightly different PSDF than stationary objects such as the turbine tower. In fact, energy moves from the lower frequency range of the spectrum to integer multiplies of the rotational frequency of the blades, that is, if the blades are rotating with a frequency of π rads^{-1} (one complete revolution every two seconds), energy in the wind gets shifted to frequencies such as π rads^{-1}, 2π rads^{-1}, 3π rads^{-1}, and so on. This phenomenon is known as rotational sampling, and is unique

to the problems at hand. Figure 4 illustrates what is known as a rotationally sampled spectrum, which represents the distribution of wind energy experienced by rotating wind turbine blades. In this figure, fSvv(f) denotes the product of frequency (f) with the power spectral density of fluctuating wind velocity Svv(f), which is a function of frequency.

2.2.2 Forced vibrations of tower including blade interaction

The wind turbine tower and blades do not vibrate independently. To account for the interaction between the two, the three rotating blades may be mathematically coupled to the tower by considering the force transmitted between them. When a blade vibrates, it experiences a shear force along its length, which is a maximum at the base of the blade. An expression for the total base shear created by the forced vibration of the three blades, $V_{BS}(t)$, may be obtained as the sum of the inertia forces experienced by each blade as

$$V_{BS}(t) = 3\sum_{i=1}^{n} m_i \ddot{x}_i \qquad (9)$$

where m_i and $\ddot{x}_i$ are the mass and acceleration of node 'i' and 'n' is the total number of nodes used to represent the blade.

This base shear may subsequently be considered to act at the top of the tower. When used in conjunction with nodal drag forces acting along the length of the tower, this allows the response of the tower to be obtained including the effects of blade/tower interaction.

2.3 Vibration suppression

The vibration suppression of structures may be addressed using control theory, whose overall objective is to make a system operate in a more desirable way (Yao, 1972). Vibration control theory can be broadly separated into two main approaches. The first - modal control - seeks to control a structure's mode of vibration. The second - optimal control - is where a structure is controlled to meet some performance criterion, such as the minimisation of the deflection of the structure. Central to the application of control theory to vibration reduction is the use of dampers (Meirovitch, 1990).

2.3.1 Classification of dampers

Vibration dampers can be classified on the basis of their functional performance and power supply requirements as passive, semi-active or active. In all cases, the role of the damper is to absorb energy from the structure that originates from a source of loading, (for example, wind or earthquakes), and to reduce the vibrations experienced by the structure.

Passive dampers do not require an external power supply; their properties are chosen based on *a priori* design criteria and do not change during the response of the structure. The effect of employing a passive device is to change the structural stiffness, thereby changing the natural frequencies and mode shapes of the structure.

However, passive devices are not always sufficient to meet the design criteria. For example, with the development of high speed ground transport technology, active dampers are required to ensure vehicle stability. An active damper requires a large power source for operation. The control forces supplied by the power source are based on the actual response of the structure and change as the response of the structure changes.

For some applications, the power requirements of active dampers may be so large that they are not economically feasible. In these cases semi-active dampers can be introduced. These dampers remain passive while response amplitudes are small but are triggered into action when the vibrations exceed a predefined threshold. They require only a small power source (Spencer and Nagarajaiah, 2003).

2.3.2 Vibration dampers

Many different types of vibration dampers exist, such as variable stiffness dampers, electro-rheological dampers, magneto-rheological dampers, tuned mass dampers and tuned liquid dampers, to mention but a few. Only tuned mass dampers (TMD) are considered in this paper. A tuned mass damper consists of a mass, a spring and a dashpot. The mass of the TMD is typically between 2% and 5% of the total mass of the structure. The TMD can be passive, active or semi-active. For a passive TMD, the ratio of the natural frequency of the TMD to that of the structure is tuned to a certain value. For an active TMD, the properties of the TMD change with the response of the structure. For a semi-active TMD, the TMD remains passive until the excitations are large enough to trigger an active TMD into action. Examples of the application of such TMDs are the installation of a 400-ton TMD on the top of the Citicorp Centre in New York and two 300-ton TMDs on the John Hancock Tower in Boston.

2.3.3 Optimal location of TMDs in a wind turbine tower

Once the control strategy and choice of damper have been decided, it is important to evaluate the optimal number and position of the dampers in a structure. A method to find the optimal location of the dampers, called the sequential search algorithm (SSA) was suggested by Zhang and Soong (1992). The SSA is a useful technique that is applicable to many areas of design and any structural form, so long as the mass, stiffness and damping matrices can be obtained. The method employs a controllability index (CI) which is a measure of the response of the structure. The response of the primary structure is calculated and the first damper placed where the CI is highest. The properties of the structure are altered by the presence of this additional damper; hence the response of the structure is recalculated. The next damper is now placed where the new CI is highest. The procedure is repeated until additional dampers cause insignificant changes to the response of the structure or until a predefined criteria has been achieved. Garcia and Soong (2002) and Shukla and Datta (1999) have provided further insight into this area of research. When TMDs are added to any DOF of the structure, the augmented model (including the added TMD) represents an N + p DOF system, where

Figure 5: Mode shapes of blade rotating at 1.57 rads^{-1}.

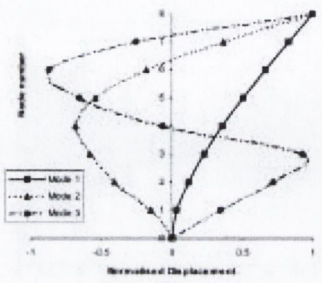

Figure 6: Tip displacement time-history of rotating blade.

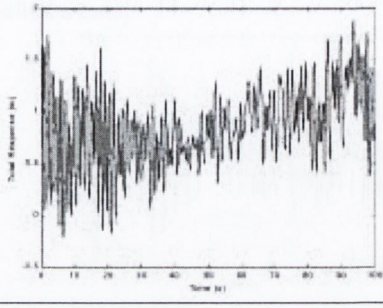

'N' denotes the number of DOF of the structure and 'p' denotes the number of additional TMDs. The response of the structure is strongly dependent on the properties of the TMD. 'p' number of TMDs are placed at the i_1, i_2, i_3,....i_p DOF (chosen based on the response of the structure) and the stiffness and damping matrices will now change.

The transfer matrix is defined as the matrix that algebraically relates the output of a system to its input. In this study, the system input is the wind velocity PSDF and the output includes the displacement, velocity or acceleration response for which the transfer matrix is formulated. Once the transfer matrix is known, the root mean square (rms) value of the response of the structure can be determined using the H_{rms} norm control technique, as given by equation (10)

$$[H]_{rms} = \left(\frac{1}{2\pi} \int_{-\infty}^{\infty} [H(\beta)][S_F(\beta)][H^*(\beta)]d\beta \right)^{1/2} \qquad (10)$$

where $[H_{rms}]$ is the rms value of the response quantity, $[H(\beta)]$ is the transfer matrix, $[H^*(\beta)]$ is the complex conjugate of $H(\beta)$ and $[S_f(\beta)]$ is the PSDF matrix. The value of $[H]_{rms}$ given by equation (10) is employed as the basis on which the vibration response of the wind turbine tower is deemed to have been minimised. A CI based on the relative rms acceleration and displacement responses of the different degrees of freedom in the tower model can be employed to quantify the extent to which this is achieved using different numbers of TMDs.

3. Results

3.1 Free vibrations of blades

The lumped mass method outlined in section 2.1.1 is used to obtain the natural frequencies and mode shapes of an idealised tapered wind turbine blade for a series of different blade rotational frequencies. This method allows for the inclusion of centrifugal stiffening due to blade rotation and the effects of this phenomenon are explored. The modal analysis capability of the finite element code ANSYS was also employed to obtain these free vibration properties, though with this method the effects due to rotation cannot be included.

The blade investigated (see Figure 2) is of rectangular hollow cross section. The rotating blade considered has a length of 30m, a width of 1.1m at both ends and a width of 3.0 m at its widest intermediate point. Three rotational frequencies were considered: 0 rads^{-1} (stationary), 1.57 rads^{-1} (one cycle every four seconds) and 3.14 rads^{-1} (one cycle every two seconds). Table 1 presents the values of natural frequency obtained from ANSYS and from the reduced order model (ROM). The two approaches may be compared at 0 rads^{-1}, with the ROM showing about a 10% difference from the ANSYS results. It is worth noting that the ANSYS results contain about three times the number of degrees-of-freedom more than the ROM, insuring a greater level of accuracy. From Table 1, it is evident that as the rotational speed of the blades increase, their natural frequencies increase, or the blade gets stiffer. Figure 5 shows the first, second and third modes obtained using the ROM which includes blade rotation at 1.57 rads^{-1}.

3.2 Forced vibrations of rotating blade

Figure 6 illustrates the tip displacement time-history of the blade described in the previous section when subjected to a dynamic wind load, calculated using the mode acceleration method. The mean wind velocity at the blade point of rotation was taken as being 20ms^{-1} and the rotationally sampled spectrum described in section 2.2.1, was used to simulate the fluctuating wind velocity component. The blade was assumed to be rotating at a frequency of 3.14 rads^{-1}, and modal damping ratios used were 1% of critical. The maximum tip blade displacement may be observed to be approximately 1.8m.

Figure 7 illustrates the time-history of the shear force created at the base of the vibrating blade. This shear force will ultimately be transferred on to the top of the tower. The maximum observed base shear is approximately 26 kN.

3.3 Forced vibrations of coupled blades/tower

Three rotating blades (as section 3.2) were coupled to a prismatic steel tower of height 60m, width 2.65m and thickness 12mm. The tower carries a nacelle of approximately 20 tonnes. A separate dynamic analysis was carried out to obtain the natural frequencies and mode shapes of the tower. Two separate cases were considered:

Figure 7: Base shear time-history of rotating blade.

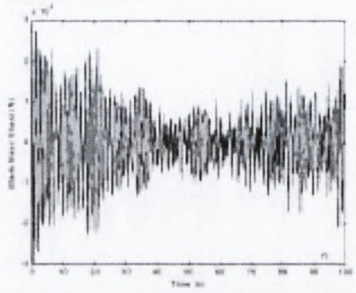

Figure 8: Displacement time history of tower carrying lumped mass of blades.

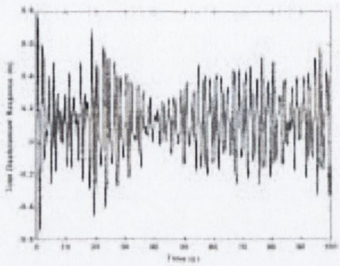

a) three rotating blades connected to the top of the tower allowing blade/tower dynamic interaction; and, b) the mass of three blades added to the mass of the nacelle, accounting for the blade mass but excluding dynamic interaction.

In these two cases, the tower is acted upon by random wind drag force which is correlated over the height of the tower, with a mean wind velocity profile exponent of 0.16. Figure 8 presents the displacement time-history at the top of the tower due to wind loading and the transferred shear force of the three rotating blades. The maximum displacement is approximately 0.75m.

Figure 9 presents the tower tip displacement time-history obtained due to wind loading when the mass of the three blades is simply lumped with the nacelle mass. The maximum observed displacement is approximately 0.15m. It is evident from comparing these two displacement maxima, that the inclusion of blade/tower coupling provides a more realistic estimation of the response of a wind turbine tower.

3.4 Suppression of tower vibrations

The SSA was employed to show the procedure of identifying the optimal location of multiple TMDs (MTMDs) in a wind turbine tower subjected to dynamic wind loading. For illustration, a discrete model of a hypothetical tower with five degrees-of-freedom (DOF), is considered as a numerical example. The tower was modelled as a steel prismatic cantilever, with the specifically chosen dimensions of height 44m, average width of 2.7m and an average thickness of the tower shell of 5mm. This was done in order to obtain natural frequencies close to the realistic natural frequencies for a wind turbine tower of such height. The tower carries a lumped mass to represent the mass of the nacelle and rotor system The first three natural frequencies of the entire system were calculated as 4.39 rads^{-1}, 29.5 rads^{-1} and 85.3 rads^{-1}. The PSDF suggested by Harris (1971) is employed and Rayleigh damping is assumed.

Following the SSA, the first TMD is placed at the node where the rms response (both acceleration and displacement) is observed to be highest. This was found to be at the top node, or fifth DOF.

The natural frequency of the TMD is determined with reference to the natural frequency of the structure. The stiffness of the TMD placed at the top node is set to $\alpha\omega_1^2 m_p$, where ω_1 is the fundamental natural frequency of the primary structure, m_p is 5% of the mass at the top of the structure and α is a tuning parameter, being the ratio of the frequency of the primary structure to that of the TMD. A viscous damping value of 1% in the TMD is assumed.

Figure 10 shows how the choice of α influences the maximum acceleration found at the fifth DOF. It is clear that the maximum decrease in the response of the structure occurs for α = 1.1. A decrease of 27% in both the maximum rms acceleration and displacement response in the primary structure is achieved. This method is repeated until the last damper results in an insignificant change to the structural response. Table 2 presents the results obtained using the numerical example presented in first paragraph of section 3.4. It shows the degrees-of-freedom positions (also see Figure 10) where the TMDs were placed at, along with their values of tuning parameter, α and mass ratio. As MTMDs are placed at different degrees-of-freedom, the displacement and acceleration responses are observed to decrease subsequently. With a MTMDs at the 5th, 4th, 3rd and 2nd DOF, a percentage reduction of 46% and 44% of original tower displacement and acceleration respectively, are observed.

4. Conclusions

Several important design implications have been addressed concerning the structural dynamic analysis of wind turbine towers. Methods were briefly presented which may be used to obtain the free vibration properties of a tapered wind turbine blade, including centrifugal stiffening of the blade due to its rotation. Blade natural frequencies were observed to increase as blade rotational frequency increased. Blade rotation also leads to the need to employ a modified rotationally-sampled wind loading spectrum in the forced vibration analysis. The response of the rotating blades were obtained in the alongwind direction only, using the blade's flapping modes. Other aeroelastic phenomena, such as vortex shedding and flutter, although of importance, were not considered in this paper.

The dynamic interaction between three vibrating blades and their supporting tower was also investigated. It was observed that when

Figure 9: Displacement time-history of coupled tower/blades system.

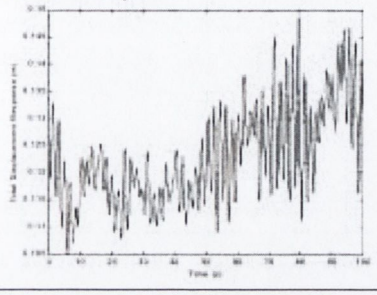

Rotating Blade Natural Frequencies (Hz)						
	Mode 1		Mode 2		Mode 3	
Ω (rads^{-1})	ANSYS	ROM	ANSYS	ROM	ANSYS	ROM
0	0.696	0.615	3.956	3.578	10.983	8.774
1.57	-	0.656	-	3.605	-	9.804
3.14	-	0.762	-	3.682	-	9.880

Table 1: Natural frequencies of rotating blade.

Table 2: 5 DOF model when CI is based on rms acceleration and displacement response.

blade tower interaction is not considered, dynamic response estimation of the tower may be considerably underestimated, especially if the fundamental frequencies of both tower and blades are similar. This is because the interaction force between the vibrating blades and tower, a resultant base shear force due to rotor system vibration, is not considered. This force is transmitted into the tower and may act to amplify tower vibrations. The magnitude of this amplification mainly depends on the flexibility of the rotating blades, so good design practise would be to ensure the blades are relatively stiff. Ignoring blade/tower interaction may lead to erroneous estimations of shear forces and bending moments used in the ultimate limit state design of the tower.

The suppression of vibrations caused by dynamic wind loading was investigated by optimally placing tuned mass dampers at several discrete nodes along the length of a tower. These dampers were found to significantly reduce the magnitude of tower response. This reduction will improve the structure's ability to survive under extreme loading conditions and may help to increase the fatigue life of the structure.

Acknowledgement

The authors would like to sincerely thank RPS-MCOS Consulting Engineers for the financial support awarded to the first and second authors enabling this work.

Figure 10: 5 + 1 DOF rms displacement response at the 5th DOF as a function of tuning parameter, α.

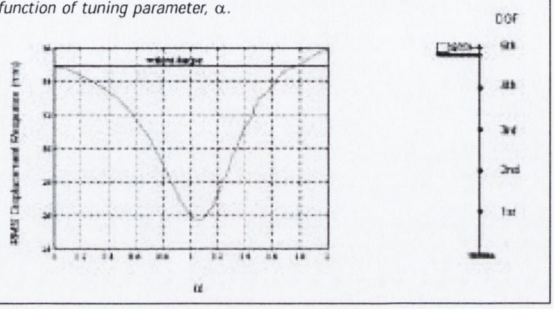

References

ASCE (1998). *Minimum Design Loads for Buildings and other Structures*, ASCE 7-98, United States.

CEN (2004). *Eurocode 1, Basis for Design and Actions on Structures – Part 1-4: Actions on Structures – Wind Actions*, European Pre-standard Env. 1991-1-4.

Davenport, A.G. (1961). The spectrum of horizontal gustiness near the ground in high winds. *Journal of Royal Meteorological Society* **87**: 194-211.

Garcia, L.D. and Soong, T. (2002). Efficiency of a simple approach to damper allocation in MDOF structures. *Journal of Structural Control* **9**: 19-30.

Harris, R.I. (1971). *The nature of wind, in the modern design of wind sensitive structures.* Construction Industry Research and Information Association, London.

Kaimal, J.C., Wyngaard, J.C., Izumi, Y., and Cote, O.R. (1972) Spectral characteristics of surface-layer turbulence. *Journal of Royal Meteorological Society* **98**: 563-589.

Meirovitch, L. (1990). *Dynamics and Control of Structures.* New York: John Wiley and Sons.

Naguleswaran, S., (1994). Lateral vibration of a centrifugally tensioned uniform Euler-Bernoulli beam. *Journal of Sound and Vibration* **176 (5)**: 613-624.

Shukla, A. and Datta, T. (1999). Optimal use of viscoelastic dampers in building frames for seismic force. *Journal of Structural Engineering* **125**: 401-409.

Spencer Jr, B.F. and Nagarajaiah, S. (2003). State of the art of structural control. *Journal of Structural Engineering* **129**: 845-856.

Von-Kàrmàn, T. (1948). *Progress in the statistical theory of turbulence. Proceedings of National Academy of Sciences.* 530-539. Washington D.C.

Yao, J. (1972). Concept of structural control. *Journal of the Structural Division*, Proceedings of the American Society of Civil Engineers **98**: 1567-1573.

Zhang, R., and Soong, T. (1992). Seismic design of viscoelastic dampers for structural applications. *Journal of Structural Engineering* **118**: 1375-1392.